THE POST-AURICULAR MUSCLE REFLEX (PAMR): ITS DETECTION, ANALYSIS, AND USE AS AN OBJECTIVE HEARING TEST

by

Greg O'Beirne

Submitted in partial fulfilment of the requirements for the degree of Bachelor of Science with Honours of the University of Western Australia
November 1998

Acknowledgements

I would like to thank my supervisor, Dr. Robert Patuzzi, for the support and enthusiasm he has shown throughout the year. He is a veritable fountain of knowledge and an inspirational teacher.

My thanks also go to Ms. Susmita Thomson for her encouragement and friendship, and for the work she did on the PAMR from 1995-97, to Mr. Greg Nancarrow for his superb advice, superlative sense of humour, and willingness to help, and to the other members of the Auditory Laboratory of the Department of Physiology for providing a cheerful and thoroughly enjoyable work environment, and for their assistance at various times during the year. They are, in no, particular order, Dr. Graeme Yates, Assoc. Prof. Don Robertson, Dr. Peter Sellick, Dr. Des Kirk, Dr. Helmy Mulders, Ms. Georgie Bennett, Mr. Robert Withnell, Dr. Si Yi Zhang, and Dr. Maria Layton. Thanks also to Dr. Sellick and Dr. Zhang for their surgical assistance.

A million thanks to Mum and Alec for all their love and encouragement over the years, and to Brad for being the best possible brother. Sadly, Alec died in March this year. He is sorely missed.

Many thanks to Doug & Mary for everything they've done during the year, and also to my Dad. Thanks especially to my friend Scott Lewis for "volunteering", albeit somewhat reluctantly, to be a subject in this study, along with Ms. Fiona Young, Andrew Young, and Robert Withnell (The Younger).

This thesis is dedicated with love to Donna, for her endless support, encouragement, love, humour, and friendship.

Abstract

A number of fundamental characteristics of the post-auricular muscle response (PAMR) have been examined in adult and infant human subjects using an automated computer-based measurement system. This system allowed simultaneous examination of the changes in background electrical activity of the PAM, and extraction of information regarding the sound-evoked PAMR waveform, such as response amplitude and peak latency.

It was found that the PAMR was best recorded using an active electrode located directly over the body of the muscle, and a reference electrode located on the dorsal surface of the pinna. In addition, it was found that during lateral rotation of the eyes towards the recording electrodes the peak-to-peak amplitude of the PAMR increased by an average of 525%. The increase in response amplitude was highly correlated with the increase in EMG observed during this manoeuvre, suggesting that the mechanisms that increase both EMG and PAMR amplitude probably occur at a common point. The voltage spectrum of the PAMR was also measured. Contrary to previous findings (Thornton, 1975), the voltage spectrum of the PAMR extended from 10 Hz to approximately 550 Hz, with a broad spectral peak centred between 70 Hz and 115 Hz.

Finally, a cheap, efficient and reliable objective hearing test was developed, using the correlation measure of the PAMR. The availability of such a device has the potential to vastly increase the number of children that are screened for hearing disorders, especially in poorer communities who do not have the funds or the expertise to establish screening programs using the currently available objective techniques of ABR and oto-acoustic emission measurement.

CONTENTS

INTRODUCTION

1.0 LIST OF ABBREVIATIONS 1
1.1 GENERAL INTRODUCTION 2
1.2 METHODS OF OBJECTIVE HEARING ASSESSMENT 5
1.2.1 WHAT ARE EVOKED POTENTIALS? 5
1.2.2 ECOCHG – ELECTROCOCHLEOGRAPHY 6
1.2.3 OAES – OTOACOUSTIC EMISSIONS 8
1.2.4 ABR – AUDITORY BRAINSTEM RESPONSES 8
1.2.5 PAMR - POST-AURICULAR MUSCLE RESPONSE 10
1.3 THE PROBLEM OF VARIABILITY 11
1.4 A BRIEF HISTORY OF THE POST-AURICULAR MUSCLE RESPONSE 15
1.5 CHARACTERISTICS OF THE PAMR 17
1.6 CURRENT KNOWLEDGE REGARDING PAMR NEURAL PATHWAYS 19
1.6.1 THE BRAINSTEM PATHWAY IN HUMANS 21
1.7 FACTORS THAT AFFECT THE PAMR 22
1.7.1A TYPE OF STIMULUS: CLICK OR TONE-BURST 22
1.7.1B TONE-BURST FREQUENCY 23
1.7.2 STIMULUS INTENSITY 24
1.7.3 STIMULUS REPETITION RATE 24
1.7.4 MUSCLE TONE 25
1.7.5 EYE MOVEMENT 27
1.7.6A ATTENTION 27
1.7.6B ADAPTATION OF THE PAMR 28
1.7.7 AGE & DEVELOPMENTAL MATURITY 29
1.7.8 SEROUS OTITIS MEDIA 30
1.7.9 ELECTRODE PLACEMENT 31
1.8 SENSITIVITY AND SPECIFICITY 31
1.9 AIMS 34

METHODS

2.0 SUBJECTS 35
2.1 EQUIPMENT 37
2.2 CLICK AND TONE-BURST GENERATOR 38
2.3 ELECTRODES 40
2.4 SIGNAL FILTERING AND AMPLIFICATION 42
2.5 LABVIEW 46
2.6 CORRELATION 49
2.7 OPTIMAL CHOICE OF CORRELATION WINDOW 51
2.8 SAFETY 53
2.9 PORTABLE EQUIPMENT SET-UP 53
2.10 ELECTRICAL ARTEFACTS 54
2.11 PAMR THRESHOLD TRACKING USING A FEEDBACK LOOP 55

RESULTS

3.1 INPUT/OUTPUT FUNCTION OF THE PAMR 60
3.2 THE EFFECT OF TONE-BURST FREQUENCY ON THE PAMR 63
3.3 DISTRIBUTION OF THE PAMR RESPONSE 68
3.4 TESTS OF BILATERAL SYMMETRY 73
3.5 THE EFFECT OF MATURATION ON PAMR LATENCY 76
3.6 THE EFFECT OF EYE MOVEMENT ON THE PAMR 79
3.6.1 "ALL OR NONE" EYE ROTATION EXPERIMENTS 81
3.6.2 GRADED EYE ROTATION EXPERIMENTS 85
3.6.3 EFFECT OF INCREASING EMG BY OTHER METHODS 87
3.6.4 SUMMARY AND CONCLUSIONS 92
3.7 IDENTIFYING SINGLE MOTOR UNIT RESPONSES IN THE PAM 93
3.7.1 AVERAGING OF RECTIFIED RAW RESPONSES 94
3.7.2 INTER-SPIKE INTERVALS IN GROSS RECORDINGS 96
3.8 SPECTRAL ANALYSIS OF THE PAMR 102
3.9 DISTORTION OF THE PAMR DUE TO SYSTEM BANDWIDTH LIMITS 113
3.10 PAMR CORRELATION MEASUREMENTS IN INFANTS 119
3.11 DEVELOPMENT OF A CHEAP, PORTABLE DEVICE FOR PAMR MEASUREMENT 124
3.11.1 FM TRANSMITTER 125
FM TRANSMITTER – PRINTED CIRCUIT BOARD LAYOUT 127
3.11.2 FM RECEIVER AND BITSTREAM CORRELATOR 128
FM RECEIVER/CORRELATOR – PRINTED CIRCUIT BOARD LAYOUT 134
3.12 PAMR THRESHOLD-TRACKING USING A STIMULUS-LEVEL FEEDBACK LOOP 134
3.12.1 ATTENUATION RAMPING RATE AND THRESHOLD-TRACKING 135
3.12.2 EFFECT OF MUSCLE TONE ON THE AUTOMATIC PAMR THRESHOLD 137
3.13 CAP THRESHOLD-TRACKING USING A FEEDBACK LOOP 143
3.14 REAL-TIME BOLTZMANN ANALYSIS OF CM WAVEFORMS 150
3.14.1 BOLTZMATRON VI 157
3.14.1.1 SIMULATION MODE 158
3.14.1.2 CAPTURE MODE 160
3.14.2 RESULTS OF THE BOLTZMANN ANALYSIS 162
3.14.3 DISCUSSION 163
3.14.4 CONCLUSION 164

DISCUSSION AND SUMMARY

4.1 SUMMARY 165
4.2 SHORTCOMINGS OF THE STUDY 170
4.3 SUGGESTIONS FOR FUTURE IMPROVEMENTS AND RESEARCH 170
4.4 CONCLUDING REMARKS 173

INTRODUCTION

1.0 List of Abbreviations

Units

dB – decibel
HL – hearing level
Hz – Hertz
s – seconds
Ω – Ohm
SL – sensation level
SPL – sound pressure level
V – volts

SI Prefixes

μ – micro-
m – milli-
d – deci-
k – kilo-
M – mega

Terms

ABR – Auditory Brainstem Response
AEP – Auditory Evoked Potential
AMLR – Auditory Middle Latency Response
AP – Action Potential
BAER – Brainstem Auditory Evoked Response
BAEP – Brainstem Auditory Evoked Potential
CAP – Cochlear Action Potential
CAR – Crossed Acoustic Response (a.k.a. the PAMR)
CM – Cochlear Microphonic
MS – Multiple Sclerosis
OAE – Oto-Acoustic Emissions
PAM – Post-Auricular Muscle
PAMR – Post-Auricular Muscle Response
SEP – Somatosensory Evoked Potential
SP – Summating Potential
VEP – Visual Evoked Potential

1.1 General Introduction

Severe congenital hearing loss is an important disability which affects approximately 0.1% of the newborn population, and around 1-2% of infants in neonatal intensive care units (Oudesluys-Murphy et al., 1996). The incidence of this hearing impairment among infants is much higher if we include less severe and acquired losses, such as those that occur as a result of illness or injury. It is essential that this neonatal hearing impairment is detected early, because significant auditory input is required during the first year of life for normal development of the central auditory system and language acquisition centres of the brain (Nober et al.,1977). In fact, evidence suggests that developmental delays occur even if only a mild hearing loss is present (Goetzinger, 1962).

The age of diagnosis of hearing impairment is usually 18 - 30 months where there are no screening programs, and even later in cases of less severe, and therefore less obvious, impairment (Oudesluys-Murphy et al., 1996). An argument in favour for the widespread of testing of every newborn infant for hearing impairment (known as "universal hearing screening"), rather than screening only those infants at a higher risk of impairment, is that it has been shown that if neonatal screening is restricted to *only* high-risk groups, then 30-50% of infants with hearing loss are not discovered (Oudesluys-Murphy et al., 1996).

At present, universal hearing screening is not carried out in Australia. Arguments against its establishment in the U.S.A. were outlined in an editorial by Bess et al. (1994). Their main concerns were that many important studies (such as those into the validity and reliability of the available techniques, and the cost/benefit ratio of early rather than late intervention) have yet to be carried out, and that if universal hearing screening were to be implemented immediately, using available techniques, this may deter the future development of more

effective early identification techniques (Bess et al., 1994). These arguments were comprehensively opposed by White et al. (1995), who claimed that Bess et al. had not included substantial relevant research data and practical experience in their analysis, and recommended that such screening programs be implemented without further delay. The only trial screening program operating in Western Australia is designed to test the feasibility of universal hearing screening using the presently available test of otoacoustic emissions (KEMH, 1997). However, this particular trial is still in its early stages, and so it is not possible to comment on its effectiveness.

Subjective methods of hearing assessment are those which require the cooperation of the subject to inform the tester (in some way) that they have, or have not, heard the sound. Behavioural audiometric methods (in which attempts are made to distract the infant with sound, or to condition them to respond to a sound in a certain way) are only effective in most children after the age of 6 months (Wilson et al., 1991), and can be problematic if the child is uncooperative or suffers from some physical or mental disability. In cases such as these, and for testing younger infants, it is more effective to use one of the available objective methods of hearing assessment. These have the advantage of being able to determine the hearing acuity of the infant without his or her active cooperation.

One such objective test involves measuring the electrical activity produced by a muscle located behind the ear, the post-auricular muscle (PAM), in response to brief acoustic stimuli. The PAM is illustrated in Figure 1.1. Although this response has been known for many years, it has largely been ignored by clinicians because of the variability in the response, both between subjects, and between testing sessions of the same subject.

The aims of this Honours project were to examine the ways in which the reliability of the PAM response (PAMR) could be improved, to investigate the physiological effects of eye movement on the PAMR, and to develop a simple, reliable, and cost-effective device capable of evoking and detecting the PAMR.

This introduction discusses the known physiology of the PAMR, its history, and the previous attempts to measure of the reflex as an indicator of hearing ability.

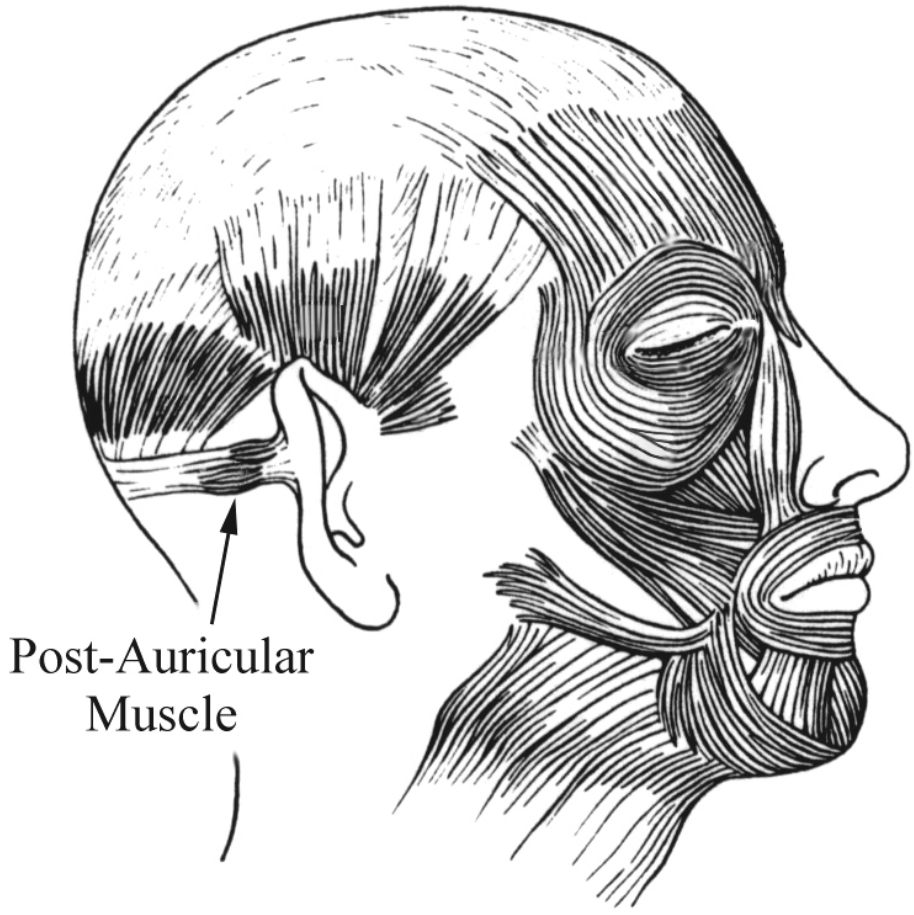

Figure 1.1: The location of the post-auricular muscle (adapted from Feneis, 1994).

1.2 Methods of objective hearing assessment

The methods of objective hearing assessment discussed here are those that make use of auditory evoked responses of one form or another. Of these objective methods, the most commonly used are electrocochleography (ECochG), tests of otoacoustic emissions (OAE), and auditory brainstem responses (ABR), also known as brainstem auditory evoked responses (BAER).

1.2.1 What are evoked potentials?

Evoked potentials are patterns of electrical activity in the peripheral and central nervous systems that are triggered by the presentation of various rapid-onset stimuli, such as flashes of light, or brief acoustic clicks or tone-bursts. The fact that sensory inputs such as these can modify *cortical* electrical potentials has been known since Caton's experiments on rabbits in 1875 (cited in Cody et al., 1964).

Generally, this evoked electrical activity can be detected using electrodes placed at various positions on the skin surface. In most applications, it is the electrical activity of the brainstem, cortex, or head musculature that is of interest. These electrical potentials are usually quite small, usually of the order of microvolts, and so can be difficult to measure within the background of electrical noise from the rest of the body (typically of much larger amplitude), itself coming from the brain, and from other muscles (such as those of the jaw or neck), or the heart (Hall, 1992).

A step towards solving the problem of how to distinguish the evoked potentials from the background noise was made by Dawson in 1951, with the development of a device to electronically average the measurements of electrical activity from repeated presentations of the stimulus (Hall, 1992). Prior to this, the standard technique for studying evoked potentials

had been to superimpose the responses on an oscilloscope or photographic plate. A major limitation of this method was that in all but a few cases, the time-locked responses were obscured by large spontaneous brain activity (Hall, 1992). With averaging techniques, the responses are summed rather than superimposed, so that time-locked potentials triggered by the stimulus will occur at the same point in time after each presentation, whereas the background noise, which is not synchronized to the stimulus or recording device, will tend to cancel out. The signal-to-noise ratio of the electrical signal increases by a factor equal to the square root of the number of observations added, according to the formula:

$$\text{signal-to-noise ratio} = \frac{\text{signal amplitude}}{\text{noise amplitude}} \times \sqrt{\text{n averages}}$$

For example, if 100 responses are averaged, the signal-to-noise ratio is increased by a factor of 10. This has implications on the time taken to carry out a particular test. To achieve the same response clarity, an evoked-response measurement procedure that has a lower signal-to-noise ratio will require a larger number of averages, and therefore will take longer, than a procedure that has a higher signal-to-noise ratio.

1.2.2 ECochG – Electrocochleography

Electrocochleography is a method by which the electrical activity of the cochlea, in particular the summating potential (SP) and cochlear action potential (CAP), are measured by means of an electrode placed near the inner ear. Clinically, the largest and clearest CAP recordings are obtained using the trans-tympanic method, in which an electrode is placed directly on the wall of the cochlea that faces the middle ear (the promontory), which necessitates puncture of the tympanic membrane by the recording needle (Mendel, 1977). In adults, this may be done under a local anaesthetic, but in infants and children it is typically carried out under general anaesthesia. General anaesthesia adds a significant cost to the test procedure (admission to hospital, extra staff, etc.), and increased risk to the subject. Nevertheless, the test provides valuable and accurate information about cochlear function at all levels, up to and including the auditory nerve. Unfortunately, it is also highly invasive, time-consuming, and expensive to perform. For these reasons, this test is generally only carried out when other methods are unsuitable, or have yielded inconclusive results. A typical averaged click-evoked electrocochleograph from an adult subject is shown in Figure 1.2.

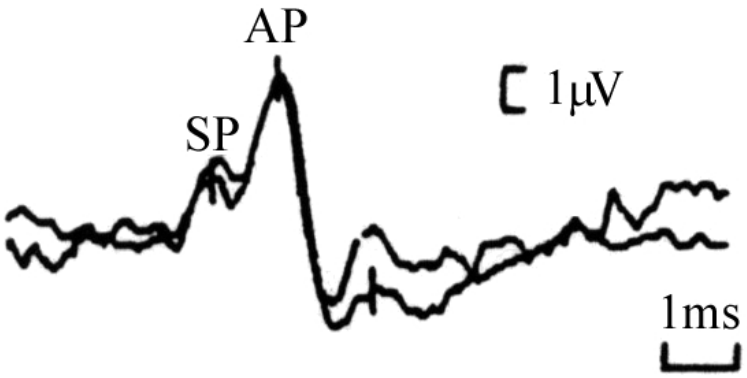

Figure 1.2: A typical click-evoked electrocochleographic measurement recorded from the promontory of an adult subject, showing the summating potential (SP) and cochlear action potential (CAP) (Hall, 1992).

1.2.3 OAEs – Otoacoustic Emissions

Otoacoustic emissions are sounds of cochlear origin that are detectable in the ear canal using a sufficiently sensitive microphone (Kemp, 1978). The major clinical importance of OAEs lies in the ability to examine the micromechanical integrity of the cochlea in a non-invasive and objective manner (Probst et al., 1991). The ability to record OAEs from a subject generally implies that any conductive hearing losses present in the subject are not greater than about 25-30 dB HL (Probst et al., 1991). OAEs are not detectable if there is middle-ear effusion (for example, during serous otitis media; Probst et al., 1991), and can be present in subjects whose cochlear mechanics are intact, but who in fact suffer from hearing loss due to retrocochlear disorders, such as brainstem abnormalities (Stein et al., 1996).

1.2.4 ABR – Auditory Brainstem Responses

The auditory brainstem responses (also known as the brainstem auditory evoked response, or BAER) are the patterns of neural activity measurable (usually from the scalp) in response to brief, rapid-onset acoustic stimuli. This activity is produced by synchronous neural firing in parts of the brainstem, and generally occurs in the first 8 ms following the stimulus. Figure 1.3 shows a typical ABR from a normal adult (Schwarz et al., 1994).

A number of distinct peaks, labelled I to VI, are clearly visible in the waveform. The neural generators for these waves have been defined, and abnormalities in the specific components can yield valuable brainstem diagnostic information (Hall, 1992).

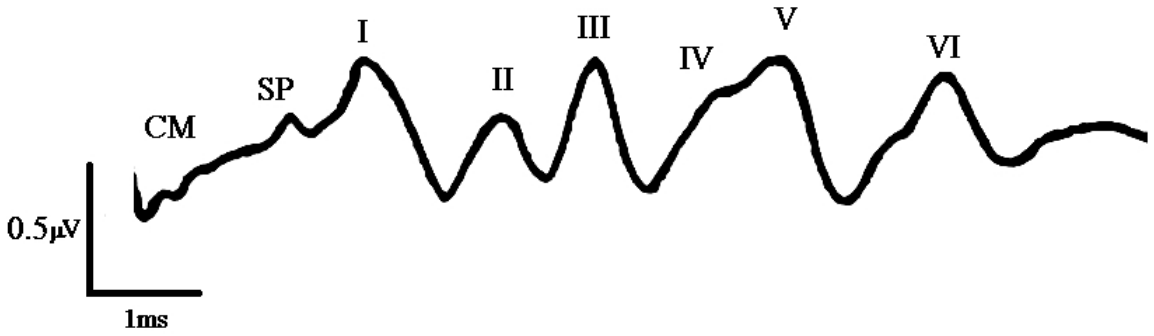

Figure 1.3: An averaged click-evoked ABR from a normal neurologic and oto-audiologic adult, showing waves I to VI., the cochlear microphonic (CM), and the summating potential (SP) [Click intensity: 110 dB peak SPL] (Schwarz et al., 1994).

Electrical activity from myogenic sources can greatly interfere with the recording of the ABR. Some of this myogenic activity may come from time-locked reflexes such as the PAMR, which are therefore not removed by averaging. To avoid this myogenic interference, the subject must be kept calm and still during testing. For patients aged between about 4 months and 6 years, sedation is often used to quieten the child (Hall, 1992). This adds additional cost to the procedure, and requires the presence of medical staff.

Due to the size of the ABR response, the electrical signals recorded from the head must be amplified up to 100,000 times before they can be processed and analysed (Hall, 1992), and the low signal-to-noise ratio of the response means that often several thousand presentations need to be averaged before the peaks can be properly identified.

Nevertheless, the ABR is widely used in clinical situations as an objective hearing test, as it is less invasive that the ECochG, and has greater sensitivity and specificity than measurements of OAEs (Oudesluys-Murphy et al., 1996). The terms sensitivity and specificity are discussed in greater detail in Section 1.8.

1.2.5 PAMR - Post-Auricular Muscle Response

The Post-Auricular Muscle Response is a large myogenic electrical response that can be measured from the skin surface over the post-auricular muscle. The response, which can be triggered by rapid-onset acoustic stimuli such as clicks and tone-bursts, consists of two peaks: a negative-going peak occurring between 12.5 and 15 ms, and a positive-going peak between 15 and 18 ms (Yoshie and Okudaira, 1969).

Figure 1.4 shows a click-evoked PAMR, recorded from a normal subject. [Note: It is common practice within PAMR research to plot negativity on the active electrode as a positive potential difference on the voltage axis of waveform graphs. This convention has been followed throughout this report].

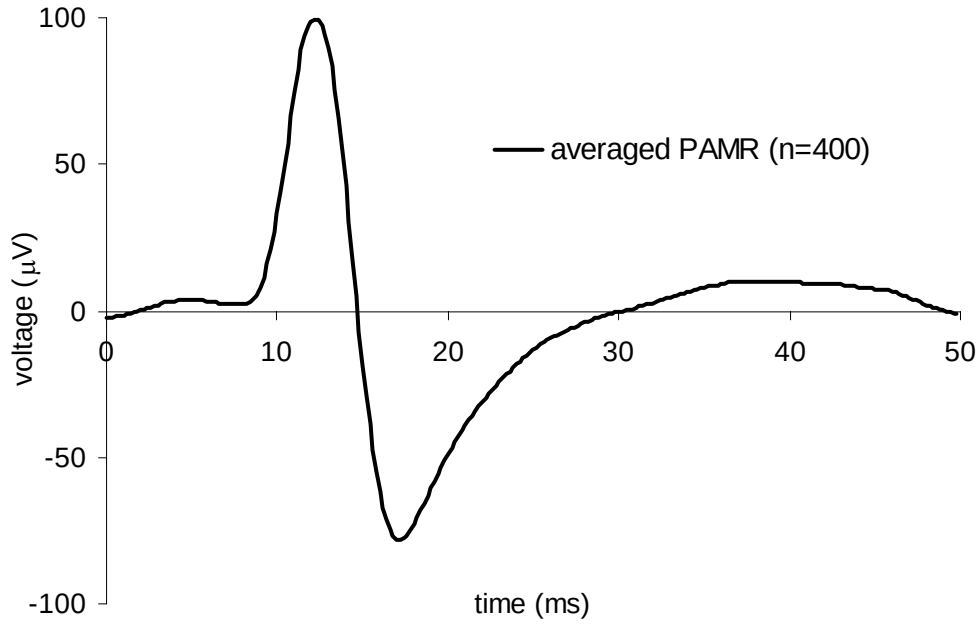

Figure 1.4: An averaged click-evoked PAMR from a normal neurologic and oto-audiologic adult (Number of averages: 400. Active electrode: PAM. Reference electrode: pinna. Filtering bandwidth: 1 Hz – 2.5 kHz. Subject: G.O'B.).

If we compare Figure 1.4 with Figure 1.3, it can be seen that the peak-to-peak amplitude of the PAMR (in this case 178 μV pp) is much larger than that of the ABR (less than 1 μV). When using surface electrodes, electrical responses from muscle tissue are generally of much greater amplitude than those with a solely neural origin. Even at more typical PAMR amplitudes (75 to 150 μV pp), the difference between the size of the neurogenic ABR and that of the myogenic PAMR is apparent.

The magnitude of the PAMR is such that, under certain conditions, it can even be seen quite clearly in the raw trace. This higher signal-to-noise ratio of the PAMR means that less amplification is required, and much less averaging is needed to detect the PAMR than the ABR.

If this is the case, why is the PAMR not used in place of the ABR as a screening test? The answer lies in the variability of the PAMR, and the difficulty that many researchers and clinicians have previously had in trying to measure the response.

1.3 The problem of variability

One of the major obstacles to the widespread usage of the PAMR as an objective hearing test has been the variability of the reflex, both in terms of the amplitude of the response, and because of the difficulty found in evoking the response in some subjects. The PAMR was described by Picton et al. (1974) as being "*highly variable from subject to subject and even within subject*s". Cody et al. (1969) found the response to be absent in at least one ear of 32% of their subjects, and absent bilaterally in 7% of their subjects. Because of this variability, they considered it unlikely that the PAMR would have any useful clinical application. Similarly, Suzuki stated that "*from the audiological point of view the most serious*

disadvantage of [the PAMR] *is the inconsistency or variability of its appearance… Such an individual variability is a very serious problem for applying the response as an index of objective audiometry. However, we should overcome this problem because the response is a very important and easily recordable one…*" (Suzuki, in Bochenek et al., 1976).

How important a response is the PAMR? What does the presence of a normal PAMR in a subject indicate, and what is indicated by an absent response?

From the available information about the PAMR reflex pathway (discussed in Sections 1.5 and 1.6), it is known that for a normal PAMR to be recorded from a subject there must be: i) adequate functioning of the regions of the cochlea that correspond to the stimulus frequencies (Gibson, 1975), ii) intact transmission of the neural output of the cochlea along the auditory nerve and through the brainstem (Douek et al., 1973), and iii) intact transmission of the evoked response from the brainstem to the post-auricular muscles, via the facial nerve (Cody et al., 1964). For these reasons, the presence of a normal PAMR is a useful indicator that all of these structures are intact and functioning.

Furthermore, there is evidence to suggest that if the response can be evoked successfully, it can provide a reasonable approximation of the subjective hearing threshold obtained using standard audiometry. For example, Gibson (1975) found that the PAMR appeared to be directly related to the subjective audiometric threshold in 90% of his subjects.

Thornton (1975) carried out studies on the use of the PAMR in the estimation of audiometric thresholds. Frequency analysis of the acoustic energy produced by his click stimuli indicated a main spectral peak at 2 kHz, and so he used the subjects audiometric

threshold at that frequency as a comparison[1]. His results are shown in Figure 1.5. Each of the data points on the graph in Figure 1.5 represents a single subject. The slope of the regression line shows an almost one to one correlation between the audiometric threshold of a subject and the sound level at which the PAM is first detectable. The mean difference between the PAMR threshold and the audiometric threshold was 9 dB, with a standard deviation of 7 dB. According to Thornton (1975), this accuracy "*is comparable to that achieved by conventional audiometry and by cortical evoked response audiometry*". His regression line crosses the PAMR threshold axis at around the 12 dB mark, which indicates that the PAMR method is 12 dB less sensitive than the standard subjective technique used by Thornton.

Figure 1.5 is also interesting because it shows that Thornton was able to evoke the PAMR in all 20 of his subjects. This response stability may be due to the methods he used to increase tone in the neck muscles, as discussed in Section 1.7.4. If this is the case, his data indicate that when the PAMR is facilitated by increased muscle tone, it can give a good estimation of hearing threshold.

Unlike Thornton's results, the PAMR threshold estimates recorded by Buffin, Connell & Stamp (1977) were not as well correlated with subjective threshold. They recorded the PAMR in 241 patients; 227 of whom were under 14 years of age, and found the PAMR present in 70% of the children whose audiograms were reasonably normal.

The format of Figure 1.6 is identical to Thornton's, in that it depicts the estimates of PAMR threshold plotted against the subjective 2 kHz pure-tone audiometric threshold. The graph shows that for a large number of subjects, the PAMR does *not* give a good indication of

---

[1] As will be discussed in Section 3.8, it is likely that Thornton's spectral analysis technique was flawed,

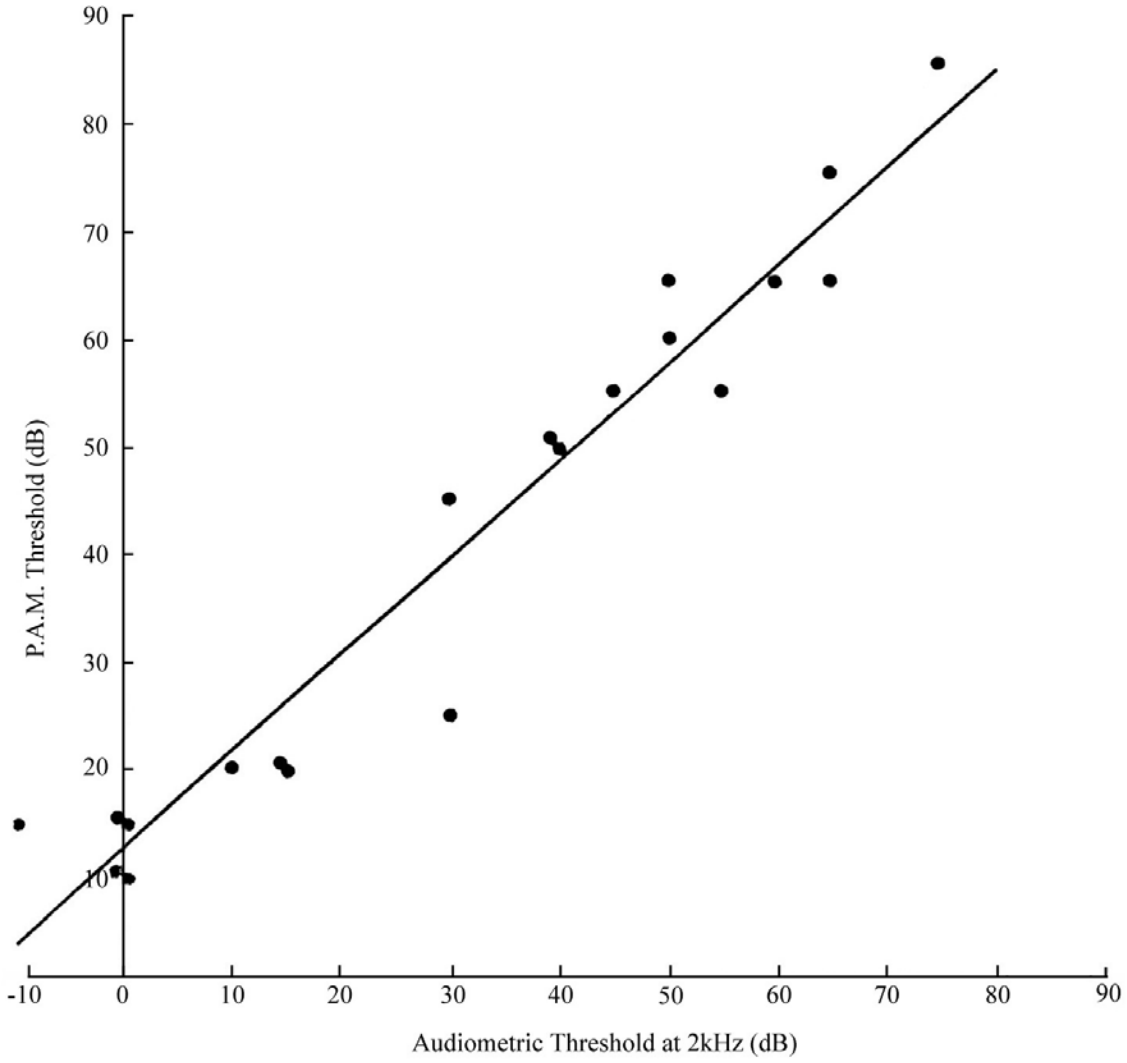

Figure 1.5: Audiometric threshold at 2 kHz plotted against the threshold estimated by the minimum click intensity at which the PAMR becomes visible. Results for 20 subjects are plotted. Note the high correlation between the two estimates (Thornton, 1975).

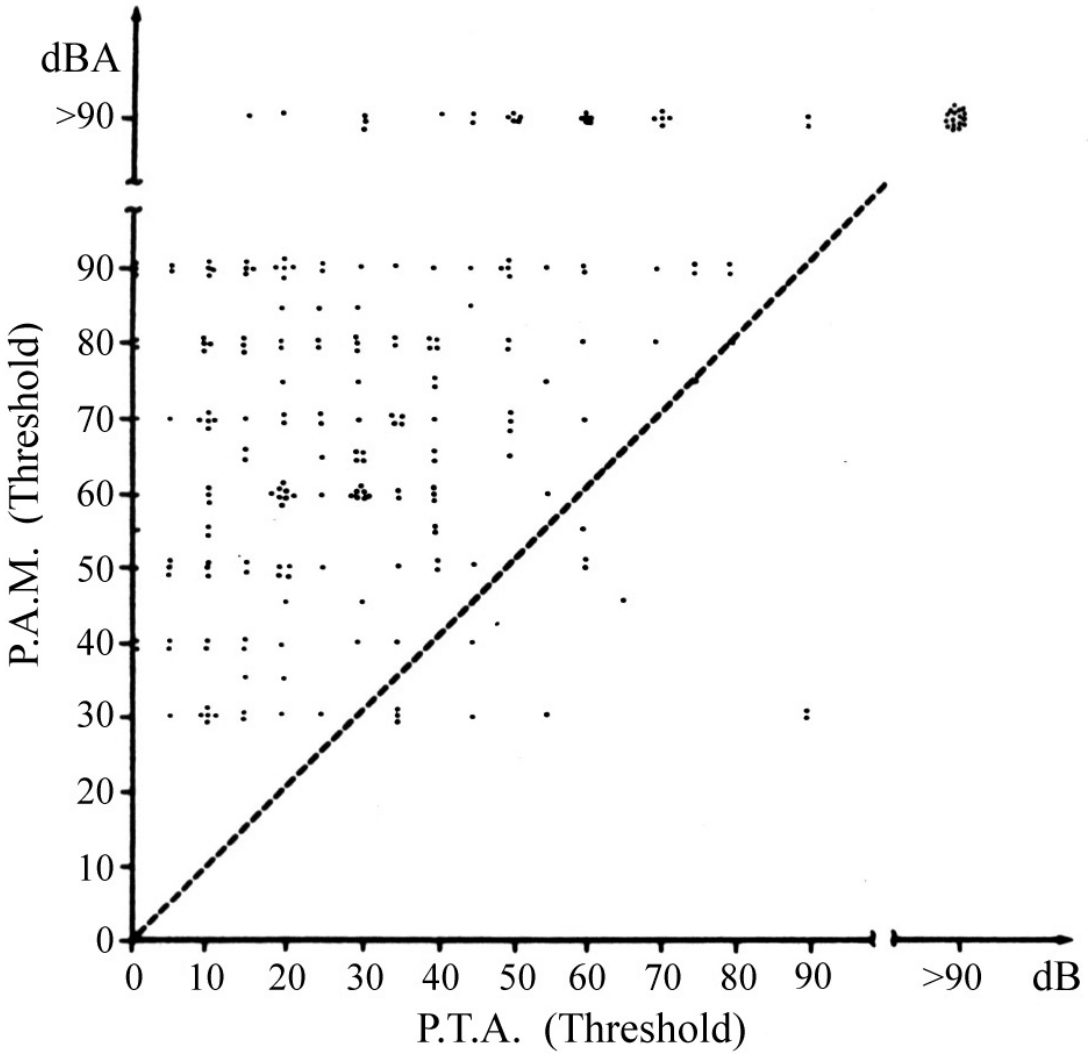

Figure 1.6: Audiometric threshold at 2 kHz plotted against the threshold estimated by the minimum click intensity at which the PAMR becomes visible. Results for 241 subjects are plotted. Note the greater distribution of data in the upper left half of the graph. (Buffin et al., 1977).

the hearing threshold. They comment that "*a good response is strongly suggestive of good hearing. A poor response has far less diagnostic value.*" They did note, however, that "*the age range of the patients under test makes it difficult to be certain that all pure tone audiograms are truly threshold measurements*".

Gibson (1975) found that there was on average a 20 dB gap between measurements of PAMR threshold and subjective threshold measurements among subjects with normal hearing or partial hearing losses. Less than 10% of his subjects failed to show a response within 30 dB of their subjective threshold.

Based on his research, he concluded that tests based on the PAMR appeared to provide an excellent method of assessing the hearing acuity of children during a clinic: "*The advantages of the test are that all manner of children, normally untestable without sedation, can be rapidly screened during the course of the actual clinic.*" He felt that the unique advantage of the PAMR was that "*since it is a muscle response, the tense child difficult to test by other means gives clear responses*." He believed the disadvantages of the test were that:

1) Click-evoked responses cannot accurately reproduce a pure-tone audiogram[2],

2) The judgement of the actual hearing threshold is not as accurate as that obtained using electrocochleography or by cortical evoked response audiometry in older children.

3) Conductive hearing losses and in particular children with serous otitis media gave poor responses[3] (this is discussed further in Section 1.7.8).

---

and so it is possible that the main spectral peak of his click stimuli may not actually have been at 2 kHz.

[2] This criticism would also apply to measurements of click-evoked ABR.

[3] Serous otitis media is also a problem for measurements of OAEs.

However, due to the speed and ease at which the response can be tested, he felt the advantages far outweighed the disadvantages, and had used the PAMR as a routine clinical tool at the Hearing and Language Clinic at Guy's Hospital, London, for a number of years (Douek et al., 1974).

1.4 A brief history of the Post-Auricular Muscle Response

Click-evoked potentials were first averaged and recorded from the human scalp by Geisler, Frishkopf and Rosenblith in 1958. In this paper they characterized many of the properties of auditory evoked potentials and, in doing so, inspired many other researchers to begin studying them.

Among other details, Geisler and co-workers noted that the responses to monaural clicks were bilateral, and that "*the threshold for the appearance of a detectable response agrees closely with the minimum intensity at which the subject reports he hears clicks*." The peak latency of the response was approximately 30 ms, but both latency and amplitude were found to vary with the intensity of the click stimulus. Because of this latency, they suggested that the response, later known as the "Auditory Middle Latency Response" (AMLR), may have been generated by the cortical neurones.

These findings triggered considerable interest from researchers at the Mayo Clinic in Minnesota (namely Bickford, Jacobson, Cody, Galbraith, Walker and Lambert), who worked together in various combinations to produce a series of important papers on evoked responses. In the first of these papers (Bickford et al., 1963), they measured a widespread response to loud (100 - 135 dB SPL) clicks that was present in facial, cranial, and limb musculature. The response, later termed the "inion response", was characterized by onset latencies of 8 - 10 ms,

and by peak to peak amplitudes that were related to tension in the muscles to the extent that the response disappeared on complete relaxation.

In 1963, Kiang and associates reported the recording of an averaged evoked response to clicks from the post-auricular area of the awake human. This post-auricular response was demonstrated to be of myogenic origin by Jacobson et al. (1964). The evidence for this finding is discussed further in Section 1.5.

Yoshie & Okudaira (1969) proved that the PAMR was of cochlear origin, and were able to quantify a number of the characteristics of the reflex. These included the relationship between stimulus intensity and the peak-to-peak amplitude and response latency. These characteristics are discussed further in Section 1.7.2. They also mentioned the ease of recording, and the stability of the PAMR, and suggested that it was suitable for use as an objective hearing test, and as a possible method of differentiation between various oto-neurogenic disorders associated with lesions in the brainstem.

Douek, Gibson, and Humphries, who carried out their research in the clinical setting of Guy's Hospital, London, were aware of the potential of the PAMR (referred to as the "Crossed Acoustic Reflex" in their laboratory) for use both as a means of localizing the anatomical site of hearing impairments, and as an objective test of hearing. They proposed that *"electro-physiological tests based on evoked responses may be used to test the integrity of the auditory pathways in the brain substance*", and carried out testing of the response in a number of patients with brainstem lesions, with abnormal, absent, or unilateral PAMRs found in many of these cases.

Similarly, the PAMR has also been used as a means of detecting subclinical demyelination in patients suspected of having Multiple Sclerosis (Clifford-Jones et al., 1979).

Multiple sclerosis (MS) is a disease characterized by multiple areas of demyelination in the central nervous system (CNS). Clinical diagnosis depends on demonstrating objective evidence of multiple lesions in the CNS white matter of a patient with a suitable history, and no alternative explanation.

Clifford-Jones et al. recorded abnormal PAMRs in 87% of subjects with clinical signs of MS, and in 69% of subclinical subjects (those with probable or possible MS). On monaural stimulation, the main abnormality found was a significant change in the latency of the second peak of the PAMR recorded from the contralateral ear (the side opposite to the stimulus). The most useful diagnostic strategy was found in testing subjects using both the PAMR and visual evoked responses (VERs), as 90% of the 66 MS patients had at least one of these responses delayed. They concluded that "*the recording of the* [PAMR] *is a valuable test of brainstem function and with the VER provides a particularly useful combination of evoked responses for the detection of subclinical demyelination*" (Clifford-Jones et. al., 1979).

1.5 Characteristics of the PAMR

The PAMR is a myogenic response that can be evoked bilaterally by both monaural and binaural cochlear stimuli. When considering the potential of the response as an objective test of hearing acuity, the most important of these three characteristics is the fact that the cochlea is the receptor of the sound stimulus that triggers the PAMR. Research into the PAMR by Yoshie & Okudaira (1969), and by Gibson and colleagues over a number of years, yielded convincing results showing that the reflex was of cochlear origin. If the response were able to be evoked by tactile, visual, or vestibular stimuli, rather than by cochlear stimulation alone, the suitability of the PAMR as a test of hearing would be severely limited.

Attempts by Gibson (1975) to record the PAMR from a number of deaf subjects with working vestibular systems failed. He also found no significant differences between his measurements of the PAMR in subjects with normal hearing, but no demonstrable vestibular function, and those with both normal hearing and normal vestibular function (Gibson, 1975). In addition, Yoshie & Okudaira (1969) recorded no response to intense clicks (100 dB SPL) from the post-auricular region in patients who suffered from severe sensorineural hearing loss, but who had normal vestibular function.

The fact that the PAMR produces a bilateral response to monaural acoustic stimuli was demonstrated by Yoshie et al. (1969). Clifford-Jones et al. (1979) reported latency differences of less than 0.6 ms between the PAMRs evoked by monaural click stimuli to the ears ipsilateral and contralateral to the recording electrodes. Douek et al. (1975) showed that the bilateralism of the response was not due to the click stimulus being transmitted via bone conduction to the other side of the head, by masking the contralateral ear. These results were later confirmed by testing patients with unilateral hearing losses (Gibson, 1975).

The crossed nature of the response found a clinical use in the research of Douek et al. (1973), who found that lesions in the brainstem can interrupt the crossing fibres and thus abolish or alter the PAMR. This was found by measuring the "crossover" of the response in a range of subjects, by comparing the responses to monaural clicks recorded from the PAMs on both sides of the head. The crossover was found to be absent in one ear of a number of patients with either proven or suspected brainstem tumours, whereas it was present in response to monaural stimuli in both ears in 12 normal subjects, and in 22 patients with varying cochlear pathology (including Ménière's disease, acoustic trauma, presbyacusis, and tinnitus). They

found the PAMR to be a simple, quick and painless tool in the assessment of intra-cerebral auditory pathways (Douek et al. 1973).

The electrical activity measured as the PAMR is of muscular, rather than neural, origin. Bickford et al. (1964) found that the response could be elicited by increasing the tone in the neck muscles by forward traction of the head. This conclusion was reached when it was found that:

i) the amplitude of the response could be markedly enhanced or abolished in suitable subjects by contraction or relaxation of the ear muscles, and

ii) local anaesthetic block of the post-auricular branch of the facial nerve abolished the response unilaterally.

1.6 Current knowledge regarding PAMR neural pathways

The neural pathway of a reflex is important in determining its clinical significance. The peripheral pathways of the PAMR have been characterised, but theories regarding the PAMR brainstem pathway have yet to be proven.

The bilateral nature of the auditory evoked responses (noted by Geisler et al., 1958), the myogenic source of the post-auricular response (Jacobson et al., 1964), and the data of Yoshie & Okudaira (1969) showing the cochlear origin of the response, led Douek et al. (1973) to propose that the reflex arc of the PAMR consisted of the following components:

cochlear receptor $\rightarrow$ auditory nerve $\rightarrow$ undetermined brainstem pathway $\rightarrow$

motor nucleus $\rightarrow$ facial nerve $\rightarrow$ post-auricular muscles

In this model, a sound stimulus is converted in the cochlea to afferent nervous information which passes via the auditory fibres of the auditory nerve to the brainstem. It is at

some point within the brainstem that the response is "split" and relayed bilaterally to motor nuclei on both sides of the head (Gibson, 1975). From here the neural activity travels along the facial nerve to the post-auricular muscles, producing an electrical response (the PAMR) which causes the muscles to contract. This electrical response from the muscle is easily detectable with surface electrodes (Jacobson et al., 1964). A model for the "undetermined" brainstem pathway was later proposed by Gibson (1975), and is discussed further in Section 1.6.1.

In a range of animals, the post-auricular muscles mobilize the pinna to locate the source of sound (Douek et al. 1973). The acoustic auricular reflex is commonly seen in the rabbit, cat, and in the guinea pig, where it is termed the Preyer reflex in honour of its discoverer. It may be hypothesised that the reason the response does not cause such visible ear movements in humans is due to the rigidity of the human pinna, and the relatively small size of the human PAM. Due to the analogues between the Preyer reflex and the PAMR, it is worth presenting the neural pathway of the Preyer reflex.

Based on the electromyographic studies of the Preyer reflex in the guinea pig, Totsuka, Nakamura and Kirikae (1954) concluded that the reflex arc for the Preyer reflex was:

cochlea $\rightarrow$ cochlear nerve $\rightarrow$ cochlear nucleus $\rightarrow$ superior olivary complex $\rightarrow$ nucleus of the lateral lemniscus $\rightarrow$ facial nucleus $\rightarrow$ facial nerve $\rightarrow$ muscle of the auricle.

The latency of the reflex at each of these components and their location is shown in Figure 1.7.

1.6.1 The brainstem pathway in humans

Based on comparison between the latency of the PAMR response and the theoretical estimates for the time taken for i) transmission of the response along peripheral and central nerve fibres, and ii) synaptic transmission and motor end plate conduction, and on knowledge

of the functioning of the various brainstem components, Gibson (1975) suggested that the most likely brainstem pathway was either:

a) ventral cochlear nucleus → superior olivary complex → nucleus of the lateral lemniscus → to perhaps a synapse in the reticular formation → facial motor nucleus.

or

b) same as above but passing to the inferior colliculus instead of the reticular formation.

It must be stressed that Gibson's model is only "an armchair theory" (Gibson, 1975) that has not been proven experimentally. It is quite similar to the Totsuka model of the Preyer reflex, with the exception that there are only four brainstem components in the Totsuka model.

In the Gibson model, the inclusion of the extra brainstem component (either the inferior colliculus or a synapse in the reticular formation), increases the time taken from the onset of the stimulus to the contraction of the post-auricular muscles to around the 8 ms onset latency of the PAMR.

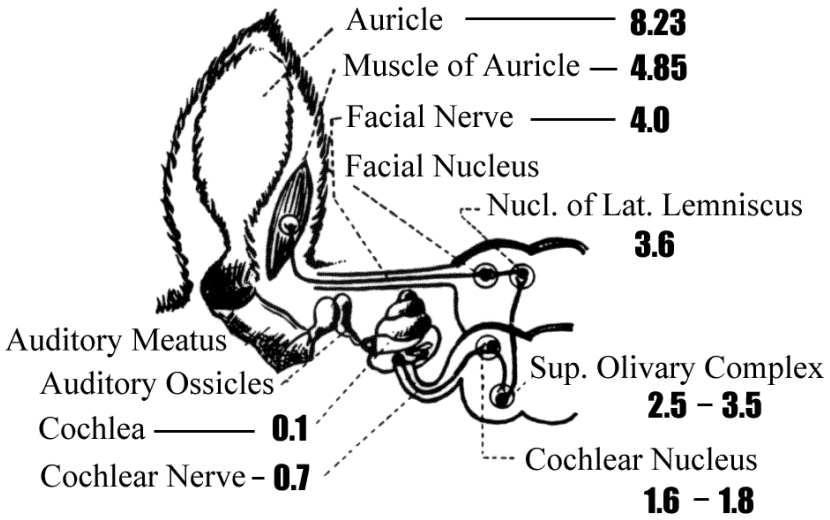

Figure 1.7: Schematic diagram of the neural pathway of the Preyer reflex in the guinea pig. The latency of the response in each component is given as milliseconds following the stimulus (Totsuka et al., 1954).

1.7 Factors that affect the PAMR

The characteristics of the acoustic stimuli used to evoke the PAMR, and a number of physiological factors, are important in determining the size, latency, and reproducibility of the PAMR, as described below.

1.7.1a Type of stimulus: click or tone-burst.

The synchronous firing of many neurones is necessary to generate an evoked response that can be measured against the background electrical activity (Hall, 1992). In the case of auditory evoked responses, different types of sound stimuli can be used to cause this firing, and can provide different information about the functioning of the sensory component of the reflex. The stimuli most commonly used are acoustic “clicks” and “tone-bursts”.

A click is an acoustic signal produced when a rectangular electric pulse of a specified duration is delivered to a transducer, such as a loudspeaker or headphone. Abrupt signals (such as rectangular electrical pulses) have a very broad energy spectrum which, when delivered to a loudspeaker, result in an acoustic signal with a wide range of frequencies (Hall, 1992). The range of frequencies contained in the stimulus also depends on the properties of the transducer, filtering effects of the ear canal and the middle-ear, and the integrity of the cochlea. On receiving the acoustic click, the cochlea is stimulated by this wide range of frequencies and the hair cells over an extensive region of the cochlear partition are activated (Hall, 1992). Clicks have been found to produce a PAMR of larger amplitude than those obtained using tone bursts (Gibson, 1975; Douek et al., 1973).

The most direct approach to obtaining frequency-specific thresholds is to use frequency-specific stimuli, such as tone-bursts. The acoustic signal generated from a tone burst of a particular frequency has a much narrower spectrum than a click, and so stimulates less of

the cochlear partition than the wide-band click, but has advantages in that it enables the hearing sensitivity at that specific frequency alone to be assessed.

1.7.1b Tone-burst frequency

The frequency of the tone-burst used to evoke the PAMR has been found to have an effect on the amplitude of the response. This is because the apical region of the cochlea involved in the reception of low-frequency sound stimuli has been found to be less effective in producing the typical, sharply-peaked evoked responses when stimulated (Hall, 1992). There are two possible reasons for this:

First, if the tone-burst is synchronous with the tone-burst gating function (i.e. the phase of the tone-burst is the same with each presentation), it is difficult to tell the difference between the phasic neural response (the frequency-following response) and the low-frequency cochlear microphonic, due to the firing characteristics of the nerves in the apical region of the cochlea. On the other hand, if the tone-burst is asynchronous with the gating function (i.e. the phase of the tone-burst relative to its onset "rolls" with each presentation), the neural response tends to "wash out" with repeated averaging.

Second, the neural circuitry that receives input from the high-frequency nerves in the basal-region of the cochlea is better at producing a response to acoustic transients, hence their role in directional hearing.

Figure 1.8 shows relationship between the stimulus frequency and the peak-to-peak amplitude of the response for a given stimulus intensity reported by Patuzzi and Thomson (unpublished).

1.7.2 Stimulus intensity

A louder auditory stimulus causes a greater degree of synchronous firing in the cochlea, and so evokes a greater amplitude response (Hall, 1992). The latency of the response also decreases with increasing stimulus intensity (by around 3 to 5 ms; Yoshie et al., 1969). An example of an input-output function for the PAMR (stimulus intensity vs. response amplitude) is shown in Figure 1.9 (Yoshie et al., 1969). Similar results were reported by Gibson (1975), who found that "*in every case, an exponential rise in the amplitude* [of the PAMR] *was encountered on increasing the stimulus intensity*". However, the units of stimulus intensity (dB) are logarithmic, and so when the response amplitude is plotted on a logarithmic scale, a linear relationship is observed.

1.7.3 Stimulus repetition rate

The repetition rate of the acoustic stimulus used to evoke the PAMR has also been found to have an effect on the response amplitude. Fatigue of a response is generally defined in terms of the percentage amplitude of the response found at higher repetition rates, compared to the amplitude of the response that is generated when stimuli are presented at a rate that allows 100% recovery between stimuli. Geisler et al. (1958) found that the peak to peak amplitude decreased with increasing stimulus rates above 10/s. Jacobson et al. (1964) reported that the PAMR could be driven to rates of 100 responses per second without evidence of fatigue or habituation. This conflicts with the data of Yoshie & Okudaira (1969), who found that the amplitude of the response diminished considerably as the interstimulus interval was reduced, as shown in Figure 1.10. According to Gibson (1975), "Kiang (1963) could identify the individual responses at rates in excess of 200 stimuli presentations per second". The amplitude of such responses, if they were indeed visible, would be presumably greatly

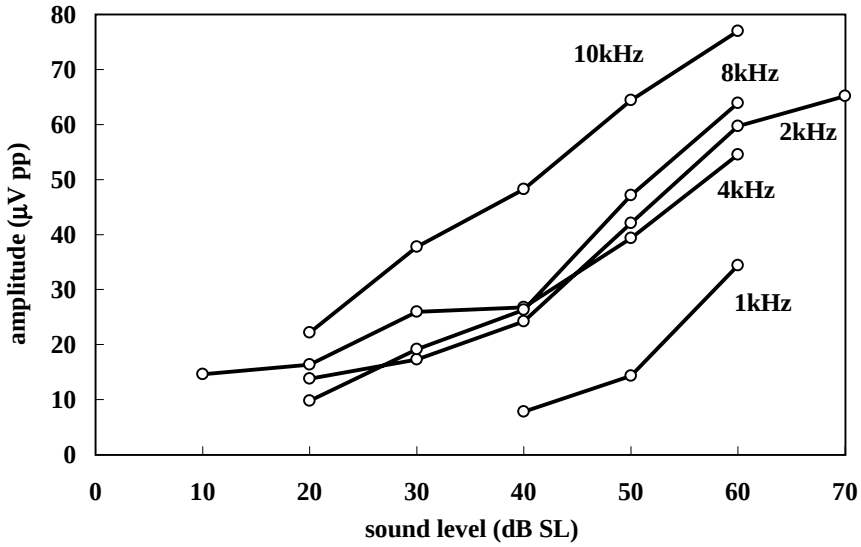

Figure 1.8: The relationship between the sound level of a tone-burst stimulus and the peak-to-peak amplitude of the PAMR, shown for tone-burst frequencies of 1 kHz, 2 kHz, 4 kHz, 8 kHz, and 10 kHz. (Patuzzi and Thomson, unpublished).

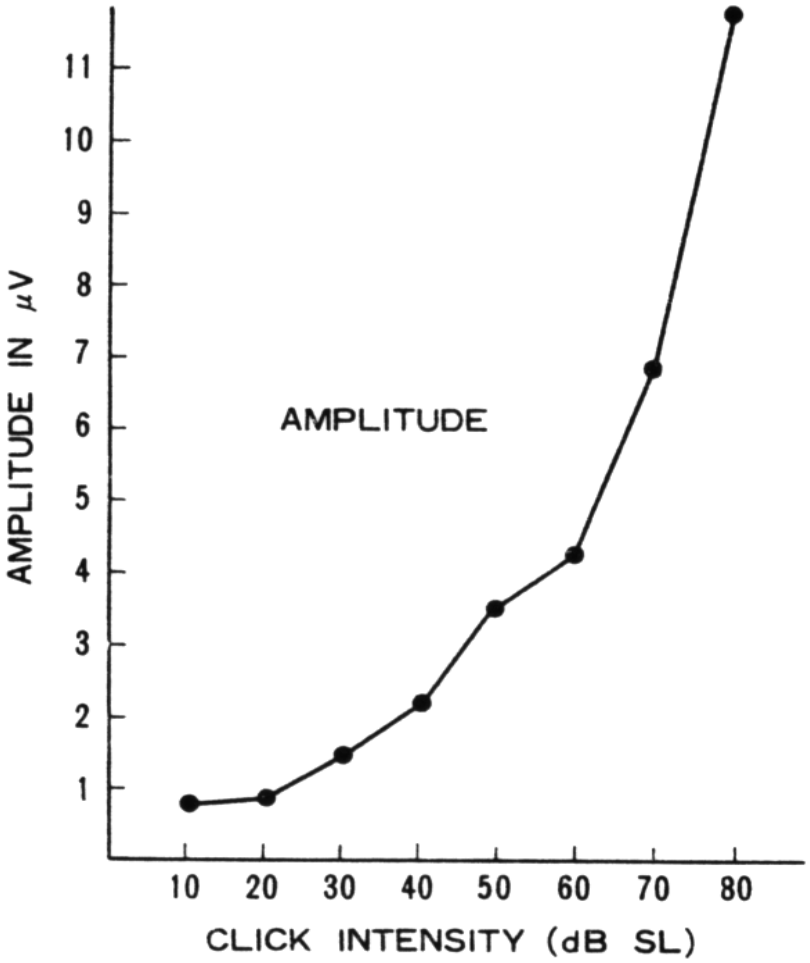

Figure 1.9: The input-output function of the PAMR, showing the peak-to-peak amplitude of the response evoked using click stimuli of sound levels between 10 db SL and 80 dB SL (Yoshie and Okudaira, 1969).

diminished. In view of the recovery data shown by Yoshie et al. (1969), later confirmed by Gibson (1975), the lack of evidence of fatigue or habituation in the responses seen by Jacobson et al. (1964) may indicate that their responses were not maximal to begin with.

1.7.4 Muscle Tone

It has been noted by many authors (mentioned below) that the amplitude, and in many cases the actual presence, of the PAMR depends on the tone of the muscle. In many circumstances when a PAMR is not recorded, methods that increase the tone in the post-auricular muscles have been found effective in facilitating a response.

These techniques include:

i) Voluntary forward flexion of the neck. The subject is instructed to hold their head as low as possible. This technique was found to increase the amplitude of the PAMR by a factor of between 3 and 10 when compared to when the head is held in an upright position (Yoshie et al., 1969). Dus et al. (1975) also found lowering of the head to increase the likelihood of obtaining the PAMR.

ii) Resisted flexion of the neck (Clifford-Jones et al., 1979). The subject tries to push their head backwards against force in the opposite direction.

iii) Similarly, the subject can attempt to maintain an upright head position when the investigator pushes on the back of the subject's head, or by using weights and pulleys to apply traction to a head-straps worn by the subject (Cody et al., 1964).

iv) Propping the head forwards with pillows was found to increase the PAMR amplitude when patients were lying down (Yoshie & Okudaira, 1969; Thornton, 1975).

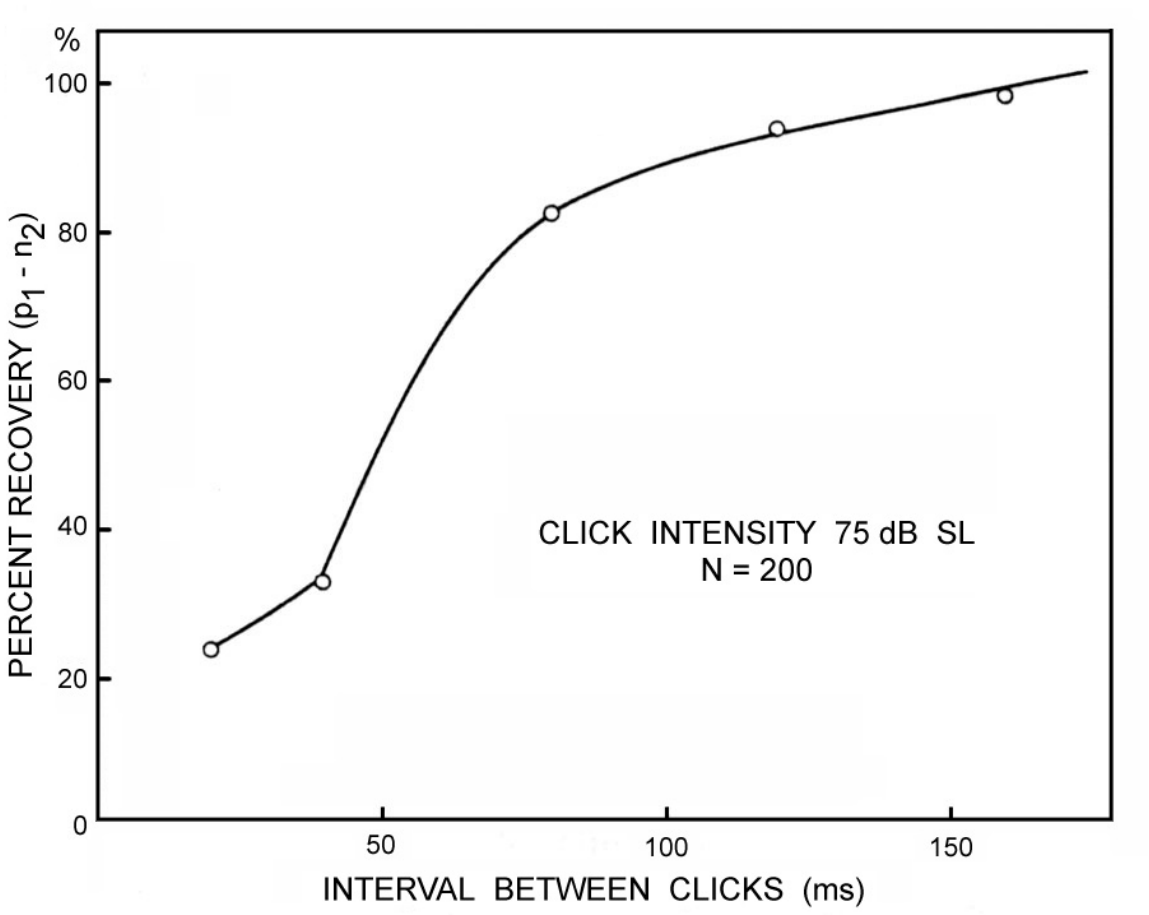

Figure 1.10: The effect of inter-stimulus interval on the peak-to-peak amplitude of the PAMR, expressed as percentage recovery of the response (Yoshie and Okudaira, 1969).

v) Smiling was found to increase the likelihood of obtaining a PAMR (in at least one ear) by 80% in normal subjects (Dus et al., 1975). Gibson (1975) found that encouraging the subject to put their chin onto their chest and give “a broad ear-to-ear grin”.

vi) Streletz et al. (1977) found that in two subjects selected for their ability to wiggle their ears, the amplitude of the response increased ten-fold during this manoeuvre.

vii) Kiang et al. (1963) reported that a flagging response could be revived by applying an electric shock to the subject’s feet.

Douek et al. (1973) used a technique whereby they averaged responses from both sides of the head simultaneously. The advantage of this method was that any lateral movements of the head and neck that decreased the response on one side would be compensated by the enhanced response on the other side. On testing 166 young children with varying degrees of hearing impairment, difficulty in carrying out the test procedure was found in only 7% of the subjects (Gibson, 1975).

Sleep has been found to cause a relaxation of the scalp musculature and hence a decrease in the amplitude of the PAMR. During their research on neurogenic AEPs, Picton et al. (1974) found that sleep was a useful tool to attenuate responses from the scalp muscle reflexes (such as PAMR) to avoid myogenic contamination of their results. They found “it was far easier to have the subject fall asleep than voluntarily relax his scalp musculature”. Streletz et al. (1977) reported that the PAMR was recorded with diminished amplitude during sleep in three subjects, and that it was not detected at all during sleep in the remaining two subjects.

1.7.5 Eye Movement

Jacobson et al. (1964) mentioned in a paper that they had found that "the response amplitude and distribution can be greatly modified by changing head position and lateral

movement of the eyes." This statement is somewhat intriguing in its brevity. Although many authors have published data on the effect that changing head position has on the PAMR, no data has been forthcoming on the effect of eye movement on the PAMR. The effect of eye movements on the PAMR has been previously studied in our laboratory (Patuzzi & Thomson, unpublished). Preliminary results (such as the one shown in Figure 1.11) indicate that the amplitude of the response roughly triples when the eyes are rotated 70 degrees from the forward position. The mechanisms by which this effect occurs are as yet unknown, and form a major component of the current study. Possible mechanisms are discussed further in Section 3.6.

1.7.6a Attention

Paying careful attention to the click stimuli has been found to have a significant effect on the magnitude of certain neurogenic components of the auditory evoked potentials (Picton et al., 1975, Lille et al., 1975, Desmedt et al, 1977). However, it does not cause any significant alteration to the PAMR response (Gibson, 1975).

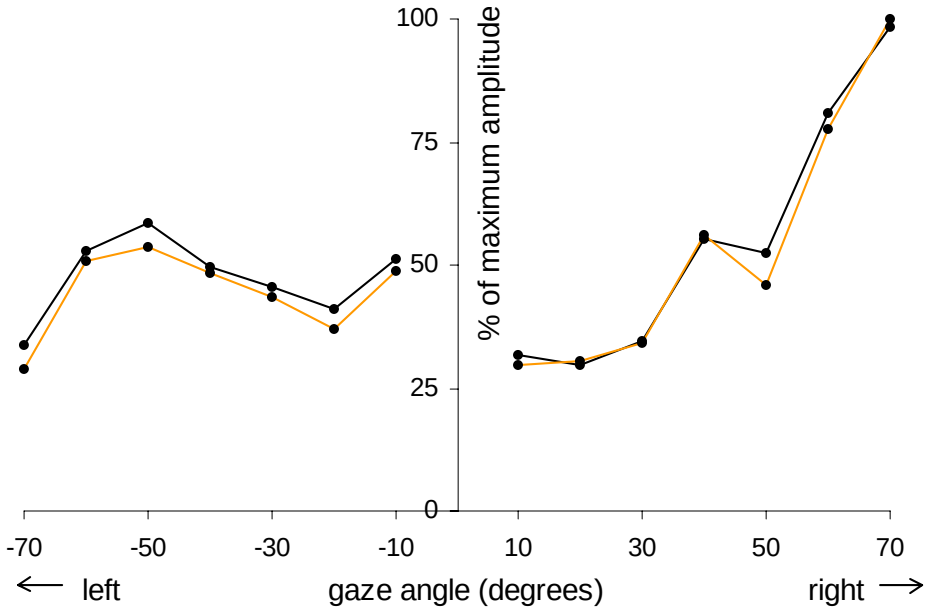

Figure 1.11: The change in peak-to-peak height of the PAMR (expressed as a percentage of the maximum peak-to-peak height) with lateral rotation of the eyes (Patuzzi, et al. unpublished). Responses are recorded from the right PAM.

1.7.6b Adaptation of the PAMR

Adaptation is usually measured as the change in the response to successive click stimuli with respect to that evoked by the first stimulus in the burst of clicks (Thornton et al., 1975). Thornton (1975) claimed that he had some evidence that "there is appreciable adaptation of the response" over 200 seconds, but did not elaborate on this statement.

Humphries et al. (1976) found that the adaptation of the responses varied from subject to subject and also between different times of testing for each subject "depending on the general mental and physical state". In some of their subjects, the averaged responses were still visible after continuous stimulation at a rate of 10/s for 15 minutes, whereas for others who were more relaxed and had low muscle tone, the responses disappeared after several minutes. Similar results were reported by Gibson (1975).

The use of the word “adaptation” is problematical in this context. If the muscle tone of a subject were to increase with time (e.g. if the subject were becoming more anxious about the procedure), their PAMR could be observed to “adapt” in a positive rather than deleterious way. Indeed, Kiang (1963) found that a flagging PAMR in one subject revived spontaneously “for no apparent reason”. Any subtle shift in posture, head position, or facial expression may have caused an slight increase in muscle tone in the post-auricular area, thereby “reviving” their PAMR.

1.7.7 Age & Developmental Maturity

When recording from infants as part of a screening program, it is important to know if the response alters with the age. ABR measurements undergo marked changes in morphology during the first 18 months of life (Hall, 1992). At birth, generally only waves I, III, & V are observed, and the other components become more distinct during the first three months after birth (Hall, 1992).

With regard to neonatal audiometric screening using the PAMR, the shape of the waveform is generally not as important as whether the response is present or absent. The available evidence suggesting the intact operation of the PAMR in early infancy comes from Gibson (1975), Buffin et al. (1977), and Flood et al. (1982). Gibson (1975) tested 11 normal babies between the ages of three months and one year, and was able to record the PAMR in all cases using stimuli of 40 dB SPL or less. Buffin et al. (1977) were able to measure the PAMR in 80% infants under 2 years of age, and reported that the latency of the PAMR is significantly extended in infancy. Flood et al. (1982) recorded a normal PAMR result from 68% of 101 infants around the age of six months. 42% of those that gave an abnormal or absent PAMR had a sensorineural hearing impairment, and the remaining 58% of those that produced

abnormal PAMRs were found to have serous otitis media at the time of the test. The effect of serous otitis media on PAMR is discussed below.

The limited amount of data available on the use of PAMR tests with young infants suggests that the PAMR is recordable in most cases, but more research needs to be done on babies under 3 months of age in order to establish normative data on the presence and morphology of the reflex at this age.

1.7.8 Serous Otitis Media

Middle-ear pathology can have a pronounced effect on evoked responses, such as OAEs, ABR, and the PAMR. Serous otitis media, or "glue ear", is a condition that is widespread among infants, and results in the filling of the middle-ear cavity with fluid, which reduces conduction of sound through the middle-ear.

Gibson (1975) found that one of the disadvantages in using the PAMR as a method of testing the hearing acuity of children was that conductive hearing losses, and in particular, children with "glue ears" gave poor responses. As discussed in Section 1.71a, a rapid-onset sound stimulus is required to elicit the reflex. Gibson attributed the failure to record responses in these children to "attenuation of the sharp onset of the click into a more gradual rise, which failed to elicit the response". Fluid in the middle-ear tends to produce a relatively greater degree of conductive hearing loss for low frequencies (i.e. those below 1000 Hz) than for those above 1000 Hz (Hall, 1992), and so Gibson's explanation that the click stimulus was low-pass filtered is unlikely. The lack of response may simply be attributable to the overall reduction in the intensity of the transmitted sound stimulus that occurs during this condition.

Flood et al. (1982) tested the PAMR in 101 infants under two years of age (usually as close as possible to six months of age). The children were later independently retested using

subjective audiometric techniques when they were of an age that they would perform reliably (i.e. when they were "at least 3½ years old"). Seventy-two of the subjects belonged to a group of low-birth-weight group. Of the infants tested, 68% gave a normal PAMR result. Of those that gave an abnormal PAMR, 42% had sensorineural deafness, and the remaining 58% were found to have serous otitis media at the time of the PAMR test. Among the infants that gave a normal PAMR, all were later found to have normal audiograms (except those who had developed serous otitis media in the time before the audiogram).

1.7.9 Electrode placement

Yoshie & Okudaira (1969) briefly studied the effect of different active and reference electrode locations on the amplitude and morphology of the measured PAMR. This procedure has since been repeated by Gibson (1975), and Buffin, Connell and Stamp (1982) for a number of electrode locations. The results of Yoshie et al. (1969) and Buffin et al. (1982) are shown in Figures 1.12A and 1.12B respectively. All of these groups recorded the PAMR at maximal amplitude when the active electrode was located directly above the post-auricular muscle.

1.8 Sensitivity and Specificity

The two terms most commonly used to define the success of a screening strategy are the *sensitivity* and *specificity* of the particular test. The sensitivity of a hearing test refers to the probability that a hearing-impaired child will fail the test, while specificity refers to the probability that a normal-hearing child will pass the test. Both of these measures of success are calculated by determining the proportion of test subjects that fall into each of the four possible outcomes of the test, named the *true-positive*, *true-negative*, *false-positive*, and *false-negative* outcomes.

A. (from Yoshie et al., 1969)

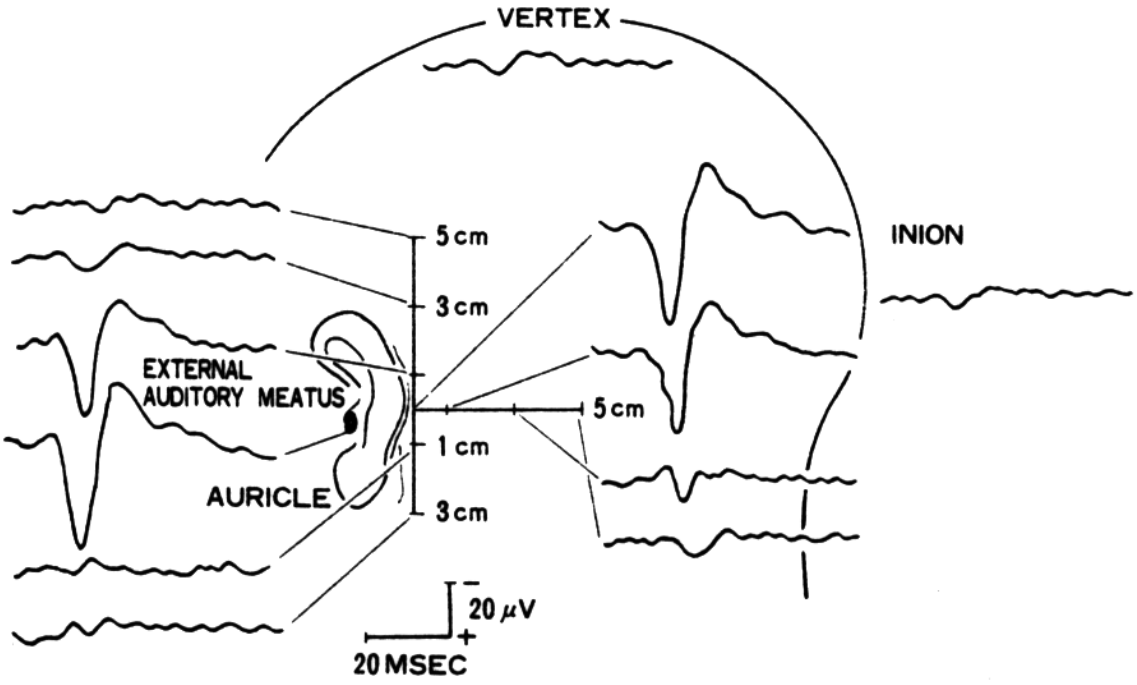

B. (from Buffin et al., 1977)

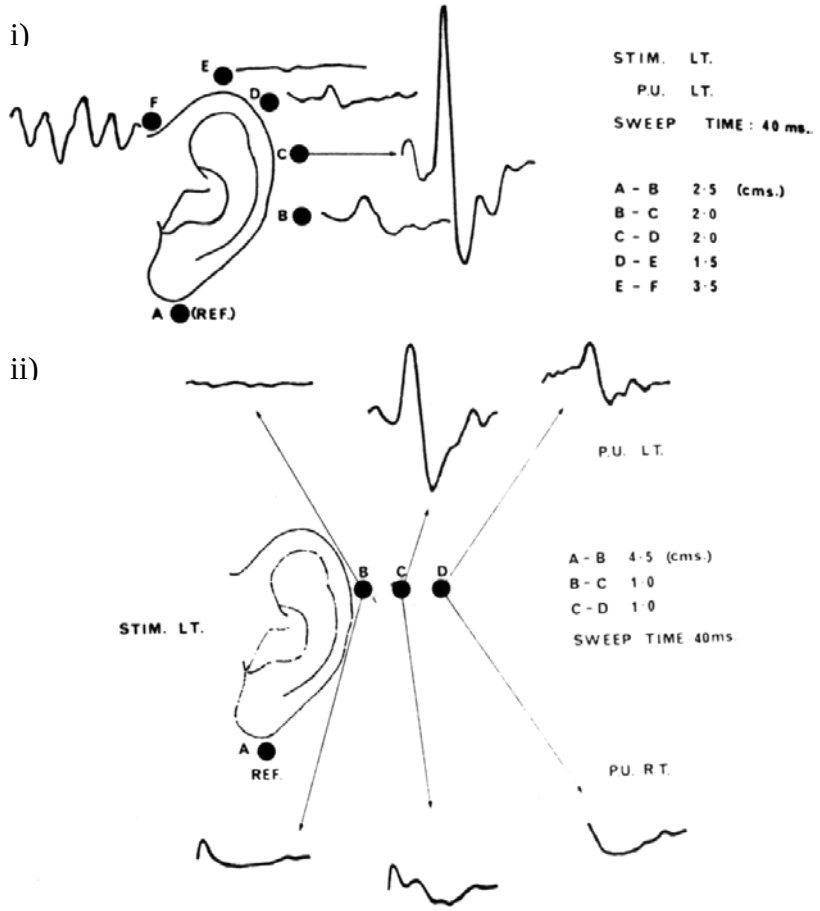

Figure 1.12: **A.** The results of Yoshie et al. (1969), showing the averaged PAMR waveforms (n = 500) recorded from various electrode positions over the scalp in response to 90 dB SL clicks. Note that the traces are plotted with negativity on the *reference* electrode as "up" in this figure.
B. The results of Buffin et al. (1977) showing the averaged PAMR waveforms recorded using i) ipsilateral monaural stimuli, (stimulus to left ear, response recorded from left ear), and ii) both ipsilateral and contralateral monaural stimuli (stimulus to left ear, response recorded from left ear – and from the right ear). The distances between the recording electrodes (in cm) are also shown. [Abbreviations: STIM. – stimulus, P.U. – "picked up" (recorded from), L.T. – "left", R.T. – "right".]

A true-positive is achieved when a hearing-impaired subject fails a hearing test, and a true-negative occurs when a normal-hearing subject passes the hearing test. Conversely, a false-positive occurs when the normal-hearing subject fails the test, and a false-negative result occurs when the hearing-impaired subject passes the test. The outcomes are summarised in Figure 1.13 below, adapted from Weber & Jacobson (1993).

The ideal hearing screening test would have a sensitivity and specificity of 100%, but in practice this is not achieved. Decisions as to what is defined as a "pass" and "fail" in a specific hearing test will affect the distribution of results into the four categories. More stringent "pass" criteria will lead to an increase in the sensitivity of the test, but reduce the specificity. Measures that allow more subjects to pass will do the opposite. The sensitivity and specificity of a number of commonly used audiometric screening tests are shown in Figure 1.14 (adapted

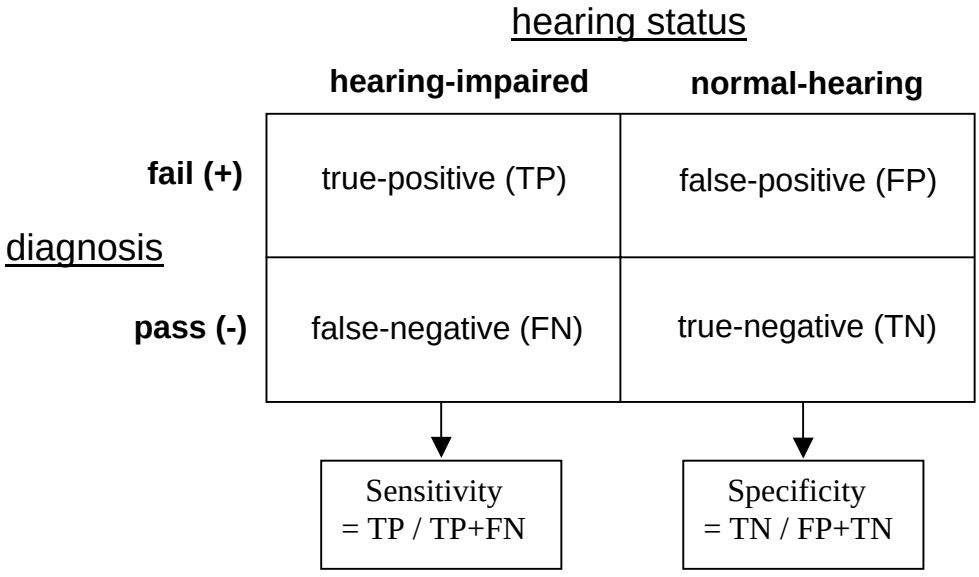

Figure 1.13: An example of the 2 x 2 matrix commonly used to categorize test results into true-positive, true-negative, false-positive, and false-negative outcomes. (Weber & Jacobson, 1993)

from Oudesluys-Murphy et al., 1996). It also allows comparison between a number of other features of the tests.

The tests compared are: i) The Ewing test – a subjective distraction audiometric test commonly performed on infants, ii) Transient-evoked oto-acoustic emissions (TEOAE) – hearing tests involving oto-acoustic emission measurement, as described in Section 1.2.3, iii) ABR – measurement of the click-evoked auditory brainstem response, and iv) ALGO – an automated ABR measurement system (Jacobson et al., 1990).

Based on the information gathered in this introduction, a column representing the PAMR has been added. There is not sufficient data available to enable calculation of the sensitivity and specificity of the PAMR, as the methods used to measure the response have varied from researcher to researcher. However, a number of other characteristics are presented below to provide a brief overview of the PAMR in relation to other hearing tests.

	EWING	TEOAE	ABR	ALGO	PAMR
Age (months)	9	0 - …	0 - …	0 – 6	0 - …
Time (mins)	5 - 30	7.2 / 16.6	± 30	14 / 19	5 – 15
Testers	2	1	1 (2)	1	1
Training	+++	+++	++++	++	++
Sound treated room?	+	+	±	-	-
Objective/Subjective	Subjective	Objective	± Objective	Objective	Objective
Sound intensity	30 – 35 dB SL	26 – 36 dB SL	All possible	35 dB SL	from 10 dB SL
Pre-term testing	n/a	+	+	+	?
Sensitivity	79.4%	76% / 50%	Gold Std.	100%	??
Specificity	97.6%	86% / 52%	Gold Std.	98.7%	??
Hearing pathway	Total	Pre-neural	Distal auditory nerve – midbrain	Distal auditory nerve – midbrain	Distal auditory nerve – midbrain
Handicapped child?	-	+	+	+	+
Screening method?	+	+	-	+	?

Figure 1.14: A table comparing the features of a number of commonly used hearing screening tests (adapted from Oudesluys-Murphy et al., 1996), and those of the PAMR.

1.9 Aims

The aims of the current study were to examine a number of fundamental properties of the PAMR, including the best methods and parameters of recording the response, and the investigation of the mechanisms by which eye-rotation potentiates the reflex. Investigation of these mechanisms necessitated the development of a computer-based automated PAMR measurement system, which allowed simultaneous examination of the changes in background electrical activity of the PAM, and extraction of information regarding the sound-evoked PAMR waveform, such as response amplitude and peak latency. With minor modifications, the automated system was also used in electrocochleographic research, including the measurement of the compound action potential (CAP) and low-frequency cochlear microphonic (CM) waveforms in guinea pigs. Both the CAP and CM are important evoked responses used in auditory research.

From a technical viewpoint, the other aims of the project were to assess correlation as a measure of the presence and amplitude of the PAMR in both adult subjects and in infants, and, most importantly, to develop a cheap, efficient and reliable objective hearing test that could be used as an alternative to the ones that are currently available. The availability of such a device would have the potential to vastly increase the number of children that are screened for hearing disorders, especially in poorer communities who do not have the funds or the expertise to establish screening programs using the currently available objective techniques of ABR and oto-acoustic emission measurement.

METHODS

Methods

A system was developed in the present study for the detection and measurement of the post-auricular muscle reflex (PAMR) in adult and infant subjects. Chronologically, the project can be divided into four stages. In the initial stages, the auditory stimulus generator was built and customised waveform capture software was written. Further development and refinement of this software continued throughout the year. In the secondary stages, the bulk of experimental results regarding the fundamental properties of the reflex were obtained. In the tertiary stages of the project, a hand-held automatic PAMR detection and measurement device was developed, and preliminary trials of this device were carried out in adult subjects. In the fourth stage of the study, the software developed for the detection of the PAMR in human subjects was successfully applied to the detection of the Compound Action Potential (CAP) in the guinea pig, and the tracking of the CAP threshold evoked using tone-bursts of a number of frequencies. At the same time, software was also developed to enable real-time Boltzmann analysis of cochlear microphonic (CM) waveforms recorded from the guinea pig. All experiments were conducted in the Physiology Department of the University of Western Australia.

2.0 Subjects

In the first and second stages of the project, subjects were chosen from the staff and students of the Physiology Department of the University of Western Australia. The pure-tone audiometric thresholds of these subjects were measured using a Diagnostic Audiometer (Model TA155) at frequencies of between 125 Hz and 8 kHz. All of these subjects were found to have

normal audiometric thresholds. The subjective click thresholds for these subjects were also measured using a custom-built click generator and voltage-controlled attenuator.

In the secondary stages of the project, adult and infant subjects were also selected from the general public. These tests complied with the University of Western Australia's Committee of Human Rights guidelines (Ethics Approval Project No. N65). Consent Forms were signed by the subjects, or in the case of infant subjects, their guardians, prior to testing. Sample copies of the Ethics Approval and Consent Forms are presented in Appendix Two.

2.1 Equipment

Schematic diagrams of the equipment systems used in the project are shown below in Figure 2.1. The operation and function of the individual hardware and software components of the systems are described in detail on the following pages.

Laboratory setup:

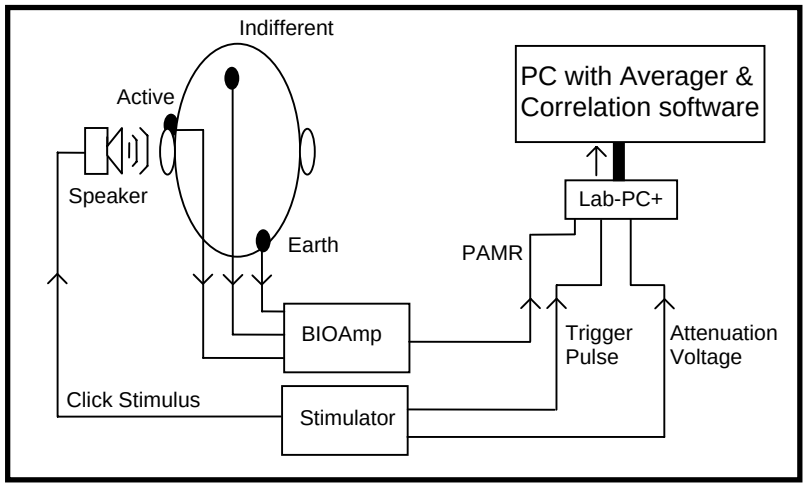

Portable setup:

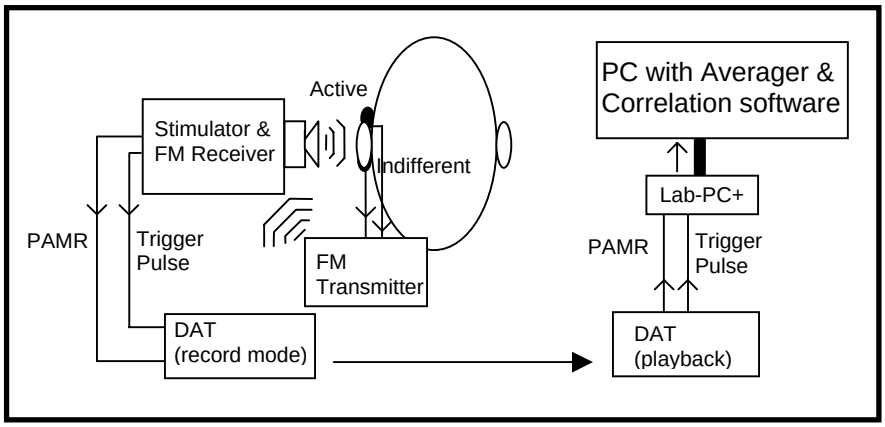

Figure 2.1: Schematic diagram of the equipment used in the current study, illustrating the interconnection between the various components, as described in the text, and differences between the laboratory and portable equipment configurations.

2.2 Click and Tone-Burst Generator

The sound stimuli used to elicit the PAMR were produced by a custom-built click and tone-burst generator. Unless otherwise specified, the acoustic clicks were produced by delivering repetitive, monophasic square-wave pulses to a pair of Philips SBC 3315 headphones. The frequency response of these headphones to uniform white noise, measured free-field by a Sennheiser MKE2-5 microphone, is shown below in Figure 2.2.

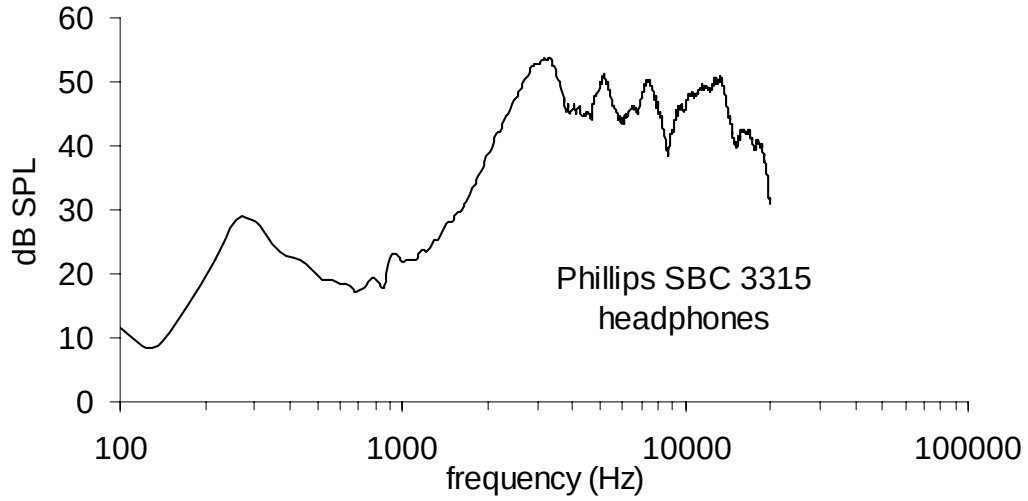

Figure 2.2: Amplitude spectrum showing the frequency response of the Philips SBC 3315 headphones to uniform white noise, measured free-field by a Sennheiser MKE2-5 microphone. (Sample rate: 44,100 samples/sec)

The output voltage of the clicks was 150 mV pp at 0 dB attenuation, which produced a 75 dB peak SPL click when delivered to the SBC 3315 headphones. The electrical square-wave pulse, the acoustic click waveform, and the frequency spectrum of the acoustic click are shown in Figure 2.3. The acoustic click waveform was recorded free-field by a Sennheiser MKE2-5 microphone at a distance of approximately 1 inch. The properties of the click

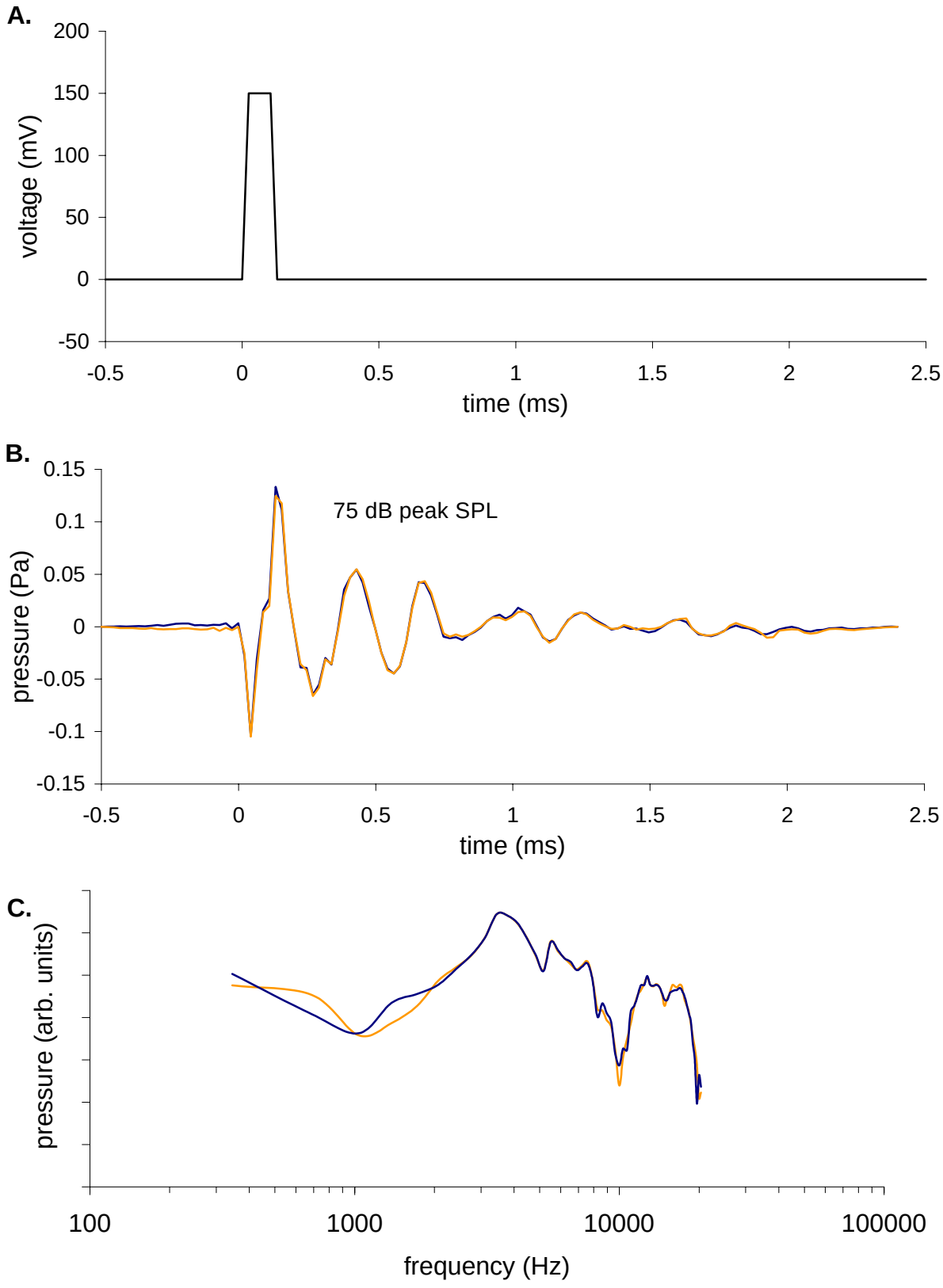

Figure 2.3: **A.** An example of the electrical square-wave pulse delivered to the SBC 3315 headphones. **B.** The resulting acoustic click waveform, recorded free-field by a Sennheiser MKE2-5 microphone at a distance of approximately 1 inch. **C.** The pressure spectrum, showing the distribution of the pressure of the acoustic click across frequencies from approximately 350 Hz to 22 kHz. (Sample rate: 44,100 samples/sec).

produced by the headphone are altered during passage through the ear canal, and so the data shown in Figure 2.3 are only an approximation.

The click generator had two rate settings: "Normal", in which clicks could be produced at adjustable rates between 7/s (140 ms period) and 18/s (56 ms period), and "Slow", which produced the clicks at 1.7/s (588 ms period). A rate of 8/s was most often used because the time taken by the LabVIEW software (see Section 2.5) to sample and carry out calculations on each waveform was, on average, 125 ms (when using a 200 MHz Pentium Processor). This rate meant that each click presentation could be processed in real-time.

The width of the square-wave pulse used to generate the click could be adjusted from 20 μs up to 100 μs. Unless otherwise stated, a click width of 100 μs was used during testing, as it was found to evoke the largest PAMR response. The click-generator circuit also provided a square-wave output that was used as a gating signal for the tone-burst generator circuit, which produced tone-bursts of selectable frequency, with a rate and width determined by the gating signal.

The sound level of the click or tone-burst stimuli could be adjusted using a voltage-controlled attenuator circuit, housed within the stimulator box. Although capable of a larger degree of attenuation (if its input signal were larger), the circuit was able to attenuate the click or tone-burst stimuli by up to 57dB before the signal disappeared into the noise floor. The attenuation level could be adjusted manually using a potentiometer, or by using a section of the attenuator circuit that smoothly and automatically ramped the attenuation up or down, depending on the presence or absence of a digital TTL (transistor-transistor logic) pulse delivered to the attenuator circuit from the PC.

The attenuator circuit also produced a DC voltage output that could be used to monitor the level of attenuation provided by the circuit. The applications of this DC voltage output in experimentation are discussed further in Section 2.11.

During the experimental series discussed in Section 3.2, pure tones were generated by a Hewlett Packard HP3325a Synthesizer/Function Generator, and gated externally to produce 38 ms tone-bursts with a rise-time of 1 ms, at a rate of 5/second. These tone-bursts were then recorded to DAT by a Denon DTR-2000 DAT recorder (Nippon Columbia Corp., Tokyo, Japan). On playing back these tone-bursts, a pair of Telephonics TDH39 transducers were used instead of the SBC 3315 headphones, as they had a better frequency response, and were therefore more suitable for delivering the tone-burst stimuli.

2.3 Electrodes

The PAMR was recorded as the difference in potential between two electrodes: the active electrode, located (in most cases) directly above the PAM, and the reference or indifferent electrode, located at some other position. The electrodes used in the preliminary studies were pre-gelled Ag/AgCl Adult ECG Electrodes (ConMed Corp., NY, USA). The conducting portion of the electrode was 2 cm in diameter, surrounded by a 1.5 cm wide, non-conducting, self-adhesive annulus. One edge of this adhesive portion of the active electrode was removed with scissors to avoid tearing a subject's hair on removal of the electrode.

Initially, recordings were made with the active electrode directly over the PAM, the reference electrode placed high on the forehead, and a ground electrode placed on the neck. Before applying the electrodes, the relevant areas of the subject's skin were cleaned by wiping with 95% ethanol to increase conductivity and aid electrode adhesion. A contact resistance of

5 kΩ between the active and reference points was typical with this brand of electrode in this placement. Approximately 350 Ω of this resistance was due to the electrodes.

"Optimum" placement of the electrodes was defined as that configuration which gave the best combination of large response amplitude, low electrical noise from both internal (biological) and external (interference) sources, and the accuracy with which the electrodes could be applied to the correct locations. Also important was the convenience of placing the electrodes, and how comfortable they were to remove (e.g. the location that required pulling out the least hair).

In order to determine the optimum placement for the active and reference electrodes, multiple electrode arrays were used to map the distribution of the PAMR on the surface of the skin above the PAM and on the dorsal surface of the pinna. Although the following information is presented in more detail in the Results section, it is necessary to briefly mention electrode placement experiments here to explain the subsequent choice of electrode placement and electrode design. With reference to a forehead electrode, the PAMR was recorded from twelve different active electrode locations (Section 3.3 of Results). During these recordings, the subject shifted his gaze horizontally to the right to obtain a larger response.

The PAMR recorded from a site directly over the body of the right PAM was found to have the largest amplitude (105 μV pp). The largest waveform recorded from the back of the right pinna had an amplitude of 50 μV pp. However, the PAMR waveforms recorded from the dorsal surface of the pinna were inverted relative to those recorded from over the PAM. The phenomenon of signal inversion on the dorsal surface of the pinna is discussed further in Section 3.3. Because these waveforms were inverted relative to each other, but were otherwise similar in shape, the PAM and pinna locations that gave the largest response amplitudes were

used as a dipole for differential recording of the PAMR. When recorded from these locations, the peak-to-peak amplitude of the PAMR was larger (155 μV pp) than that recorded from the PAM with a forehead reference (105 μV pp). Attachment of the electrodes was also easier, as described below.

A "hinged" pair of electrodes was designed such that the PAMR could be recorded from the PAM with reference to the back of the pinna. The electrode pair (Figure 2.4) was made from two thin strands of 0.71 mm diameter copper wire coiled over a folded strip of adhesive foam. After applying a small amount of conductive gel (Signa Gel, Parker Laboratories, Inc. NJ, USA) to the electrode end, the pair could be "wedged" into the V-shaped fold behind the pinna. In this position, one strand of wire was pressed against the PAM, and the other against the rear of the pinna. These two wires made the differential pair from which recordings of the PAMR were made.

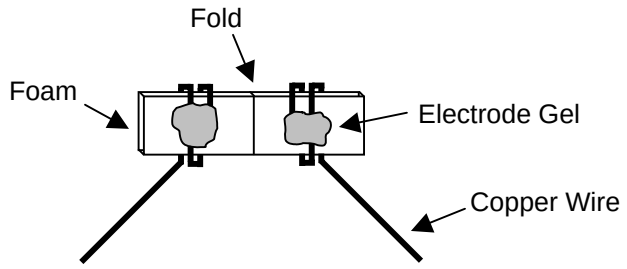

Figure 2.4: Design of the "wedge" electrode used for measurement of the PAMR.

2.4 Signal Filtering and Amplification

In the initial stages of experimentation, filtering and amplification of the signal was provided by a BIO Amp CF (ADInstruments, NSW, Australia), controlled by an Apple Power

Macintosh 7600/200, running Scope V3.5 software (ADInstruments, NSW, Australia). The BIO Amp provided a 4-pole Bessel low-pass filter (± 3% accuracy), a single-pole high-pass filter (± 0.25% accuracy), and a 2-pole notch filter that reduced interference from the mains power supply by attenuating the 50 Hz components of the signal (± 0.5% accuracy) by 32 dB. In these initial stages, the signal from the electrodes was amplified by 10,000, and filtered with a pass-band of 10 Hz to 200 Hz, and 50 Hz notch filtering. The low-pass filter settings were later changed, as data regarding the spectral composition of the PAMR were obtained.

Knowledge of the spectral composition (Fourier Transform) of the PAMR waveform was important in choosing filter settings to improve the signal-to-noise ratio (i.e. reduced the amplitude of the unwanted electrical noise in relation to the amplitude of the desired PAMR signal).

To include as much of the original frequency information of the PAMR signal in the spectral analysis, the BIO Amp filtering bandwidth was made as wide as possible (1 Hz to 5 kHz). After the test subject shifted their gaze horizontally to the right to maximise the PAMR, 160 waveforms from the right PAM were sampled at 10 kHz, and the average spectrum of the sampled waveforms was calculated by a LabVIEW Fast Fourier Transform algorithm. The LabVIEW package is discussed at greater depth in Section 2.5.

A Blackman-Harris window function was used during the Fourier transform to minimise “spectral splatter”, or “leakage” distortion (caused by the abrupt truncation of the signal to a finite length) by forcing the signal data gradually to zero at the ends of the time window (Norton, 1989).

As shown in Figure 2.5, the spectral peak of the PAMR was broadly centred between 60 and 100 Hz, with only a small proportion of frequency components above the 300 Hz region

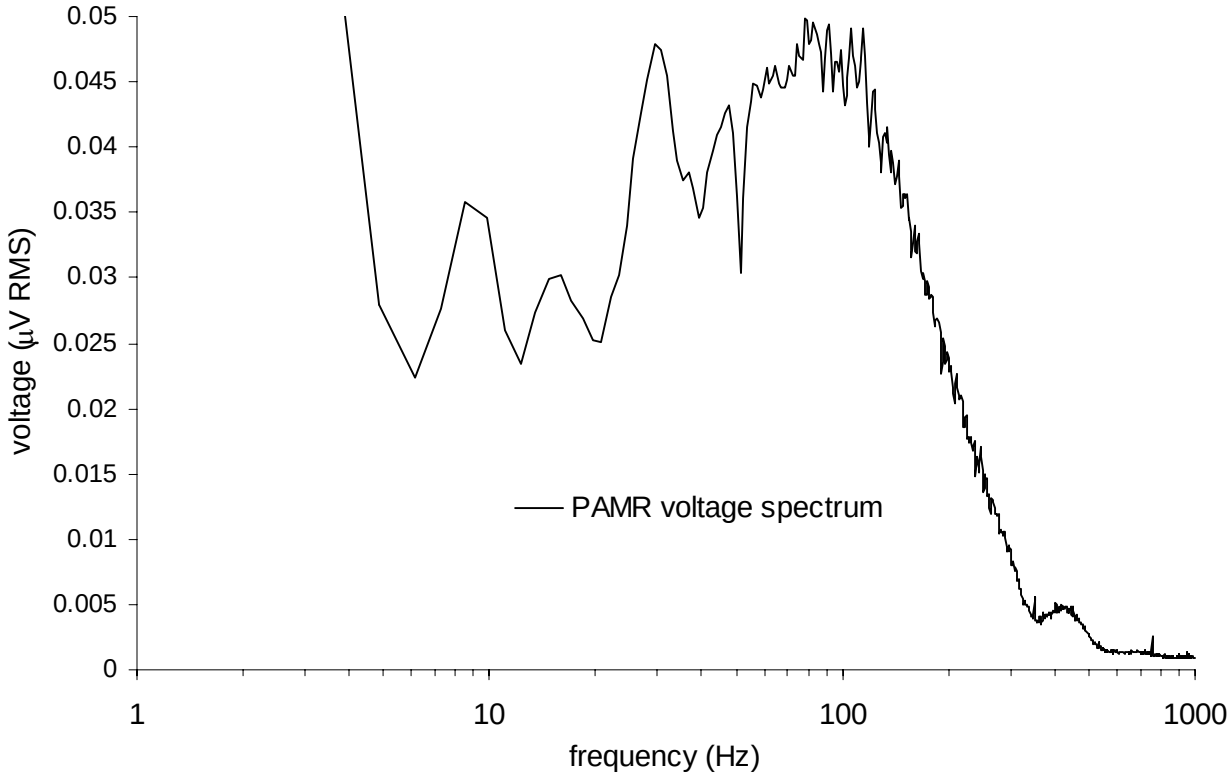

Figure 2.5: Voltage spectrum showing the average frequency composition of 160 PAMR waveforms, recorded from the right PAM with the eyes of the subject rotated hard right. (Filter bandwidth: 1 Hz - 5 kHz, 50 Hz notch. Sample rate: 10,000 samples/sec. Window: Blackman-Harris.)

of the spectrum, and almost none above 500 Hz. A large low-frequency component under 4 Hz is not shown in this figure, but can be seen more clearly in Section 3.8.

The way in which a signal is filtered is important for a number of reasons. To avoid aliasing, the signal should be low-pass filtered to remove frequency components above half the sample rate (Feuer et al., 1996). Because a sample rate of 5000 Hz was most commonly used by the waveform capture software (described in Section 2.5), the low-pass filter setting had to be at most 2500 Hz. However, as the spectrum of the PAMR showed there was only limited frequency distribution above 400 Hz, a low-pass filter setting of 300 Hz was chosen, to limit

the possibility of electrical interference at higher frequencies, and to avoid aliasing. In the months before this spectral analysis was performed, a 200 Hz low-pass filter was used.

The high-pass filter setting was set to 10 Hz, because it was the highest available setting on the BIO Amp. This AC coupling of the signal was very important, because any DC offset would artificially raise the correlation level between successive waveforms, as described in Section 2.6. This high-pass filter level did, however, have a noticeable effect on the peak amplitudes and latencies of the PAMR waveform. Shown in Figure 2.6 is an example of two averaged PAMR waveforms that were filtered with different pass-bands before sampling. The amplitude of the more filtered waveform was decreased by 14%, and its peak latencies were increased by an average of 1.5 ms.

Nevertheless, the 10 Hz high-pass setting was retained because the increased

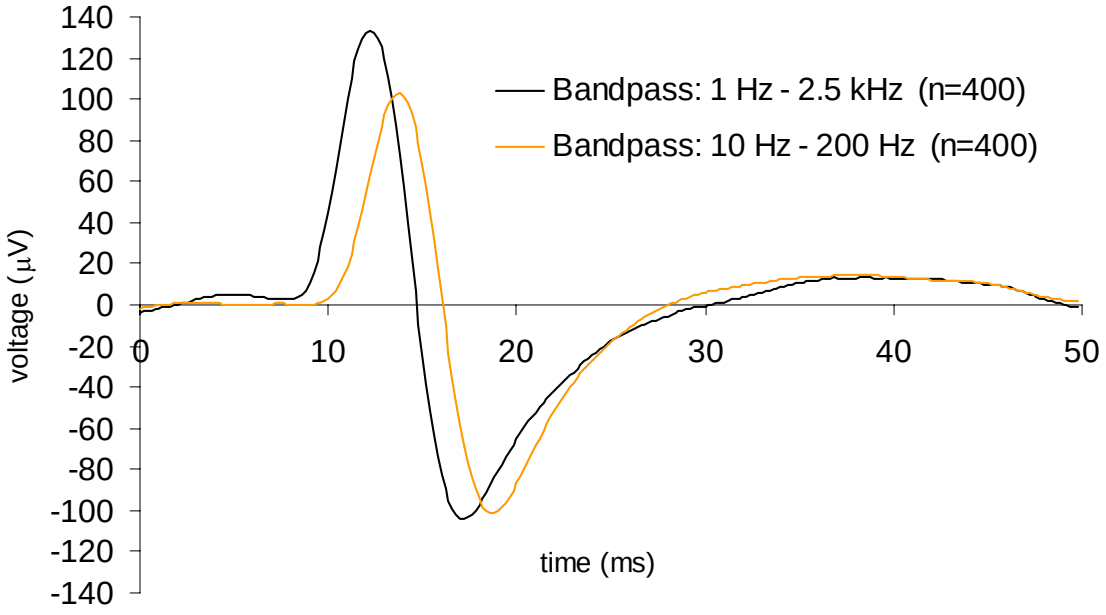

Figure 2.6: The changes in latency and amplitude of two averaged PAMR waveforms due to different band-pass filtering levels. The waveforms were recorded from the right PAM with the eyes of the subject rotated hard right.
1 – 2500 Hz PAMR: 1st peak: 133 μV at 12.2 ms. 2nd peak: -104 μV at 17.2 ms.
1 – 200 Hz PAMR: 1st peak: 103 μV at 13.8 ms. 2nd peak: -101 μV at 18.6 ms.

correlation stability gained by decreasing the low-frequency "rumble" of the PAMR waveforms outweighed these morphological changes.

The 50 Hz notch filter greatly reduced mains interference, while having a negligible effect on the amplitude of the PAMR, as shown in Figure 2.7.

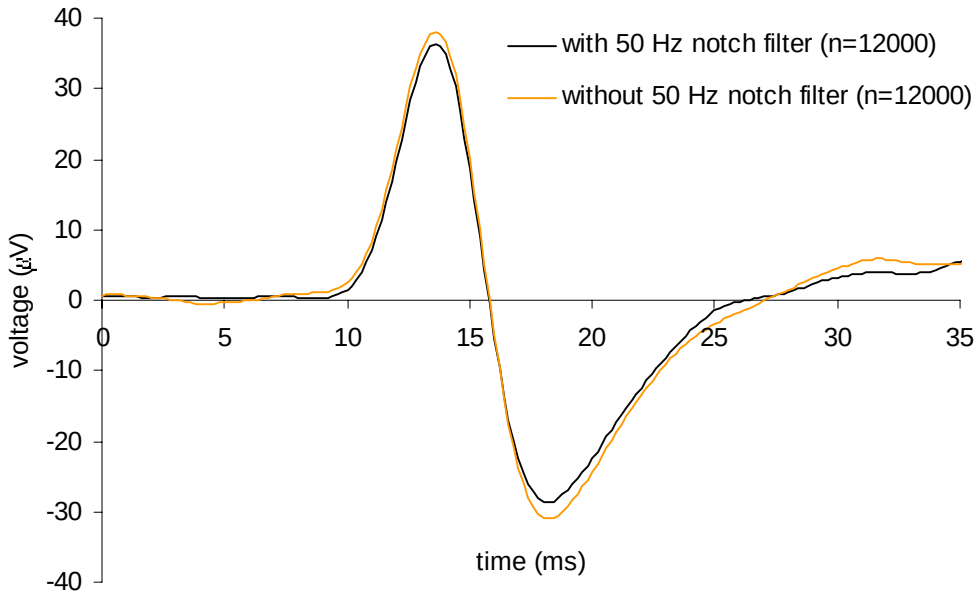

Figure 2.7: The 50 Hz notch reduced electrical interference, while causing no significant change in peak latency or amplitude. The waveforms were recorded from the right PAM with the eyes of the subject rotated hard right. (Filtering: 10 Hz to 200 Hz, with and without 50 Hz notch).

2.5 LabVIEW

Waveform capture was primarily carried out using a PC fitted with a Lab-PC+ Digital I/O card (National Instruments Corp. TX, USA). The sampling of the waveform data via the Lab-PC+ card and its subsequent analysis were controlled by software written with LabVIEW (National Instruments Corp. TX, USA). LabVIEW is a graphical programming development environment based on the G programming language. In LabVIEW, programs are written in the

form of block diagrams known as “virtual instruments” (or VIs), in which data move along “wires” between icons representing variables and functions. Each VI may contain other VIs, which are then referred to as sub-VIs. The block diagrams of the VIs written by the author for this project are presented in Appendix One. LabVIEW was chosen as a software development tool in this project because of the relative speed and ease with which the complicated programming tasks (such as waveform capture, graphical displays, data manipulation and file handling) could be completed, and the ease with which programs could be later modified to suit changing requirements.

Waveform capture was triggered externally by a square-wave pulse from the stimulus box that was synchronous with the click sound. The 36 ms on either side of the trigger pulse (a total of 72ms) were sampled at a rate of 5000 Hz, and stored as a 1-dimensional array of numbers representing the instantaneous signal voltage at sample points 0.2 ms apart.

After each waveform acquisition, the array was multiplied by a correction factor to compensate for the gain of the BIO Amp, and to change the units from volts (V) to microvolts (μV). The mean voltage of the waveform array was also subtracted in order to remove any possible DC offset that could artificially increase the correlation value, as described in Section 2.6. The waveform array was then split into its pre-trigger and post-trigger waveform segments (36 ms each). The pre-trigger waveform segment was sampled in a period relative to the click stimulus in which no muscle activity *synchronised to click stimuli* was measurable. The muscle activity that was present was not time-locked to the click stimuli. This lack of synchronised activity was confirmed by the result that averaging the pre-trigger waveform segment over a large number of presentations produced a flat line. This division of the waveform into pre-trigger and post-trigger segments is illustrated in Figure 2.8.

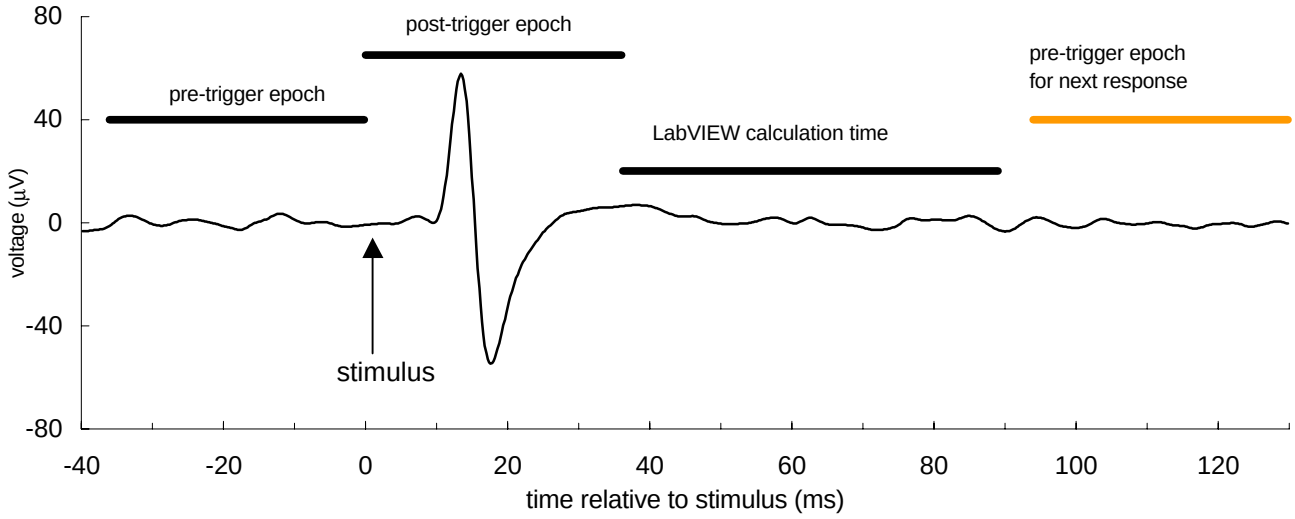

Figure 2.8: The division of the waveform into the pre-trigger and post-trigger segments (or epochs). The 36 ms pre-trigger epoch was used for the calculation of the background EMG, and the 36 ms post-trigger epoch contained the PAMR itself. The time taken for the LabVIEW VI to carry out the calculations on the waveforms (averaging, extraction of latency, peak to peak amplitude etc.) was less than 53 ms.

Because this activity was measured from the vicinity of the PAM, but was not part of the PAMR, the root-mean-square (RMS) amplitude of the unsynchronised muscle activity in the pre-trigger "sham" epoch was calculated, and used as a measure of the amount of background electromyographic noise (unsynchronised EMG). However, if a click rate greater than around 14 per second (72 ms period) was used, the duration of the pre-trigger waveform segment was decreased in order to prevent the inclusion of the "tail" of the PAMR from the previous stimulus in the current EMG calculation.

The fact that the RMS amplitude of the pre-trigger epoch was a measure of background EMG was confirmed by experiments that showed that there was no significant difference between the means of the background EMG levels recorded with and without auditory stimuli, as shown in Figure 3.6.14 of Section 3.6.

The post-trigger epoch (the 36 ms window that contained the PAMR if it was present) was displayed in a window of the "front panel" (graphical screen output) of the VI (Figure 2.9), before being sent to the averaging and correlation sub-VIs. In the averaging process, the incoming *n*th PAMR waveform was arithmetically added to an array of the summed previous waveforms. This sum array was then divided by *n* to give the averaged PAMR waveform, which was then displayed in another front panel window (Figure 2.9). A number of array functions (described in Appendix One) were performed on the averaged PAMR waveform to find the time (in milliseconds) and magnitude (in microvolts) of the largest positive and negative peaks of the waveform, and to calculate the peak-to-peak height of the waveform. These data, and the output from the Correlator VI (described below), were then saved to a file for spreadsheet analysis and graphing.

2.6 Correlation

Calculation of the correlation value between successive raw PAMR waveforms was used as a method of signal detection in this project. The level of correlation between two sampled waveforms was calculated in the following manner. For these calculations, the captured waveforms were stored as arrays of 180 equally spaced sample points over 36 ms, with the numerical value of each sample representing the instantaneous signal voltage at a particular moment in time after the trigger pulse. This array of numbers is referred to here as the waveform function, x(t). In calculating the correlation value between two of these waveforms [$x_1(t)$ and $x_2(t)$], we were interested in the similarity of the numerical values of the samples that occurred at the same moment in time after each trigger pulse. This was done by multiplying the numerical value of each sample in the first waveform by the corresponding sample in the second waveform. If $x_1(1)$ and $x_2(1)$ were both positive values, or both negative values, the product of the two would be positive. Conversely, if $x_1(1)$ and $x_2(1)$ had different signs, the product of the two would be negative. The sum of these products $\sum_{i=0}^{179} x_1(i).x_2(i)$ [that is, $x_1(0).x_2(0) + x_1(1).x_2(1) + x_1(2).x_2(2) + \ldots + x_1(179).x_2(179)$] was therefore a measure of the correlation of the waveforms $x_1(t)$ and $x_2(t)$. However, although it is true that a greater correlation between the two waveforms will result in a larger sum of the products, this simple correlation value also depended on the amplitude of the signals. For example, the sum of the products of $2x_1(t)$ and $2x_2(t)$ will be twice that of $x_1(t)$ and $x_2(t)$, although the pairs of waveforms themselves are equally similar. That is, the simple correlation value $\sum_{i=0}^{179} x_1(i).x_2(i)$ would depend on signal magnitude, and therefore such factors as electrode placement, contact resistance, and signal amplification. To remove the effects of scaling the waveforms, the

correlation value was normalised to a value lying between –1 and +1 by dividing the simple correlation value $\sum_{i=0}^{179} x_1(i).x_2(i)$ by the square root of the product of $\sum_{i=0}^{179} x_1(t)^2$ and $\sum_{i=0}^{179} x_2(t)^2$.

Any DC offset in the waveforms also increased the correlation value obtained. When the mean values of the waveforms $x_1(t)$ and $x_2(t)$ were both above zero (in the case of a positive DC offset), or both below zero (in the case of a negative DC offset), there was an increased probability that the multiplication of individual array elements would result in a positive value, thereby increasing the sum of the products of the arrays, $\sum_{i=0}^{179} x_1(i).x_2(i)$. This increase in the simple correlation value was not totally removed by the normalisation factor: Whereas a DC offset is reflected in the simple correlation value as an increased level of similarity between the two waveforms, it appears in the normalisation factor as the equivalent of an increase in waveform amplitude, because the arrays $x_1(t)$ and $x_2(t)$ are squared before being summed and multiplied by each other. To avoid this artificial correlation increase, any DC offset in the incoming signal was reduced prior to calculation by high-pass filtering the signal at 10 Hz. The effect that this filtering has on waveform morphology is discussed further in Section 3.9.

The correlation between successive waveforms can be used as a method for detecting the presence of a time-locked signal buried in noise, because the correlation value of the waveforms containing the same time-locked signal must, on average, be higher than that of random noise: the correlation value of waveforms containing only random noise will average to zero, whereas the correlation value of waveforms containing some time-locked signal will average to a value above zero.

The *difference* in correlation value between waveforms that contain a response and those that do not can be maximised by limiting the time window over which the correlation is calculated to a window that contains the response. That is, the correlation value is “diluted” if

the window includes times where no response could possibly be present. The correlation calculations were limited to a specific time window by multiplying the waveform arrays by a "window" array (consisting of zeros and ones) that discarded the data not within the chosen period prior to calculation. The selection of this optimal time window is described below.

2.7 Optimal choice of correlation window

The simplest method of choosing a correlation window for PAMR detection was to adjust the window so that the correlation was calculated only over the time course of the PAMR (i.e. using window "start" and "stop" times of approximately 10 ms and 25 ms after the click stimulus). Although this window gave a greater correlation value than when the correlation was calculated over the entire 36 ms waveform, it was not necessarily the window that gave the highest possible correlation, as some parts of the PAMR waveform are less stable than others. In addition, the optimal window for clinical use may not be the one that gives the highest correlation: other important factors in the choice of a correlation window included how "robust" the resulting value was: that is, did the window allow for a shift in peak latency and magnitude when the sound level of the click stimulus was altered.

In order to choose empirically the optimal window for PAMR detection, a VI was written (see "Optimum Correlation Window VI", Appendix One) which systematically calculated the average correlation value for 180 successive waveforms (containing the PAMR and the background EMG noise) using every possible combination of window start and stop times (in whole milliseconds).

Using the PAMoMATIC VI (see Appendix One), 180 waveforms were recorded from the right PAM of a subject whose gaze was shifted to the right during recording to maximise the response. These raw waveforms were stored in a data file for repeated use by the Optimum

Correlation Window VI. The output of this VI was a file containing the "start" and "stop" times defining the correlation window, and the average correlation value (for the 180 sampled waveforms) calculated with that window. The results were then plotted as a contour map, enabling visual interpretation of the data. This was repeated using waveforms evoked by four different click-stimulus sound levels: 45 dB, 35 dB, 25 dB, and 15 dB SL. These sound levels were chosen so that the correlation contours for both maximal and minimal PAMR responses could be compared. The correlation contour maps for the four click-stimulus sound levels are shown in Figure 2.9.

For each of the stimulus levels, the maximal correlation window was found to be from 12.5 ms to 14 ms. As shown in Figure 2.9, this window was located directly above the first peak of the PAMR. A local minimum found for a window of 15 ms to 15.5 ms is due to the fact that this is the zero-crossing point in the PAMR waveform (i.e. the transition from the first peak to the second). As the PAMR component of each waveform is close to zero amplitude near this point, the background noise components cause any sample close to this point that is positive in sign in one waveform to be just as likely to have a negative value in the next, which drives the correlation closer to zero in this region.

Based on the information obtained from these experiments, a correlation window of 10 ms to 24 ms was chosen as it provided a good level of correlation, and was resistant to any shifts in peak latency with stimulus intensity or maturation.

2.8 Safety

Safety of the subject must always be a primary consideration in any experimental or clinical situation. The BIO Amp used in the initial stage of experimentation contained optocoupled components that allowed the subject to be electrically isolated from mains voltage

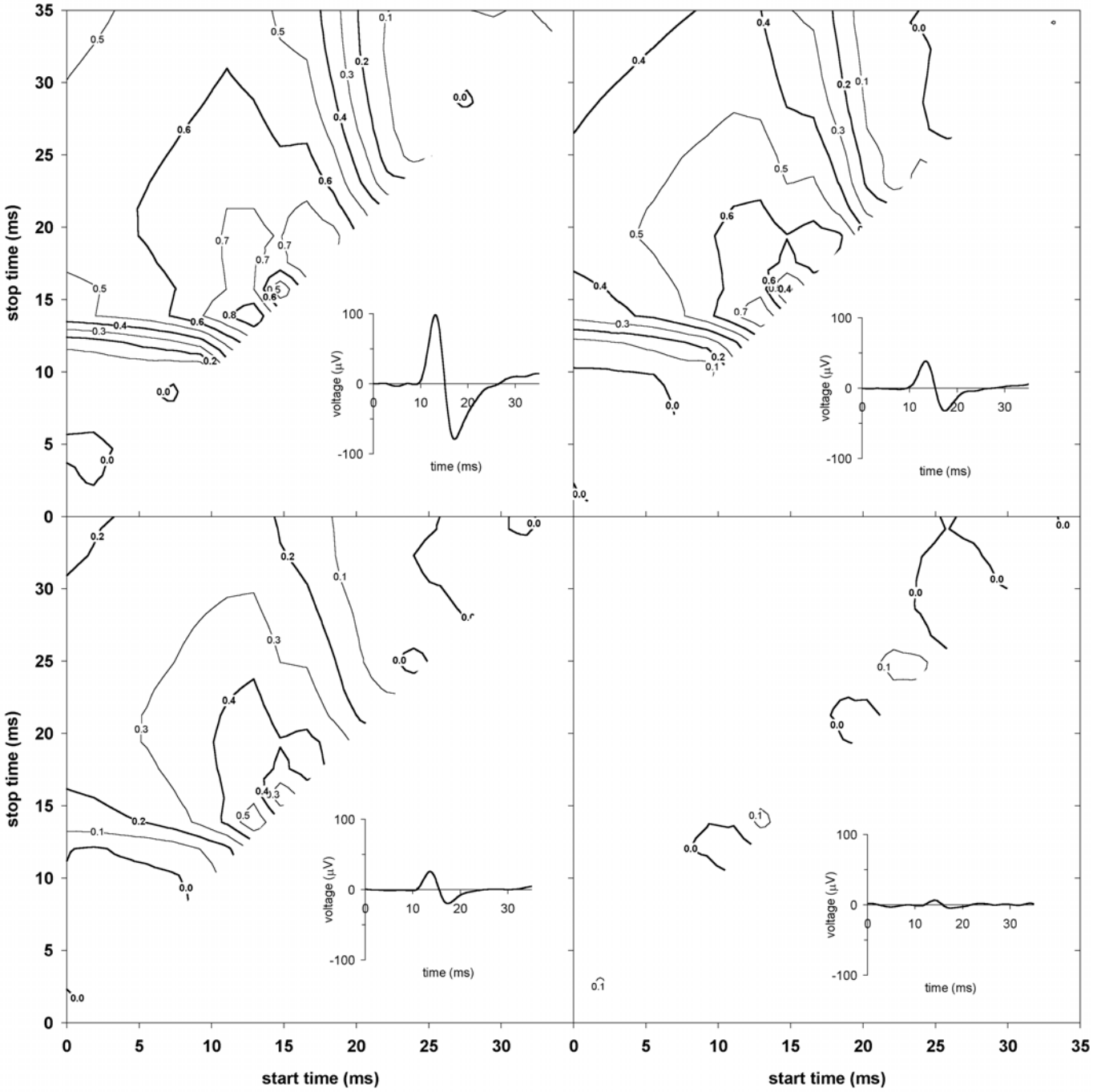

Figure 2.9: Correlation contour maps showing the average correlation value calculated using every possible window start and stop times (in millisecond intervals) for 180 sampled waveforms. The waveform averaged from these 180 raw waveforms is also shown in each plot. Stimulus levels of 45 dB, 35 dB, 25 dB and 15 dB SL were used (shown in the plots at the top-right, top-left, bottom-right, and bottom-left respectively). For each of the stimulus levels, the maximal correlation window was found to be from 12.5 ms to 14 ms. The gaze of the subject was shifted horizontally to the right during recording of the waveforms.

during recording, and provided protection against power surges of up to 3.75 kV_{rms}. In the portable equipment set-up, complete electrical isolation of the subject was provided by the FM radio link, described below.

2.9 Portable equipment set-up

In the portable set-up shown in Figure 2.1, the BIO Amp was replaced by a small, battery powered FM transmitter, which acted as both a filter and an amplifier, and also served to electrically isolate the subject from the recording apparatus. The FM transmitter is discussed in detail in Section 3.11.

A DTR-2000 Digital Audio Tape (DAT) recorder (Denon Corp., Japan) was used to record the output of the FM receiver and the trigger pulse from the stimulator onto separate audio channels, to enable off-line analysis of the subject's responses. The recorded trigger pulse was used to synchronise the data acquisition by LabVIEW or any other signal analysis package.

The DAT recorder itself had a pass-band of 2 Hz to 22 kHz, and a flat frequency-response over this range. This pass-band and frequency response cannot be matched by conventional amplitude-modulated tape-recorders.

The ability of the DAT recorder to accurately record and reproducibly playback the PAMR waveform data was confirmed in a series of calibration experiments. A set of 2000 consecutive PAMR waveforms were sampled and analysed on-line by LabVIEW while being simultaneously recorded to DAT. Once the LabVIEW analysis was completed, the waveforms that were recorded to DAT were played back and analysed by LabVIEW in the same way. Other than changes in waveform amplitude due to the gain of the DAT recorder, no other differences in the waveforms from the two sources were observed.

2.10 Electrical Artefacts

Artefacts and interference caused by electrical sources are common problems in electrophysiological measurement. In this project, electrical interference from fluorescent light sources and computer monitors in close proximity to the recording electrodes was frequently observed. While this was reduced to an extent by filtering, it was also controlled for during testing by either turning off the lights and monitors in question, or by moving the subject a distance from the monitor where this interference was minimal.

While the BIO Amp filters were able to reduce the degree to which electrical interference picked up by the electrodes was transmitted through to the recording apparatus, other strategies had to be employed in order to minimise electrical artefacts that occurred *after* this filtering and amplification stage (i.e. between the BIO Amp and the Lab-PC+ data acquisition card).

For example, a computer located about 3m away from the subject was found to be the cause of a high frequency electrical interference that entered the power supply of the test equipment via the mains power supply. This interference was successfully reduced by the simple installation of a Continuous Power Filter Spike Arrester Model 350 (Australian Protective Electronics, Australia) to the power supply of the computer.

A more problematic electrical artefact was discovered when it was noticed that the correlation value (calculated by the Correlation VI) would not fall below 0.2, even when there was no PAMR present. Examination of surrounding electrical equipment revealed that the source of the raised correlation level was the stimulus box trigger pulse, which had been increased in both width and amplitude in order to improve the ability of the waveform capture software to trigger from this input. However, as the Lab-PC+ inputs for the signal waveform

and the trigger pulse were located next to each other on a terminal block, the trigger pulse was of large enough amplitude and width that there was capacitive pick-up between the two across the terminal block and parallel cable joining the terminal block to the Lab PC+ card, creating a DC pedestal in the signal waveform. To eliminate this artefact, the trigger pulse was attenuated, and a 1 μF coupling capacitor and parallel shunt resistance to ground were added to the signal waveform inputs to further AC couple the signal. This fixed the correlation problem and, although the trigger pulse was attenuated, it was still of sufficient width to enable successful triggering by the LabVIEW software. As a further precaution against DC offsets, a VI was written that subtracted the mean of the sampled waveform array. By ensuring the mean value of the waveform was zero, any DC offset was, by definition, removed.

2.11 PAMR threshold tracking using a stimulus attenuation level feedback loop

A series of experiments was carried out in which the attenuation level of the sound stimulus was automatically adjusted to maintain a constant correlation level. The initial aim of these experiments was to use the software to determine the sound level threshold at which the PAMR could be first detected (the PAMR threshold). The same technique, using a variation of the same software, was later applied to the automatic tracking of the compound action potential (CAP) threshold in the guinea pig.

In the custom built electronics (described in Section 2.2), the stimulus attenuation level could be adjusted manually using a potentiometer, or by using a voltage-controlled attenuator (VCA) circuit (housed within the stimulation circuitry) that smoothly and automatically ramped the attenuation up or down, depending on the presence or absence of a digital TTL (transistor-transistor logic) voltage level delivered to the attenuator circuit from one of the digital outputs of the Lab-PC+ card.

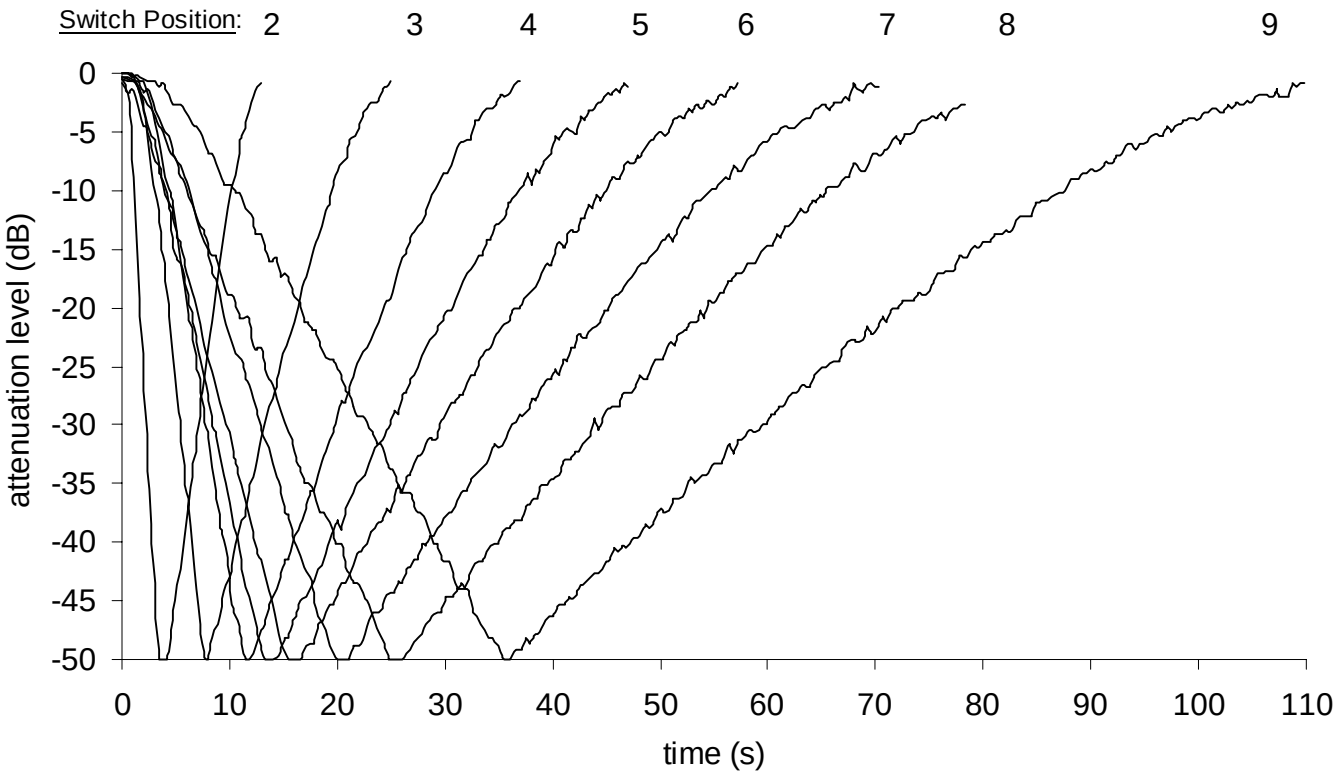

Figure 2.10: The ramping rate of the voltage-controlled attenuator could be adjusted using a multi-position switch on the stimulus box. The speed with which the attenuation level (in dB) changed is shown above for a number of switch positions.

The speed with which the attenuation level was ramped upwards or downwards could be chosen from 9 pre-set switch positions. The first switch position gave an "infinite" ramping rate, in that the TTL voltage level determined whether the sound stimulus was at either maximum attenuation or minimum attenuation. The ramping characteristics of the other eight switch positions are shown in Figure 2.10. The ramping rates were uniformly asymmetric: the attenuation level increased at approximately 2.5 times the rate that it decreased (± 10%).

The VCA circuit produced a DC voltage output proportional to the decibel attenuation of the stimulus signal, which was used to monitor the level of attenuation provided by the circuit. The DC voltage was calibrated against the corresponding peak-to-peak height of the

click stimulus square-wave pulse, using an oscilloscope. As there was a logarithmic relationship between peak-to-peak pulse height and DC attenuation voltage, the peak-to-peak heights of the waveforms were converted to an equivalent attenuation level in decibels, and linear regression used to fit an attenuation function to this data. The slope of this curve indicated that the DC output of the attenuation circuit dropped by 10.8 mV per dB of attenuation. Using this function, a VI was written to convert the DC voltage into an attenuation level in decibels that could be monitored by the front panel VI (see Appendix One).

This feature, combined with the ability to adjust the stimulus attenuation level using the VI software, allowed a software feedback loop to be written which automatically raised or lowered the level of attenuation of the click-stimulus based on the whether the average correlation level between consecutive waveforms was above or below a certain desired level. This automatic technique is a variation of the Békésy audiometric method (von Békésy, 1947), in which a human subject adjusts the stimulus attenuation level based on whether they can hear the stimulus or not.

In this study, a comparison was made between the subjective click threshold (the sound level at which the subject can first hear the clicks), and the automatically detected PAMR threshold (the sound level at which the PAMR is first detected by the correlation method).

The stimulus SPL was adjusted manually by the subject using a potentiometer on the VCA box. Once the threshold was found, the level of attenuation was read from a meter on the front panel VI. Automatic PAMR threshold detection was then carried out using the VI developed for the task. The present automated technique calculated the correlation level between successive PAMR waveforms over the 10 to 16 ms post-stimulus time window. An average correlation level of 0.2 over 5 stimulus presentations was decided upon as the

minimum level of correlation required to indicate the presence of the PAMR. The 0.2 average correlation level was found to provide the best estimate of PAMR threshold: an average level of 0.1 was too commonly achieved during random fluctuations, whereas a level of 0.4 was found to overestimate the stimulus intensity required to visualise the PAMR.

Having chosen this detection criterion, if the PAMR was deemed to be not present, a TTL output from the Lab-PC+ card was turned on, thus causing the attenuation level to decrease. As the stimulus became more intense, the PAMR increased in amplitude relative to the background noise, which was reflected by the increase in correlation level above 0.2. When the average correlation level for 5 stimulus presentations rose above 0.2, the TTL output from the Lab-PC+ card was turned off, and the attenuation progressively became greater, so that the sound stimulus was not sufficiently intense to elicit the PAMR. This procedure was repeated with two other subjects under a number of experimental conditions.

With each stimulus presentation, the output from the VI, which included the current attenuation level (in dB), was recorded to an output file for later analysis. The results for these experiments are shown in Section 3.12. The methods, results and discussion for the CAP threshold tracking experiments using the same software are presented in Section 3.13.

RESULTS

3.1 Input/output function of the PAMR

The input/output function of a response plots the way in which the response amplitude changes with increased sound level of the stimulus. This has been studied previously in the PAMR by a number of researchers (Yoshie et al., 1969; Gibson, 1975; Buffin et al., 1977; Patuzzi et al., unpublished). The input/output function recorded by Yoshie et al. (1969) was shown in Figure 1.9 of the Introduction.

In the present study, the peak-to-peak amplitude and peak latency of the PAMR was recorded from the right PAM of one subject at a number of stimulus sound levels. Also measured during this period were the correlation level between successive PAMR waveforms, and the background EMG of the PAM.

Shown in Figure 3.1.1 are the averaged PAMR waveforms (n = 200) evoked using click stimuli, with sound levels increasing from 0 dB SL to 80 dB SL in 10 dB increments. It can be seen that, although small, the PAMR was present at stimulus levels just 10 dB above threshold. With increasing stimulus level, the peak-to-peak amplitude of the response increased monotonically over the 80 dB range, from 6.8 μV (± 1.3 μV) at 10 dB SL to 127.3 μV pp (± 4.5 μV) at 80 dB SL. The latency of the peaks of the PAMR were observed to decrease with increasing stimulus level. The average first-peak latency of the response decreased from 15.5 ms at 10 dB SL to 13.2 ms at 80 dB SL. The second-peak latency decreased from 21.9 ms at 10 dB SL to 19.12 ms at 80 dB SL. The relationship between stimulus level and peak-to-peak amplitude is shown in Figure 3.1.2, while Figure 3.1.3 shows the decrease in latency of both peaks of the PAMR with increasing stimulus level.

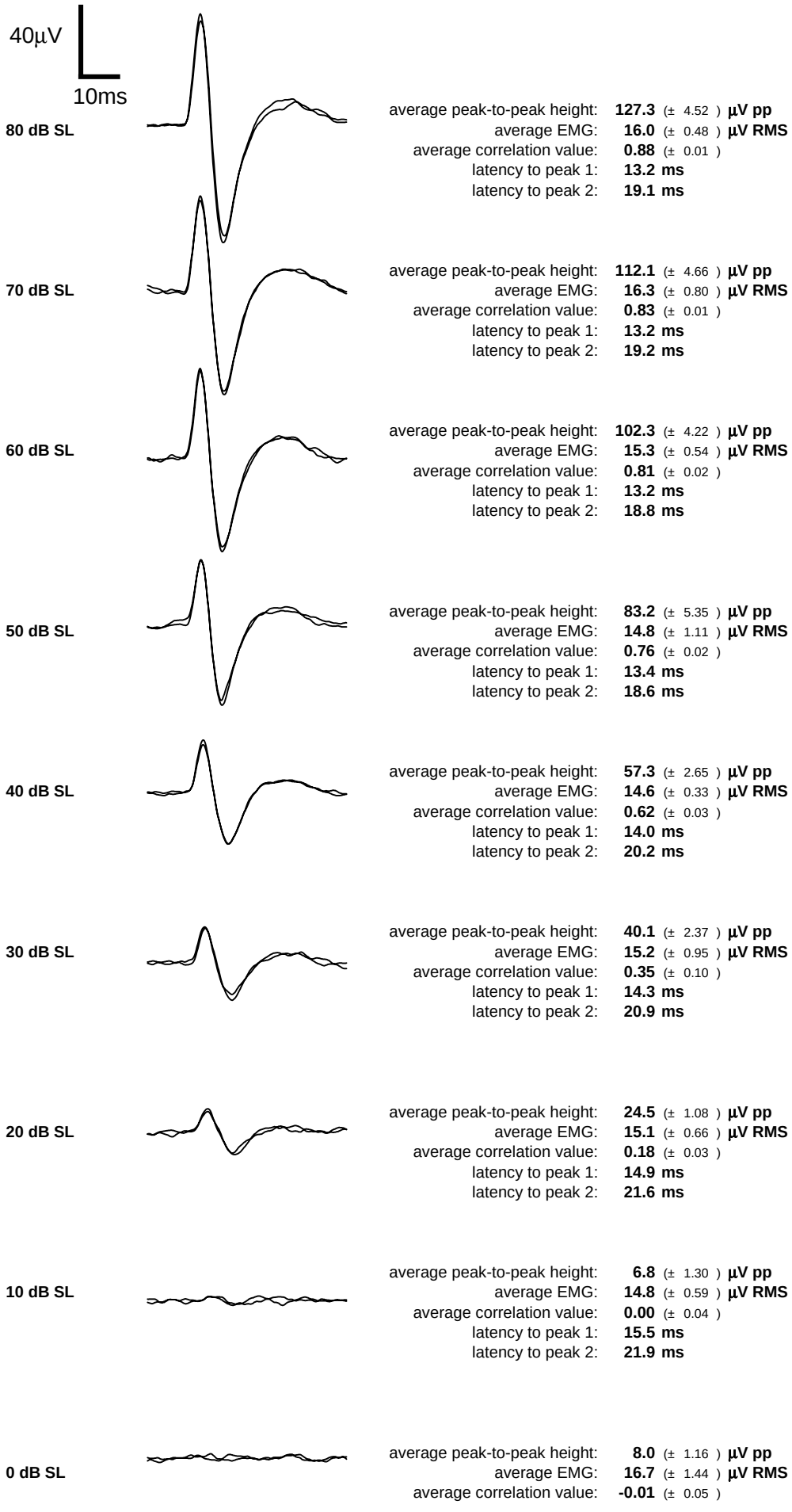

Figure 3.1.1: Averaged PAMR waveforms (n = 250 per trace) from one subject showing the change in response amplitude and latency with increasing stimulus sound level. (filter bandwidth: 1 Hz to 500 Hz).

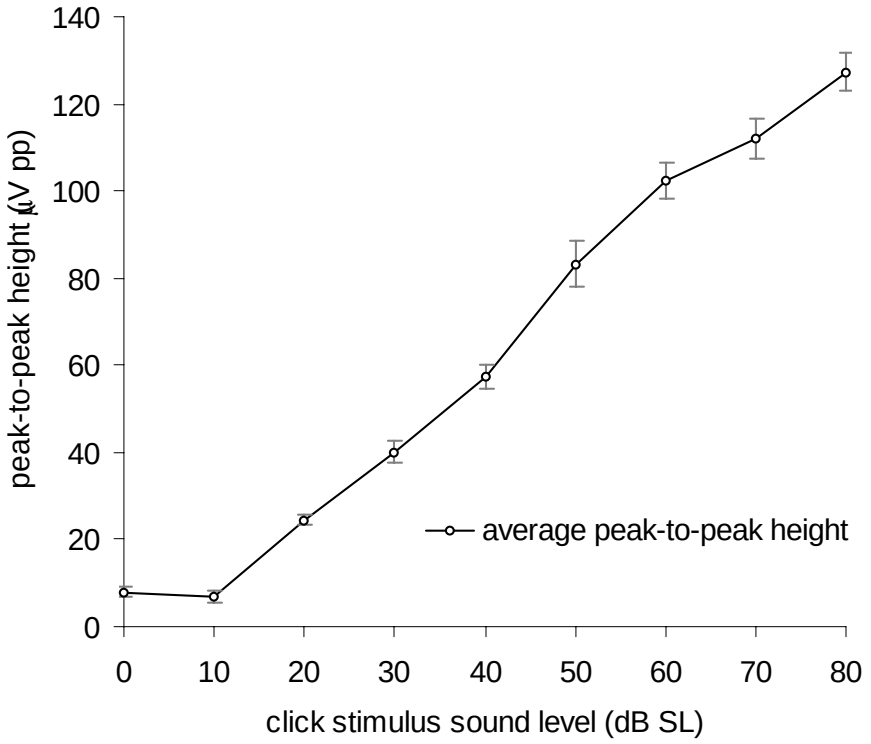

Figure 3.1.2: The relationship between the click stimulus sound level (dB) and the peak-to-peak amplitude of the PAMR. Averaged measurements (n = 500) from one subject are shown.

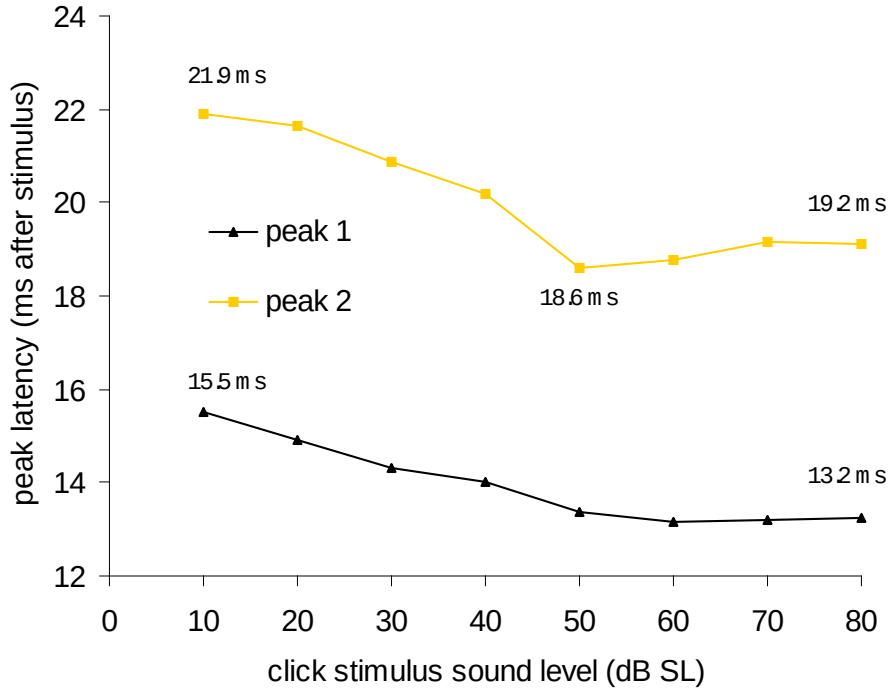

Figure 3.1.3: The relationship between the click stimulus sound level (dB) and the latency of the first and second peaks of the PAMR. Averaged measurements (n = 500) from one subject are shown.

Discussion

Our findings regarding the decrease in response latency with increasing stimulus sound level are consistent with those of Yoshie et al. (1969), Gibson (1975), Buffin et al. (1977) and Patuzzi et al. (unpublished). Yoshie et al. reported a decrease in latency of around 3 to 5 ms with high stimulus sound levels. Our results regarding the increase in response amplitude with increasing sound level are similar to those previously reported, however, the input-output function shown in Figure 3.1.2 has a more linear appearance (similar to that reported by Buffin et al., 1977) than the "exponential" shaped curves reported by Yoshie et al. (1969) and Gibson (1975). Our results are from one subject only, and so this variation may be due to individual differences among subjects.

High sound-level stimuli cause a greater degree of synchronous firing in the afferent neurones of the cochlea than is caused by lower sound-level stimuli, and so evoke a greater amplitude response (Hall, 1992). The decrease in response latency with increasing sound level is presumably due to the excitatory post-synaptic potential (EPSP) in one or more of the neurones in the neural pathway reaching a firing threshold sooner with higher-intensity stimuli than with low-intensity stimuli, and so producing action potentials in the auditory nerve earlier. Also, the delays involved in synaptic transmission are less with higher-intensity stimuli than with low-intensity stimuli (Hall, 1992).

3.2 The effect of tone-burst frequency on the PAMR

While clicks are more commonly used in testing the PAMR, it is possible to use tone-bursts to obtain some indication of the functioning of the cochlea at different frequencies. The responses obtained with tone-bursts have been found to be of lower amplitude that those obtained using click stimuli (Douek et al., 1973; Gibson, 1975). Cody et al. (1969) tested the PAMR using *only* tone-bursts, and found that the responses obtained with frequencies of 500 Hz, 1 kHz and 2 kHz, were similar to each other, whereas Patuzzi et al. found that the peak-to-peak amplitude of the response varied with different tone-burst frequencies (as shown in Figure 1.8 of Section 1.7.1b).

In the present study, a series of experiments were carried out in which the PAMR was evoked using a range of tone-burst frequencies and stimulus intensities. Pure tones with frequencies of 500 Hz, 1 kHz, 2 kHz, 4 kHz, 8 kHz, 16 kHz and 32 kHz were generated by a Hewlett Packard HP3325a Synthesizer/Function Generator, and gated externally to produce 38 ms tone-bursts with a rise-time of 1 ms, at a rate of 5/second. The tone-bursts were not phase-locked to the gating function. These tone-bursts were recorded to one channel of a digital audio tape (DAT) using a Denon DTR-2000 DAT recorder (Nippon Columbia Corp., Tokyo, Japan). A trigger pulse was recorded on the other channel of the DAT to synchronise the LabVIEW data acquisition with the onset of the tone-burst. Because the DAT recorder had a pass-band of 2 Hz to 22 kHz, the 32 kHz tone-burst was not, itself, recorded onto the DAT, but was used as an internal control for any electrical artefacts produced by the gating of the tone-burst. Because the anti-aliasing filter on the input of the DAT recorder had filtered out everything above 22 kHz (as proved by visual inspection of the tone-burst waveform on an oscilloscope), any response evoked during the 32 kHz tone-burst section of the DAT at a

particular attenuation level would be caused by a gate artefact alone. This allowed the influence of any gate artefact on the responses evoked by other frequencies at the same level of stimulus attenuation to be assessed.

The tone-bursts were played back using a Sony TCD-D7 Tape-Corder (Sony Corp., Japan). The output from the DAT player was amplified by a Realistic SA150 Integrated Stereo Amplifier (Tandy Corp., Japan), attenuated using a Hewlett Packard 350D resistive attenuator, and delivered binaurally to the subject via a pair of Telephonics TDH-39 headphones. Any filtering of the tone-burst signal in the playback chain was compensated for by determining the sound level of the stimuli in decibels relative to the subjective threshold of the subject.

Shown in Figure 3.2.1 are the responses obtained using tone-burst frequencies of 500 Hz, 1 kHz, 2 kHz, 4 kHz, 8 kHz, and 16 kHz at stimulus levels from threshold (0 dB SL) to 80 dB SL in 10 dB steps. To illustrate the reproducibility of the data, two averaged responses (n = 100) are overlayed for each frequency/intensity combination. Shown in Figure 3.2.2 is the same data as that shown in Figure 3.2.1, but with the waveforms scaled to the same peak-to-peak amplitude.

The data show that the PAMR was able to be evoked using stimulus levels of 40 dB or less at all frequencies above 1 kHz, and using a stimulus level of 50 dB at 500 Hz. The PAMR was most sensitive to tone-bursts at 2 kHz, requiring sound levels only 20 dB above subjective threshold to obtain a response clearly distinguishable from the background noise. The visual detection PAMR audiogram is shown in Figure 3.2.3. Similar results to these were obtained during the same experiment performed earlier in the year on the same subject, and are plotted on the PAMR audiogram of Figure 3.2.3 for comparison. Also plotted is data from another subject, recorded by Patuzzi et al. (1995).

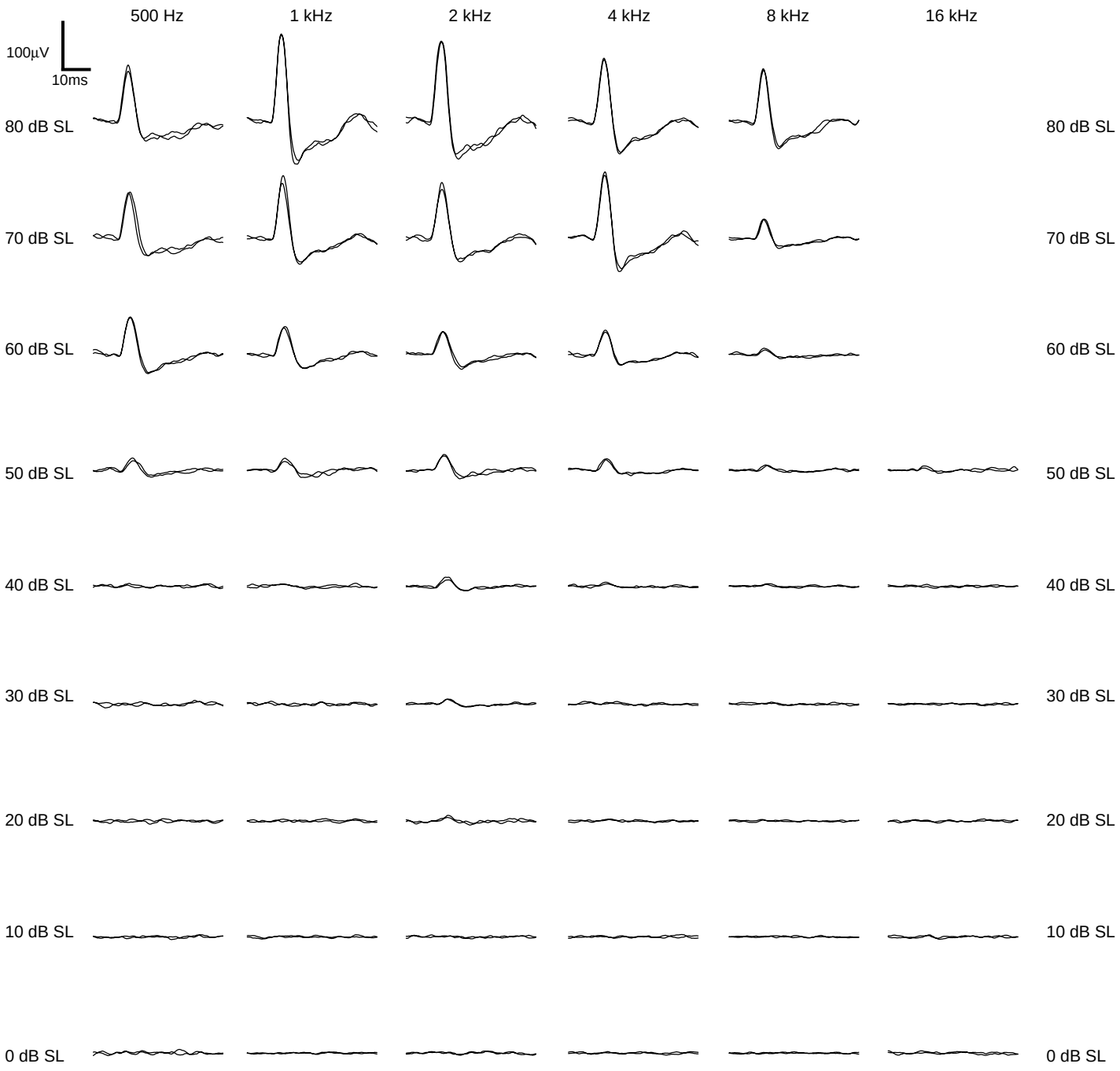

Figure 3.2.1: Averaged PAMR waveforms (n = 100 per trace) evoked obtained using tone-burst frequencies of 500 Hz, 1 kHz, 2 kHz, 4 kHz, 8 kHz, and 16 kHz at stimulus levels from threshold (0 dB SL) to 80 dB SL in 10 dB steps. (Recording bandwidth: 3 Hz - 1 kHz)

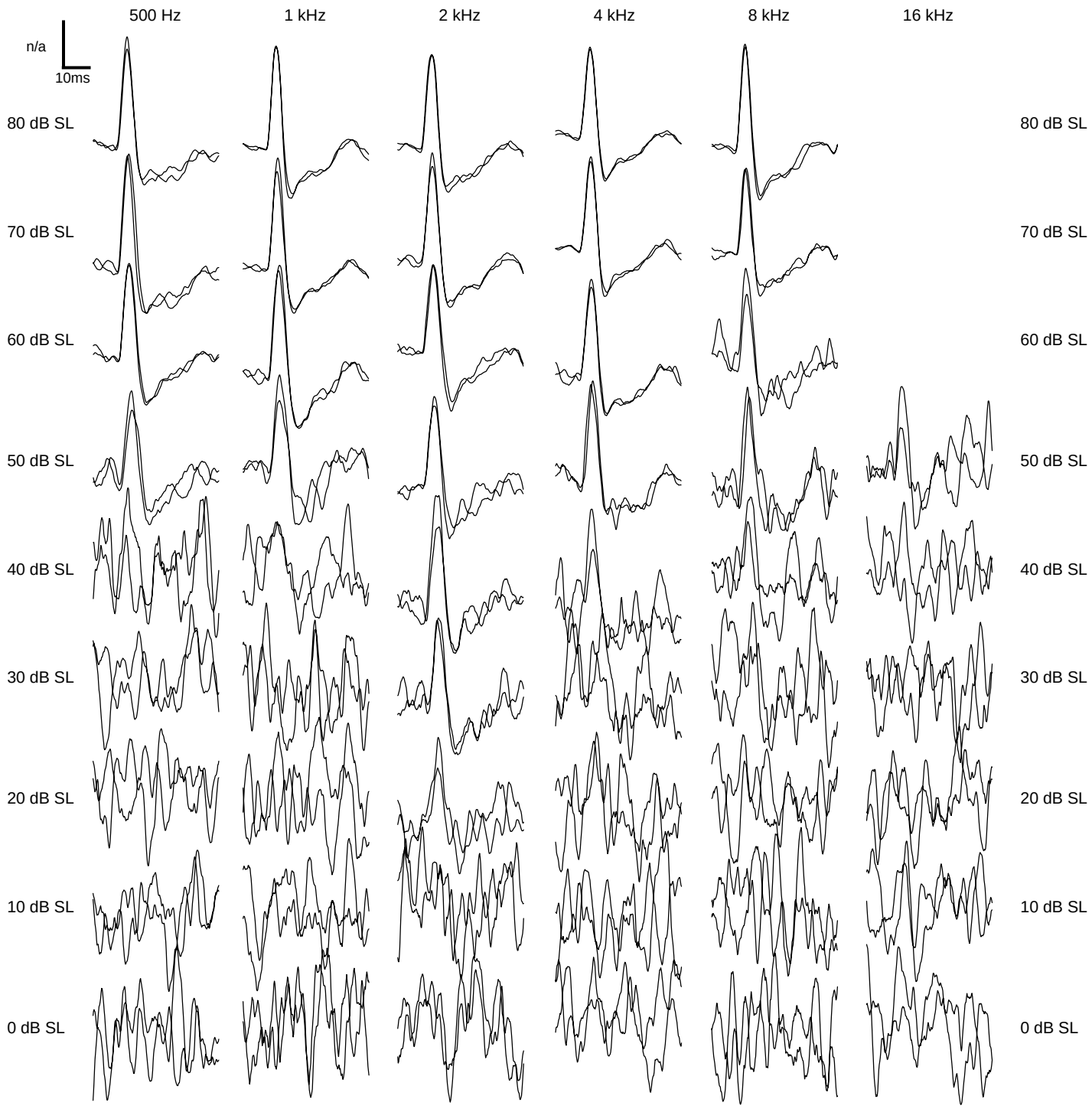

Figure 3.2.2: Averaged PAMR waveforms (n = 100 per trace) evoked obtained using tone-burst frequencies of 500 Hz, 1 kHz, 2 kHz, 4 kHz, 8 kHz, and 16 kHz at stimulus levels from threshold (0 dB SL) to 80 dB SL in 10 dB steps. The waveforms have been scaled to the same peak-to-peak amplitude to allow comparison of the shape of the waveform. (Recording bandwidth: 3 Hz - 1 kHz)

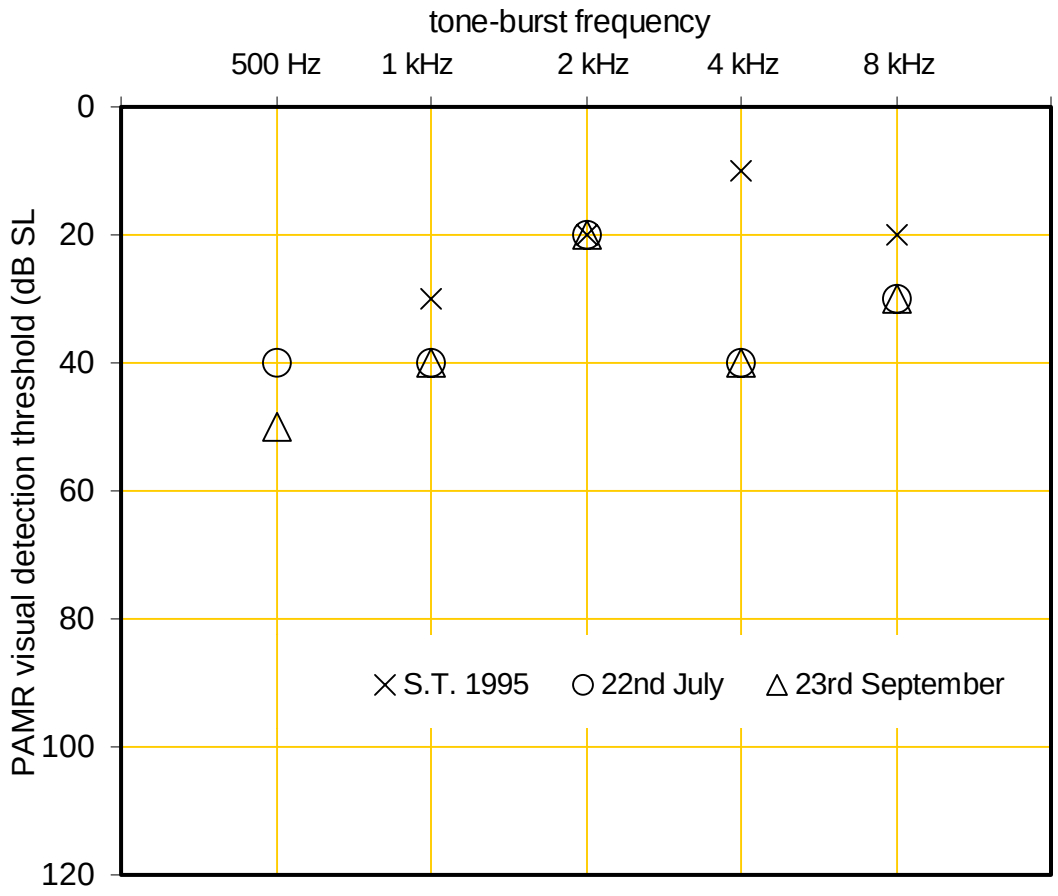

Figure 3.2.3: The visual-detection audiogram of the PAMR, showing the stimulus levels (dB above subjective threshold of the subject) required to evoke a recognisable PAMR response at different tone-burst frequencies, from 500 Hz to 8 kHz. Data from two separate experiments in this study are shown, as is data from a similar experiments carried out by Patuzzi and Thomson (1995).

Figure 3.2.4 shows the input/output function of the PAMR obtained using the different tone-burst frequencies. In this experiment, the largest peak-to-peak amplitude was obtained using 1 kHz tone-bursts at 80 dB SL. For stimulus intensities of 70 dB and below, the 8 kHz responses were of lower peak-to-peak amplitude than those obtained using frequencies of 4 kHz and below.

Attempts to evoke a response from the control (the absent 32 kHz tone-burst) section of the stimulus tape failed at all but the highest DAT output levels (at which a small PAMR, presumably, caused by the gate artefact, was observed). These high levels were not used with tone-burst frequencies between 500 Hz and 8 kHz, even at levels of up to 80 dB SL. However,

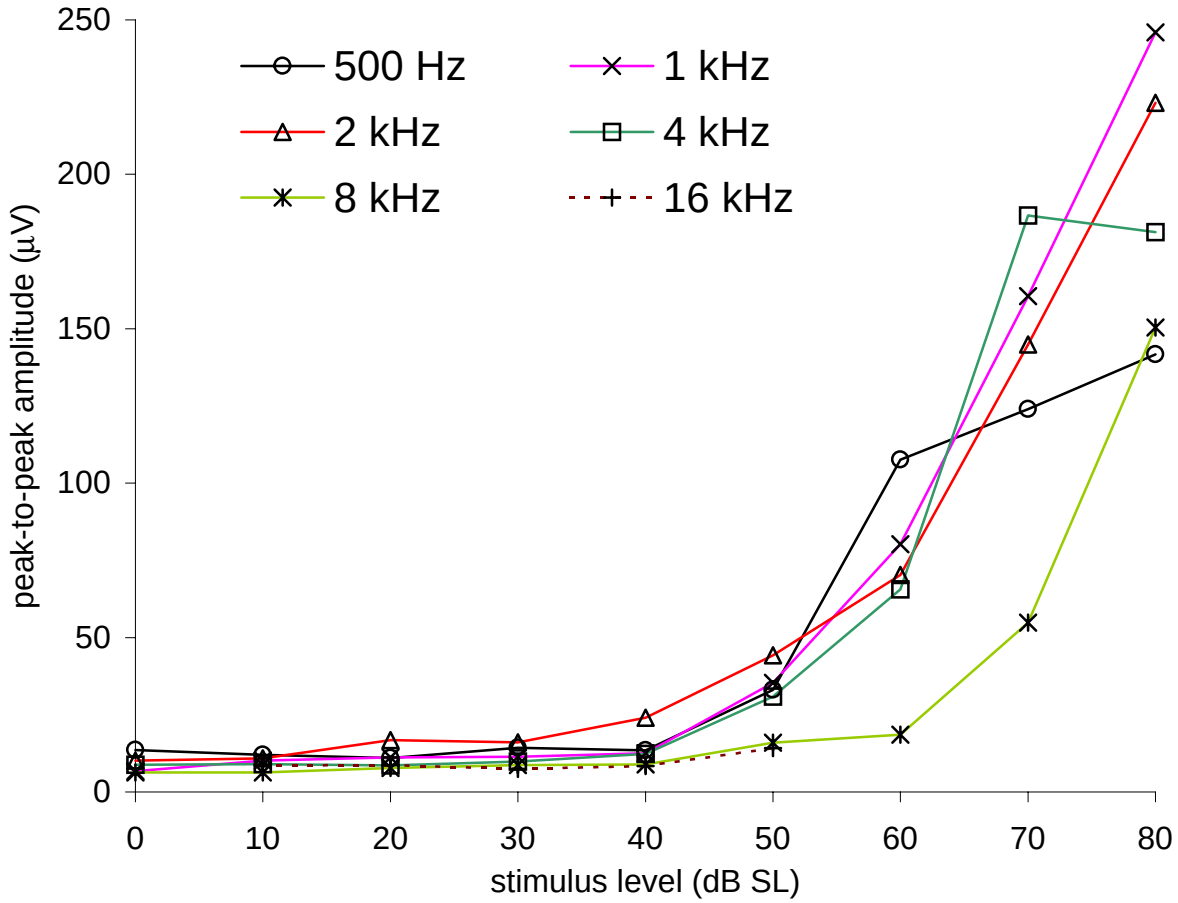

Figure 3.2.4: The input/output function of the PAMR obtained using tone-burst frequencies of 500 Hz, 1 kHz, 2 kHz, 4 kHz, 8 kHz and 16 kHz, at stimulus levels from threshold (0 dB SL) to 80 dB SL in 10 dB increments.

they were used with the 16 kHz tone-bursts above 50 dB SL, and so the results obtained for 16 kHz tone-bursts of 60 dB, 70 dB and 80 dB SL were not included in Figures 3.2.1 and 3.2.2.

Discussion

Our data indicate that, in this subject at least, it is possible to evoke the PAMR using tone-bursts of frequencies up to 8 kHz, and possibly higher. This result is important from an audiometric testing point of view, as it indicates that the PAMR has the potential to be used as an objective hearing test that can give frequency-specific information about the hearing acuity of the subject. Conventional objective screening methods such as ABR and TEOAEs normally only use click stimuli, although they can also be evoked with tone-bursts.

For most frequencies (except 500 Hz on one occasion), a response was obtainable using a stimulus level of 40 dB HL[1] or less. For comparison, a "pass" result in clinical ABR screening is often given if a response is obtained using click stimuli at 30 to 40 dB HL (Oudesluys-Murphy et al., 1996; Hall, 1992). For subjective pure-tone audiometric tests, a subject can often pass an examination if he or she has hearing losses not greater than 25 dB HL.

Gibson (1975) has stated that, in his experience, click stimuli had to be employed in clinical situations "*otherwise the responses are disappointing and inconsistent*". He found that higher-frequency tone-burst stimuli did produce consistent results, but "*it was unnecessary to use them clinically since these higher frequencies were well enough presented by the filtered*

[1] Because the subject had normal hearing [pure-tone audiometric thresholds of between 0 dB HL and –5 dB HL for frequencies between 125 Hz and 8 kHz], the assumption was made that, in his case, sensation level (SL) and hearing level (HL) were equivalent.

clicks". The results obtained from this particular subject were quite consistent, as demonstrated by the two sets of data plotted in Figures 3.2.1 and 3.2.3. The responses obtained using tone-bursts of 500 Hz and 1 kHz were just as consistent as those obtained with higher frequencies. However, because these results are from one subject only, they are not necessarily indicative of results that would be obtained across a larger population.

3.3 Distribution of the PAMR response

The distribution of the PAMR around the post-auricular area has been studied previously by many researchers (Yoshie et al., 1969; Picton et al., 1974; Streletz et al., 1977; Buffin et al., 1977). The results of Yoshie et al. (1969) and Buffin et al. (1977) were shown in Figure 1.12 of Section 1.7.9.

In the present study, the distribution of the response over the post-auricular area and the dorsal surface of the pinna of one subject was studied using an array of 12 small electrodes. Averaged responses (n = 900 traces per average) from these 12 active electrode locations were recorded using a forehead reference electrode and a recording bandwidth of 10 Hz to 200 Hz (with a 50 Hz notch filter). These results are shown in Figure 3.3.1.

In this particular subject, the PAMR was found to have the largest amplitude (108 μV pp) when recorded from directly over the body of the post-auricular muscle (electrode location PAM 5 on Figure 3.3.1). The response was found to have decreased amplitude when recorded further away from the main body of the muscle, consistent with resistive attenuation of the electrical potentials by the skin and tissue. As shown in Figure 3.3.1, an inverted version of the PAMR waveform was found on the dorsal surface of the pinna. The largest of these pinna waveforms had an amplitude of 48 μV pp, recorded from electrode location Pinna 2. There was also a latency shift of 0.8 ms associated with the inverted waveform. Figure 3.3.2 shows the averaged response recorded from electrode location "PAM 5" and superimposed with the response recorded from location "Pinna 2". The pinna waveform has been inverted so as to allow more direct comparison of the differences in latency between the two waveforms.

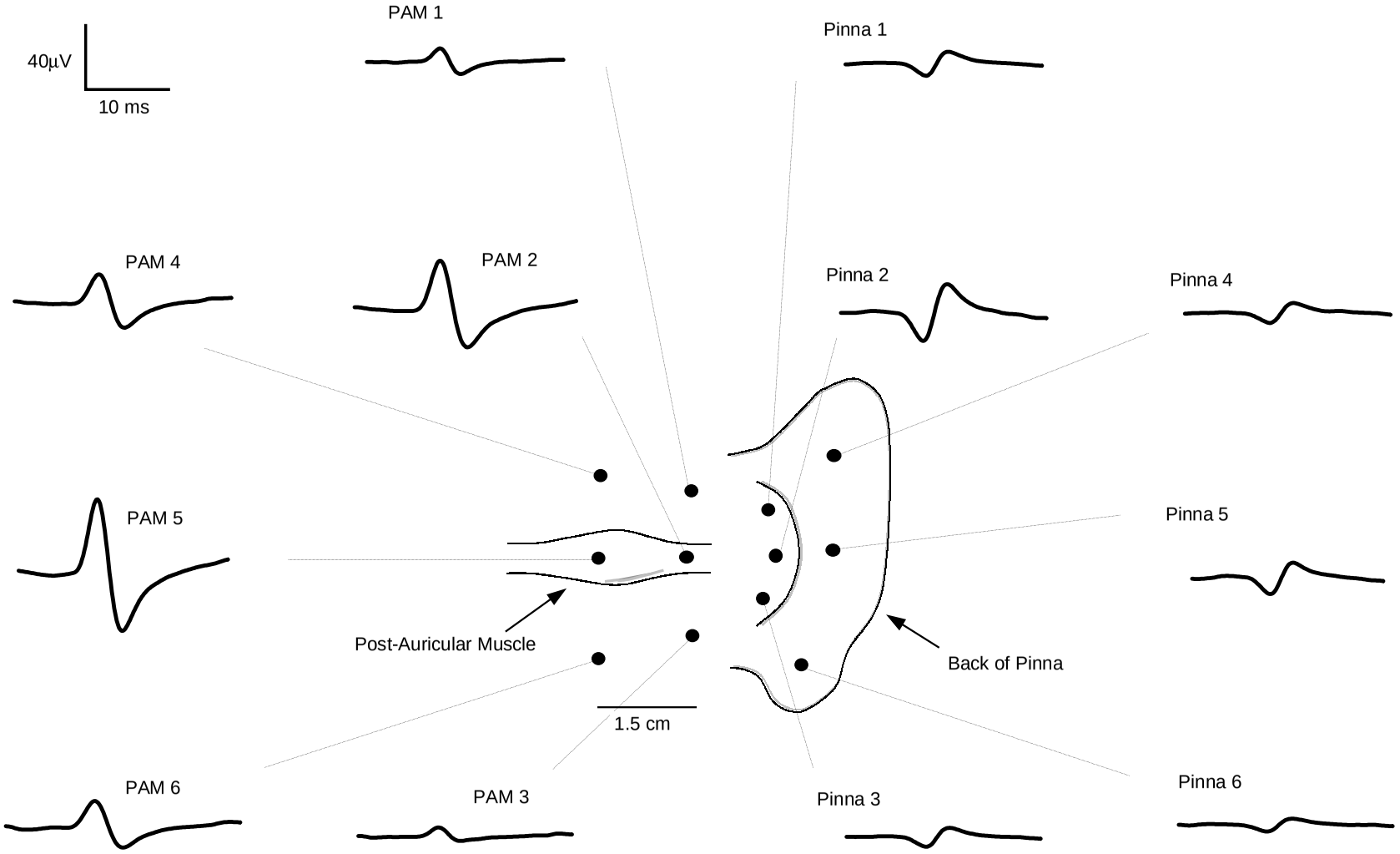

Figure 3.3.1: Averaged PAMR waveforms (n = 900) recorded using 12 different active electrode locations over the post-auricular area and the dorsal surface of the pinna. Note that the PAMR waveforms recorded from the pinna are inverted relative to those recorded from the PAM. (45 dB SL clicks. Reference electrode: forehead. Recording bandwidth: 10 Hz - 200 Hz, 50 Hz notch filter.)

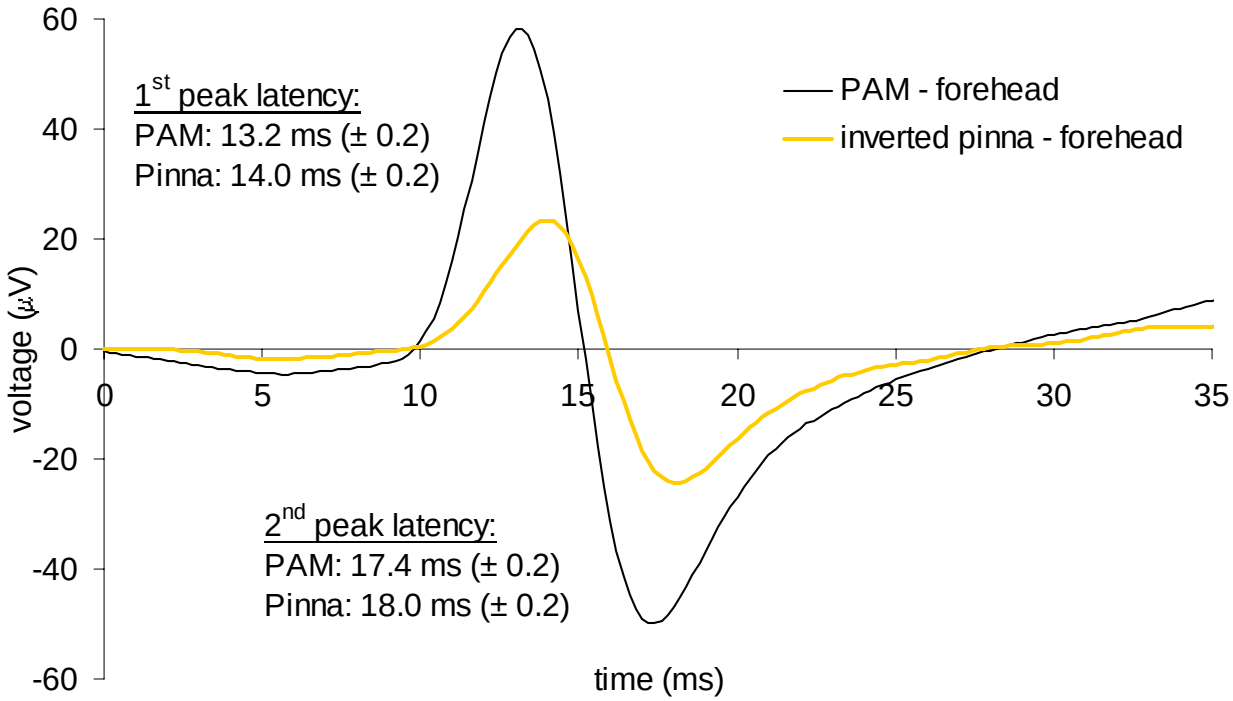

Figure 3.3.2: Comparison of the maximal responses recorded from the PAM and the pinna. The pinna waveform has been inverted to emphasise the differences in latency between the two waveforms. (Each trace is an average of 900 waveforms evoked by 45 dB SL clicks. Reference electrode location: forehead. Recording bandwidth: 10 Hz – 200 Hz, 50 Hz notch filter).

Discussion

Our results concerning the inversion of the PAMR waveform on the pinna are consistent with those of Streletz et al. (1977), who measured the distribution of the PAMR in one subject, and reported that "*a large negative potential with a peak latency of 14 ms is present in the post-auricular region*", and that "*a positive potential of the same latency is recorded with lesser amplitude from the auricle and earlobe*". With regard to the PAMR inversion on pinna, Streletz et al. (1977) stated that "*this may be explained by the occurrence of a compound muscle action potential arising in the post-auricular muscles which spreads toward its tendinous insertion on the ear structures (Katz and Miledi, 1965).*"

Katz and Miledi (1965) carried out a series of experiments on the propagation of electrical activity in single muscle fibres, and found that the extracellular potentials generated in response to intracellular electrical stimulation of the muscle were predominantly *negative-going* when recorded above the body of the muscle, but were predominantly *positive-going* when recorded above the myotendinous junction (the point at the end of the muscle where the body of the muscle attaches to the tendon). Their results are shown in Figure 3.3.3 below.

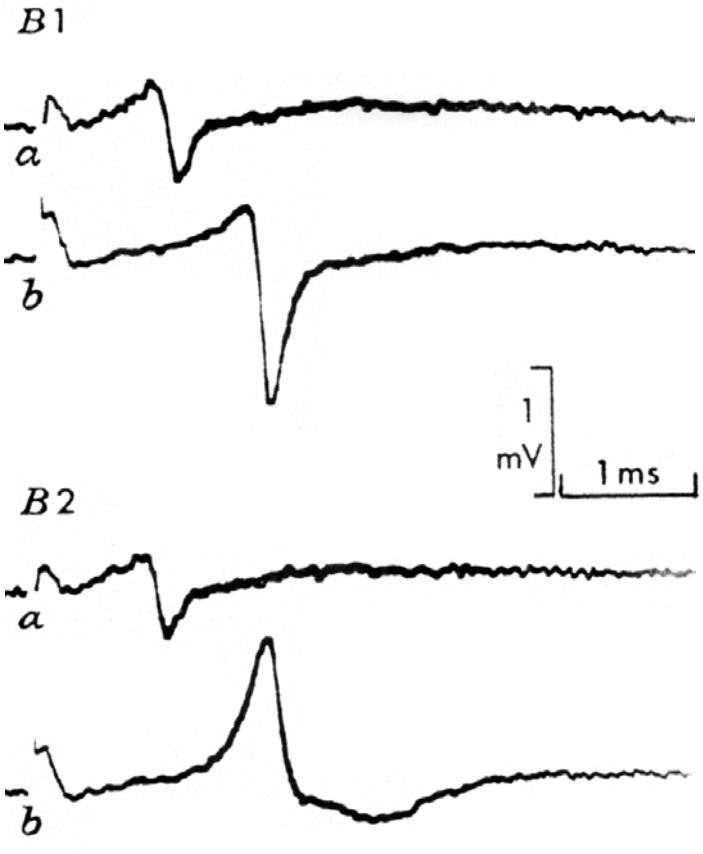

Figure 3.3.3: The extracellular "spikes" recorded by Katz and Miledi in response to intracellular electrical stimulation of a single muscle fibre. Trace *a* in both B1 and B2 is the recording from an extracellular electrode placed 1000 μm from the myotendinous junction on the surface of a single muscle fibre. Trace *b* is the recording made 250 μm from the junction (B1) and a 0 μm from the junction (B2). Note that while the spike in trace *b* of B1 is predominantly negative-going, the spike in trace *b* of B2 is predominantly positive-going. (adapted from Katz and Miledi, 1965).

The tendinous aponeurotic end of the post-auricular muscle inserts into a cartilaginous ridge (called the "ponticulus") on the cartilage of the pinna (Feneis, 1994), and it is therefore likely that the inverted PAMR waveform recorded from the pinna is the result of conduction of the predominantly positive-going extracellular potentials from the tendinous insertion of the PAM to the pinna (Streletz et al., 1977). Although this inversion was *demonstrated* by Katz and Miledi, it is not *explained*.

Because the PAM and pinna waveforms were inverted relative to each other, but were otherwise similar in shape, the PAM and pinna locations that gave the largest response amplitudes were used for differential recording of the PAMR, as discussed in Section 2.3. When recorded from these locations, the peak-to-peak amplitude of the PAMR was larger (155 μV pp) than that recorded from the PAM with a forehead reference (105 μV pp). This is shown in Figure 3.3.4.

There has been some discussion in the literature with regard to the relative advantages and disadvantages of using an "active" reference location, such as the pinna, in recording evoked responses (Picton et al., 1974; Wolpaw et al., 1982). Although we found a very slight latency difference between waveforms recorded with a forehead reference and those recorded with a pinna reference (approximately 0.2 ms), this disadvantage was, in our opinion, far outweighed by the many advantages gained by this electrode placement, including an improved signal-to-noise ratio (as described in Section 3.8), more convenient placement of the electrode pairs (as described in Section 2.3) and, as described below, the elimination of blink artefacts.

The forehead reference location the we had originally used generally lies directly above the frontalis muscle, which is electrically active during eyebrow movements and reflex blinking, and is also the source of another myogenic sonomotor reflex potential (Picton et al.,

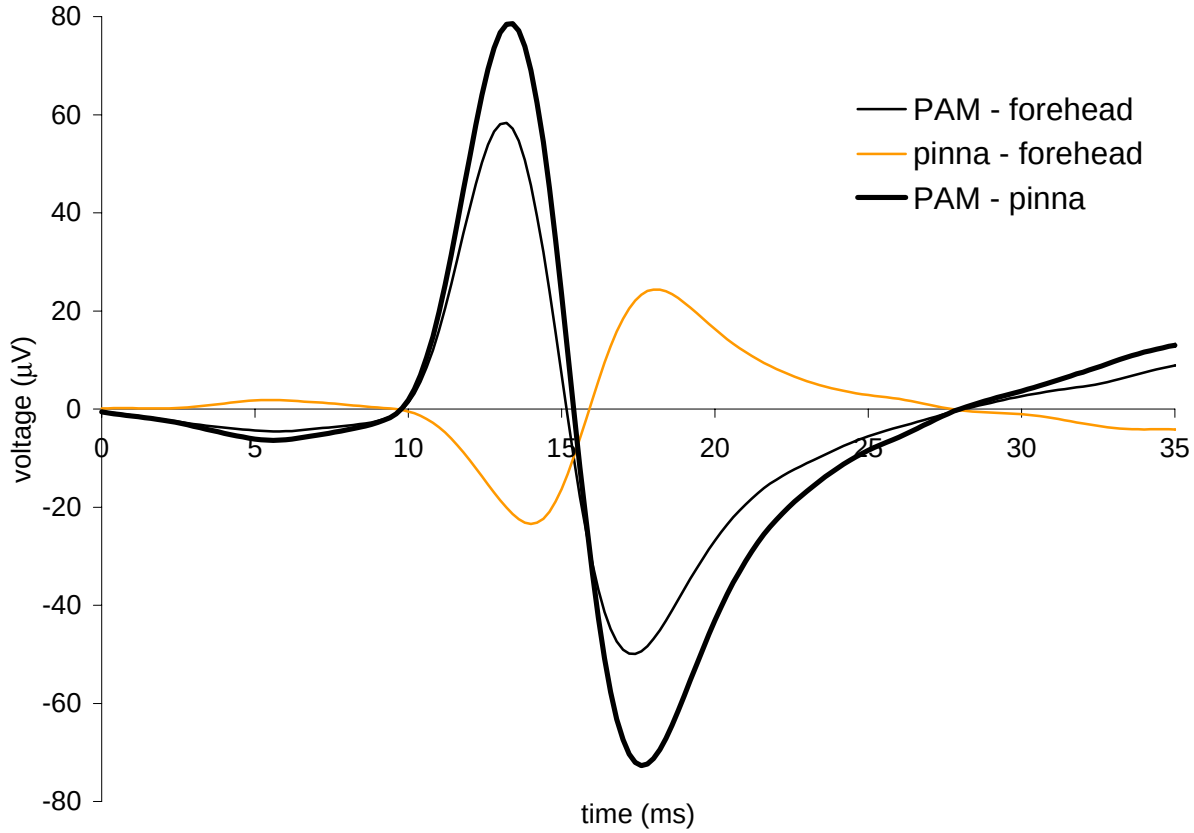

Figure 3.3.4: Averaged PAMR waveforms (n = 900) recorded from PAM location 5 with reference to the forehead (PAM - forehead), pinna location 2 with reference to the forehead (pinna - forehead), and the waveform that results when the pinna waveform is subtracted from the PAM waveform (PAM - pinna). This is equivalent to making a differential recording between the PAM and the pinna.

1974). A large electrical artefact was often observed during blinking, as shown in Figure 3.3.5 below. This artefact was particularly troublesome if it occurred during an averaging period. The pinna reference location entirely eliminated this artefact, as shown in the lower trace of Figure 3.3.5.

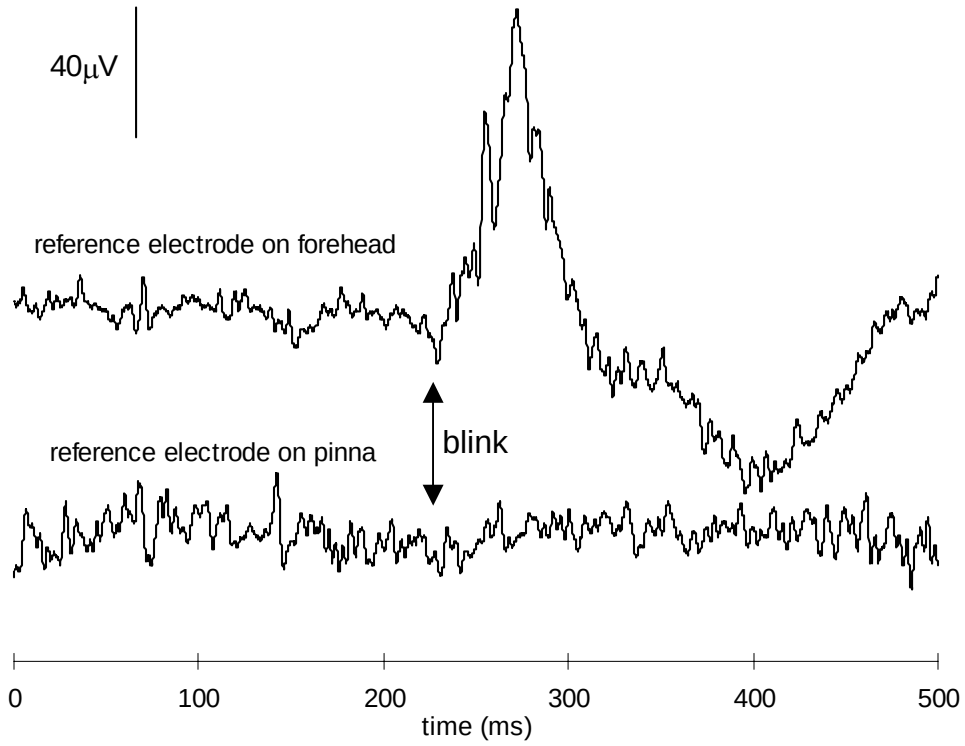

Figure 3.3.5: The reference electrode location had a substantial effect on the interference to the averaging process caused by blink artefacts. The top trace shows the electrical activity recorded from the PAMR during a single 500 ms time period, while using a forehead reference electrode. The bottom trace shows another 500 ms time period, recorded with a pinna reference electrode. Note that although the experiment involved the subject blinking at the same time in each trace, any evidence of the blink artefact is absent in the bottom trace. (filter bandwidth: 1 Hz – 200 Hz).

3.4 Tests of bilateral symmetry

As discussed in the introduction, the PAMR produces a bilateral response from monaural sound stimuli (Yoshie et al., 1969). That is, a click or tone-burst stimulus delivered to *one* ear will produce a PAMR response on *both* sides of the head. Headphones were used to deliver binaural stimuli to subjects throughout this study, but in clinical testing situations, it has been found that young children often do not tolerate headphones and so it becomes necessary to used free-field stimulation, using a loudspeaker (Gibson, 1975). Depending on the direction that the subject is facing, free-field stimuli may often be louder in one ear than the other, and so it was necessary to determine how the ear used in reception of the stimuli affects both the magnitude and latency of the evoked response. We studied this in *one* subject, comparing the two extreme cases of stimulus direction: ipsilateral-monaural stimuli (where sound is delivered to the ear on the same side of the head as the recording electrodes only) and contralateral-monaural stimuli (where sound is delivered to the ear on the opposite side of the head as the recording electrodes only). The latency and magnitude of the response waveforms were also compared to those evoked using binaural stimuli (where sound is delivered to both ears simultaneously). Our hypothesis was that the PAMR evoked by binaural stimuli was equivalent to the sum of the PAMRs evoked by sound stimuli delivered individually to the left and right ears, as is often the case with the amplitude of wave V of the ABR (Hall, 1992).

Any latency differences between the monaurally- and binaurally- evoked PAMR waveforms were also of practical importance, because the correlation measure of the PAMR, calculated over a particular “window”, has been demonstrated to be sensitive to shifts in the latencies of the peaks.

To eliminate the possibility of obtaining misleading results due to specific differences in the ear or PAM on one side of the head (for example, threshold differences), experiments carried out on the right side of the head were repeated on the left side, and the corresponding results were pooled. That is, the data from responses recorded from the right PAM to stimuli in the right ear were pooled with the data from responses recorded from the left PAM to left ear stimuli, and the data from responses recorded from the right PAM to stimuli in the left ear were pooled with the data from responses recorded from the left PAM to right ear stimuli**.**

These results are shown in Figure 3.4.1. The average (n = 2400) peak-to-peak amplitudes for the PAMRs evoked by contralateral and ipsilateral stimuli were 80 μV and 72 μV respectively. The peak-to-peak amplitude of the averaged PAMR evoked by binaural stimuli was 142 μV. The latencies of the averaged PAMRs were 13.8 ms (± 0.26 ms) with ipsilateral stimuli, 14.3 ms (± 0.39 ms) with contralateral stimuli, and 13.9 ms (± 0.18 ms) with the binaural stimuli. The first-peak latencies of the contralaterally- and ipsilaterally-evoked monaural PAMRs are significantly different from each other (unpaired t-test, $p = 0.05$). The first peak latency of the binaural waveform was significantly different from those of both the monaurally-evoked PAMRs (unpaired t-test, $p = 0.05$).

The monaural sum waveform, consisting of the ipsilaterally and contralaterally evoked PAMRs, was also compared to the binaurally evoked PAMR waveform. The magnitudes of the peak-to-peak amplitudes of the two monaural PAMRs summed to 152 μV, which was within 10% of the 142 μV peak-to-peak amplitude recorded with binaural stimulation. The first-peak latency of the monaural sum waveform was 14.1 ms, compared to 13.9 ms with binaural stimuli.

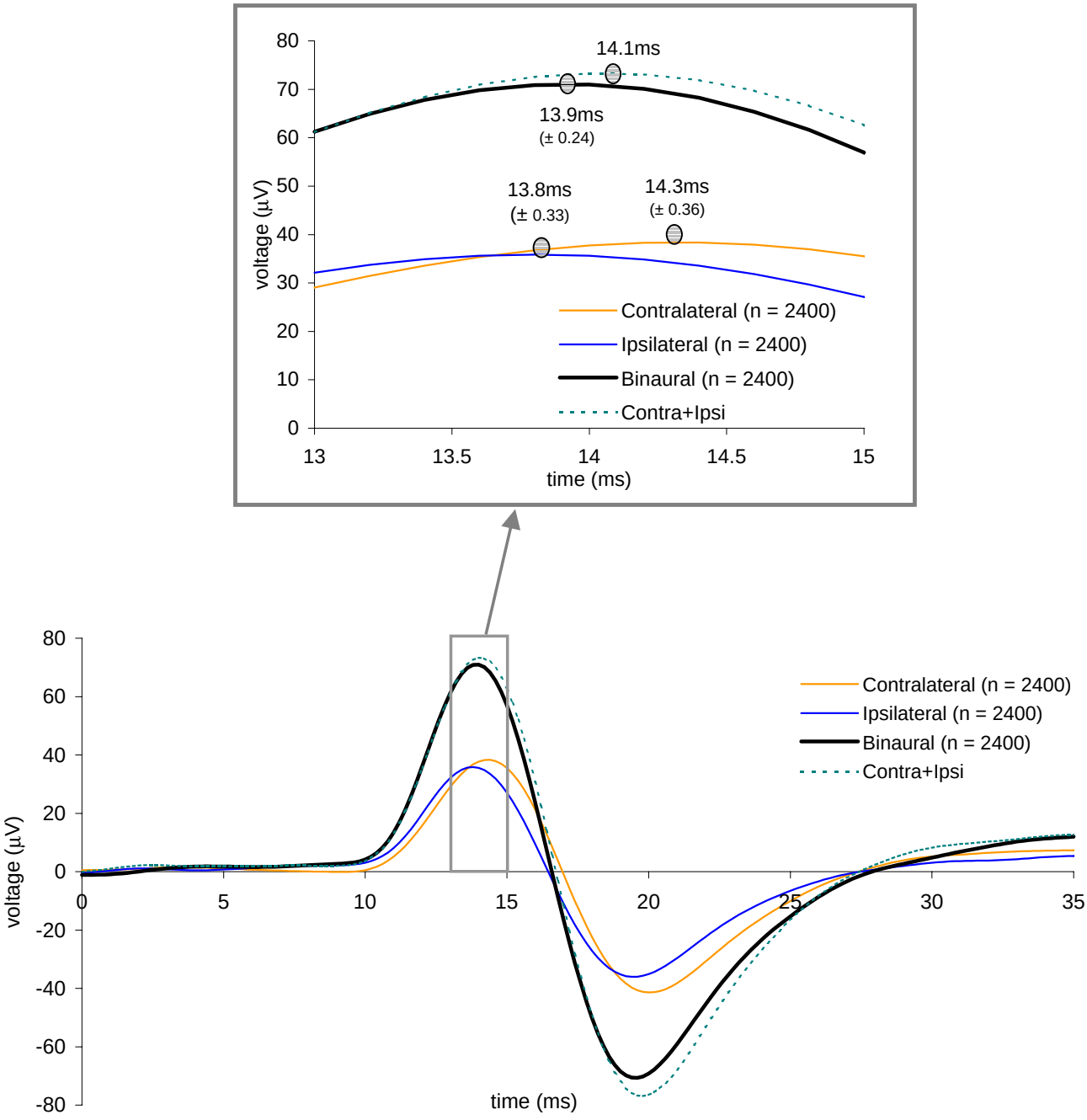

Figure 3.4.1: Averaged PAMR waveforms (n = 2400) recorded using ipsilateral-monaural, contralateral-monaural, and binaural click stimuli. Also shown is the sum of the two monaural waveforms. The first peak latencies for the ipsilateral-monaural, contralateral-monaural, and binaural waveforms are significantly different from each other (unpaired t-test, p = 0.05).

Discussion

Our results showed a difference in the mean latencies of the ipsilaterally- and contralaterally-evoked monaural waveforms of 0.5 ms. This result is consistent with that of Clifford-Jones et al. (1979), who reported mean inter-side latency maximum differences of 0.6 ms (± 0.3 ms). Our data also show that the responses from binaural stimuli were roughly equivalent in both magnitude and latency to the sum of the two monaural waveforms. This is consistent with binaural response being equivalent to a summation of the neural activity from both cochleae at a common point in the reflex pathway.

The differences in the first-peak latencies of the mean waveforms evoked with contralateral-monaural (n = 2400), ipsilateral-monaural (n = 2400), and binaural stimuli (n = 2400) were significantly different from each other. The first-peak latency difference of 0.5 ms between the mean responses evoked with contralateral-monaural and ipsilateral-monaural stimuli is consistent with there being a slight difference in the length of the neurones through the crossed and uncrossed pathway through the brainstem. The latency difference is too short for there to be an extra synapse in the contralateral pathway (as approximate synaptic delays of at least 0.7 ms were found by Totsuka et al., 1954).

This latency difference was taken into account when deciding the time-window over which to calculate the correlation level of the successive PAMR waveforms in the electronic PAMR device discussed in Section 3.11. Although the correlation contour chart shown in Figure 2.9 of Section 2.7 indicated that the *largest* correlation value with binaural stimuli was achieved when the correlation was calculated from 13 ms to 14 ms (i.e. directly over the first peak of the PAMR), this window would be not be effective for contralateral monaural stimuli,

because the peak falls outside of this small range. Based on the data from this experiment, and those described in Sections 2.7 and 3.5, a correlation window of 10 to 24 ms was used instead.

3.5 The effect of maturation on PAMR latency

When recording from infants as part of a screening program, it is important to know if the response alters with the age. The shape of the response to expect from infants is important when using visual-detection techniques to identify a response. For example, ABR measurements undergo marked changes in morphology during the first 18 months of life (Hall, 1992). At birth, generally only waves I, III, & V are observed, and the other components become more distinct during the first three months after birth (Hall, 1992). Also of importance from a testing viewpoint is how the different shape of the response will alter the effectiveness of any automated response-detection system, such as the correlation level of successive waveforms. For this reason, the averaged PAMR waveforms recorded from a small number of infant subjects were compared with those of an adult subject in order to examine any differences in response latency.

In the present study, the PAMR was recorded from two infant subjects. One subject was one year old, while the other was 4½ months old. Averaged waveforms from these two subjects are presented in Figure 3.5.1. Also shown for comparison is an averaged waveform recorded from an adult subject. The responses from all three subjects were evoked using 45 dB click stimuli delivered via headphones, and were recorded with a bandwidth of 10 Hz to 500 Hz.

We found that while the responses recorded for the one-year-old subject were similar in latency to adult responses, the responses recorded from the four-and-a-half-month-old subject occurred on average 2 ms later than those of the adult. The second peak of the averaged PAMR recorded from the four-month-old subject occurred 5.8 ms after that recorded from the adult subject.

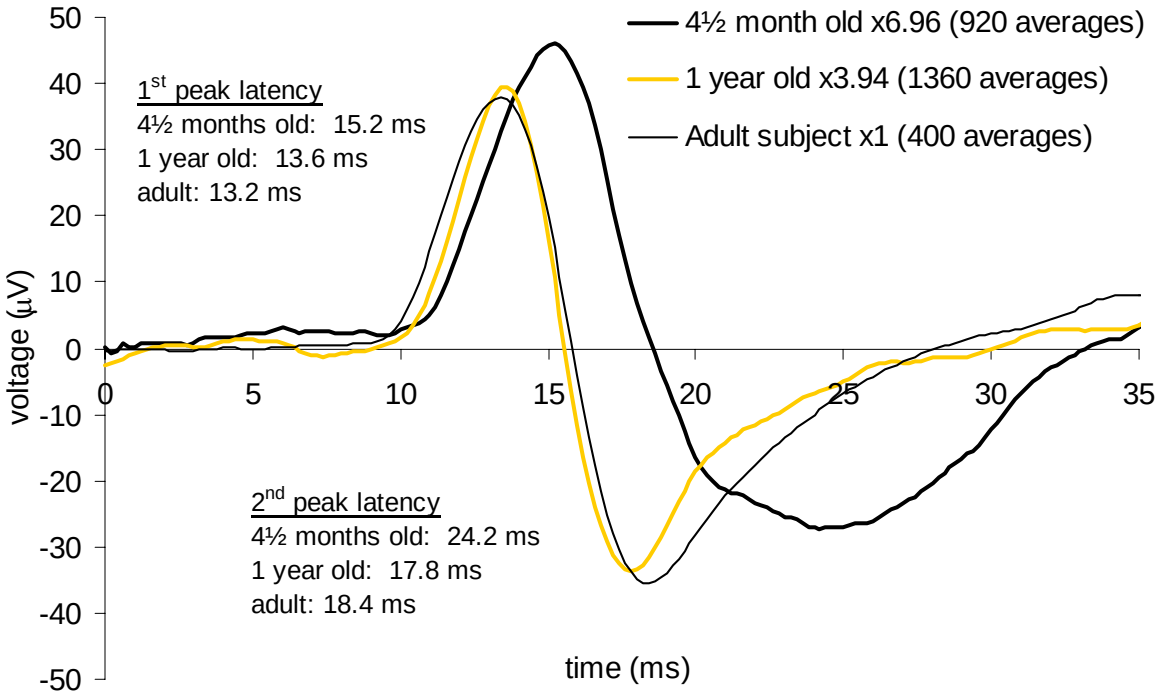

Figure 3.5.1: Averaged PAMR waveforms recorded from two infant subjects and one adult subject, illustrating the decrease in response latency with increase maturation. The responses from the two infant subjects have been scaled to the same peak-to-peak amplitude as the response from the adult subject to emphasise the differences in peak latency. Actual peak-to-peak amplitudes for the 4½ month old, 1 year old, and adult subject were 10.5 μV pp, 18.6 μV pp and 73.4 μV pp respectively. (Click intensity: 45 dB HL. Recording bandwidth: 10 Hz – 500 Hz)

Discussion

Although our sample size was very small, and therefore not necessarily indicative of the characteristics of the entire population, our results are consistent with those of Buffin, Connell, and Stamp (1977). Buffin et al. recorded the PAMR from 241 subjects and reported that the latency of the PAMR was significantly extended in infancy. This extended response latency has been attributed to a number of variables, including incomplete myelination and reduced synaptic efficiency in the central nervous system (Eggermont, 1985; Goldstein et al., 1979), which decrease the conduction velocities of the responses along their neural pathways. This latency data was taken into account when choosing the optimum correlation window for the electronic correlator device, so as to improve its reliability for use in infant *and* adult subjects.

3.6 The effect of eye movement on the PAMR

As discussed in the Introduction, it was briefly mentioned by Jacobson et al. (1964) that the amplitude of the PAMR "*can be greatly modified by changing head position and lateral movement of the eyes*". While many authors have published data on the effect of head position on the PAMR, no data regarding the effect of eye movement on the PAMR have been published.

The effect of eye rotation on the peak-to-peak amplitude of the PAMR was studied by Patuzzi and Thompson (unpublished). Their results, presented in Figure 1.11 of Section 1.7.5, show that the peak-to-peak amplitude of the response roughly tripled when the eyes were rotated by 70 degrees. Unfortunately, their results do not reveal the mechanisms of this increase.

The current model of the neural pathway of the PAMR was discussed in Section 1.6.1, and is summarised in Figure 3.6.1. In this model, sound stimuli are converted in the cochlea to afferent nervous information that passes via the auditory fibres of the auditory nerve to the brainstem. Gibson (1975) suggested a brainstem pathway consisting of the ventral cochlear nucleus, superior olivary nucleus, the nucleus of the lateral lemniscus, and then to either the reticular formation or the inferior colliculus. It is at some point within the brainstem that the response is "split" and relayed bilaterally to the motor nuclei of the facial nerve on both sides of the head (Gibson, 1975). From here, the neural activity travels along the facial nerve to the post-auricular muscles, producing an electrical response (the PAMR) which causes the muscles to contract.

We must also consider the neural drive for ipsilateral rotation of the eyes. This drive passes via the abducens nucleus, along the abducens nerve, and causes a contraction of the

lateral rectus muscle of the ipsilateral eye (Feldon et al., 1987). In accordance with Hering's Law, with drive to the *lateral rectus* of the ipsilateral eye, there occurs an equal and simultaneous drive to the *medial rectus* of the contralateral eye (passing via the oculomotor nucleus and the oculomotor nerve; Feldon et al., 1987). For simplicity, only the neural drive to the *lateral rectus* is illustrated in Figure 3.6.1.

In view of the neural pathway of the PAMR, we considered it likely in this study that the potentiation of the auditory reflex with eye rotation occurred in one of two ways, illustrated in Figure 3.6.1. If eye rotation potentiated the PAMR at some point along the reflex pathway through the brainstem, we would expect that eye rotation would increase the size of the sound-evoked response without altering the level of background EMG in the muscle. However, if the enhancement of the reflex with eye rotation occurred at the motor nucleus of the facial nerve, then we would expect that eye rotation would increase the amplitude of the sound-evoked PAMR and the background EMG simultaneously.

3.6.1 "All or none" eye rotation experiments

In the present study, the effect of eye movement on a number of characteristics of the PAMR was examined using custom-designed virtual instruments capable of simultaneously measuring and averaging the peak-to-peak amplitude and latency of the PAMR, the EMG of the PAM, and the correlation level between successive PAMR waveforms, as discussed in Appendix One. A series of experiments was carried out in which subjects were instructed to rotate their eyes ipsilaterally (that is, towards the side of the head on which the measurements of the PAMR were being made) as far as they could, and the changes in peak-to-peak amplitude of the averaged response and the EMG were measured simultaneously. The level of correlation of the successive waveforms was also calculated.

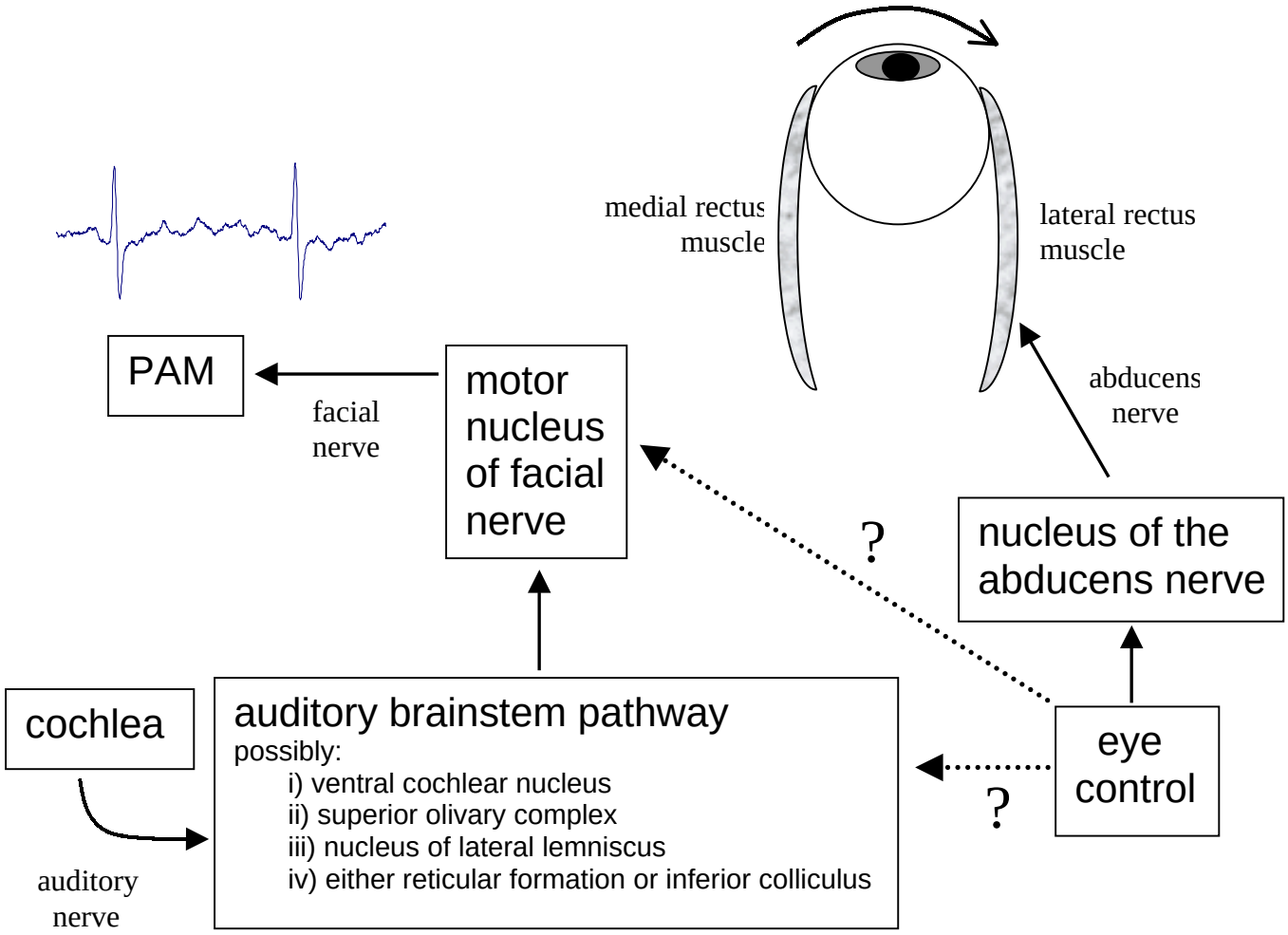

Figure 3.6.1: Two of the possible mechanisms for the observed potentiation of the PAMR during eye rotation. The reflex pathway of the PAMR, including the proposed brainstem pathway (Gibson, 1975), is shown on the left of the diagram. The dotted lines illustrate the hypotheses that eye rotation could exert influence at either the level of the brainstem pathway or at the motor nucleus of the facial nerve.

The experiment was carried out as follows. The subject was seated comfortably and instructed to relax, as this would hopefully reduce their muscle tone during the first 20 runs of the experiment. Electrodes were then attached (the active electrode placed directly above the right PAM, the reference electrode on the forehead), and click stimuli were presented to the subject at a rate of 8/s. Each "run" consisted of 20 stimulus presentations, the results of which were averaged and saved to a file for later analysis.

In order to produce a baseline comparison, the eyes of the subjects faced forward for the first 20 runs (approximately 50 seconds). After this time, they were instructed to shift their gaze hard to the right. An audible "beep" was produced by the software every 20 runs in order help the subjects rotate their eyes at the correct moment. The "hard right" gaze condition was maintained for a period of 20 runs, after which time the subjects shifted their gaze back to the forward position, where the eyes remained for a further 60 runs (approximately 150 seconds). This procedure was repeated ten times, with a short break between each set of 100 runs. The results of this eye-rotation task are shown in Figures 3.6.2 to 3.6.5, for four different subjects. The error bars shown in the figures are the standard deviations of the 10 repeats. The pure-tone audiograms carried out on these subjects across the frequency range 125 Hz to 8 kHz showed no hearing losses greater than 10 dB HL.

In all four subjects, the eye rotation manoeuvre caused a sharp increase in the EMG of the PAM, which was accompanied by a simultaneous increase in peak-to-peak amplitude of the PAMR. The average increases in EMG with eye rotation for each subject were 136% ± 9%, 297% ± 8%, 256% ± 11%, and 62% ± 8%, shown in trace A of Figures 3.6.2 to 3.6.5, respectively. The increases in peak-to-peak amplitude of the PAMR (over the same period) for each subject were 727% ± 18%, 207% ± 8%, 1050% ± 15%, and 117% ± 10% shown in trace B of Figures 3.6.2 to 3.6.5, respectively.

In all four subjects, the time-course for the increase and decrease in the PAMR peak-to-peak amplitude was qualitatively similar to the time-course for the increase and decrease in the magnitude of the EMG. The peak-to-peak amplitudes of the responses were correlated with the magnitude of the EMG in the four subjects, with correlation coefficients (r) of 0.90, 0.86, 0.95 and 0.80 observed between the two variables (n = 1000). These data are shown in Figures

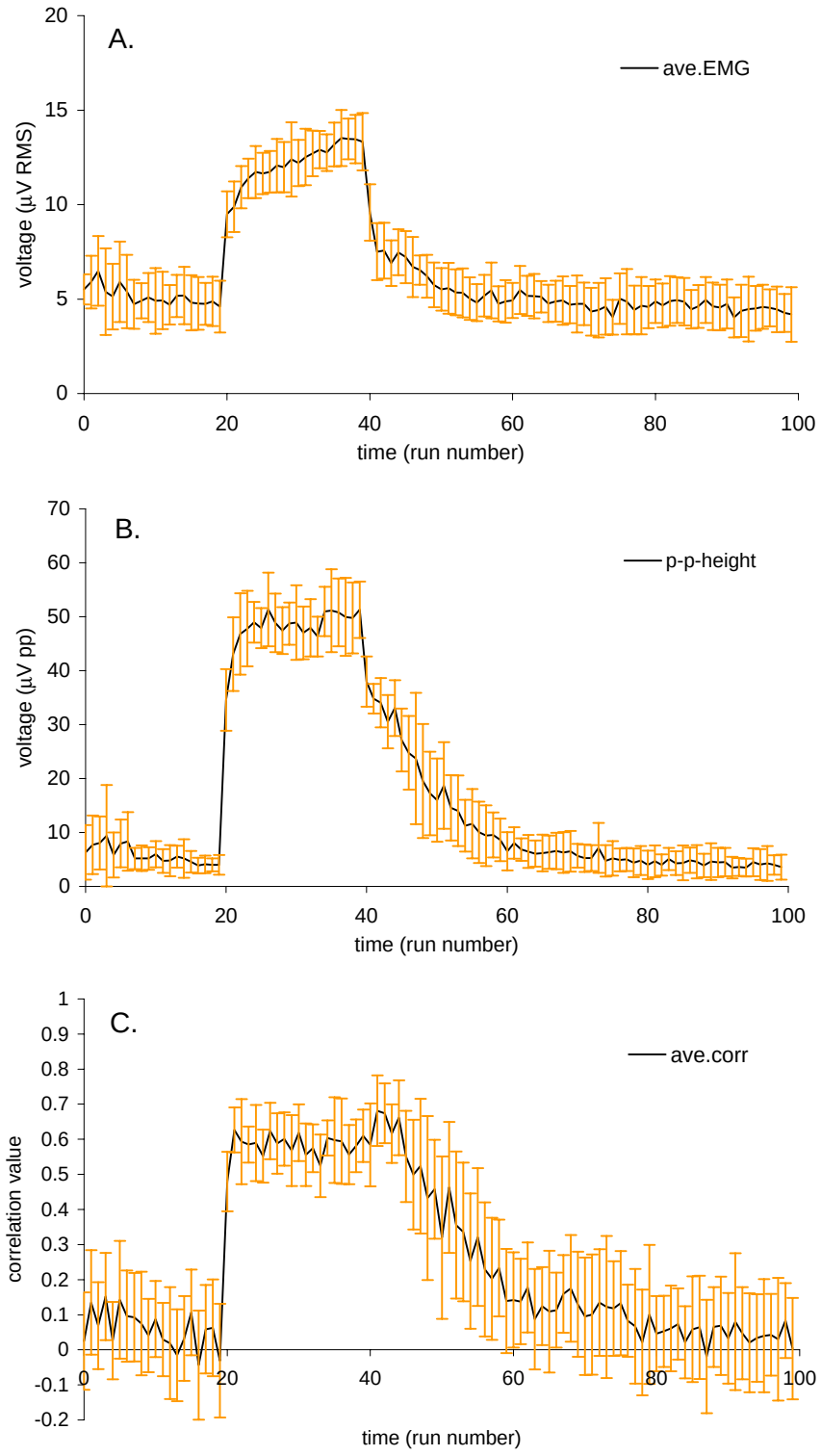

Figure 3.6.2: The effect of ipsilateral eye movement on **A.** the muscle tone of the PAM, **B.** the peak-to-peak height of the averaged PAMR waveform, and **C.** the average correlation level between consecutive PAMR waveforms. The gaze of the subject (G.O'B.) was shifted hard towards the recording electrodes between runs 20 and 40. Each run consisted of 20 averages. Shown here is the averaged results for 10 sets of 100 runs, and the standard deviation between the 10 sets. (Recording bandwidth: 10 Hz – 200 Hz, 50 Hz notch. Click rate: 8/s.)

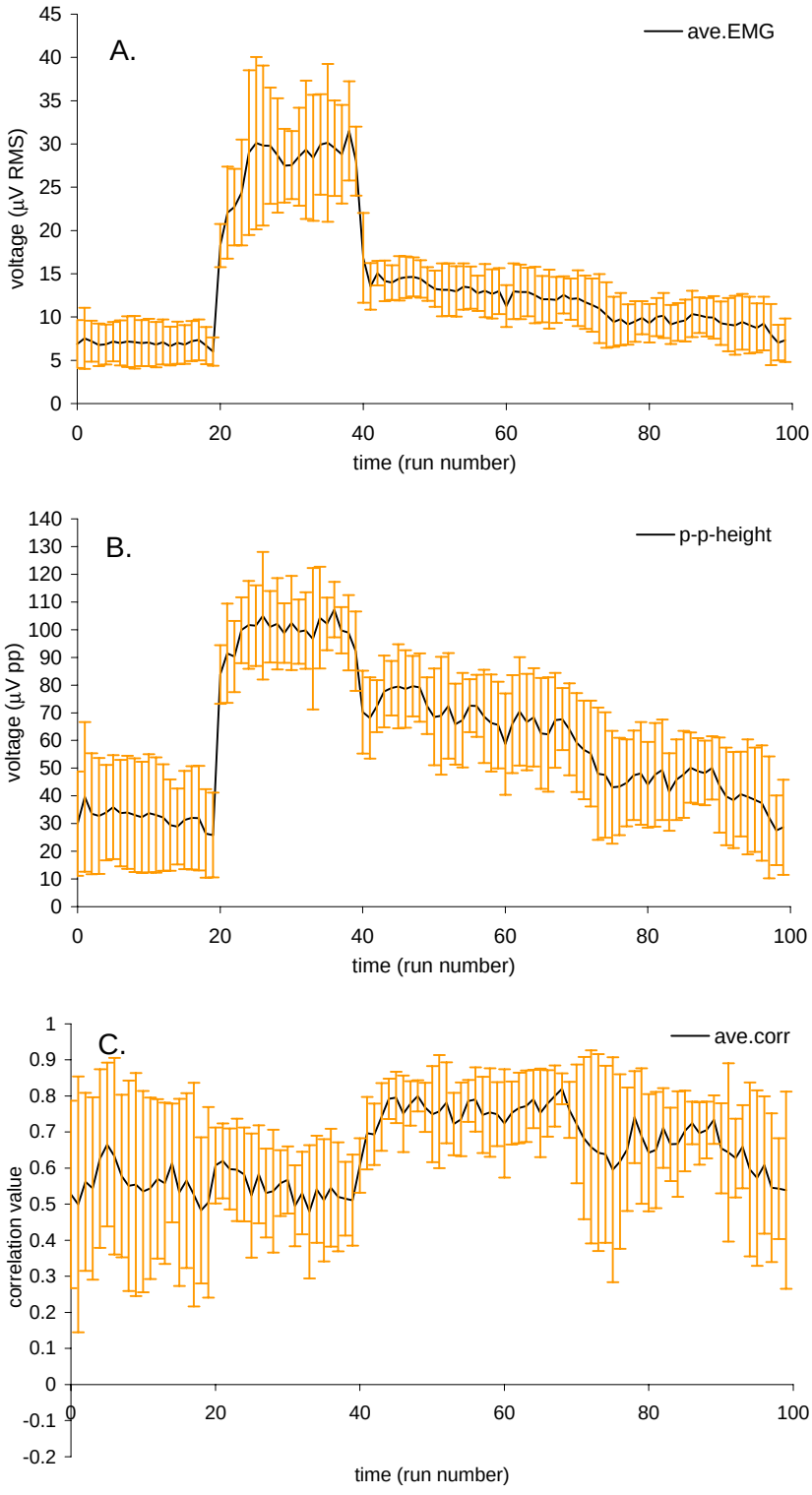

Figure 3.6.3: The effect of ipsilateral eye movement on **A.** the muscle tone of the PAM, **B.** the peak-to-peak height of the averaged PAMR waveform, and **C.** the average correlation level between consecutive PAMR waveforms. The gaze of the subject (D.B.) was shifted hard towards the recording electrodes between runs 20 and 40. Each run consisted of 20 averages. Shown here is the averaged results for 10 sets of 100 runs, and the standard deviation between the 10 sets. (Recording bandwidth: 10 Hz – 200 Hz, 50 Hz notch. Click rate: 8/s.)

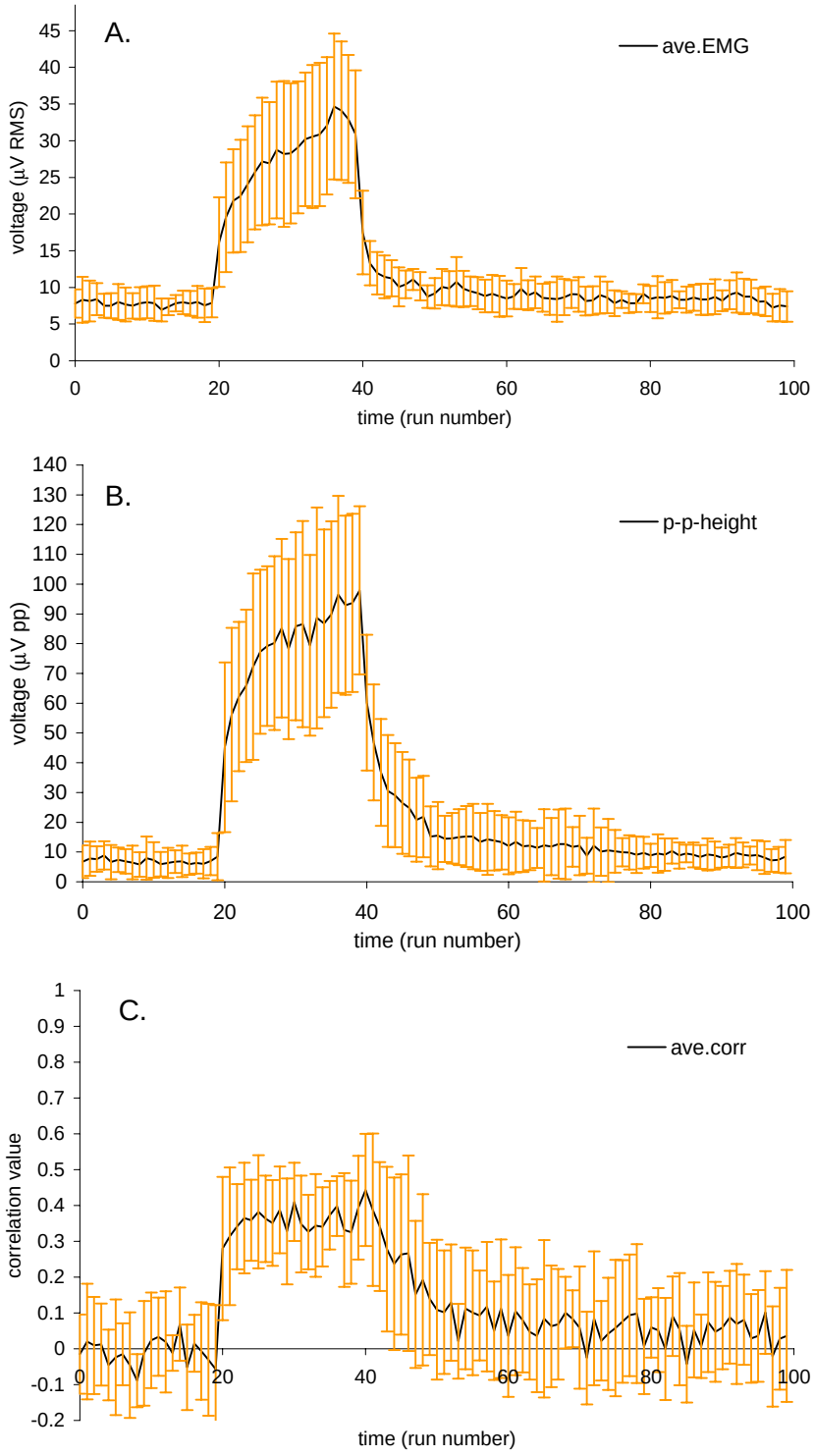

Figure 3.6.4: The effect of ipsilateral eye movement on **A.** the muscle tone of the PAM, **B.** the peak-to-peak height of the averaged PAMR waveform, and **C.** the average correlation level between consecutive PAMR waveforms. The gaze of the subject (R.P.) was shifted hard towards the recording electrodes between runs 20 and 40. Each run consisted of 20 averages. Shown here is the averaged results for 10 sets of 100 runs, and the standard deviation between the 10 sets. (Recording bandwidth: 10 Hz – 200 Hz, 50 Hz notch. Click rate: 8/s.)

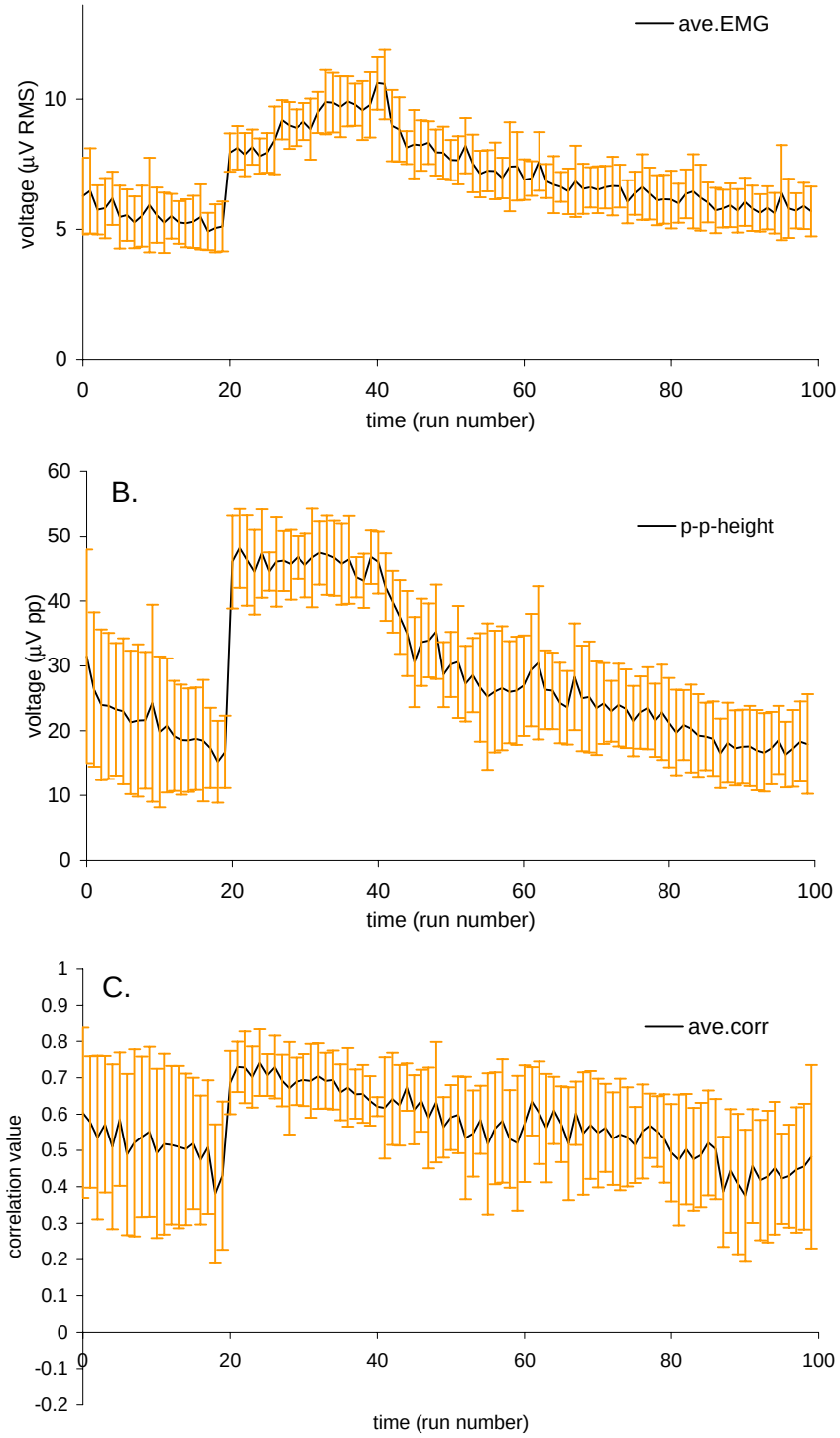

Figure 3.6.5: The effect of ipsilateral eye movement on **A.** the muscle tone of the PAM, **B.** the peak-to-peak height of the averaged PAMR waveform, and **C.** the average correlation level between consecutive PAMR waveforms. The gaze of the subject (S.T.) was shifted hard towards the recording electrodes between runs 20 and 40. Each run consisted of 20 averages. Shown here is the averaged results for 10 sets of 100 runs, and the standard deviation between the 10 sets. (Recording bandwidth: 10 Hz – 200 Hz, 50 Hz notch. Click rate: 8/s.)

3.6.6 A, B, C, and D, respectively. The relationship between the EMG and peak-to-peak amplitude of the PAMR is essentially a linear one, except in subject D.B. (Figure 3.6.6 B), which follows a linear trend until the EMG exceeds approximately 15 μV RMS, after which there is a decreased rate of growth in PAMR amplitude with increased EMG.

The correlation levels between the successive waveforms calculated by the software before, during, and after the eye rotation manoeuvre are shown in graph C of Figures 3.6.2 to 3.6.5. The correlation level increased during eye rotation in subjects G.O'B., R.P., and S.T. (Figures 3.6.2, 3.6.4, and 3.6.5, respectively). In subject D.B., however, the average correlation level over the 10 repeats remained relatively unchanged during the transition from eyes-forwards to eyes-right (Figure 3.6.3). However, an increase in correlation from 0.55 (± 0.04) to 0.70 (± 0.07) was observed when the eyes were returned to the forwards position after 20 runs. In this subject, the PAMR was clearly present during the first eyes-forward period (runs 0 – 19), with an average correlation level of 0.56 (± 0.05). When the eyes of this subject were rotated to the right (runs 20 - 39), the peak-to-peak amplitude of the PAMR increased, but the EMG increased to such a level that any increase in correlation gained by the increased PAMR amplitude was "cancelled" by the increased background noise due to the increased EMG. When the eyes were returned to the forwards position, the EMG was reduced to a level that was higher than the pre-rotation level. It can be assumed that this EMG level was still sufficient to enhance the evoked response, but not high enough to disrupt the correlation, and so the ratio of the peak-to-peak amplitude to the EMG increased, thus causing an increase in correlation level.

The relationship between correlation level, peak-to-peak amplitude of the PAMR, and EMG magnitude during the eye rotation experiments can be seen more clearly in Figure 3.6.7.

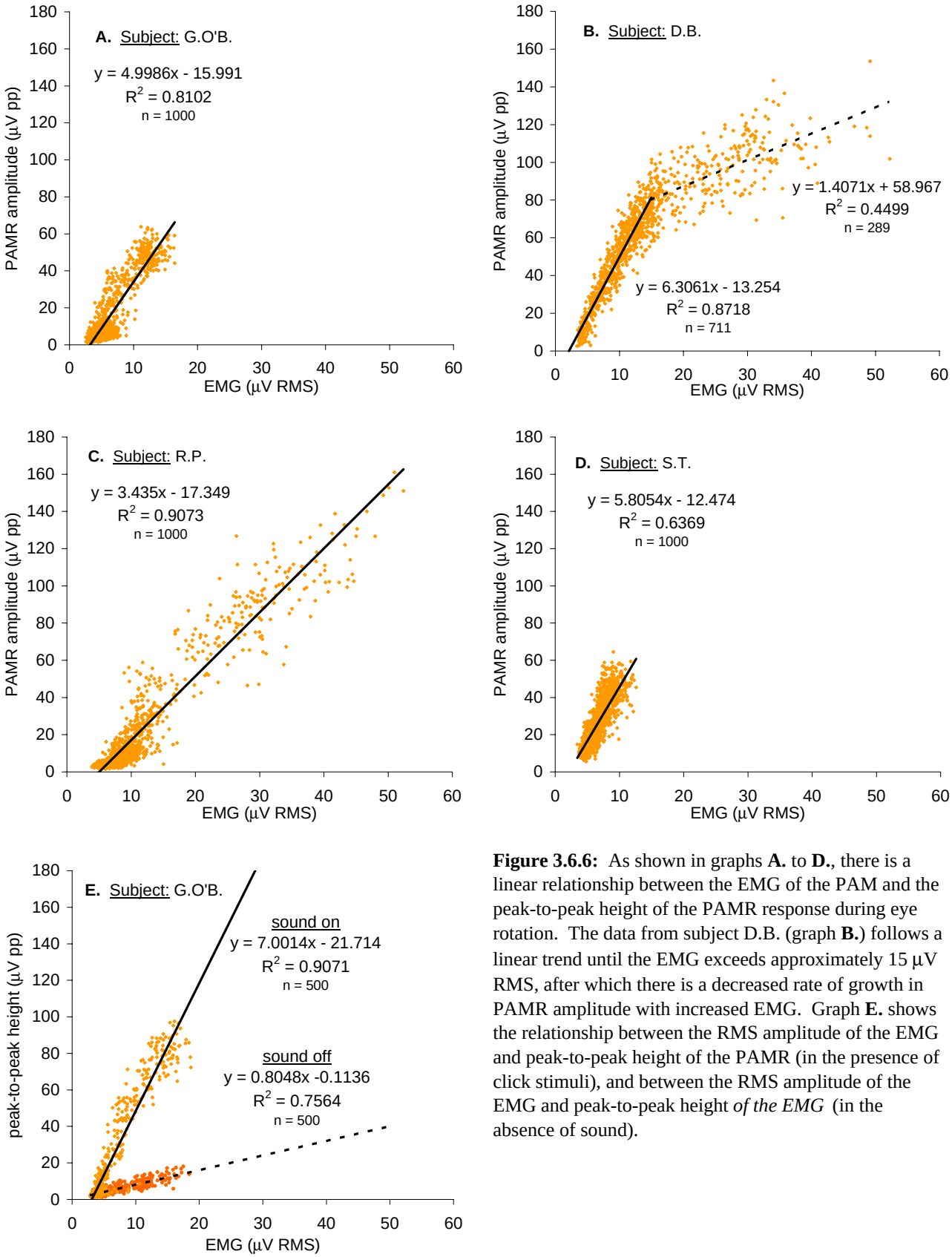

Figure 3.6.6: As shown in graphs **A.** to **D.**, there is a linear relationship between the EMG of the PAM and the peak-to-peak height of the PAMR response during eye rotation. The data from subject D.B. (graph **B.**) follows a linear trend until the EMG exceeds approximately 15 µV RMS, after which there is a decreased rate of growth in PAMR amplitude with increased EMG. Graph **E.** shows the relationship between the RMS amplitude of the EMG and peak-to-peak height of the PAMR (in the presence of click stimuli), and between the RMS amplitude of the EMG and peak-to-peak height *of the EMG* (in the absence of sound).

This figure shows the correlation level (for 100 runs from each of the four subjects) plotted against the signal-to-noise ratio (or SNR), calculated by dividing the peak-to-peak amplitude of the PAMR by the RMS amplitude of the background EMG of the PAM. A linear relationship between the correlation level and the signal-to-noise ratio was observed, with a correlation level of 0.96 amongst the pooled data. The applications of this linear relationship between signal-to-noise ratio and correlation level are discussed in more detail in Section 4.

The eye rotation experiment described above was also carried out on a normal-hearing subject (S.L.) in whom it was quite difficult to record a PAMR. His results are shown in Figure 3.6.8. In this case, the eye rotation caused the EMG of the PAM to increase by 160% compared to the eyes-forward condition. Although the peak-to-peak amplitude measurements increased by 200% during this period, it must be remembered that the peak-to-peak measure of the waveform simply calculates the difference between the maximum and minimum points in an array, and is not, in itself, an indication of the size of the *sound-evoked* response, unless the sound-evoked response has a larger peak-to-peak amplitude than the background noise. That is, without a PAMR, the peak-to-peak amplitude measured represents the background EMG alone. In this case, the averaged waveforms showed no recognisable PAMR, and there was no significant change in the average correlation level before, during and after the eye rotation period. That is, in this subject, eye rotation was not sufficient to elicit the PAMR, although there was a small increase in EMG from 2.5 μV RMS to 6.5 μV RMS. This subject is discussed further in Section 3.6.3.

3.6.2 Graded eye rotation experiments

Because we had the ability to simultaneously measure changes in EMG, and peak-to-peak amplitude of the waveform, it was decided to repeat the graded eye rotation experiment of

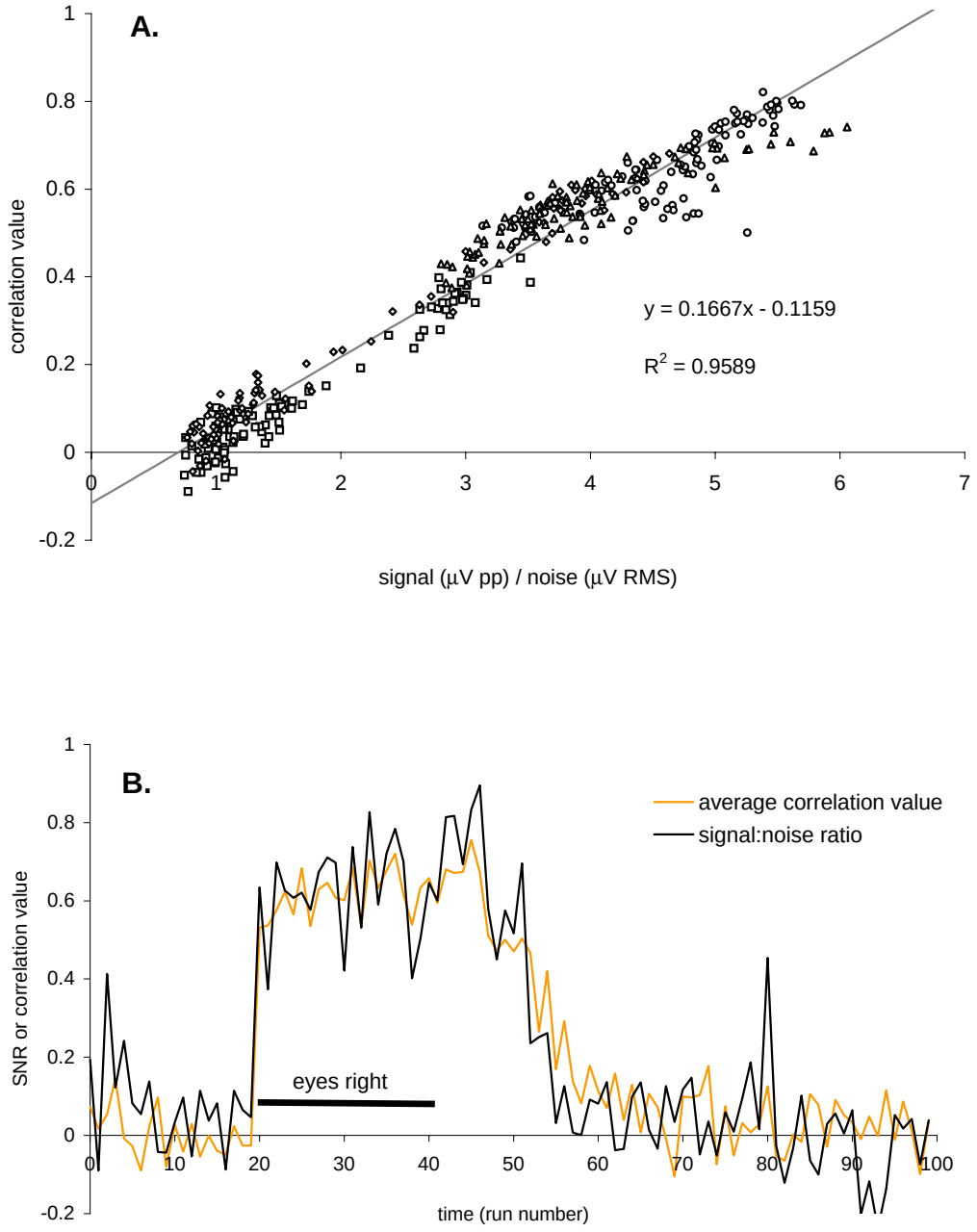

Figure 3.6.7: **A.** A strong correlation is observed between the average correlation level between successive waveforms and signal-to-noise ratio, defined by the peak-to-peak height of the response (µV pp) divided by the background EMG (µV RMS). The results for four subjects are shown, as is a regression line for the pooled data. The R^2 correlation coefficient shown (0.96) is the correlation between the pooled data and the regression line. **B.** As predicted by graph A., similar results are observed for the changes in correlation level and signal-to-noise ratio during an eye rotation experiment for one subject (G.O'B.).

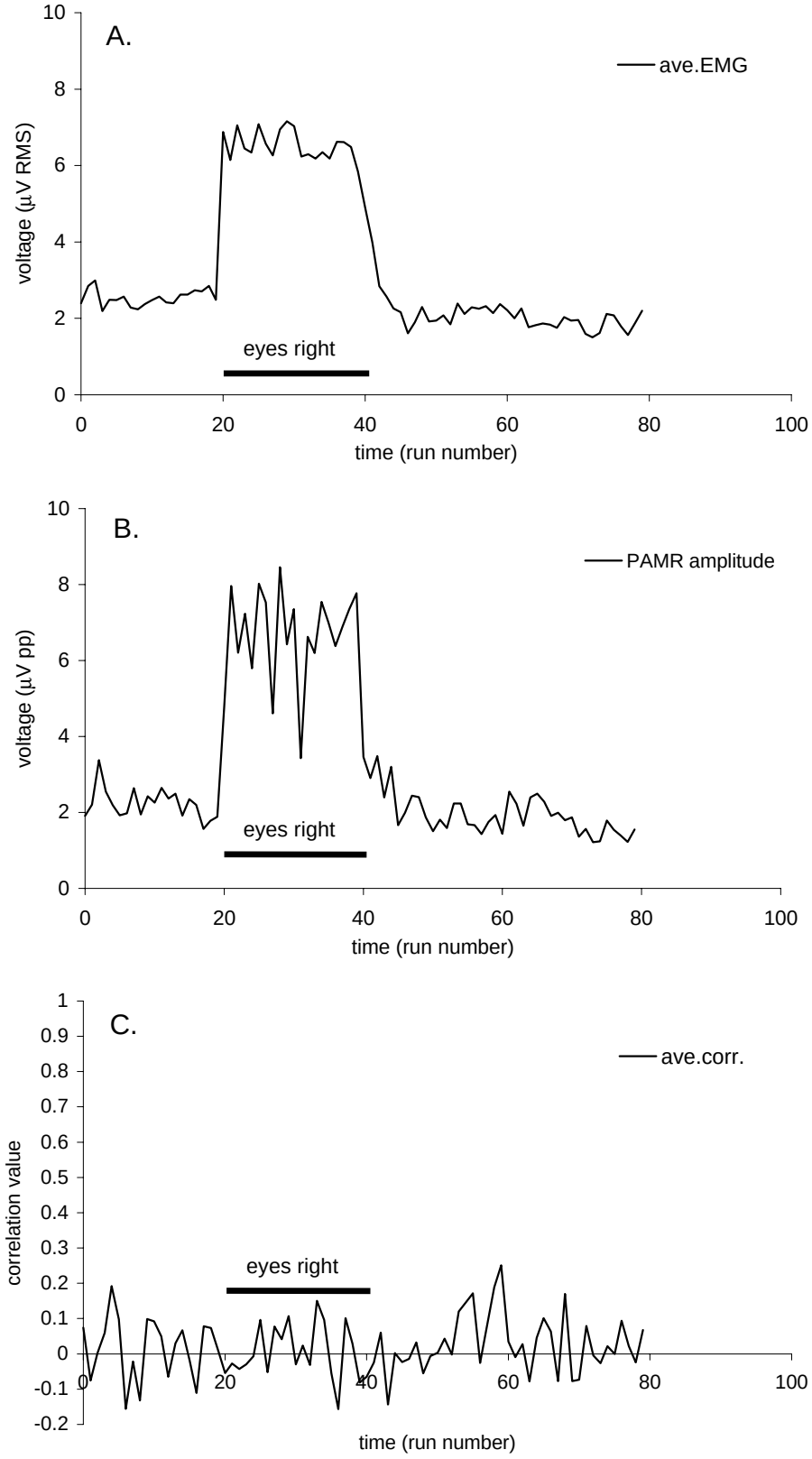

Figure 3.6.8: The effect of ipsilateral eye movement on **A.** the muscle tone of the PAM, **B.** the peak-to-peak height of the averaged PAMR waveform, and **C.** the average correlation level between consecutive PAMR waveforms from a subject (S.L.) in whom it was difficult to evoke the PAMR. The gaze of the subject (S.L.) was shifted hard towards the recording electrodes between runs 20 and 40. Each run consisted of 20 averages. Shown here is result for a single set of 80 runs. (Recording bandwidth: 10 Hz – 200 Hz, 50 Hz notch. Click rate: 8/s.)

Patuzzi and Thomson (unpublished; shown in Figure 1.11 of Section 1.7.5), to observe the changes in EMG that occurred. The eye rotation was also conducted over ± 70 degrees to observe the differences between the effects of ipsilateral and contralateral eye rotation. This was done using a device that held the head in a fixed position and provided visual targets for fixation of the gaze at 10-degree increments from 0 to ± 70 degrees. The results for this graded eye rotation task are shown in Figures 3.6.9 and 3.6.10 for two subjects (G.O'B. and S.T.).

For the subject G.O'B., whose results are presented in Figure 3.6.9, it can be seen that there was a large increase in the EMG recorded from the left PAM when the eyes were rotated hard towards the left side (Figure 3.6.9 A). Although there was a higher resting EMG level in the right PAM than in the left at the time of recording, the EMG levels were largest in the right PAM when the eyes were rotated towards the right side, as shown in Figure 3.6.9 C. A large increase in the peak-to-peak amplitude of the PAMR was observed during the ipsilateral eye rotation, as seen in Figures 3.6.9 B and D.

The results from subject S.T. are shown in Figure 3.6.10. These results show higher levels of EMG recorded during ipsilateral eye rotation than during contralateral eye rotation (Figure 3.6.10 A and C), although this increase is not as large in the left PAM as it is in the right PAM.

One problem with the data from this experiment was that each 140 degree set of eye rotation was done in two halves, 0 to +70 degrees and then 0 to –70 degrees, with a short break (approximately 1 minute) between the two measurement halves to allow the EMG of the subject to return to resting levels. The measurement for zero degrees shown in Figures 3.6.9 and 3.6.10 is the average of the two zero degree measurements. Unfortunately, in the case of subject S.T., the relaxation period was not long enough for the EMG in the PAM to decrease to

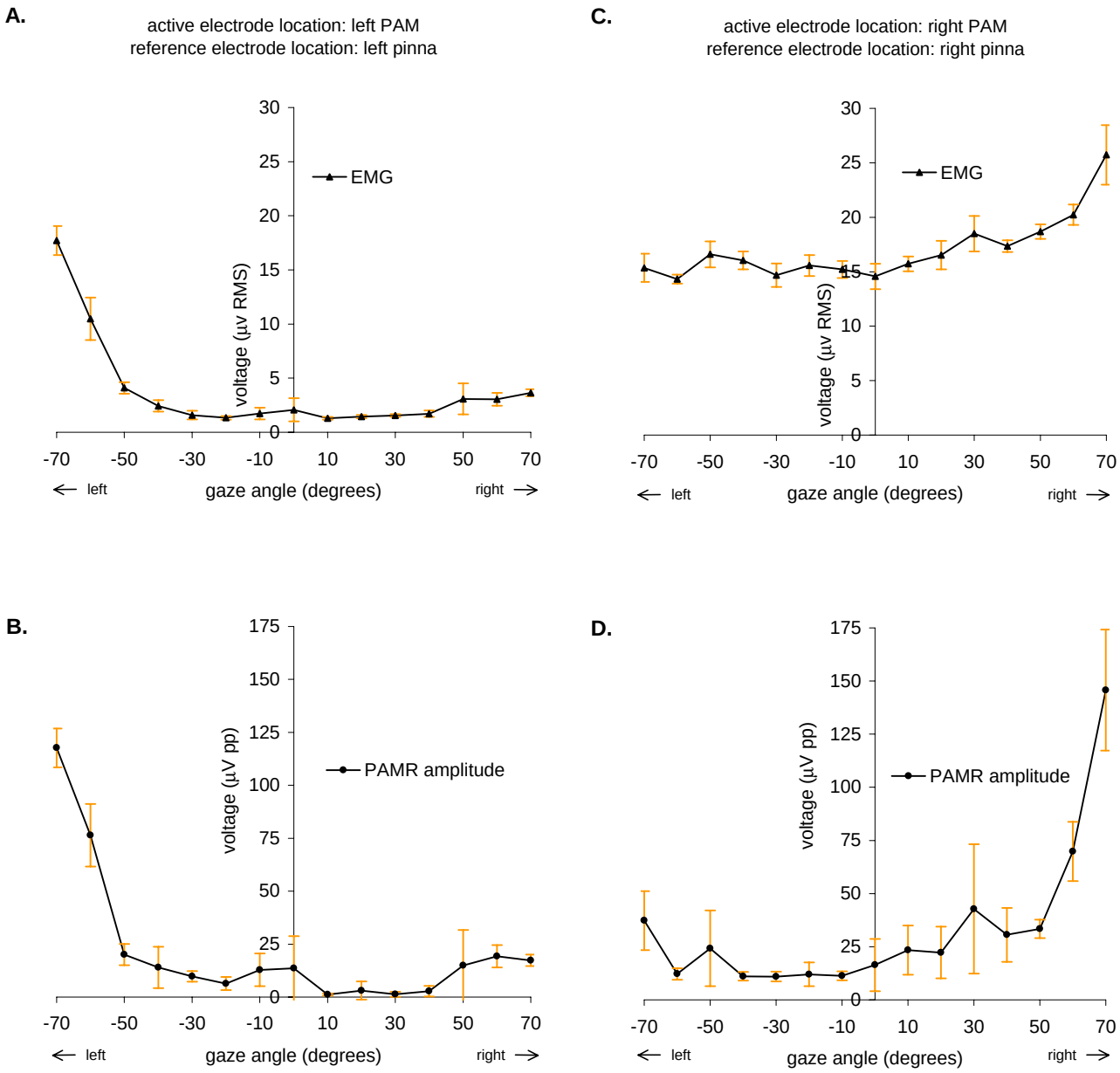

Figure 3.6.9: The change in EMG and peak-to-peak height recorded from the left PAM (figs. A. and B.), and the right PAM (figs. C. and D.) of subject G.O'B. during eye rotation over a 140° range. Note the larger increases in EMG and PAMR amplitude for large ipsilateral rotation (towards the far left and far right of the page), and the slight increase in EMG and PAMR with large contralateral rotation (towards the centre of the page).

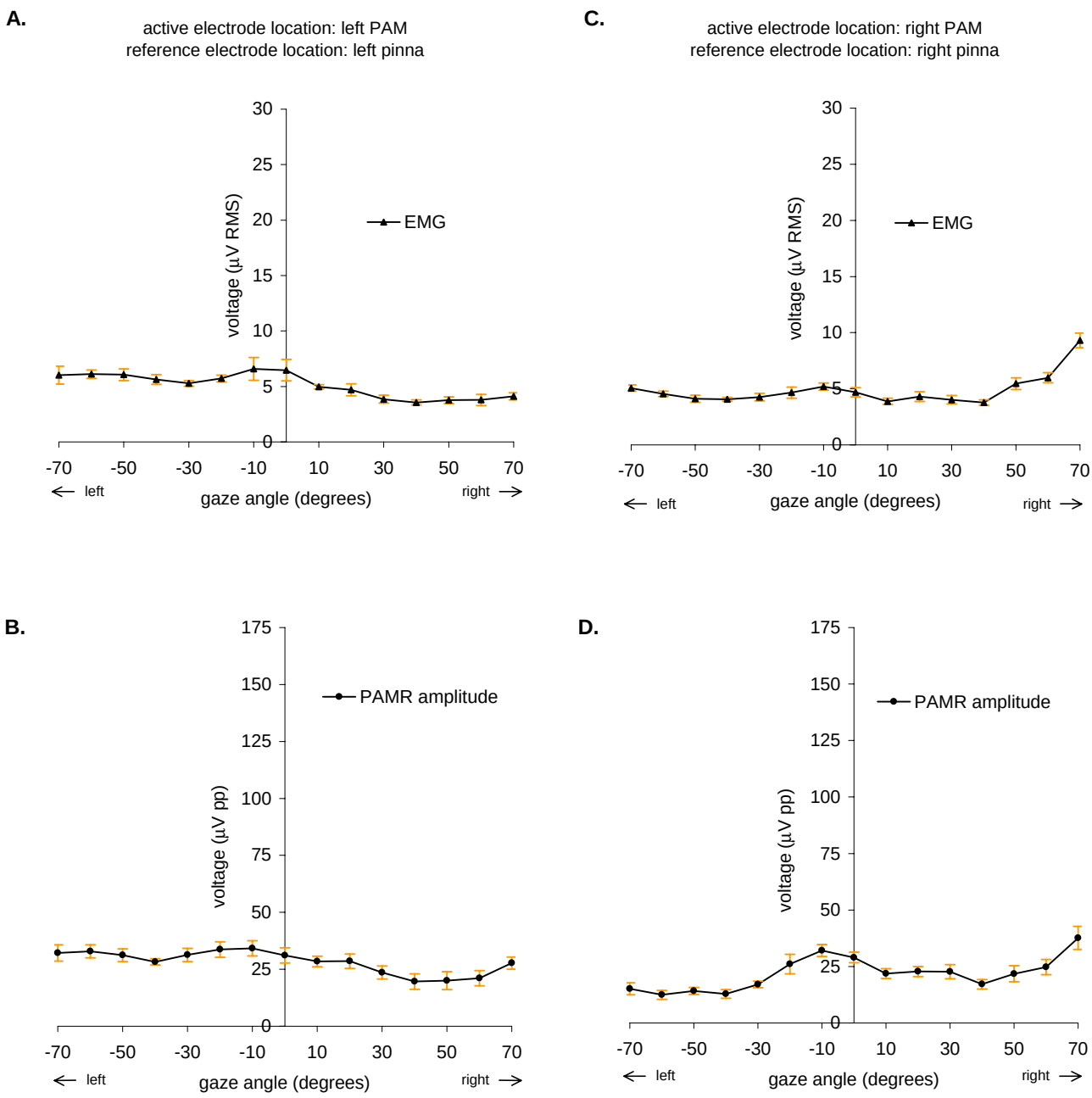

Figure 3.6.10: The change in EMG and peak-to-peak height recorded from the left PAM (figs. A. and B.), and the right PAM (figs. C. and D.) of subject S.T. during eye rotation over a 140° range. Note the increases in EMG and PAMR amplitude for large ipsilateral rotation (towards the far left and far right of the page), and the slight increase in EMG and PAMR with large contralateral rotation (towards the centre of the page). The extent of the increase in both EMG and PAMR with eye rotation are not as large as those observed in subject G.O'B. (see text).

resting levels, and so the higher EMG level observed at the –10 degree measurement was largely due to the residual EMG caused by the +70 degree measurement (Figure 3.6.10). However, due to time constraints and subject availability, it was not possible to repeat these measurements. The data from subject S.T. are presented here because they further illustrate the relationship between the *direction* of eye rotation and the increase in EMG and PAMR peak-to-peak amplitude.

Figure 3.6.11 re-plots the data of Figures 3.6.9 and 3.6.10, and shows the relationship between EMG and PAMR peak-to-peak amplitude recorded from both PAMs during the graded eye rotation manoeuvre, for subjects G.O'B. and S.T. The data for subject G.O'B. (Figure 3.6.11 A and B) show a linear relationship between the two variables. The average EMG recorded from the right PAM at rest is centred around 15 μV RMS, while the EMG from the left PAM is below 5 μV RMS at rest. The data from ipsilateral eye rotation at large angles tend towards the upper right halves of the figures (as labelled in Figure 3.6.11), while those from the contralateral eye rotation tend to be placed at the low-EMG, low-PAMR end of the data. The data from subject S.T. show a similar pattern, but to a lesser extent.

3.6.3 The effect of increasing EMG by other methods on PAMR amplitude

Shown in Figure 3.6.8 were the results of the eye rotation manoeuvre from a subject (S.L.) in whom it was difficult to evoke the PAMR. As discussed earlier, the averaged waveforms from this subject showed no recognisable PAMR, and there was no significant change in the average correlation level before, during and after the eye rotation manoeuvre. In this subject, eye rotation alone was not sufficient to elicit the PAMR. Attempts were then made to use other methods to increase the muscle tone of the subject, and therefore elicit the PAMR.

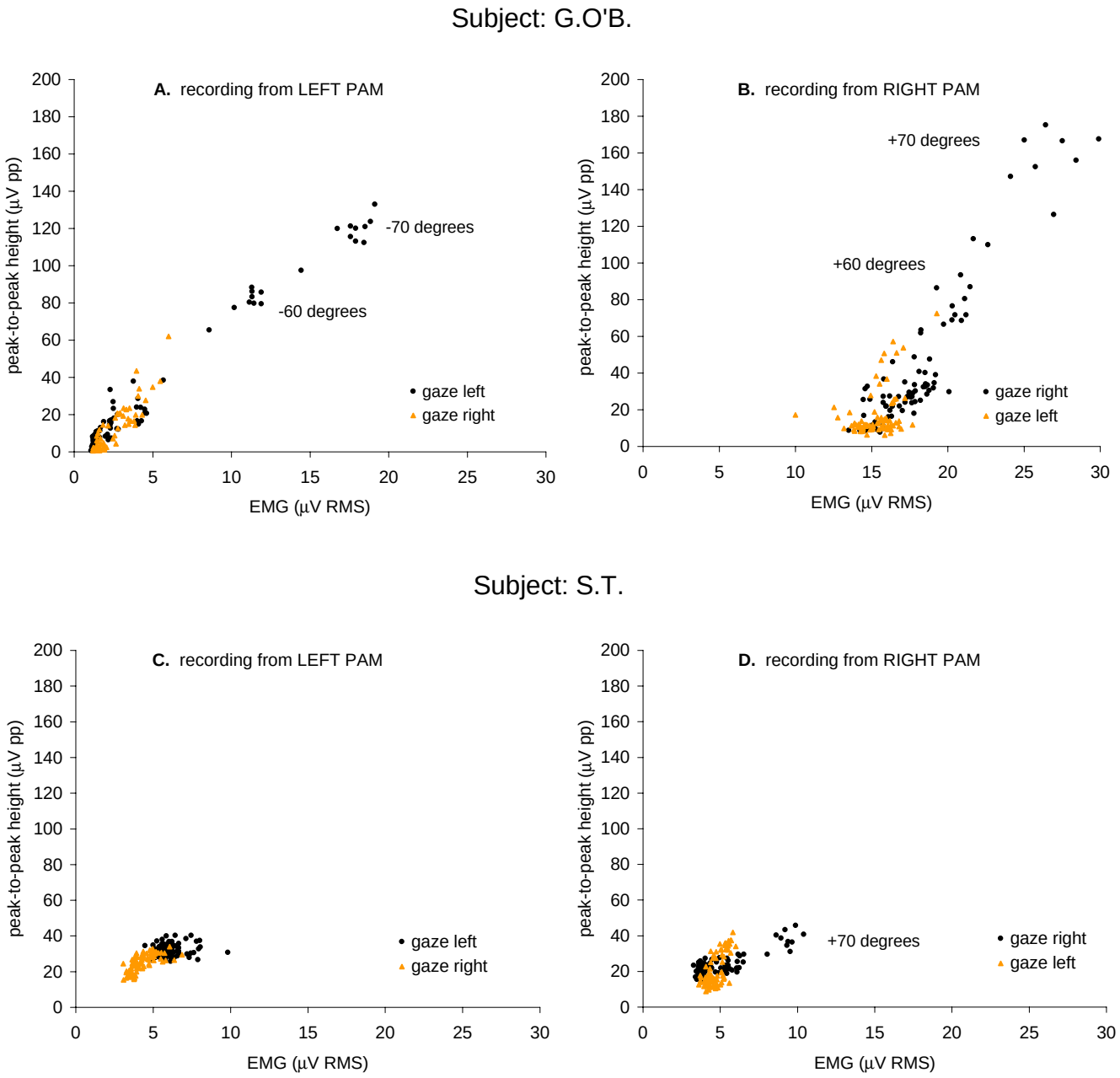

Figure 3.6.11: The relationship between peak-to-peak height of the PAMR and background EMG during graded eye-rotation. The data shown is the same as that presented in Figures 3.6.9 and 3.6.10. Responses for both subjects are shown at the same scale to illustrate the range of variation among subjects. The data for subject G.O'B. recorded from the right PAM (B.) showed a higher minimum background EMG level than was recorded from the left PAM (A.). In all figures, the points due to ipsilateral eye rotation (black) extend further along the EMG and PAM amplitude axes than do those for contralateral eye rotation (grey). Also shown is the grouping of some of these data points with the degree of ipsilateral eye rotation.

The subject was unable to voluntarily contract his post-auricular muscles (by "wiggling the ears"), and so the methods used in the attempt to record a response from this subject were smiling (Dus et al., 1975; Gibson, 1975), and resisted flexion of the neck, where the subject tried to maintain an upright head position when the head was i) pushed forwards by the investigator (Cody et al., 1964; Clifford-Jones et al., 1979), and ii) pushed backwards by the investigator (Clifford-Jones et al., 1979). The averaged waveforms (n = 100 traces per average) resulting from these manoeuvres are shown in Figure 3.6.12 A, B, and C. Although all of these traces showed a reproducible peak between 12 and 15 ms, the waveforms are not *clearly* identifiable as the PAMR.

However, it was possible to record a PAMR that was morphologically normal when this subject held his chin firmly on his chest. This voluntary forward flexion manoeuvre was similar to that used by Yoshie et al., 1969 and Dus et al., 1975. The averaged waveforms from the subject during this manoeuvre are shown in Figure 3.6.13 A in the presence and absence of sound stimuli. The peak-to-peak amplitude of the averaged PAMR waveform over this period (n = 90) was only 11.6 μV pp. This small amplitude was did not appear to be due to an average of consistently small responses, but was due to a sporadic response of moderate amplitude. This is demonstrated in Figure 3.6.13 B, which shows that when 18 of the single waveforms containing the PAMR were averaged, a peak-to-peak amplitude of 36 μV was recorded. The latencies of the first and second peaks of both the waveforms in Figure 3.6.13 (14.8 ms and 18.6 ms, respectively, for Figure 3.6.13 B) were within normal adult ranges.

Discussion

The data from the experiments described above show that the increase in the peak-to-peak amplitude of the PAMR with eye rotation coincided with an increase in the EMG of the

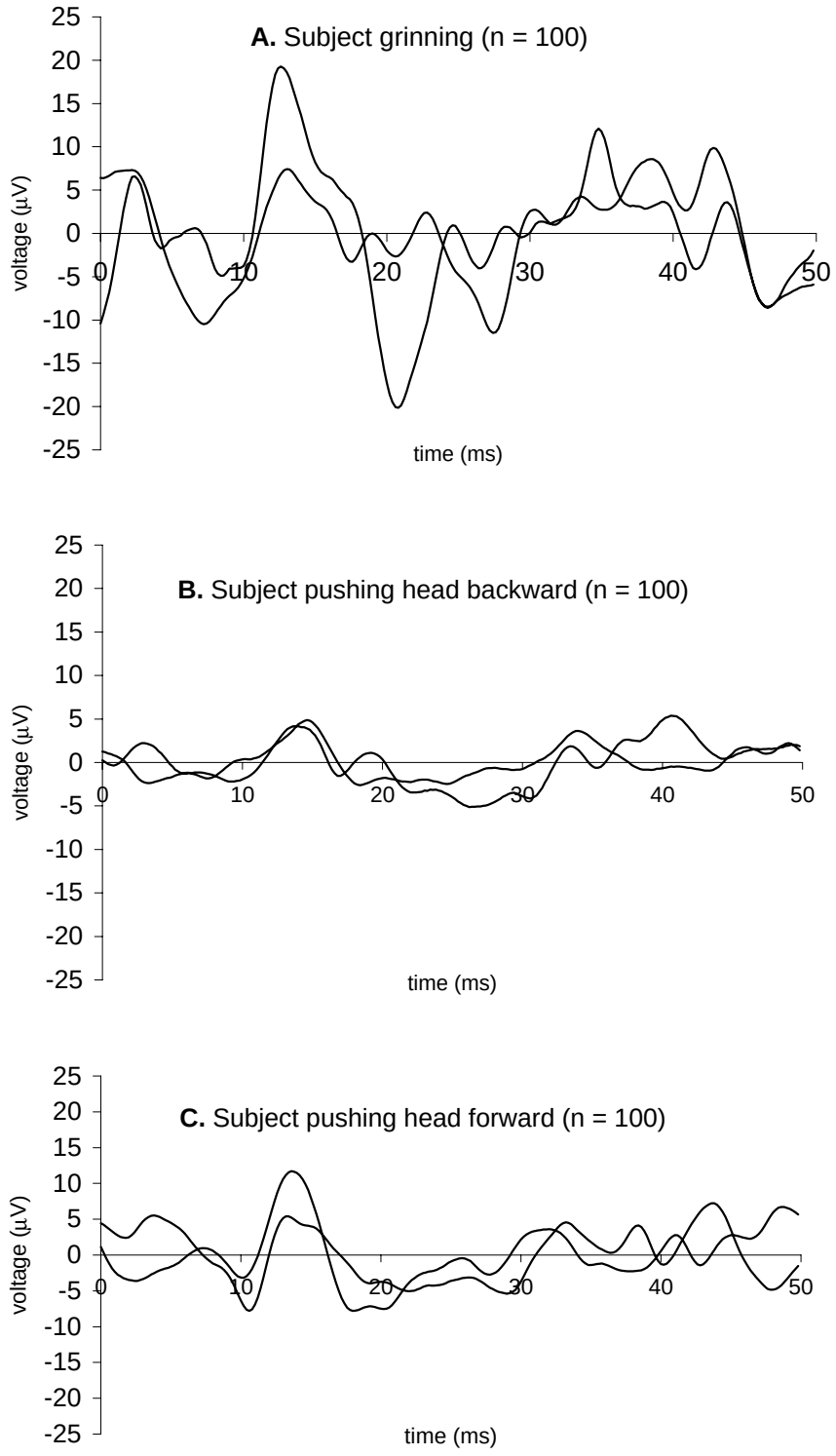

Figure 3.6.12: Manoeuvres used in attempts to obtain a PAMR response in subject S.L. included (**A.)** smiling, and resisted flexion of the neck, where the subject tried to maintain an upright head position when the head was (**B.)** pushed forwards by the investigator and (**C.**) pushed backwards by the investigator. Two traces are superimposed in each graph, with each trace being the average of 100 response waveforms. (Recording bandwidth: 10 Hz to 500 Hz).

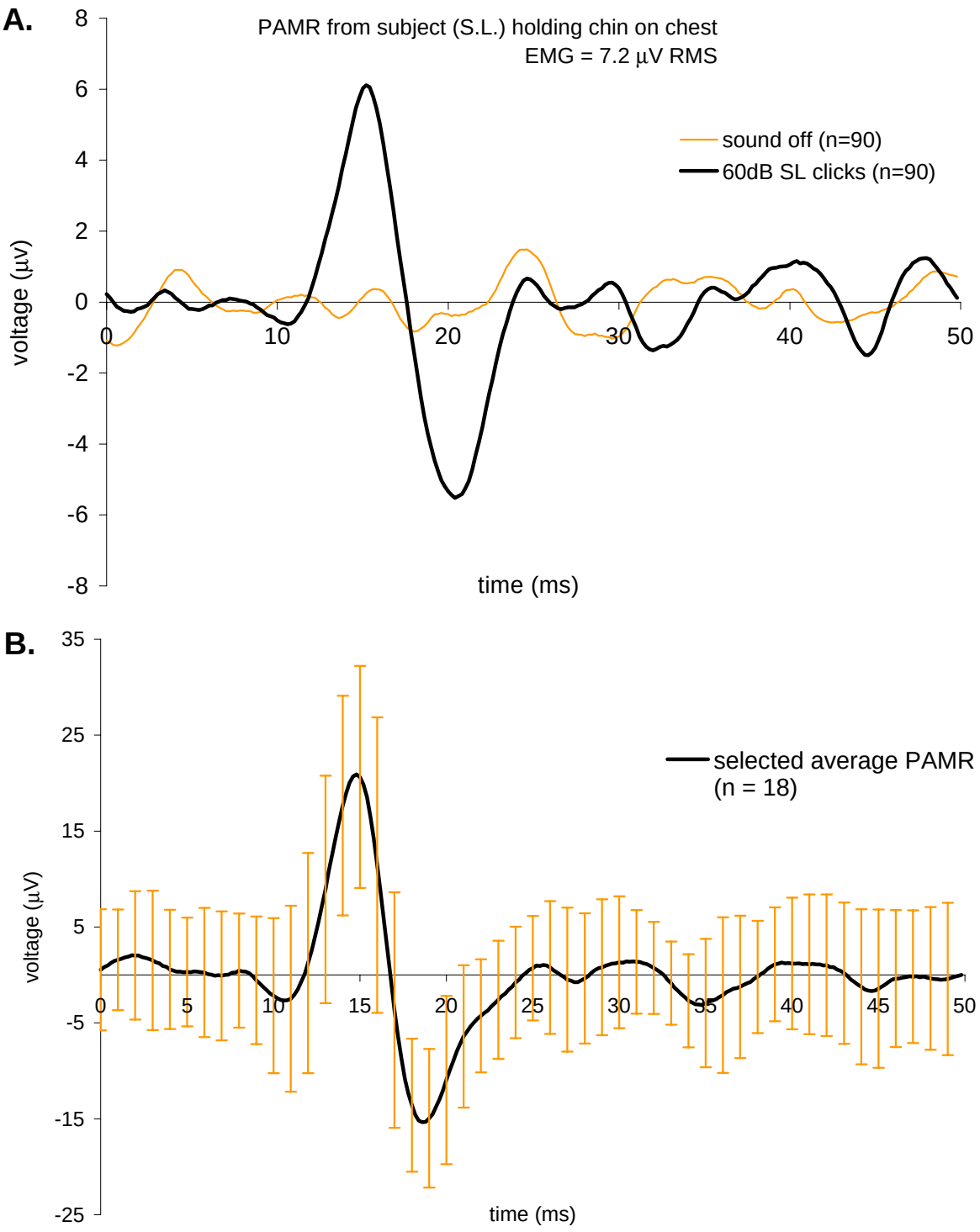

Figure 3.6.13: **A.** Morphologically "normal" averaged PAMR waveform (n = 90) recorded from a subject in whom eye rotation was not sufficient to evoke a response. The response was facilitated by having the subject hold his chin firmly against his chest, which produced an EMG level of 7.2 µV RMS in the PAM. The response was not observed in the absence of clicks. **B.** The low peak-to-peak height of the response shown in A. is due to a "dilution" of the contribution of large responses to the average by smaller or absent responses. When 18 of the larger responses were selectively averaged, a peak-to-peak height of 36 µV pp was observed.

PAM. Of course, the strong correlation between the two variables does not imply causality. However, the arguments in favour of a *causal* relationship between EMG and PAMR amplitude are:

i) in most cases, any method that increases the EMG of the PAM (from a low level to a high level) also increases the amplitude of the PAMR *if it is present* (for example, in Figure 3.6.13),

ii) any action that increases the peak-to-peak amplitude of the PAMR (other than altering the acoustic stimulus) will also increase the EMG of the PAM (for example, Figures 3.6.2 and 3.6.6), even when the action is performed in the absence of sound stimuli (for example, as shown in Figure 3.6.14 overleaf).

If these results are viewed in terms of our initial hypothesis (and not our final one, as described below), they suggest that the increases in EMG and PAMR amplitude are likely to be caused by a change in membrane potential of neurones in the motor nucleus of the facial nerve.

Our results showing the increase in EMG with eye movement are consistent with those of Joseph and Boussaoud (1985), who reported that cat eye movements to visual targets were accompanied by electromyographic discharges in the muscles controlling the pinna. They studied this phenomenon quantitatively in one cat by implanting electrodes in the pinnae muscles and by recording EMG along with visual saccades. Their results showed that "*in 90% of cases (396 times out of 450), eye movements towards mixed "auditory and visual" or even purely "visual" targets were accompanied by EMG volleys.*" This is important, because it suggests that the mechanisms by which eye rotation affects the movement of the pinna (for example, in movements towards visual targets) do not require auditory input, and therefore do not necessarily involve the auditory pathway that is responsible for movement of the pinna

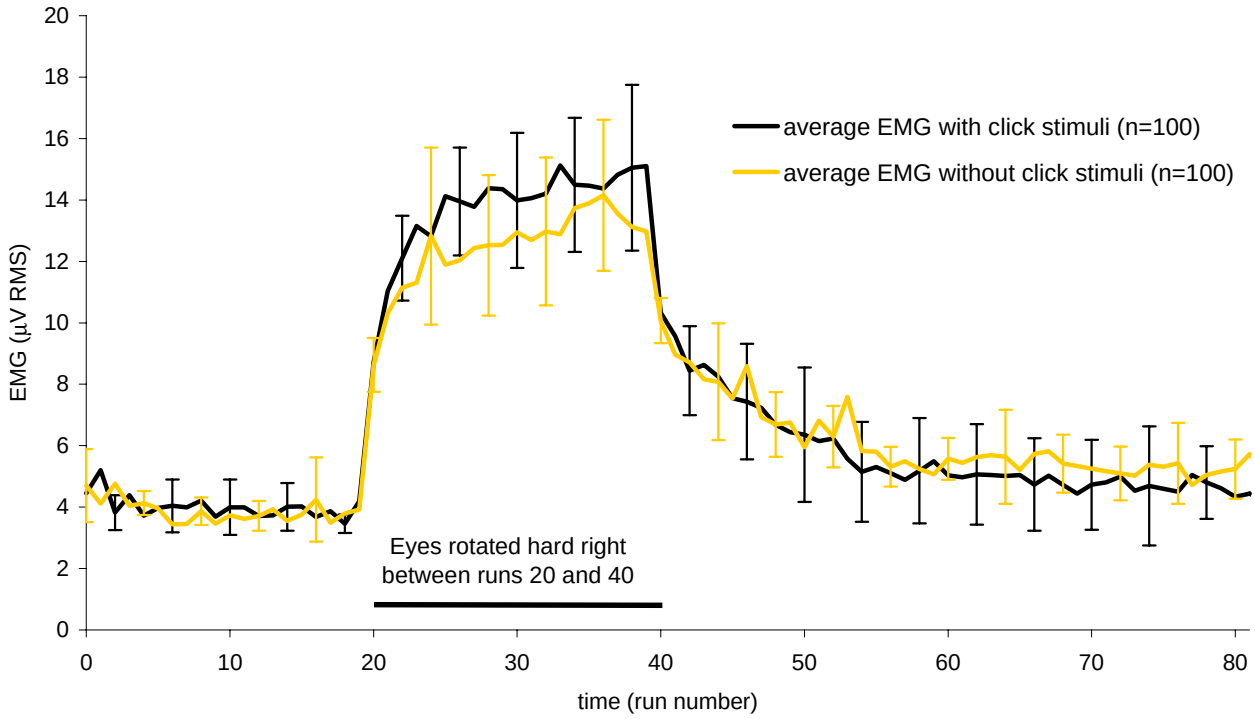

Figure 3.6.14: Ipsilateral eye rotation causes an increase in EMG of the PAMR that is the same both in the presence and absence of click stimuli. Each point is the average EMG amplitude recorded over 100 stimulus presentations (45 dB SL clicks). The error bars shown are the standard deviation between the five sets of 80 runs.

during *sound* localisation. Further evidence for this independence is found in the results of Populin and Yin (1998) who have recently observed a close association between eye and pinna movements of cats to visual targets. They found that movements of the pinna to auditory targets were stereotyped and consistent, and were made up of two parts: a short-latency component time-locked to the onset of the sound (likely to be the PAMR itself), and a second long-latency component that was highly correlated with the eye movement. Populin et al. (1998) suggest that the distinct characteristics of these two components indicates that they may be controlled separately

Populin et al. also made the observation that this close association between eye and pinna movements to visual targets is consistent with the effects of electrical stimulation of the superior colliculus of the cat, which evokes coordinated movements of the eyes, pinna and whiskers (Stein and Clamann, 1981). Neuroanatomical tracing studies carried out by Henkel and Edwards (1978) have suggested that the "*superior colliculus control of pinna movements is mediated entirely by indirect connections with the facial nucleus*", and that "*these connections occur mainly in a paralemniscal zone in the lateral midbrain*". They suggested that these connections may also occur in the cuneiform nucleus of the midbrain, the region around the oculomotor complex, and the reticular formation dorsal to the superior olive (Henkel et al., 1978). However, Feliciano et al. (1995) have identified the paralemniscal zone in the lateral midbrain as being part of the auditory brainstem, because it receives projections from the primary auditory neocortex in the rat.

The findings of Henkel et al. and Feliciano et al. raise some questions about our initial hypothesis. Our hypothesis was that if eye rotation potentiated the PAMR at some point along the reflex pathway through the brainstem, we would expect eye rotation to increase the size of

the sound-evoked response without altering the level of background EMG in the muscle, whereas if the enhancement of the reflex with eye rotation occurred at the motor nucleus of the facial nerve, then we would expect that eye rotation would increase the amplitude of the sound-evoked PAMR and the background EMG simultaneously. What was *not* considered in this hypothesis was the possibility that *all* neural drive to the post-auricular muscles, be it reflex-related or voluntary, passes through the auditory brainstem before reaching the motor nucleus of the facial nerve. This may be sensible, as the pinnae are essentially auditory organs, the movements of which play a large part in sound localisation in many animals. This possibility is supported by the evidence of Henkel et al. (1978), and Feliciano et al. (1995), discussed earlier. If this were the case, then any potentiation of the reflex that occurred in the auditory brainstem would *also* result in an increase in the EMG recorded from the PAM, *and* an increase in the peak-to-peak amplitude of the sound-evoked PAMR.

The eye rotation experiments described here have shown that the PAMR amplitude and the EMG of the PAM are highly correlated, and that this correlation exists regardless of the means used to increase the EMG. However, the only conclusion we can draw from these experiments is that the mechanisms that increase the EMG *and* the PAMR probably occur at a common point (because of the shared time-course), but *we do not have any evidence to determine whether this common point is the motor nucleus of the facial nerve or in the auditory brainstem*. This is because we do not have any clear evidence that all neural inputs to the PAM do not *also* pass through the auditory brainstem on their way to the motor nucleus of the facial nerve.

The slight increase in EMG and PAMR amplitude observed with large (>60 degree) *contralateral* eye rotation could be the result of neural drive to the *medial rectus*. However, a

more likely explanation is that this increase is due to the same mechanism that causes the increased EMG during ipsilateral eye rotation, but with the neural drive coming from synergistic rather than voluntary contraction of the *lateral rectus* during contraction of the *medial rectus*. Such synergistic innervation is common among antagonistic muscle pairs, and prevents "wobble" during eye movements, and also limits damage due to excessive contraction or extension (Boeder, 1961; Burde and Feldon, 1985).

Summary and conclusions

The advantage of using eye rotation in enhancing the PAMR experimentally is that it is easier to obtain a graded increase in EMG of the PAM by altering the angle of the gaze, rather than increasing or decreasing the degree to which the subject tries to pull back on their ears, which can cause excessive muscle noise in the recordings. Additionally, not all subjects can voluntarily contract their PAM muscles, whereas most can rotate their eyes.

Subjects who are old enough can be instructed to rotate their eyes, while subjects who are too young to understand such instructions can be coaxed into fixating their gaze on an object (such as food or a toy) and, by moving the object or the child, can be made to follow its movements with their eyes. Indeed, such distraction techniques are commonly used in infant behavioural audiometry (Gerber, 1977). Examples of the effectiveness of this coaxing in our experiments can be found in Section 3.10.

In summary, the above experiments have found that the enhancement of the PAMR during eye movement coincides with increased electrical activity (EMG) in the post-auricular muscle observed during this manoeuvre, and that any procedure which increases electrical activity in the PAM enhances the PAMR if it is present. The similar time-courses of these changes indicate that the mechanisms that increase the EMG *and* the PAMR probably occur at

a common point. However, due to a lack of neuro-anatomical evidence, we cannot distinguish whether this common point is the motor nucleus of the facial nerve, as we had originally thought, or in the auditory brainstem. Despite the lack of evidence as to the precise mechanisms by which it occurs, ipsilateral rotation of the eyes was found to be a convenient and efficient method of enhancing the PAMR in most of our subjects, including infants (as shown in Section 3.10).

3.7 Attempts at identifying single motor unit responses in the PAM

As discussed in the Introduction, the electrical potential recorded as the is produced by the firing of muscle action potentials (MAPs, also referred to as "spikes") in the PAM in response to a sound stimulus, such as a click or tone-bursts. As summarised in Figure 3.6.1 of Section 3.6, these MAPs occur as the result of neural action potentials from the facial motor nucleus, which travel down the facial nerve to the PAM. These MAPs in the PAM also occur in the absence of sound stimuli, and form the largest component of the EMG recorded from the electrodes situated on the skin surface above the PAM, as demonstrated in Figure 3.8.1 of Section 3.8. Recordings of MAPs from single motor units were first made by Katz and Miledi (1965), and were shown in Figure 3.3.3 of Section 3.3.

This Section briefly describes some observations, made during the present study, that were a result of attempts to identify MAPs from individual motor units in surface, both in the absence and presence of click stimuli.

The electrical activity of single motor units of the PAM has been studied previously by De Grandis and Santoni (1980) using needle electrodes inserted into the body of the muscle. They found that "*the averaged* [motor unit] *responses to a click exhibited an initial component with a markedly constant latency, similar to the averaged surface response*"[1]. In addition to the "*initial component*" of the response, De Grandis and Santoni (1980) reported that "*later and smaller components were also observed with variable latency*". Example waveforms

[1] This is consistent with Jacobson et al. (1964), who reported that "*when unit activity is sampled from an optimal region of the muscle, a close match between the average from the surface and unit recordings can be obtained*".

demonstrating these initial and later MAPs are shown in Figure 3.7.1. The post-stimulus time histogram of MAPs from single motor units reported by De Grandis and Santoni is shown in Figure 3.7.2. The post-stimulus time histogram (PSTH) shows the percentage presence of spikes from 34 motor units distributed into of 2.5 ms intervals after the clicks. The main peak in this histogram was found at the 10 – 12.5 ms interval (comprising the first peak of the averaged PAMR waveform), with other peaks of progressively smaller amplitude present 25 ms, 37 ms, and 50 ms after the stimulus.

In the present study, attempts were made to identify these apparently repetitive patterns of MAPs in the electrical activity recorded from the surface of the PAM. This was done in two ways: i) by averaging the "rectified" versions of the click-evoked raw trace, and ii) by using a peak-detection algorithm to calculate the inter-spike intervals observed both in the presence or absence of the click stimulus.

3.7.1 Averaging of rectified raw responses

Attempts were made in the present study to correlate the peaks in the PSTH of De Grandis and Santoni (1980) with those of the averaged PAMR waveform. The only peaks that had been observed in the averaged PAMR were i) the first peak observed 12 - 15 ms after the click stimuli, ii) the second peak occurring between 18 and 24 ms, and iii) a small, rounded peak of variable latency (usually between 30 and 40 ms) that often followed the second peak (for example, at around 37 ms in the trace shown in Figure 1.4 on page 10).

However, as the peaks in the De Grandis & Santoni PSTH were observed to become smaller (and progressively broader) with increasing post-stimulus time, it was possible that the absence of peaks after 40 ms was due to a "washing out" of the average, as the peaks of one response fall into the troughs of other responses. To avoid this cancellation, raw PAMR

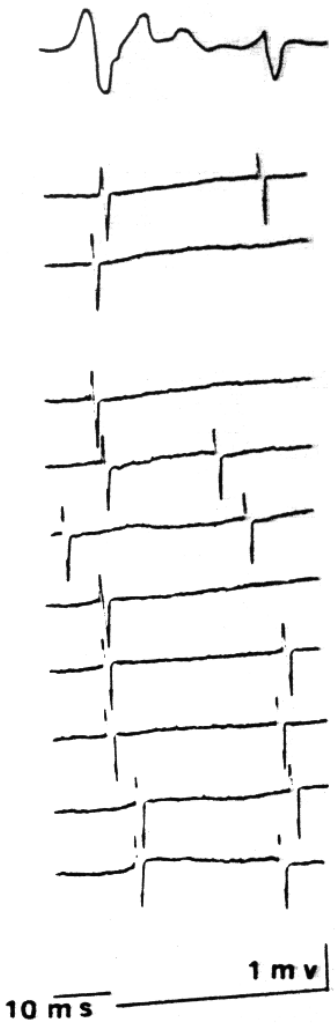

Figure 3.7.1: Ten consecutive motor unit responses recorded with single-fibre EMG electrode inserted into the PAM. The top trace shows the averaged response to 50 stimuli. These traces show the spikes coinciding with 12.5 ms and 25 ms peaks in the post-stimulus time histogram below (De Grandis and Santoni, 1980).

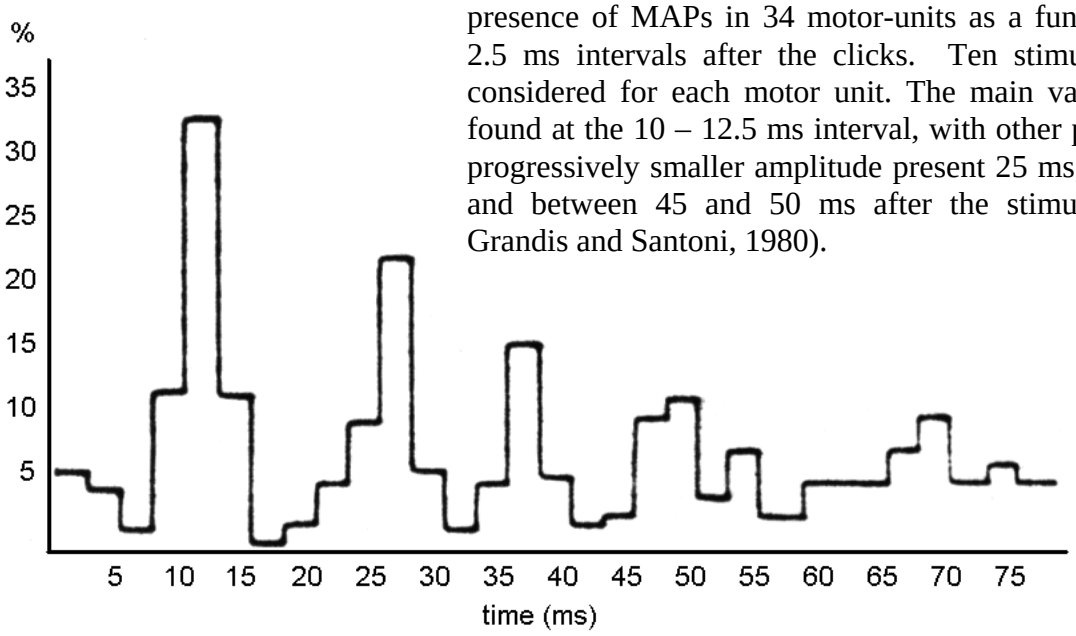

Figure 3.7.2: The post-stimulus time histogram of the presence of MAPs in 34 motor-units as a function of 2.5 ms intervals after the clicks. Ten stimuli were considered for each motor unit. The main value was found at the 10 – 12.5 ms interval, with other peaks of progressively smaller amplitude present 25 ms, 37 ms, and between 45 and 50 ms after the stimulus (De Grandis and Santoni, 1980).

waveforms of 100 ms duration were digitally full-wave-rectified before averaging. That is, the absolute-value of the voltages in the waveform array were calculated, and this absolute-value waveform was then averaged. The results of this averaging of 200 PAMR waveforms are shown in Figure 3.7.3. On magnification of the absolute-value waveform, a small upward rise (of approximately 0.8 μV) was observed at 46 ms, followed by a larger, pointed peak (approximately 2 μV above the background noise level) with a latency of 56 ms.

These observations are consistent with the PSTH described by De Grandis and Santoni (1980). Just as the synchronous firing of MAPs 12 ms after the click stimulus (shown in the PSTH of Figure 3.7.2) results in the normal PAMR peaks at 12 ms and 18 ms, it is possible that the slightly less synchronous firing of MAPs from different units between 45 and 50 ms (shown in the PSTH) results in this "smeared" rise at 46 ms and peak at 56 ms. In the absolute-value averaged waveform shown in this particular example, the second peak (18 ms) is larger than the first peak (12 ms). Similarly, the peak at 56 ms is larger that that at 46 ms, indicating that they could be due to the negative and positive peaks of the smeared firing between 45 and 50 ms after the synchronising click.

3.7.2 Inter-spike intervals in gross recordings of electrical activity

Calculating PSTHs of spike activity from single motor units is a relatively simple procedure, as each spike originates from the same motor unit. However, while it is possible to observe single spikes in gross recordings of electrical activity of the PAM (as shown in Figure 3.8.1 of Section 3.8), the task of identifying a preferred repetition rate of these spikes is complicated by the fact that the recordings made from the skin surface above the muscle is a recording of the activity of multiple motor units, usually firing concurrently.

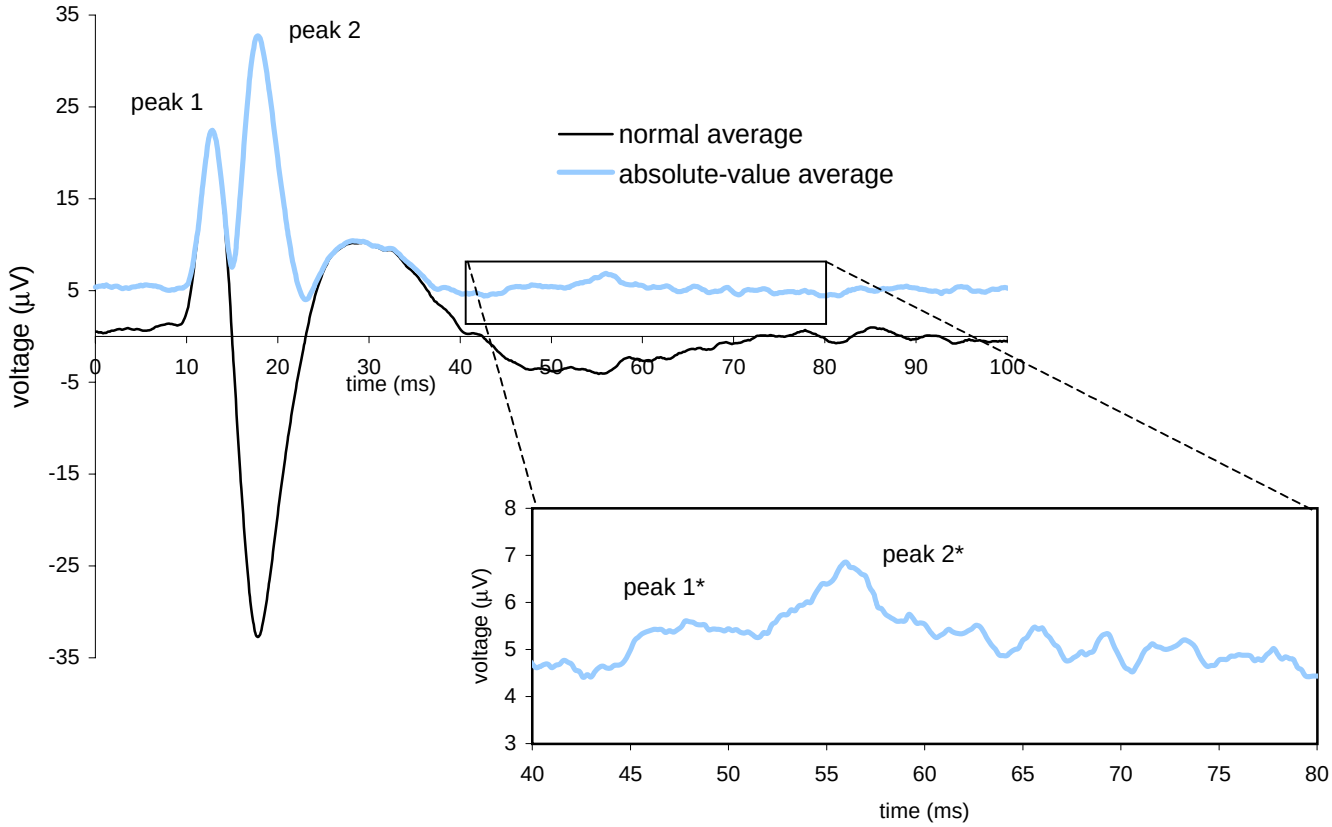

Figure 3.7.3: Averaged normal PAMR waveforms and full-wave rectified PAMR waveforms (n = 200). According to the post-stimulus time histogram of De Grandis and Santoni (1980), peak 1 and peak 2 are due to synchronous firing of MAPs in the PAM 12 ms after the click stimuli. If this is the case, then peaks 1* and 2* shown in the inset are possibly due to the slightly less synchronous firing of MAPs between 45 and 50 ms after the click stimuli.

In an attempt to examine this spontaneous (i.e. non-sound-evoked) firing activity in the PAM, a VI containing a peak-picking algorithm was used to calculate the inter-spike intervals in traces of spontaneous activity recorded from the PAM. The pulse used to trigger the acquisition of this data was from by the custom-built click generator, which produced clicks at 588 ms intervals in the "slow" setting, as described in Section 2.2. The traces from the PAM were therefore recorded in 500 ms sections, separated by an 88 ms gap, during which time each waveform was saved to file.

Once these 500 ms waveforms had been recorded, they were fed to the peak-picking VI, which recorded the locations (time in ms after the trigger pulse) and peak amplitudes (in μV *above* zero) of the MAPs present in the waveforms. Our working hypothesis was that the responses from a single motor-unit would be similar in amplitude, because they were a similar distance from the recording electrode, and were propagated along muscle fibres that had the same electrochemical properties. Therefore, when the MAPs of similar amplitude were grouped together and analysed, it was hoped that it would be possible to discover the preferred firing intervals of the MAPs.

There were, however, problems which prevented any meaningful information from being extracted using this technique. The first problem was that there was a small but significant amount of low-frequency "rumble" in the recordings. These low-frequency components caused a great deal of variation in the peak amplitudes of the spikes, which contaminated the procedure of grouping of the spikes by amplitude. However, when the low-frequency components were filtered out, the phase-distortion and reduction in amplitude of the spike caused by the high-pass filtering also reduced any differences in peak-amplitude between spikes from different motor units, and so the data from the peak-picking algorithm was useless.

In an attempt to solve this problem, the peak-picking algorithm was heavily modified (over a period of a week) so that it was capable of "picking" both the positive and the negative peaks, so that the peak-to-peak amplitude could be used instead. However, it was extremely difficult and time-consuming to match the data from the negative peaks with that from the positive peaks, and so this avenue of investigation was not pursued.

During the period over which these experiments took place, a large number of 500 ms waveform sets were recorded. It was noticed that while the waveforms were being recorded and simultaneously displayed on the front panel of the VI, it often appeared as if a spike was stationary on the screen from trace to trace, or was moving slowly across the screen with each new trace. At first these observations were dismissed as animation-like illusions. However, they occurred so regularly that it was decided to examine the raw waveforms for these instances.

In order to do this, the raw waveforms were plotted along a single 500 ms time axis, but with consecutive waveforms plotted above each other (offset along the vertical axis), so that the patterns of activity could be examined. An example of this type of plot is shown in Figure 3.7.4. Starting from the bottom trace in this figure, and moving upwards, a particular point between 0 and 500 ms in each trace occurs 588 ms after the corresponding point in the trace below it. In this trace, the spikes often seemed to be aligned in diagonal or vertical "runs" of between 3 and 5 spikes. To determine whether the regularity of these runs of spikes was real, or just imagined, the inter-spike intervals of a number of sets were examined. Shown in Figures 3.7.5 and 3.7.6 are examples of traces where MAPs appear to have occurred with very long inter-spike intervals (ISIs).

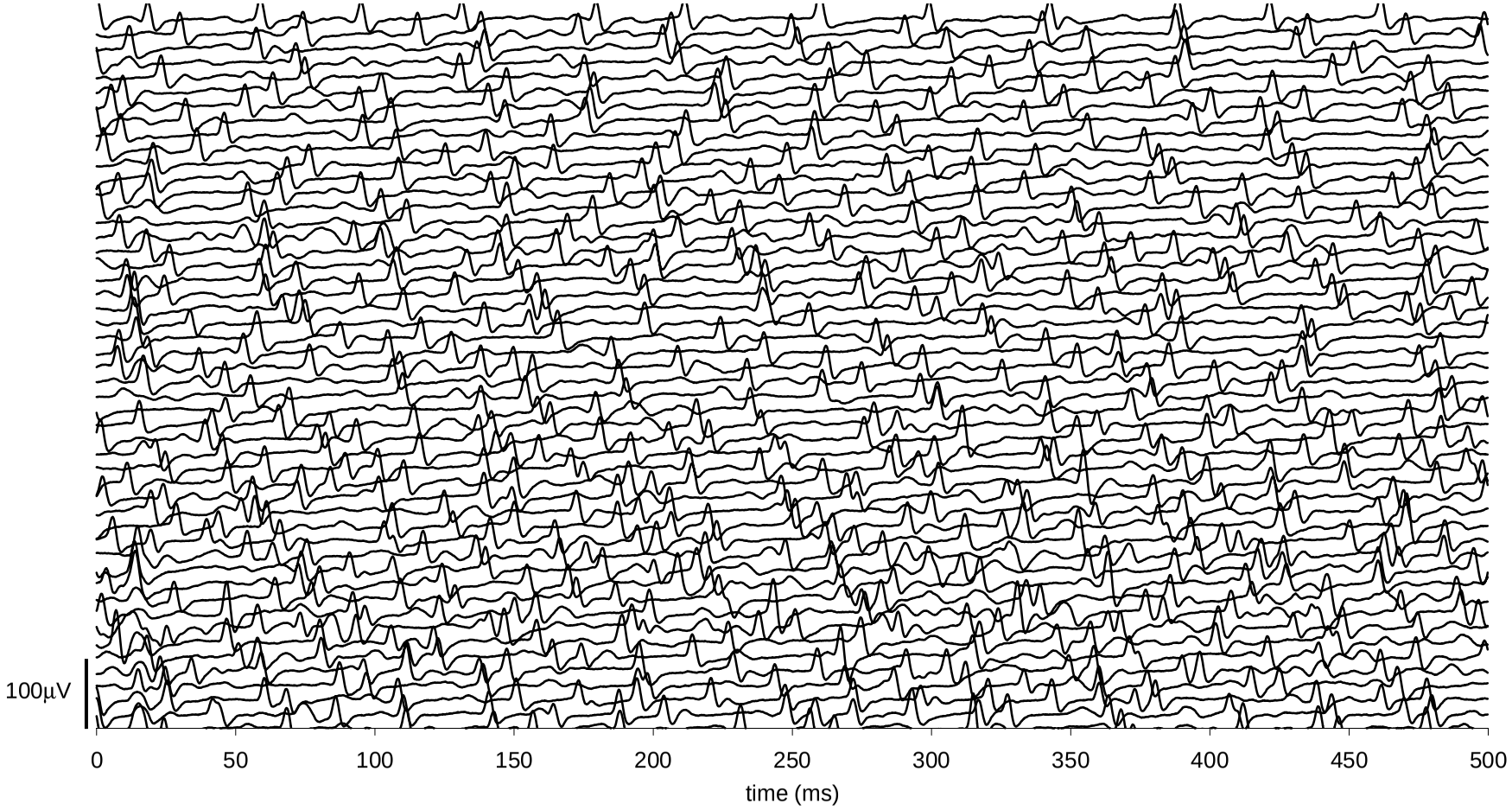

Figure 3.7.4: An example of the gross electrical activity recorded from the surface of the PAM. Each trace is 500 ms long, and there is a gap of 88 ms between the "500 ms" mark of one trace and the "0 ms" mark of the trace above it.

For example, in Figure 3.7.5, *at least* five sets of long-ISI spikes were observed. These spikes have been coloured for identification. The intervals between these possible groupings in Figure 3.7.5 were as 594.7 ms ± 1.85 ms (blue), 575.4 ms ± 1.8 ms (green), 578.6 ms ± 0.8 ms (orange), 582.5 ms ± 0.4 ms (yellow), and 588.7 ms ± 1.3 ms (pink). These groupings were highly regular. In this figure, the standard deviations of the coloured groupings were, on average, just 0.2 % of the long inter-spike interval.

In Figure 3.7.6, the interval between the blue-coloured spikes was 596.46 ms ± 2.14 ms (this standard deviation equivalent to 0.36 % of the inter-spike interval). Several other examples of this apparent long-ISI were observed, but are not presented here.

Discussion

The "absolute-value" technique discussed in Section 3.7.1 made it possible to identify what appears to be peaks due to the synchronous firing of MAPs between the 45 ms and 55 ms time intervals. This is consistent with the firing patterns shown in the PSTH reported by De Grandis and Santoni (1980). The peaks in the histogram between 45 ms and 55 ms are smaller and broader than the earlier peaks (12 ms, 25 ms), indicating that the firing of MAPs from different units is less synchronised than the firing reflected in earlier peaks of the histogram. The later peaks are not apparent in normally-averaged waveforms, as the peaks from one stimulus are likely to be cancelled by the troughs from another. By averaging the full-wave rectified versions, this cancellation effect is avoided, and any peaks (be they positive-going or negative-going) appear in the averaged waveform. This smearing of later PSTH peaks after a synchronising stimulus (the click, in this case) is common across neural populations, due to slight differences in electrical properties and preferred intervals across a fibre population.

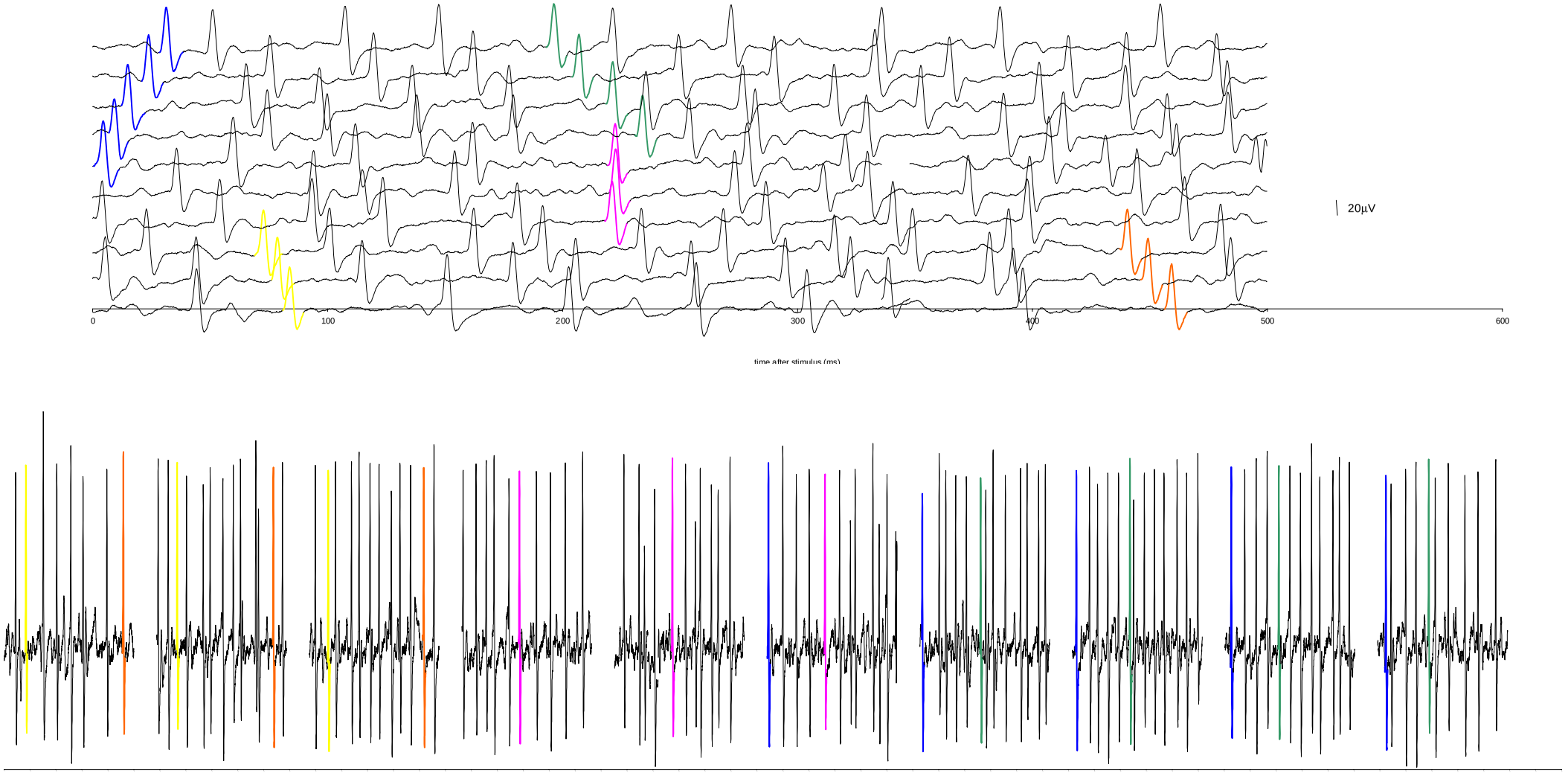

Figure 3.7.5: An example of the long-inter-spike interval "runs" of MAPs in the electrical activity recorded from the PAM. The top set of traces is similar to that in Figure 3.7.4. The bottom trace presents this same spike data as a single recording of approximately 5.8 seconds. The average inter-spike intervals for the coloured groupings were 594.7 ms ± 1.85 ms (blue), 575.4 ms ± 1.8 ms (green), 588.7 ms ± 1.3 ms (pink), 582.5 ms ± 0.4 ms (yellow), and 578.6 ms ± 0.8 ms (orange). The standard deviations of the coloured groupings were, on average, just 0.2 % of the long inter-spike interval.

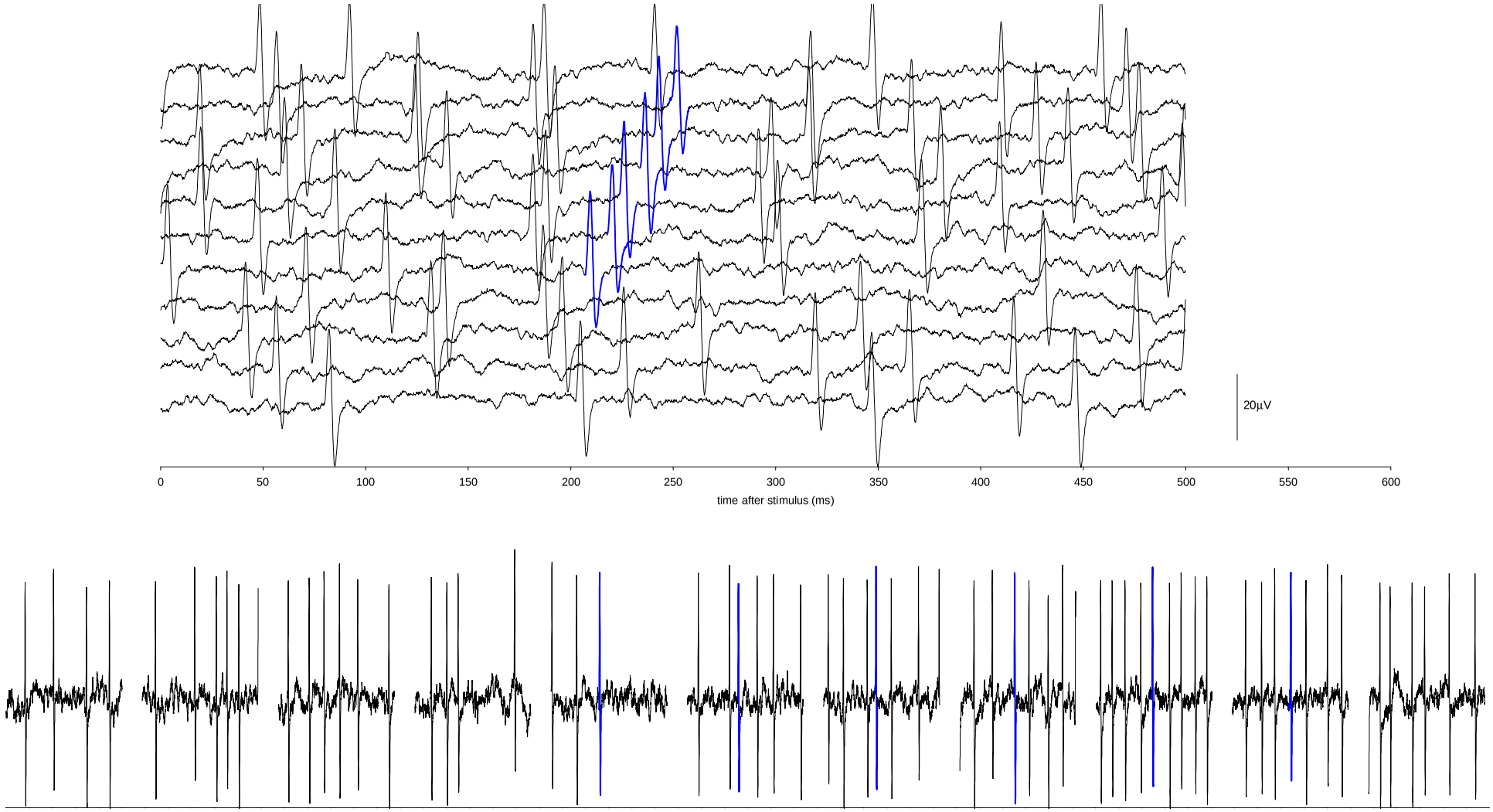

Figure 3.7.6: Another example of the a long-inter-spike interval "run" of MAPs in the electrical activity recorded from the PAM. The top set of traces is similar to that in Figure 3.7.4. The bottom trace presents this same spike data as a single recording of approximately 6.4 seconds. The average inter-spike interval for the blue grouping was 596.46 ms ± 2.14 ms (this standard deviation equivalent to 0.36 % of the inter-spike interval).

The findings discussed in Section 3.7.2 (the long inter-spike interval "runs" of MAPs) are not consistent with the preferred firing intervals observed in the PSTH of De Grandis and Santoni (1980). However, their histograms showed the firing that occurred after a click stimulus, whereas the traces shown in Figures 3.7.5 and 3.76 were recorded in the absence of click stimuli.

The regularity of these runs suggests that this firing was not random. The traces were examined to see if these patterns were better described by the interaction of short ISI MAPs, but the regularity of the firing observed was not adequately accounted for by this possibility. The long inter-spike intervals reported above are all within 15 ms (or 3%) of the trigger interval of the data acquisition system (588 ms). It is the similarity between these rates that made these patterns visible to the eye. Many of the spikes shown in Figures 3.7.4 to 3.7.6 could not be matched with others with intervals that were close to 588 ms. It is likely that there are a large range of firing rates of the MAPs, and that we only noticed those with intervals close to our data-acquisition interval. It is possible that if a different trigger interval (for example, of 400 ms, or 700 ms) had been used instead of 588 ms, then any MAPs with ISIs similar to 400 or 700ms would have been noticed.

These firing rates may also have been caused by repetitive firing of neurones that innervate with the motor nucleus of the facial nerve, as described in Section 3.6. For example, the firing rates observed in Figure 3.7.5 and 3.7.6 could be similar to those in neurones controlling voluntary contraction of the PAM, or of the neurones connecting the superior colliculus.

Alternatively, the long-ISI runs of MAPs may actually be sound-evoked responses to noise in the recording environment. The traces were recorded in the absence of click stimuli,

but the recordings were not conducted in a sound proof room. Although no such noise was noticed at the time, it is possible that there were repetitive sharp-onset noises due to electrical equipment, and so on. Although this seems unlikely, to reduce this possibility, it would have been better to carry out these experiments in a completely silent environment.

In summary, the averaged rectified signals show evidence of repetitive firing with an interval of about 45 ms, consistent with the observations of De Grandis and Santoni (1980), but the peak-picking algorithms we used were not successful in the time available. There is also some evidence for much longer preferred intervals (about 590 ms). Just whether these preferred intervals come from the neurones of the facial nucleus or cells innervating them is unclear.

3.8 Spectral analysis of the PAMR

Spectral analysis of the electrical potentials recorded from the post-auricular region was used as a tool to examine i) the contribution of the PAM potentials to the electrical activity recorded from the skin surface above the PAM, ii) the improvement in signal-to-noise ratio achieved when the reference electrode was placed on the dorsal surface of the pinna, rather than the forehead, and iii) the effect that eye rotation has on PAM electrical activity, both ipsilateral (looking towards the same side of the head as the recorded PAM) and contralateral (looking towards the side of the head opposite to the recorded PAM).

As shown in Section 3.7, spontaneous muscle action potentials, or "spikes", often occur in the PAM in the absence of sound stimuli, and it is the presence of these spikes that determines the tone of the muscle. The word "spontaneous" is used here to distinguish those PAM spikes *not* evoked by sound stimuli. Recordings of this electrical activity were made from electrodes placed over the right PAM of a subject in whom clear spikes could be elicited by very slight voluntary contractions of the muscle.

During one PAMR recording session for this subject, it was observed that when the subject was at rest, in the absence of sound stimuli, the spikes were either absent, or present at an average amplitude of 79 μV (± 2.6 μV). The opportunity was taken to measure the voltage spectrum of the electrical activity for both of these states, shown in Figure 3.8.1 overleaf, so that the contributions of both of these components to the overall voltage spectrum could be determined. A Blackman-Harris window function was used during the recording of these voltage spectra, for reasons discussed in Section 2.4.

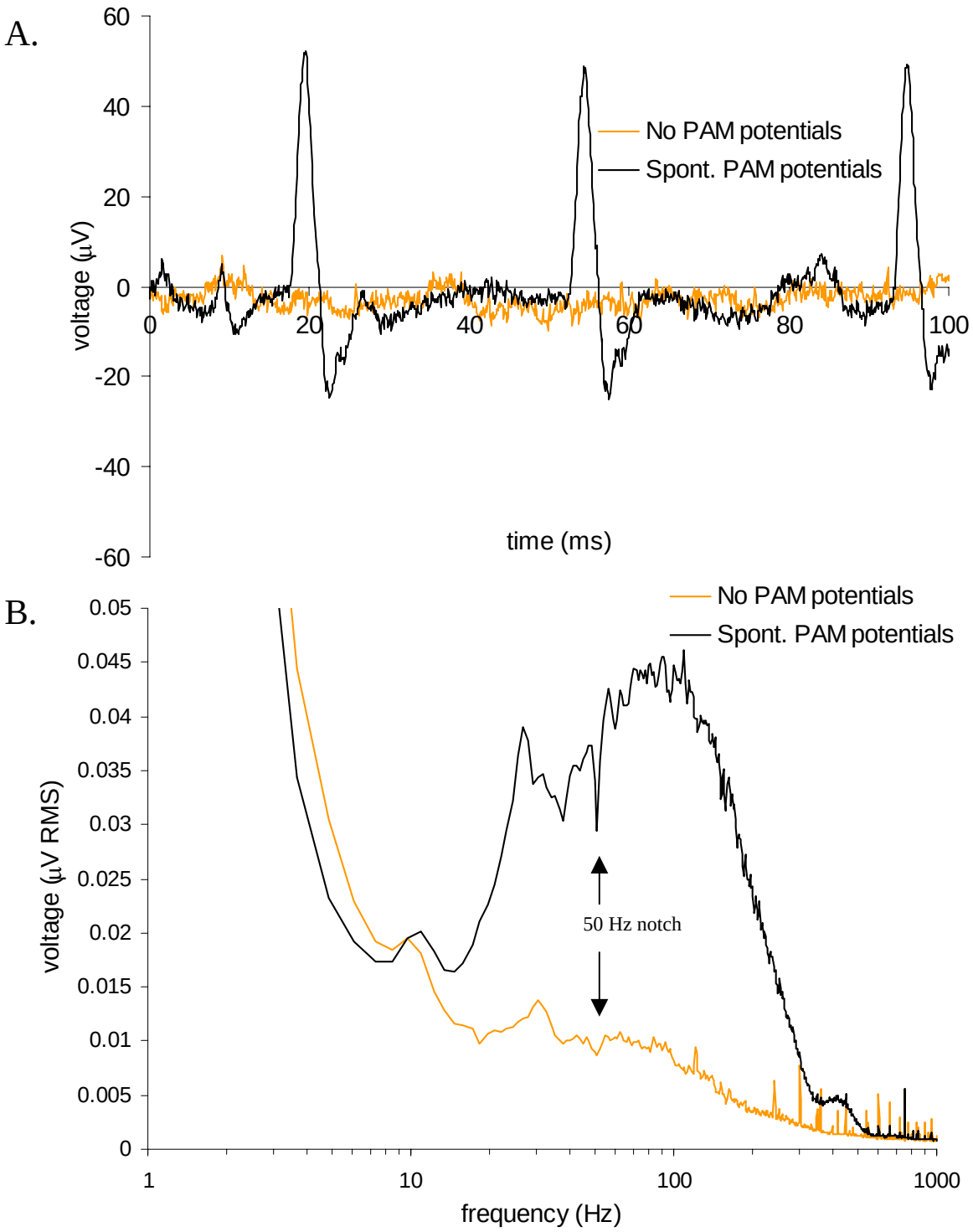

Figure 3.8.1: **A.** Two waveforms recorded from the PAM of a normal adult subject. In one of the traces, three spontaneous muscle action potentials can be observed. The almost identical morphology and amplitude of the three spikes indicated that they were likely to originate from the same motor unit. **B.** The voltage spectra for both these waveforms. The electrical activity attributable solely to the presence of the PAM spikes extended from 10 Hz to approximately 550 Hz, with a broad spectral peak centred between 70 and 115 Hz. Recording bandwidth: 1 Hz to 5 kHz, with a 50 Hz notch filter. Active electrode: PAM. Reference: pinna.

The sample rate of the data acquisition system was 10,000 samples/sec, to allow a high-pass limit of 5 kHz to be used during the recordings.

The spontaneous PAM spike time waveform, shown in Figure 3.8.1 A., showed only a slight increase in background electrical activity during the intervals between the spikes. The length of the inter-spike intervals for the spontaneous potentials varied over the 2 minutes that the spectra were calculated, with a standard deviation of 14 ms about the mean inter-spike interval of 40 ms.

The voltage spectrum for the spontaneous PAM spikes showed a broad peak centred around 100 Hz, with the signal distributed evenly between 70 Hz and 115 Hz. In comparison, the spectrum for the background noise (i.e. when there are no PAM spikes present) showed no such peak. The large voltages in the low-frequency region of the spectrum (i.e. below 5 Hz) were not due to these spikes, but were most likely caused by distant muscle activity, such as from the jaw or neck. The vertical axis in Figure 3.8.1 B has therefore been scaled to show the relevant portions of the voltage spectra in greater detail. Visible in both spectra was the effect of the 50 Hz notch filter, which reduced the interference from the mains power supply.

The effect of eye rotation on the spectral characteristics of the PAM electrical activity is shown in Figure 3.8.2. Voltage spectra were recorded from the right PAM during three conditions of eye rotation, in the absence of sound. The spectra presented in Figure 3.8.2 are averages of 400 individual spectra for each condition. During ipsilateral eye rotation, the gaze of the subject was shifted hard towards the active PAM electrode. Conversely, during the contralateral eye rotation, the subjects gaze was hard in the opposite direction. During the “eyes forward” condition, the eyes of the subject were facing forwards in a relaxed manner. Spontaneous PAM spikes were observed in the raw trace during the eyes forward period.

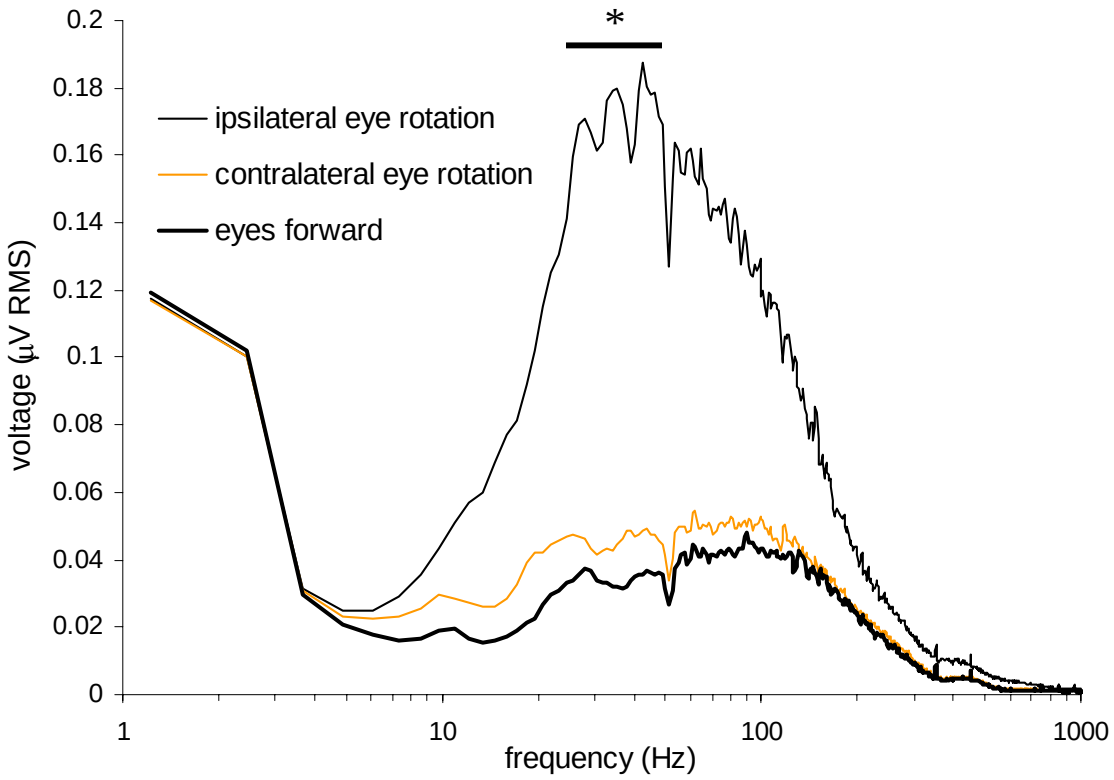

Figure 3.8.2: The voltage spectra recorded from the right PAM for three conditions of eye rotation: ipsilateral eye rotation, contralateral eye rotation, and eyes forward. The total increase in electrical activity between 1 and 1000 Hz (compared to eyes forward) was 163% during ipsilateral eye rotation, and 16% during contralateral eye rotation. Each spectrum is an average of 400 individual spectra. Recording bandwidth: 1 Hz to 5 kHz. Active electrode: PAM. Reference electrode: pinna.

When compared to the "eyes forward" condition, the voltage spectrum recorded during ipsilateral eye rotation showed an average 250% increase in electrical activity (RMS voltage) in the region between 50 Hz and 150 Hz, and an average 400% increase in the region between 25 Hz and 50 Hz (marked with an asterisk on Figure 3.8.2). The slight increase in electrical activity (approximately 20% between 50 and 100 Hz) during contralateral eye rotation is consistent with the increase in PAMR peak-to-peak height observed during this manoeuvre, as shown in Figures 3.6.9 and 3.6.10 of Section 3.6.2.

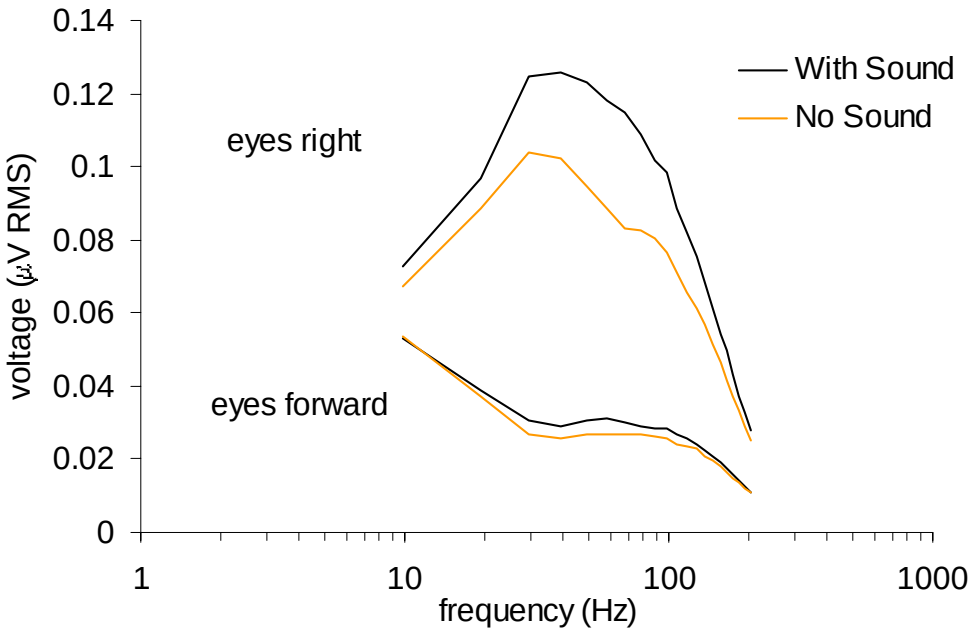

Figure 3.8.3: The voltage spectra recorded from the right PAM with the eyes forward and right, with the click stimuli either on or off. Note the increase in electrical activity when the click stimuli were present. Each spectrum is an average of 1200 individual spectra. Recording bandwidth: 10 Hz to 200 Hz, no notch filter. Active electrode: PAM. Reference electrode: pinna.

An increase in electrical activity was also observed when the PAMR was evoked by click stimuli, compared to the spontaneous PAM potentials recorded in the absence of sound. Figure 3.8.3 above shows an increase in electrical activity in the 25 Hz – 100 Hz region of 12% for the eyes forward condition, and 28% for the eyes right condition.

The effect of reference electrode location on the PAM voltage spectrum was also studied. Initially, a forehead electrode had been used as the reference location for the active electrode placed directly over the PAM. However, it was found that greater response amplitudes could be obtained by placing the reference electrode on the dorsal surface of the pinna, as shown in Figure 3.3.4 of Section 3.3. This electrode placement also had the effect of eliminating blink artefacts, as shown in Figure 3.3.5 of Section 3.3.

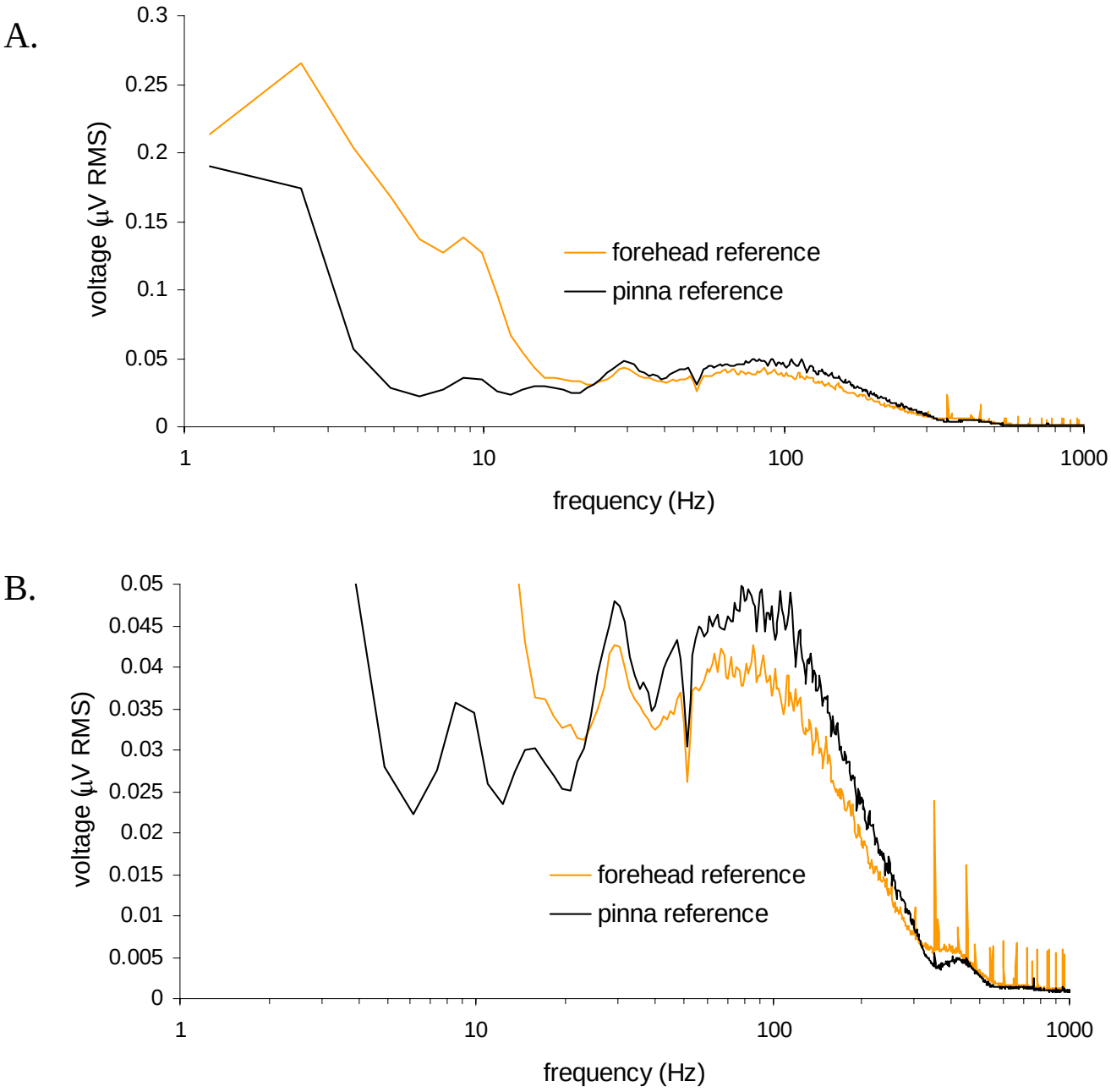

Figure 3.8.4: A. The voltage spectra recorded from the PAM with the reference electrode place on the forehead, and with the reference electrode placed on the dorsal surface of the pinna. Note the increased low-frequency "rumble" obtained with the forehead reference. **B.** A scaled version of A., showing the region between 25 Hz and 1000 Hz in greater detail. Note the increase in signal voltage between 25 Hz and 300 Hz, and the decreased higher-frequency electrical interference obtained with the pinna reference electrode. The recording bandwidth for both spectra was from 1 Hz to 5 kHz.

To compare the differences in PAM voltage spectra obtained with the reference electrode on the forehead and the dorsal surface of the pinna, 400 recordings of the voltage spectra were made with each reference electrode location. The averages of these spectra are shown in Figure 3.8.4. It can be seen from the spectra in Figure 3.8.4 A that electrical activity in the region below 25 Hz was, on average, 110% greater when the reference electrode was placed on the forehead than when the electrode is placed on the pinna. In the region between 25 Hz and 300 Hz, the electrical activity recorded with the pinna reference electrode was, on average, 20% greater than that recorded with a forehead reference, as shown in Figure 3.8.4 B. In the region above 300 Hz, an increased level of interference caused by electrical equipment was observed when a forehead reference was used.

Discussion

As shown in Figure 3.8.1, the voltage spectrum of the electrical activity recorded from the surface of the skin above the PAM can be separated into components that are due to i) the firing of muscle action potentials from the PAM, and ii) electrical activity from other sources, such as neural activity, distant muscle activity, and external electrical interference. The voltage spectrum of the electrical activity attributable to the firing of spontaneous PAM action potentials extends from 10 Hz to approximately 550 Hz, with a broad spectral peak centred between 70 Hz and 115 Hz.

These findings conflict with the spectral analysis of the PAMR carried out by Thornton (1975). Thornton found that the main spectral peak of the PAMR occurred at 600 Hz, and that the spectrum extended from approximately 100 Hz to 1.6 kHz, as shown in Figure 3.8.5.

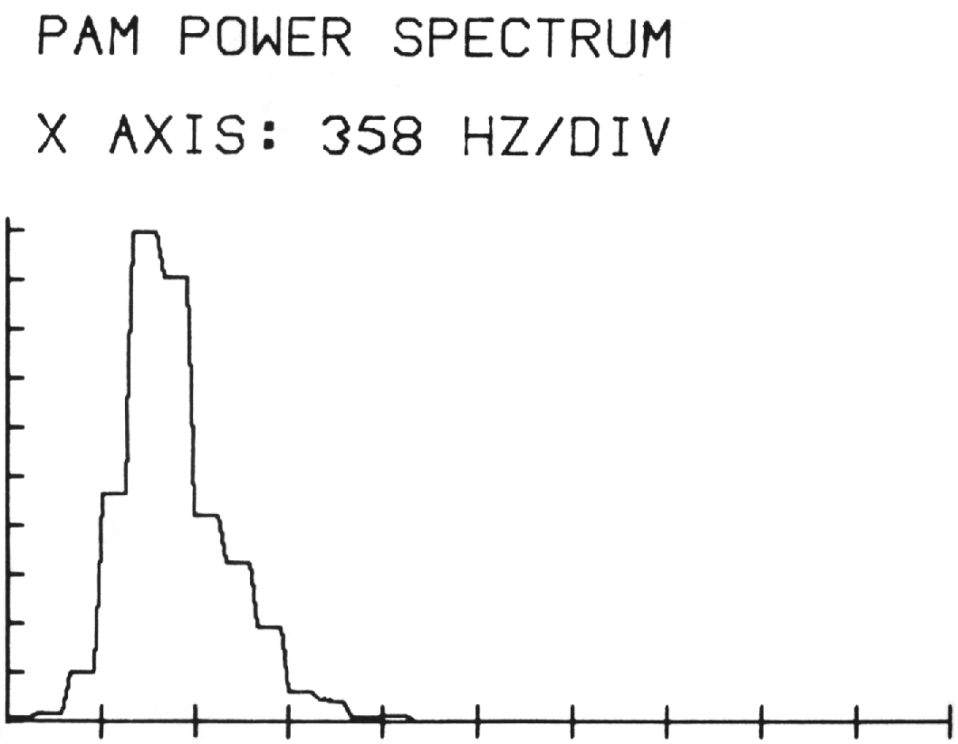

Figure 3.8.5: The power spectrum of the PAMR recorded by Thornton, showing that "the main spectral peak is at about 600 c/sec and the spectrum extends from approximately 100 c/sec to 1.6 kc/sec" (Thornton, 1975).

No other measurements of the PAMR voltage spectrum could be found in the literature, and so Thornton's results have gone unquestioned for 23 years. In his book on evoked responses, Hall (1992) cites Thornton's results regarding the spectrum of the PAMR, despite mentioning in a previous sentence the somewhat conflicting statement that "a filter setting of approximately 1-200 Hz was used in purposeful measurement of the PAM response" (Hall, 1992).

Figure 3.8.2 shows that the increase in EMG recorded from the PAM during ipsilateral eye rotation (see Section 3.6) occurs in the same frequency range as the spontaneous PAM action potentials, but with an increased distribution of voltage between 25 Hz and 50 Hz, compared to the region between 50 Hz and 150 Hz. The changes in voltage distribution during this manoeuvre indicate that with tonic contractions of the PAM caused by ipsilateral eye

movement, there is a component of the voltage spectrum recorded from above the PAM that derives from sources other than the muscle action potentials of the PAM itself. One possible source of this electrical activity is the contraction of the *lateral rectus* muscle, the extraocular muscle responsible for this particular eye rotation.

The increased electrical activity that occurs with both ipsilateral and contralateral eye rotation, shown in Figure 3.8.2, is consistent with the effects of gaze angle on PAMR amplitude discussed in Section 3.6.2.

Figure 3.8.3 shows the spectrum of the increased electrical activity observed in the presence of click stimuli. This increase is likely to be caused by a combination of the following factors. As described in Section 3.4, the magnitude of the PAMR evoked by binaural click stimuli is approximately twice that of the PAMR evoked by monaural stimuli, and twice the average magnitude of spontaneous PAM spikes. Therefore, it would be expected that there would be a large increase in the magnitude of the electrical activity observed in the spectrum when the binaural click stimuli were introduced. However, the repetition rate of the click stimulus used was only 8/s (125 ms period). Since this stimulus rate is significantly less than the spontaneous firing rate of the PAM potentials, the proportion of the spontaneously occurring PAM spikes that are actually modified in amplitude by the click stimuli would be quite low. The percentage increase in PAM electrical activity that was caused by the click when the eyes of the subject were rotated to the right was more than twice that recorded when the eyes faced forwards. This can be attributed to the increased number of active PAM motor units during voluntary contraction of the PAM.

Figure 3.8.4 illustrates the advantages of using a pinna reference electrode location instead of a forehead reference. As shown in Figure 3.8.1, the voltage spectrum of the electrical activity due to the firing of muscle action potentials from the PAM (rather than the background noise) extends from 10 Hz to approximately 550 Hz, with a broad spectral peak centred between 70 Hz and 115 Hz. The pinna reference electrode placement increased the magnitude of the "signal" component of the electrical activity (i.e. that activity due to the PAM itself), while decreasing the "noise" from other sources, such as the large voltage activity observed in the sub-15 Hz region, and the non-physiological electrical interference indicated by the sharply pointed peaks in the spectrum observed above 300 Hz.

The decreased non-physiological electrical interference encountered when the pinna reference electrode location was used is likely to be caused by the active and reference electrodes being physically closer together. For a point-source of electrical interference, this reduction of the amplitude of the interference occurs because the interference signal recorded by the active electrode is more similar in phase and magnitude to an interference signal recorded by a *nearby* reference electrode than that recorded by a more distant reference electrode. Therefore, the subtraction of the reference signal from the active signal (as occurs in differential recordings) results in greater cancellation of the interference signal when the reference and active electrodes are closer together. Electrical noise of physiological origin is also reduced for similar reasons. In addition, the forehead reference electrode generally lies directly above the frontalis muscle, which is electrically active during eyebrow movements and reflex blinking (as demonstrated in Figure 3.3.5 of Section 3.3), and is also the source of another myogenic sonomotor reflex potential (Picton et al., 1974).

The reduction in the low-frequency “rumble” that was achieved with the pinna reference electrode location also served to increase the reliability of the correlator as a method of signal detection, as discussed in Section 2.6.

3.9 Distortion of the PAMR due to system bandwidth limits

When recording evoked potentials, it is important that filter settings are chosen that improve the signal-to-noise ratio of the desired potential. This is primarily achieved by filtering out the extraneous biological signals, such as background muscle and neural activity, and noise from external sources, such as electrical equipment. As shown in Figure 3.8.1 of Section 3.8, the PAMR waveform contains frequency components between 15 Hz and 500 Hz, with a main peak broadly centred around 100 Hz. Filtering the waveform to remove frequency components outside of this range would improve the signal-to-noise ratio. However, when a signal passes through a filter, it is modified in amplitude and/or phase (Ifeachor, 1993), which can distort the shape of the waveform. The severity of this modification depends on the characteristics of the filter, and the high- or low-pass frequencies at which the signal is filtered.

The effect of different low-pass filter limits on the morphology of the PAMR waveform is shown in Figure 3.9.1. A set of 400 PAMR waveforms were recorded with a filter bandwidth of 1 Hz to 5 kHz, and averaged. The averaged waveform was then digitally filtered offline with low-pass limits of 1 kHz, 500 Hz, 200 Hz, 100 Hz, and 50 Hz, using a 2nd-order Bessel filter function on LabVIEW.

As the degree of filtering was increased, there was a reduction in the amplitude of the signal from 90 μV pp when low-pass filtered at 5 kHz, to 38 μV pp when low-pass filtered at 50 Hz. A temporal shift in the PAMR waveforms was also observed with successive reduction of the low-pass filter limit. The latency of the first peak of the waveform increased from 12.8 ms when filtered with a 5 kHz low-pass limit, to 15.8 ms when filtered with a low-pass limit of 50 Hz.

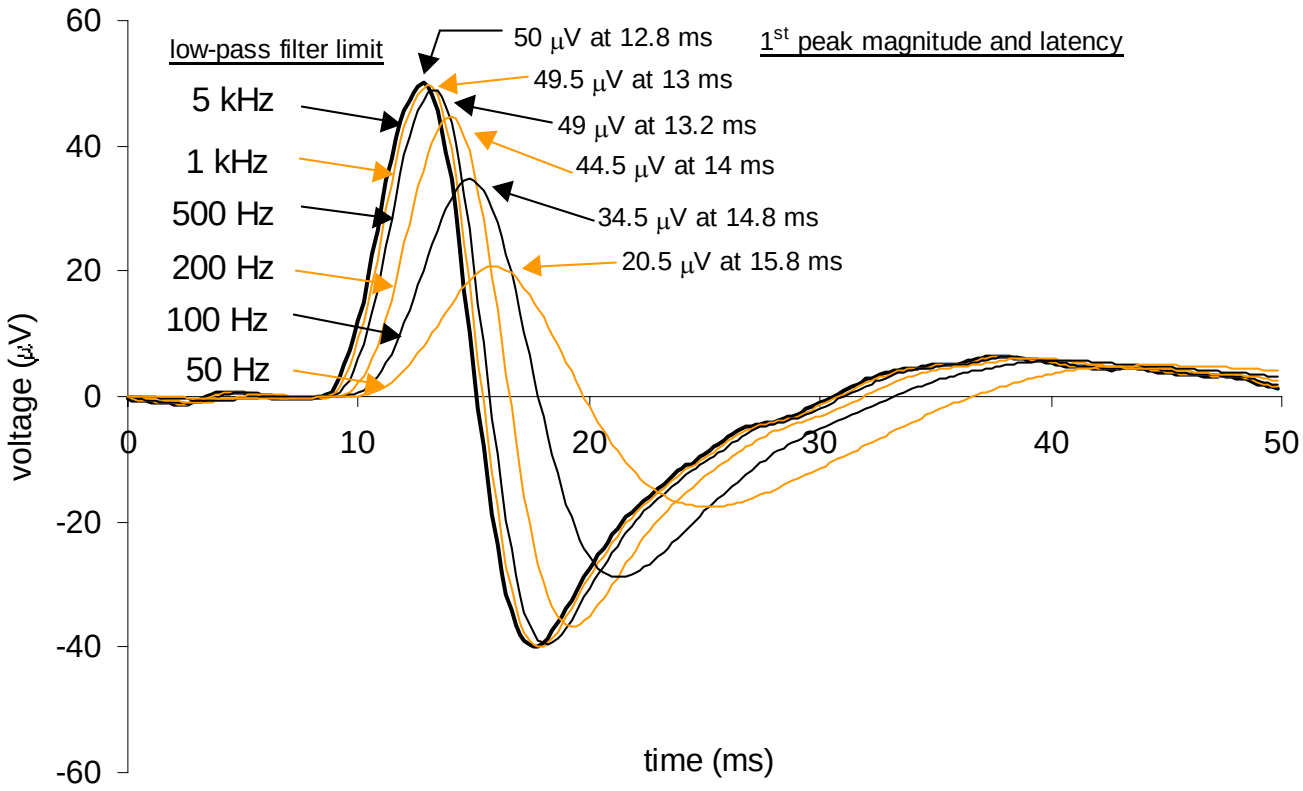

Figure 3.9.1: The changes in latency and magnitude of the first peak of the PAMR caused by digitally filtering an averaged waveform (n = 400) with low-pass filter limits of 1 kHz, 500 Hz, 200 Hz, 100 Hz, and 50 Hz. The original waveforms making up the average were recorded with a bandwidth of 1 Hz – 5 kHz.

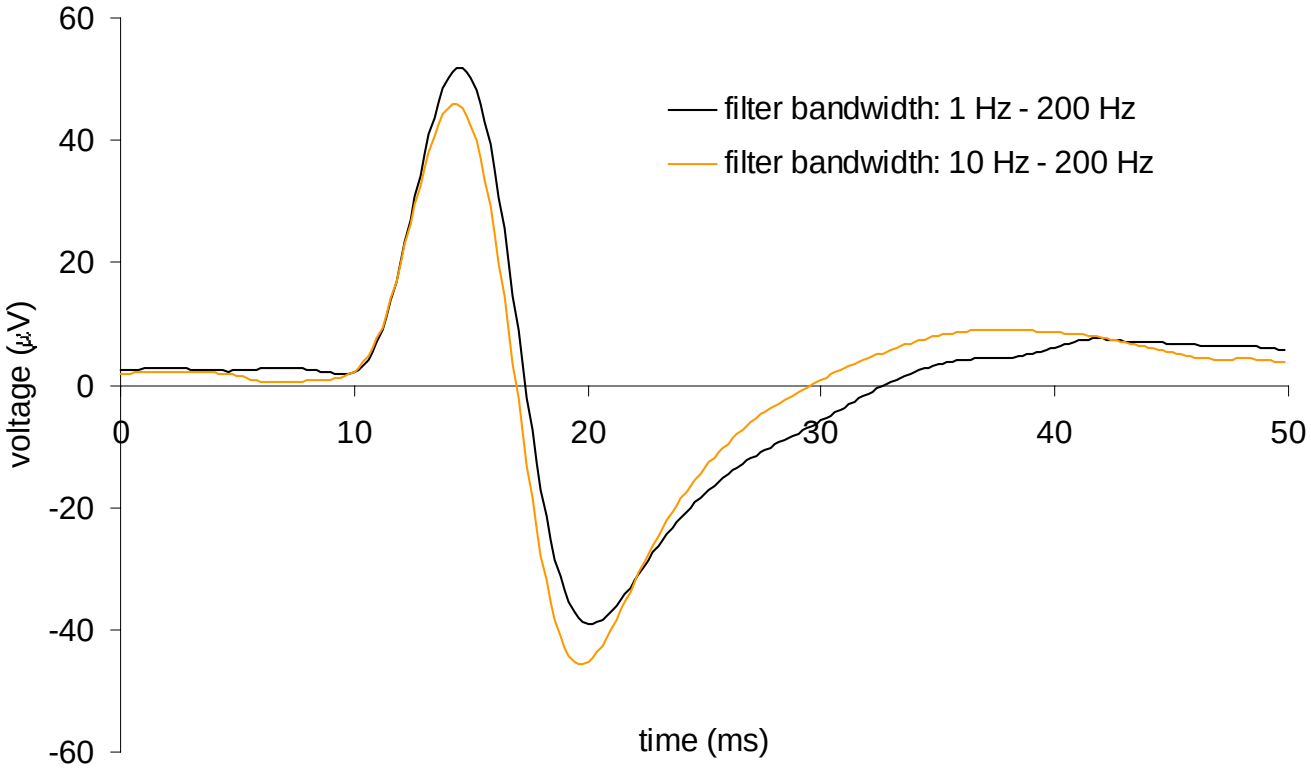

Figure 3.9.2: A slight decrease in PAMR latency is observed when the high-pass filter limit is increased from 1 Hz to 10 Hz. In this example, the first peak latency decreased from 14.5 ms (± .13 ms) to 14.3 ms (± .14 ms), while the second peak latency decreased from 20.2 ms (± .29 ms) to 19.7 ms (± .17 ms).

For studies in which the correlation levels between successive waveforms were calculated, a high-pass filter setting of 10 Hz was used during the recording process as it reduced the artificial elevation of correlation levels caused by DC components in the signal (as described in Section 2.6). This high-pass filter setting caused a slight decrease in the peak latencies of the PAMR waveform, as shown in Figure 3.9.2 above.

The distortion of the PAMR due to system bandwidth limits has been discussed previously by Thornton (1975a), in which he studied the effect on PAMR waveform morphology of reducing the low-pass frequency limit of his PAMR recording system from 4 kHz to 500 Hz, 200 Hz, and 100 Hz.

Thornton's results suggested that the previously described PAMR waveforms, consisting only of a negative-going and positive-going peak (e.g. Yoshie et al., 1969; Douek et al. 1973) were actually distorted versions of the real PAMR, caused by recording the response using systems with insufficient bandwidth. Thornton believed that the PAMR actually consisted of five peaks, labelled P_1, N_1, P_2, N_2 and P_3, and that it was by excessive low-pass filtering that the response was reduced to two peaks. Shown in Figure 3.9.3 (from Thornton, 1975a), is (A) the five-peak PAMR complex (recorded with a low-pass limit of 4 kHz), which was then digitally low-pass filtered at limits of (B) 500 Hz, (C) 200 Hz, and (D) 100 Hz.

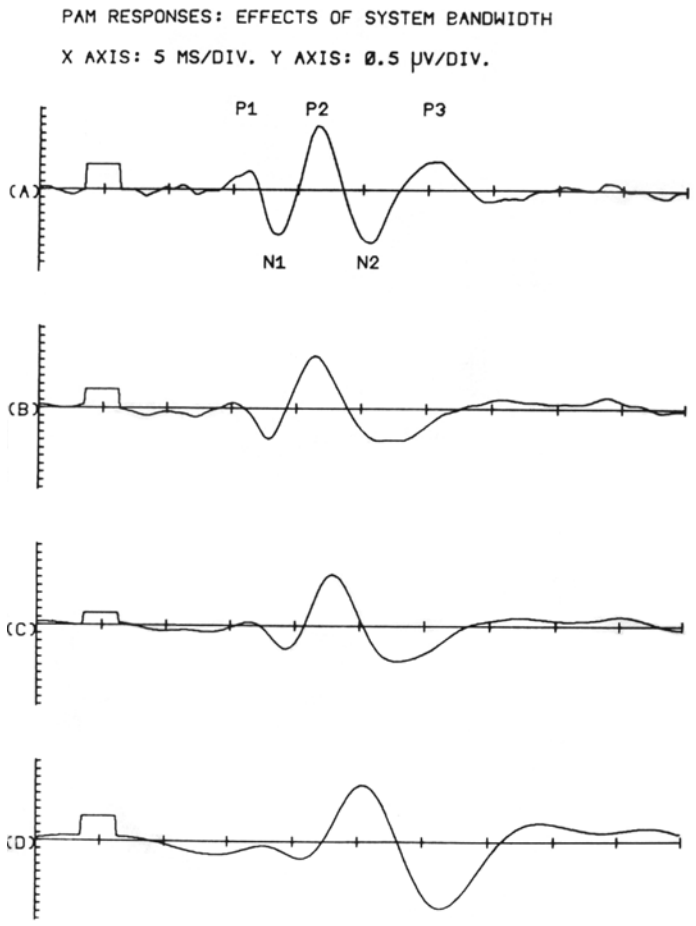

Figure 3.9.3: Thornton's data showing what he believed to be the distortion of the real PAMR waveform (A), recorded with a low-pass limit of 4 kHz, by filtering with low-pass limits of (B) 500 Hz, (C) 200 Hz, and (D) 100 Hz (Thornton, 1975a).

Thornton's data *does* show that low-pass filtering can distort the shape of a waveform, but unfortunately the PAMR waveform he started with was, itself, distorted. In his paper entitled "Distortion of averaged post-auricular muscle responses due to system bandwidth limits" (1975a), Thornton described his responses as having been recorded with high-pass frequency limits of "between 1 and 20 Hz", and a low-pass limit of 4 kHz. However, in his paper entitled "The use of the post-auricular muscle responses" (1975b), published later that year, he described the recording bandwidth of his system as being from 100 Hz to 4 kHz.

To examine whether a 100 Hz high-pass limit was the cause of the distorted PAMR waveform shown in trace (A) of Figure 3.9.3, a set of 400 PAMR waveforms were recorded with a bandwidth of 1 Hz to 2.5 kHz, and averaged. This averaged waveform was then digitally high-pass filtered at 100 Hz, using a 4th order Butterworth function on LabVIEW. The original waveform and this filtered version are shown below in Figure 3.9.4.

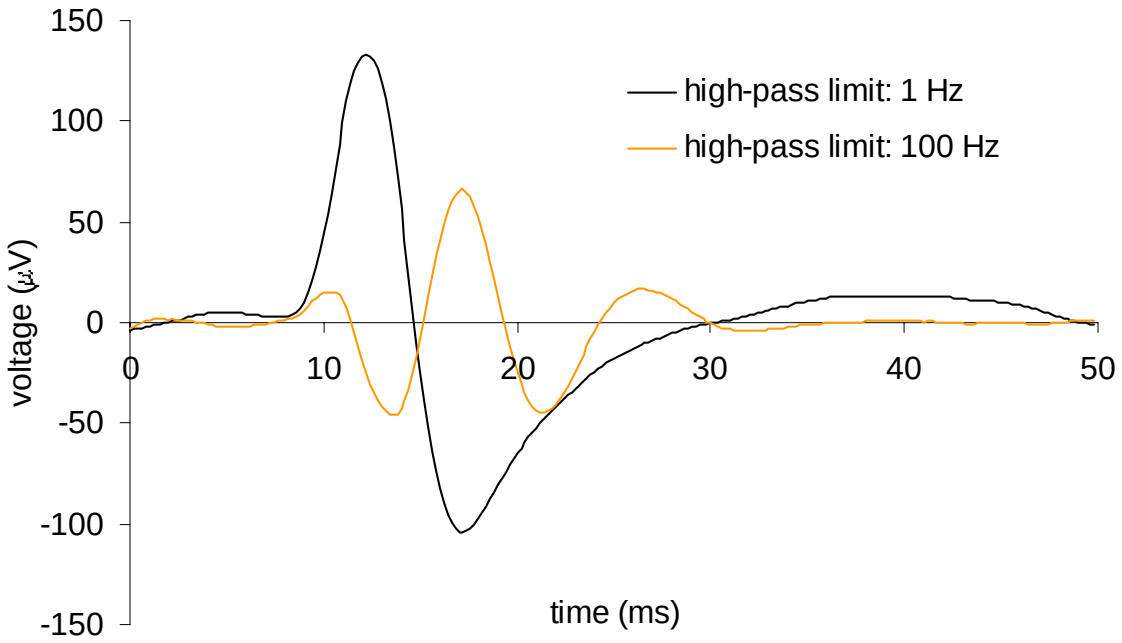

Figure 3.9.4: An averaged PAMR waveform (n = 400) recorded with a bandwidth of 1 Hz to 2.5 kHz, and the distortion caused when the same waveform is digitally high-pass filtered at 100 Hz (using a 4th order Butterworth function).

The similarity between the filtered waveform shown in Figure 3.9.4, and Thornton's PAMR from Figure 3.9.3 A, suggests that the high-pass limit of Thornton's system was 100 Hz for both studies (1975a and 1975b), apparently without him realising it. In other words, all Thornton's waveforms were distorted by his measurement system. This is problematic since his work has been used as a definitive reference in this field, cited by many subsequent authors (e.g. Robinson et al., 1977; Clifford-Jones et al., 1979; Spehlmann, 1985; Hall, 1992).

Discussion

The results presented here suggest that minimal distortion of the PAMR occurs when a recording bandwidth of 1 Hz - 5 kHz is used. If this bandwidth is decreased to 10 Hz - 500 Hz, the net increase in PAMR peak latency is less 0.5 ms. A high-pass limit of 10 Hz was preferred as it reduced the transient DC "bounces" that occurred with neck or jaw movements, and blinking. In young children, these DC movements are quite common, and so this high-pass limit is essential if the correlation method is to be used successfully. It was judged that the benefits of the reduced electrical interference and increased reliability of the correlation method outweighed the slight changes in peak latency that occurred with the decreased bandwidth.

However, this shift in peak latency due to filtering must be taken into account when choosing the time window over which to calculate the correlation level of successive waveforms. As shown in Figure 2.9 of Section 2.7, the time window must contain at least one of the peaks of the PAMR in order for the correlation method to be effective in detection of the waveform.

3.10 PAMR correlation measurements in infants

One of the aims of this study was to assess the effectiveness of using successive-waveform correlation level as a measure of hearing acuity in infants. Recordings of PAMR activity were made in two infant subjects, and the correlation measure of the response was examined. The results of one of these infants (A.Y.) are presented here in detail. The results obtained from the other infant subject (R.W.) were similar, but are discussed briefly.

Successive waveforms from the one-year old subject were measured over the 25 minute experimentation period using the PAMoMATIC VI developed for the task, and were also simultaneously recorded to DAT for offline analysis. The waveforms were recorded with the active electrode over the left PAM of the subject, the reference electrode on the pinna, and an earth electrode on the leg. The pass-band for the online recordings was 10 Hz to 500 Hz, while the recording pass-band of the DAT recorder was 2 Hz to 22 kHz. However, for consistency, the waveforms from the DAT were filtered with a bandwidth of 10 Hz to 500 Hz on playback. A detailed description of the movements and activities of the subject and the experimental conditions was taken down during the experimental period, and this information was then compared to the measured correlation levels at these times. The data are presented in chart form in Figures 3.10.1 to 3.10.5.

Within 40 seconds of beginning the test, the average correlation level (n = 80) had reached 0.25, indicating that the subject had produced a statistically significant PAMR in response to the click stimuli. The correlation level fluctuated between 0.1 and 0.35 over the next two minutes, before decreasing to below 0.05 around the 2:30 mark. At the 3:00 minute mark, the subject was coaxed into rotating his eyes towards the left side (the side that had the recording electrodes). In doing so, the correlation level increased to around 0.175. The subject

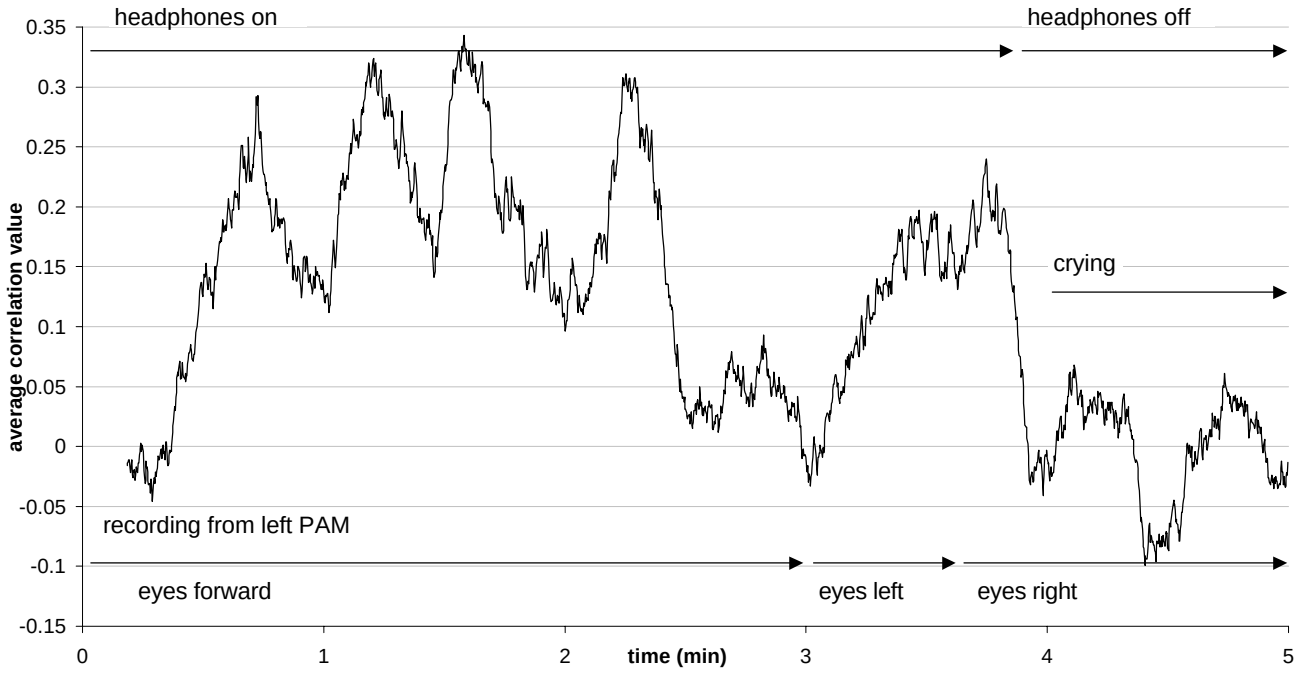

Figure 3.10.1: Data from a one-year-old subject showing the correlation level of successive PAMR waveforms, the actions of the subject, and other relevant experimental conditions, recorded over a 5 minute period (0 min - 5 min). (Click rate: 8/s. Correlation window: 10 ms - 24 ms. 80 running-point average.)

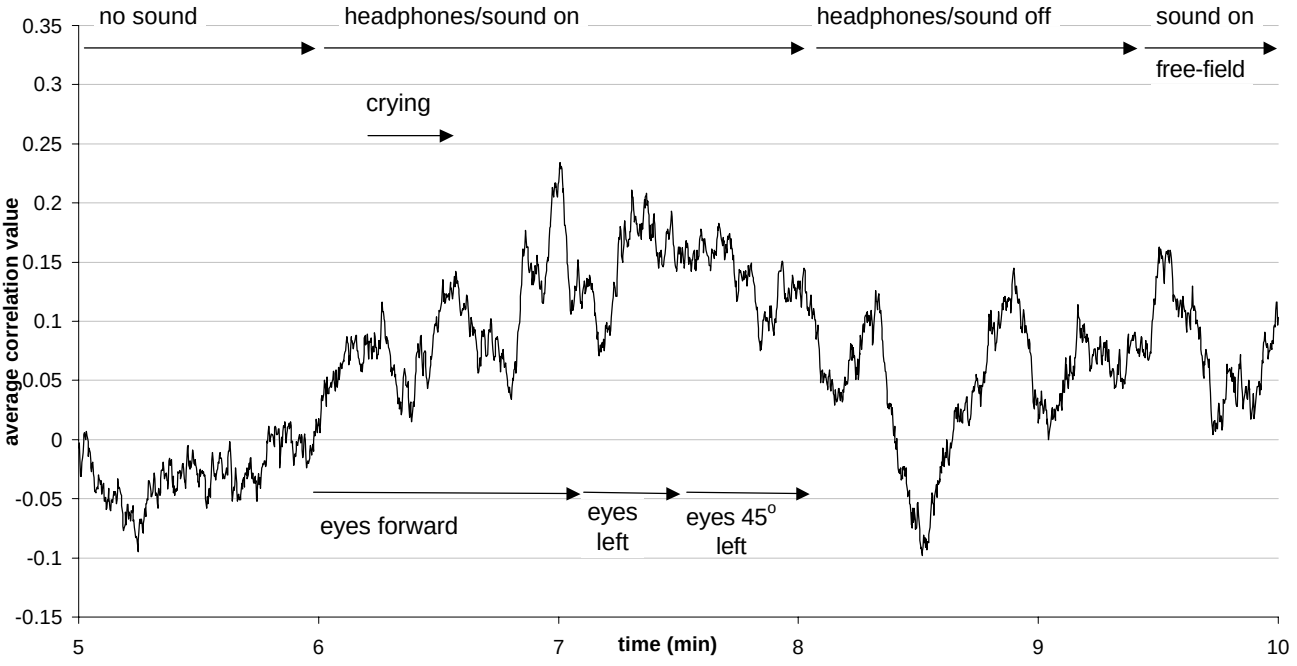

Figure 3.10.2: Data from a one-year-old subject showing the correlation level of successive PAMR waveforms, the actions of the subject, and other relevant experimental conditions, recorded over a 5 minute period (5 min - 10 min). (Click rate: 8/s. Correlation window: 10 ms - 24 ms. 80 running-point average.)

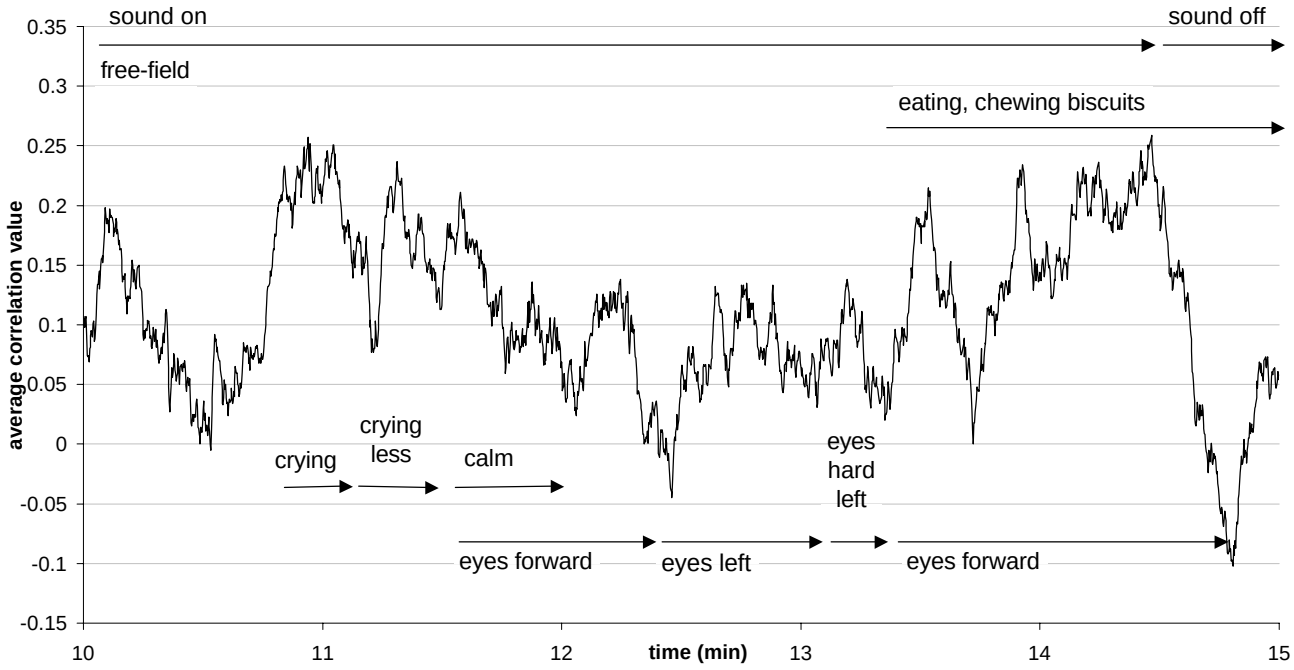

Figure 3.10.3: Data from a one-year-old subject showing the correlation level of successive PAMR waveforms, the actions of the subject, and other relevant experimental conditions, recorded over a 5 minute period (10 min - 15 min). (Click rate: 8/s. Correlation window: 10 ms - 24 ms. 80 running-point average.)

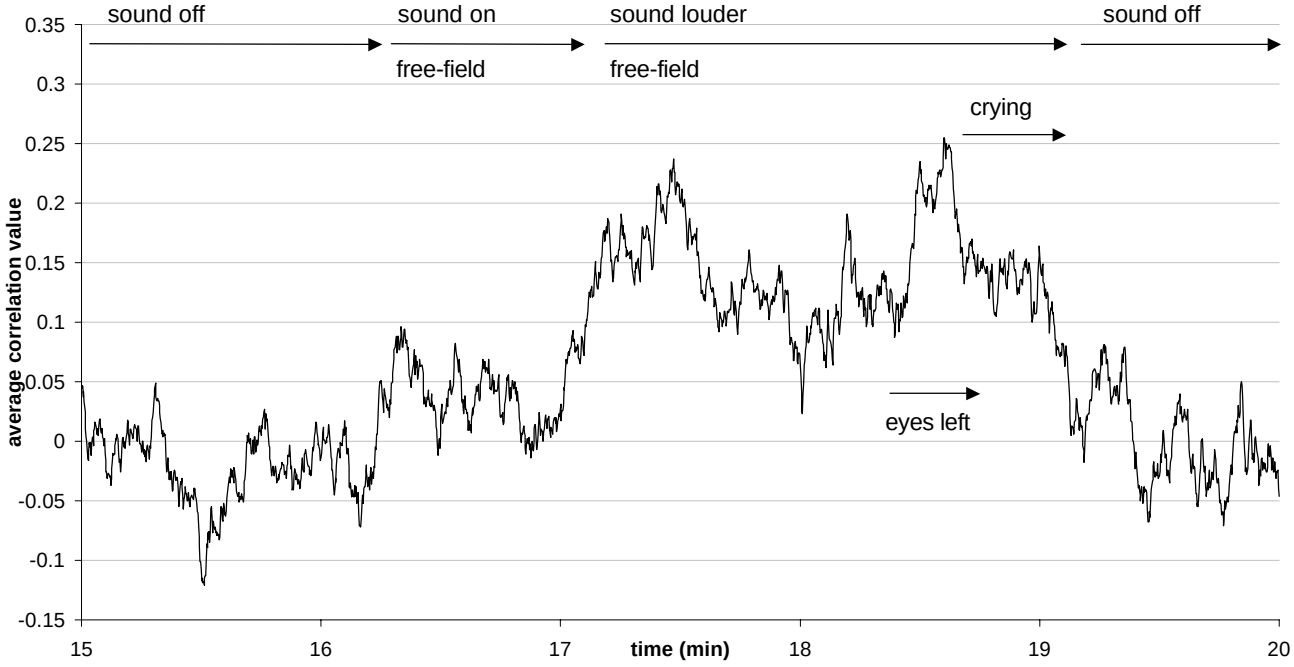

Figure 3.10.4: Data from a one-year-old subject showing the correlation level of successive PAMR waveforms, the actions of the subject, and other relevant experimental conditions, recorded over a 5 minute period (15 min - 20 min). (Click rate: 8/s. Correlation window: 10 ms - 24 ms. 80 running-point average.)

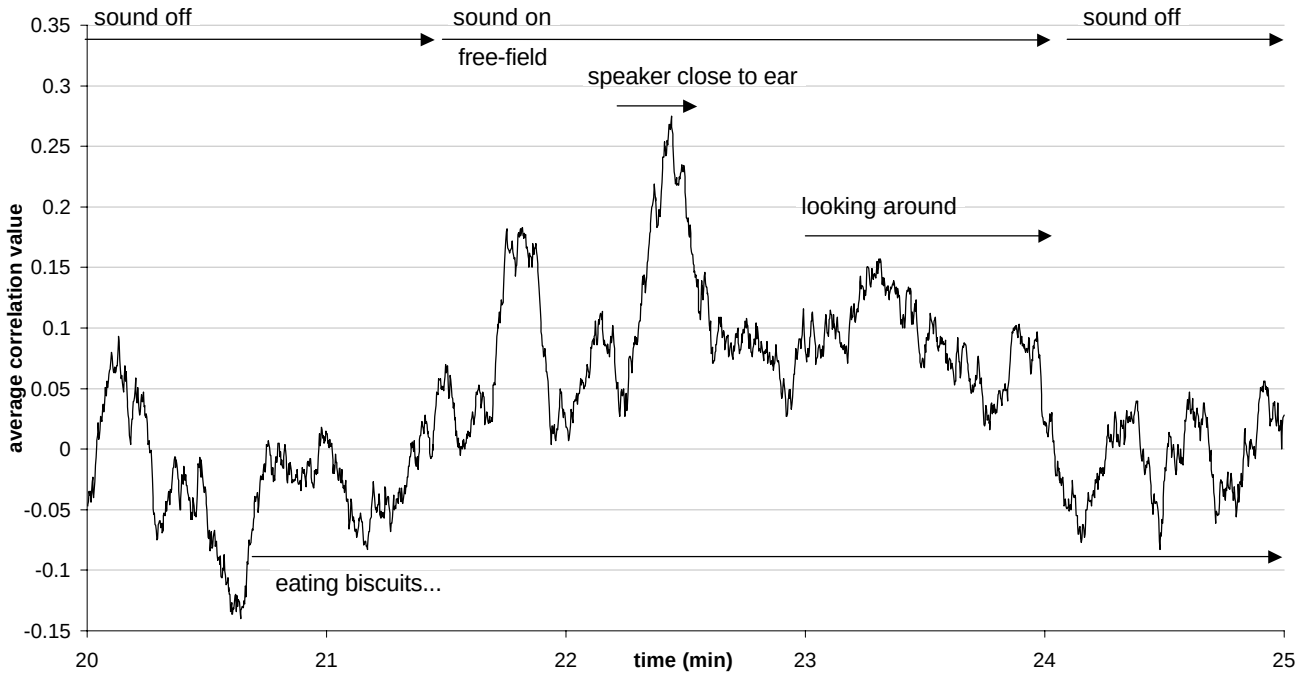

Figure 3.10.5: Data from a one-year-old subject showing the correlation level of successive PAMR waveforms, the actions of the subject, and other relevant experimental conditions, recorded over a 5 minute period (20 min - 25 min). (Click rate: 8/s. Correlation window: 10 ms - 24 ms. 80 running-point average.)

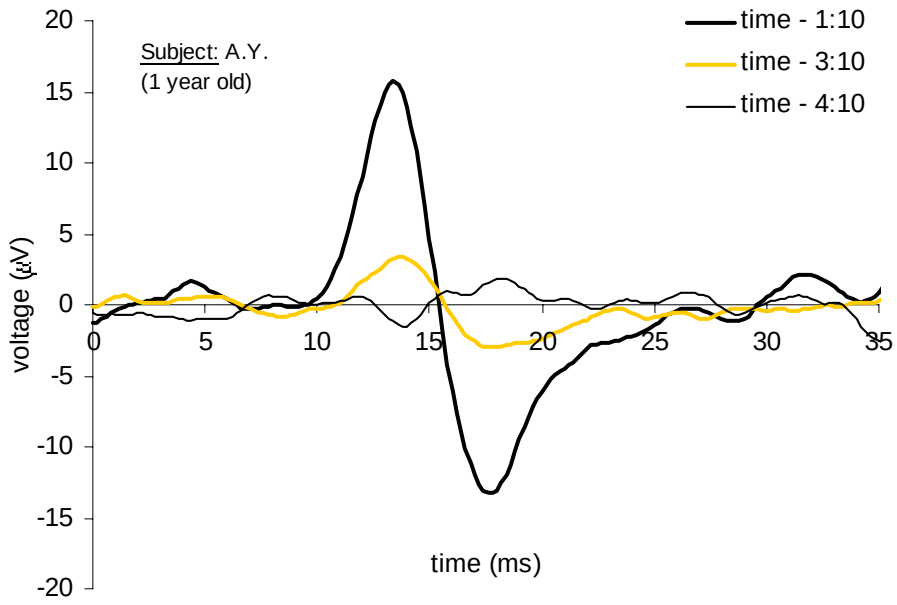

Figure 3.10.6: Averaged PAMR waveforms (n = 200) recorded from one infant subject at various starting times during the first 5 minutes of the experiment. The times correspond to those shown in Figure 3.10.1. Click intensity: 45 dB HL (traces 1 and 2), 0 dB HL (trace 3). Recording bandwidth: 10 Hz – 500 Hz.

then became agitated and began to cry, and so the headphones were removed (although, for the sake of science, they could have been left on). In the absence of sound stimuli, the correlation fell to around zero (-0.02 ± 0.04). Increases in the sound level of the click stimuli were the likely causes of the increases in correlation at 17:00, and at 22:10 (Figures 3.10.4 and 3.10.5).

Instances were observed in which increased muscle tone in the head and neck caused an increase in the correlation level (such as in Figure 3.10.3). For example, the correlation was increased (~11:00) while the subject was crying, and also between 13:40 and 14:40 while the subject was exercising his jaw muscles and swallowing (eating biscuits).

A similar experiment was carried out using a four-and-a-half month old subject (R.W). The maximum average correlation level recorded in this subject was 0.65 ± 0.21. An example of an averaged PAMR waveforms recorded from this subject during a high-correlation period is shown in Figure 3.10.7.

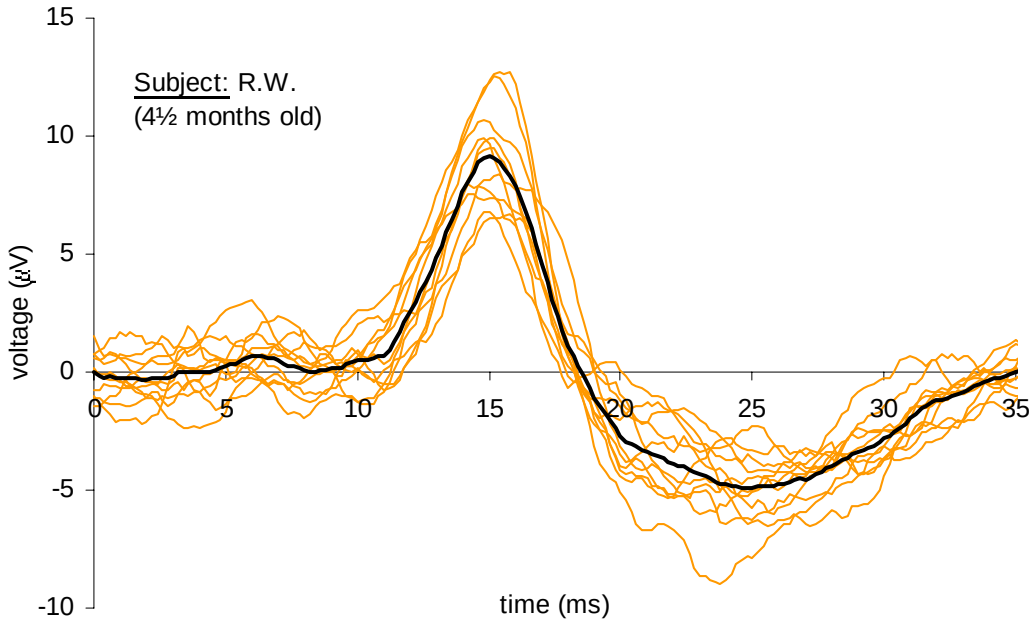

Figure 3.10.7: Averaged PAMR waveforms [grey: n = 20, and black: n = 400] recorded from an infant subject (R.W.). The average correlation during this period was 0.31 ± 0.35. (Recording bandwidth: 10 Hz – 500 Hz.)

Discussion

The correlation measure proved useful in indicating the presence of the PAMR in both the infant subjects. When the time waveforms corresponding to the higher correlation periods of the traces in Figures 3.10.1 to 3.10.5 were examined, the PAMR was found to be present (as shown in trace 1 of Figure 3.10.6). This was also clear at the time of recording, because the averaged waveforms (n=20) were continuously displayed. Similarly, periods with low correlation corresponded to low-amplitude or absent PAMR waveforms (as shown in traces 2 and 3 of Figure 3.10.6, respectively). As care was taken to avoid electrical artefacts and DC offsets in the recording and playback chains, there were no occasions in which an average correlation level above 0.15 was found in the absence of sound stimuli (a correlation level above 0.2 was used as the indication of the presence of the PAMR).

The question arises as to the best method of using the correlation data in a testing situation. Because of the dynamic fluctuations in the PAMR amplitude, one method would be to display the average correlation level over the past, say, 30 seconds on a panel meter. This would require the constant observation of the tester to monitor the results. So that the tester does not have to be present during the entire procedure, the average correlation level could be plotted (against time) on paper using a simple chart recorder, as was done in Figures 3.10.1 to 3.10.5, which would allow the tester to see how often the correlation value was above zero, and by how much. Alternatively, a peak meter could be used to display the highest correlation level recorded during the previous *n* minutes of the test. This would allow a tester more time to attending to other subjects/patients.

If care is taken to avoid electrical artefacts (such as 50 Hz mains interference) and DC offsets, as described in Sections 2.6 and 2.10, then the correlation measure of the PAMR is reliable, useful, and convenient measure of the presence or absence of the response. It has the advantage of allowing the size and stability of an evoked-response to be assessed without the need for averaging and displaying the waveform itself. This reduces the cost of the measurement system, and provides a quantitative measure of the size of the response in relation to the background noise.

The disadvantages of using the correlation measure are that i) the correlation level can be elevated by electrical artefacts [however, our equipment and techniques were designed to avoid this problem], and ii) characteristics of the waveform such as the latency of the peaks and the overall shape of the waveform cannot be assessed with just the correlation measure. This second point is relevant if using the PAMR as a diagnosis tool for Multiple Sclerosis, as

described in Section 1.4 (Clifford-Jones et al., 1979), or for subtle diagnosis of brainstem abnormalities (Gibson, 1975; Yoshie et al., 1969).

3.11 Development of a cheap and portable device for measurement of the PAMR

In many communities, the most significant obstacles to the introduction of universal hearing screening are economics and time (Bess et al., 1994). Subjective tests of hearing are only effective in most children after the age of 6 months (Wilson et al., 1991), and so in order to test children under this age, objective hearing tests must be used. Screening regimes utilizing one of the available objective hearing tests can be expensive to implement, both in terms of the equipment and number of staff required (Weber et al., 1994).

One of the aims of this project was to develop a cheap, efficient, and reliable objective hearing test that could be used as an alternative to those that are currently available. This aim was achieved by the development of a hand-held device that generated an acoustic click, and then used correlation to detect an evoked response in waveforms transmitted from the PAM of subject by a small, battery-powered amplifier/FM transmitter combination, described below.

3.11.1 FM transmitter

An amplifier and FM transmitter combination was used in the recording and transmission of the signals from the PAM of the subject, as it provided a simple, lightweight means of amplifying the signal, and allowed electrical and physical isolation of the subject from the recording equipment. The circuit diagram for the transmitter is shown in Figure 3.11.1, and the printed circuit board layout is shown in Figure 3.11.2.

The active electrode (from the PAM) was connected to Input 1 of the circuit, and the reference electrode (from the pinna) was connected to V_{SS} via Input 2, as shown in Figure 3.11.2. The AC coupling of the input from the active electrode was due to a 1 μF capacitor (C1 in Figure 3.11.2) placed in series, and a later capacitive coupling to the FM transmitter stage (C4). The AC

signal was amplified by passing it through two of the inverters on the MC14069UB Hex Inverter chip, biased into their linear operating region by a 1 MΩ feedback resistor. This amplified AC signal was then resistively attenuated to reduce frequency modulation of the voltage-controlled oscillator (VCO) part of the circuit, so that the deviations from the carrier frequency were not large enough to cause the receiver to lose lock. The VCO slightly increased or decreased the frequency of the 20 kHz oscillation (nominal) depending on the voltage signal from the AC amp. The FM signal was then broadcast via the antenna (a copper-coated fibreglass plate covering the transmitter circuit) to the receiver unit held nearby.

The FM amplifier/transmitter circuit was powered by a 3V lithium battery (Model CR2025, Kodak, Japan), and drew a current of approximately 40 μA, which meant that the circuit could be used continuously for several months between battery changes. The circuit was produced using surface-mount, rather than through-hole, technology because it reduced the size and weight of the complete circuit, and was less susceptible to electrical interference. A photograph of the FM transmitter is shown in Figure 3.11.3.

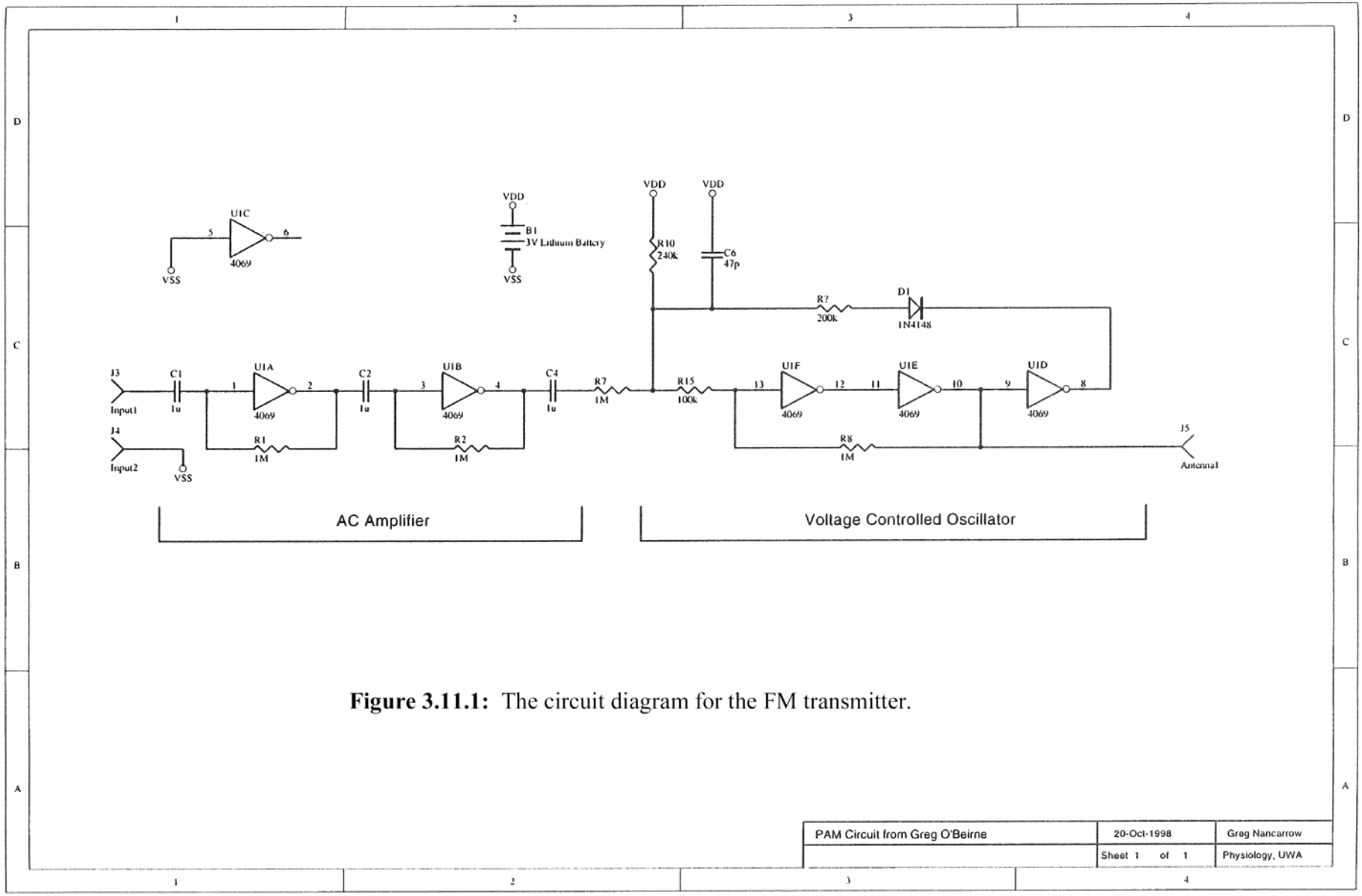

Figure 3.11.1: The circuit diagram for the FM transmitter.

FM transmitter – printed circuit board layout

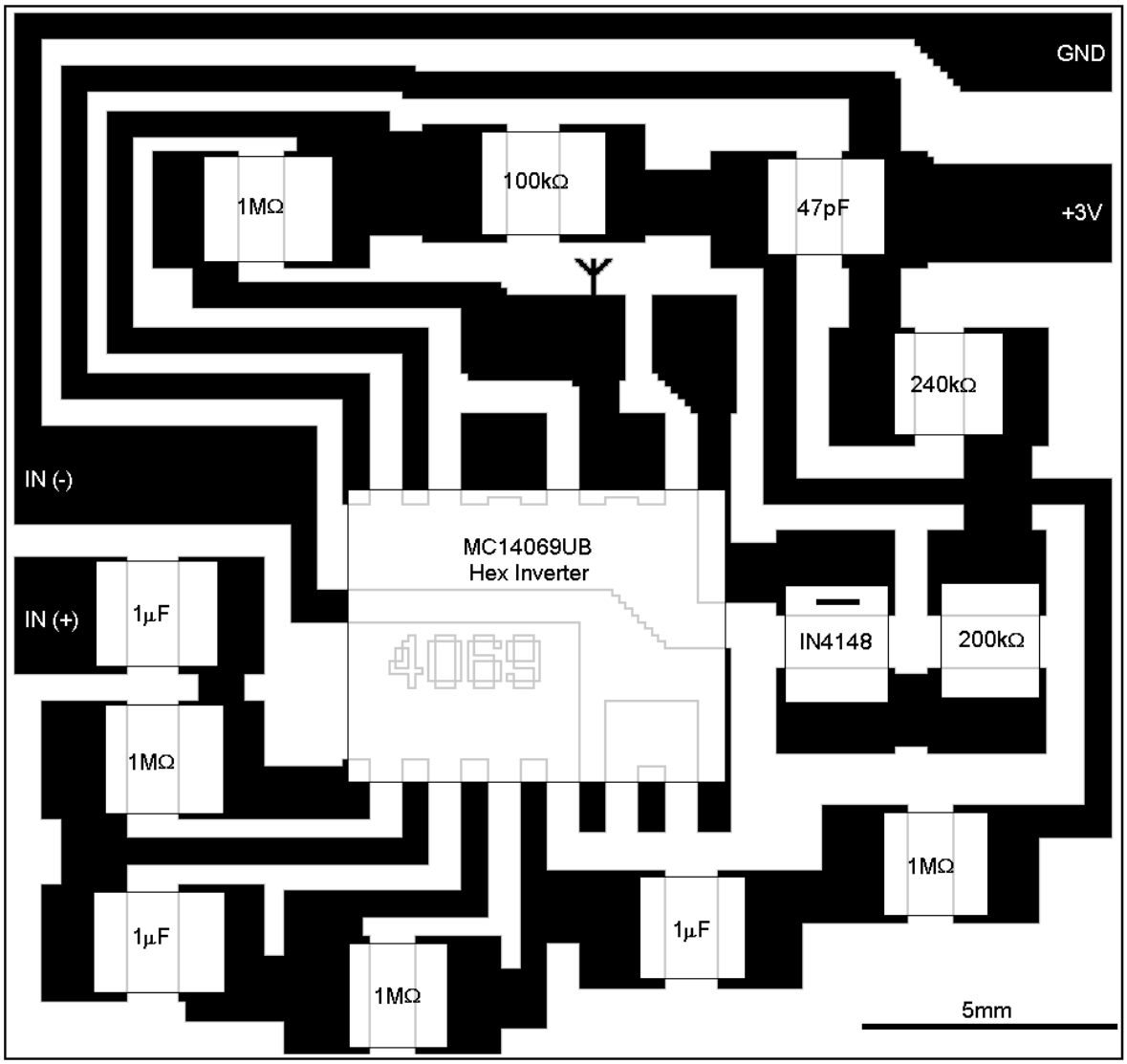

actual size: 

Figure 3.11.2: The printed circuit board layout for the FM transmitter circuit.

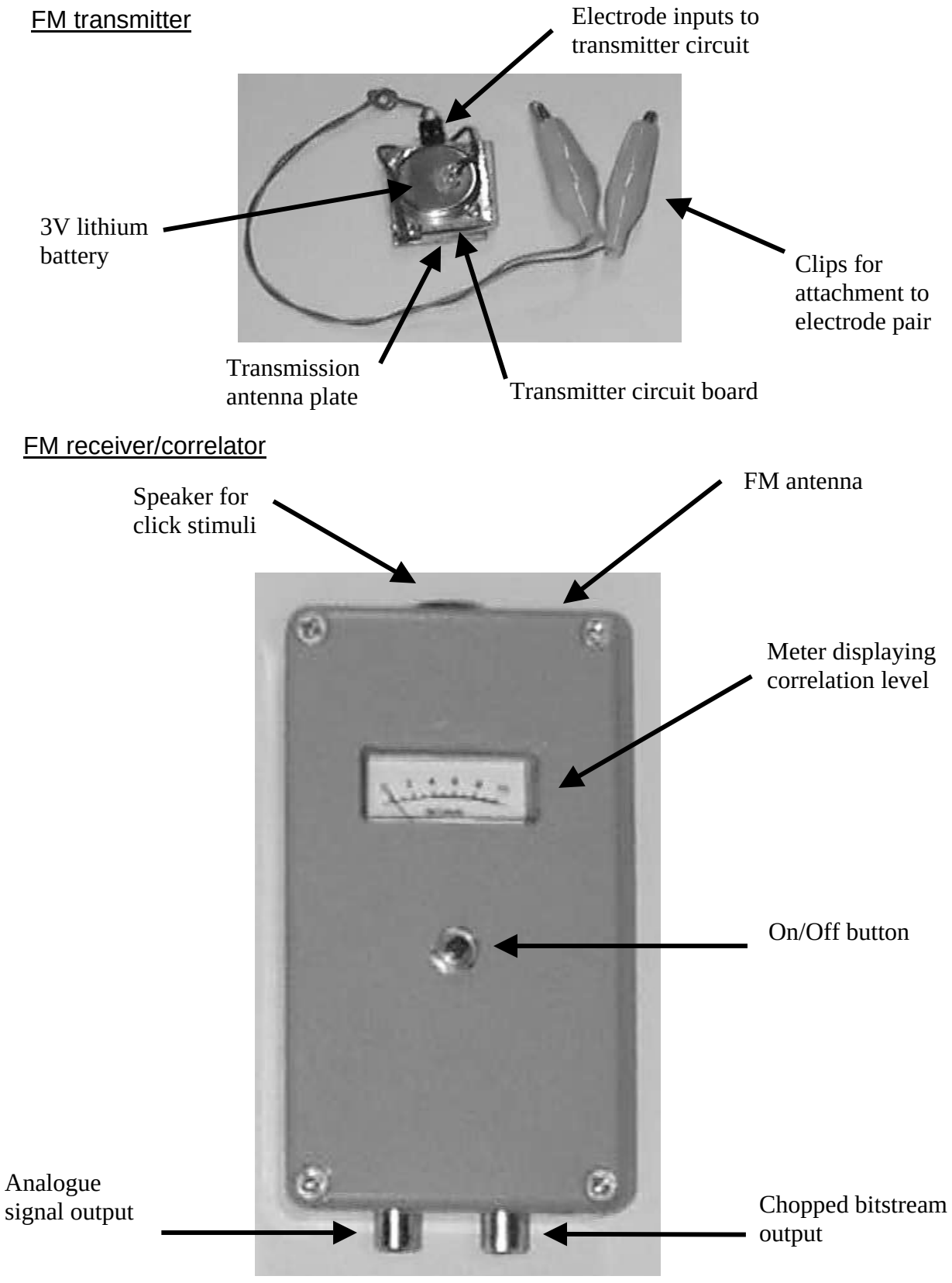

Figure 3.11.3: Photographs of the FM transmitter and FM receiver/correlator devices. The dimensions of the FM transmitter were 25 mm (L) x 21 mm (W) x 8 mm (H, including battery). The dimensions of the FM receiver/correlator device were 125 mm (L) x 64 mm (W) x 35 mm (H).

3.11.2 FM receiver and bitstream correlator

The receiver (shown in Figure 3.11.3) contained the electronics required to:

i) generate the acoustic click used to evoke the response

ii) to receive and demodulate the incoming FM signal from the transmitter

iii) convert the resulting analogue signal to a bitstream

iv) perform the correlation calculations on a selected portion of the successive bitstream waveforms, and

v) display the resulting correlation voltage on a meter on the front of the box.

The circuit diagram for the receiver/correlator is shown in Figure 3.11.6, and the printed circuit board layout is shown in Figure 3.11.7. The device was powered by a single nine-volt battery, drawing a current of 20 mA. The stimulus used to evoke the PAMR was a click, generated by an oscillator (a Schmitt trigger in parallel with a resistor and resistor/diode series combination, which charged and discharged a timing capacitor). The brief pulses generated by this oscillator were buffered by a transistor before being fed to a small headphone speaker mounted on the front of the receiver box. The pulses from the Schmitt trigger were also used to synchronize the correlator with the input signal containing the PAMR, discussed shortly.

The incoming FM signal from the antenna was first passed through two stages of amplification. The first stage (one of the JFET input op-amps on an LF353 chip) amplified the entire signal from the antenna, while the second stage of amplification greatly boosted the gain of the narrow frequency band (centered around 20 kHz) that contained the modulated signal from the transmitter. This filter/amplifier was made by placing a “twin-T” notch filter in the negative feedback path of the op-amp.

The FM signal was then demodulated using a 4046 phase-locked loop chip. The resulting demodulated AC signal could be measured from the "Analogue Output" on the receiver unit, shown in Figure 3.11.6. The demodulated output was also fed to a comparator, which converted the AC signal to a bitstream (i.e. to a high or low voltage level depending on whether the instantaneous voltage of the signal was above or below a zero baseline). The demodulated signal had to be AC coupled in order for the bitstream approximation to be suitable for use in the correlation calculations. DC offsets, if present, would artificially elevate analogue correlation calculations, as described in Section 2.6, but the effect is much more severe when calculating bitstream correlation levels, due to the all-or-none ("above or below zero") decisions of the comparator, as illustrated in Figure 3.11.4.

With each stimulus presentation, the bitstream response waveform (at time = *t*) was fed to one input of an "exclusive OR" (XOR) gate, and also to the 128-bit shift register for storage (delay). At the same time, the bitstream response from the previous stimulus presentation (at time = *t-1*) was read out of the shift-register and inverted by a Schmitt trigger, before being fed into the other input of the XOR gate. The bitstream output from the XOR gate was equivalent to the binary product of the "raw" and "delayed-and-inverted" waveforms (the *t* and inverted *t-1* bitstreams).

Using information derived from the correlation contour plots described in Section 2.7, and the results of the bilateral symmetry experiments described in Section 3.4, the PAM window was adjusted so that the correlation was calculated over the period of the waveform between 10 and 24 ms. The correlation level of the *t* and uninverted *t-1* waveforms was, in logical terms, the time-integral of the NOT XOR of the bitstreams over this "PAM window". The equivalence of "(*t*) NOT XOR (*t-1*)" and "(*t*) XOR (NOT *t-1*)" is demonstrated in Table 3.11.5.

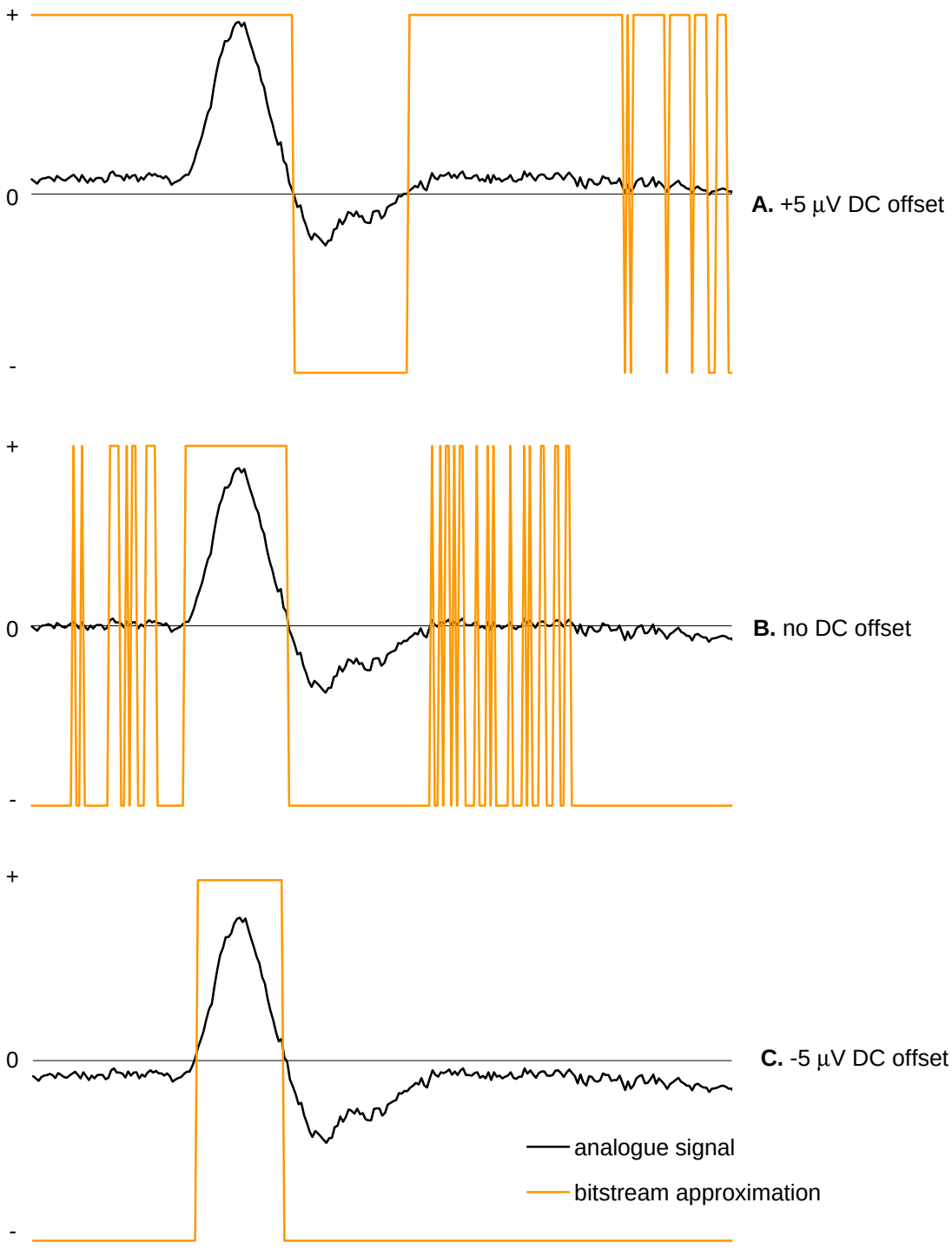

Figure 3.11.4: A demonstration of the effect that DC offsets in the response waveform have on the bitstream approximation process, due to the all-or-none ("above or below zero") decisions of the comparator.

As a result of the calculation described above, the greater the level of correlation of the *t* and *t-1* bitstreams, the greater the ratio of 1s to 0s in the product bitstream. A tri-state output system was required in order to calculate the average correlation level, because it prevented the charge on the capacitor from changing during the periods between PAM responses. To achieve this tri-state time-integration, the NOT XOR bitstream was fed to a pair of NAND gates and diodes, generating a tri-state charging of the 33 μF storage capacitor. This tri-state output increased the charge on the capacitor for high correlation levels, decreased the charge on the capacitor for low correlation levels, and blocked the charge/discharge path of the capacitor in the periods outside the "PAM window". The period over which the correlation was calculated (the PAM window) was controlled by the output of a Schmitt trigger, synchronised by the 0.1 Hz stimulus generator.

t	*t-1*	NOT XOR
0	1	**0**
0	0	**1**
1	1	**1**
1	0	**0**

t	NOT *t-1*	XOR
0	0	**0**
0	1	**1**
1	0	**1**
1	1	**0**

equivalent

Table 3.11.5: The correlation level between the *t* and *t-1* bitstream is determined by the logical function " *t* NOT XOR *t-1*". To make the implementation of the electronics simpler, the correlation was actually calculated as "*t* XOR NOT*t-1*", which produced the same result, as the truth tables above demonstrate.

The net charge, and therefore voltage, on the storage capacitor was buffered by an op-amp, in order to prevent it being loaded by the meter, which displayed the DC correlation voltage. The correlation voltage was normalised to a value between zero to one by adjusting a variable resistor in setting up the equipment.

The receiver circuit was produced using standard through-hole technology (rather than surface-mount) because i) the receiver unit was hand-held and did not have to be miniaturized to the same extent as the transmitter, and ii) most of the weight of the receiver unit (under 250g) was due to the nine-volt battery, meter, and die-cast aluminium box, rather than the circuit-board and components.

The combined gain of the transmitter and receiver units was 69.5 dB (± 1 dB). This gain was calculated by simultaneously comparing the peak-to-peak heights of responses recorded directly from the electrodes via the BioAMP with those recorded from the FM transmitter via the analogue out of the receiver unit.

Discussion

As described above, a cheap, portable system was developed for the measurement of the PAMR as an objective test of hearing.

Rather than using wires to connect the subject and the correlator device, an amplifier/FM amplifier combination was used, as it allowed electrical and physical isolation of the subject from the recording equipment. Although the recording equipment was, in this case, battery-powered and therefore presented no risk to the safety of the subject, the electrical isolation provided by the FM link meant that the subject did not have to be earthed in order for a clean signal to be recorded. It also reduced the chances that an infant subject would grab at any wires.

The transmitter unit worked well, providing a clear signal over approximately 15cm. Weighing under 10g, the transmitter was light enough to be attached to the self-adhesive electrodes, but care had to be taken that the transmitting antenna plate was facing towards the receiver unit for the FM signal to be clear.

Although there were a few problems with the FM receiver and correlator design (as described below), we were able to successfully receive signals from the transmitter and use the device to measure the PAMR correlation level from two subjects on a number of occasions. However, during the trials of the device, we found a number of ways in which the functioning of the device could be made more robust. For example, the FM demodulator chip often lost lock to the carrier frequency if there were fluctuations in the battery power supply. To remedy this, a large "smoothing" capacitor was placed in parallel with the power supply. Although this improved the situation, the phase-locked loop chip still required tuning on occasions. These power fluctuations could also be eliminated by placing a voltage-regulator in the circuit.

There was also a recurring problem with the correlator. The frequency of the high-frequency clock had to be adjusted from time to time to bring the raw and delayed waveforms into alignment (or time-registration). If either too few or too many bits were fed to the shift register during the PAM window, the raw and delayed bitstreams drifted slightly out of time-registration, which lowered the correlation level. This could be remedied in future by using a high-frequency clock to drive a single counter chip, which would generate the "PAM window" and control the tri-state output of the correlator circuit. Such a measure would significantly improve the robustness of the device, and eliminate the need for repeated adjustment. No problems were found with the analogue-to-bitstream conversion process (the comparator),

because the 10 Hz high-pass filtering on the FM transmitter circuit ensured that the waveforms were sufficiently AC-coupled.

As it stood, the device was light-weight, portable, cheap, and functional, but required regular tuning. With the modifications described above, the device has the potential to become a reliable tool for quick, effective testing of the PAMR. As can be seen from the schematic diagrams in Figures 3.11.1 and 3.11.6, both the transmitter and the receiver/correlator box are built from cheap and simple components that are readily obtainable almost anywhere in the world.

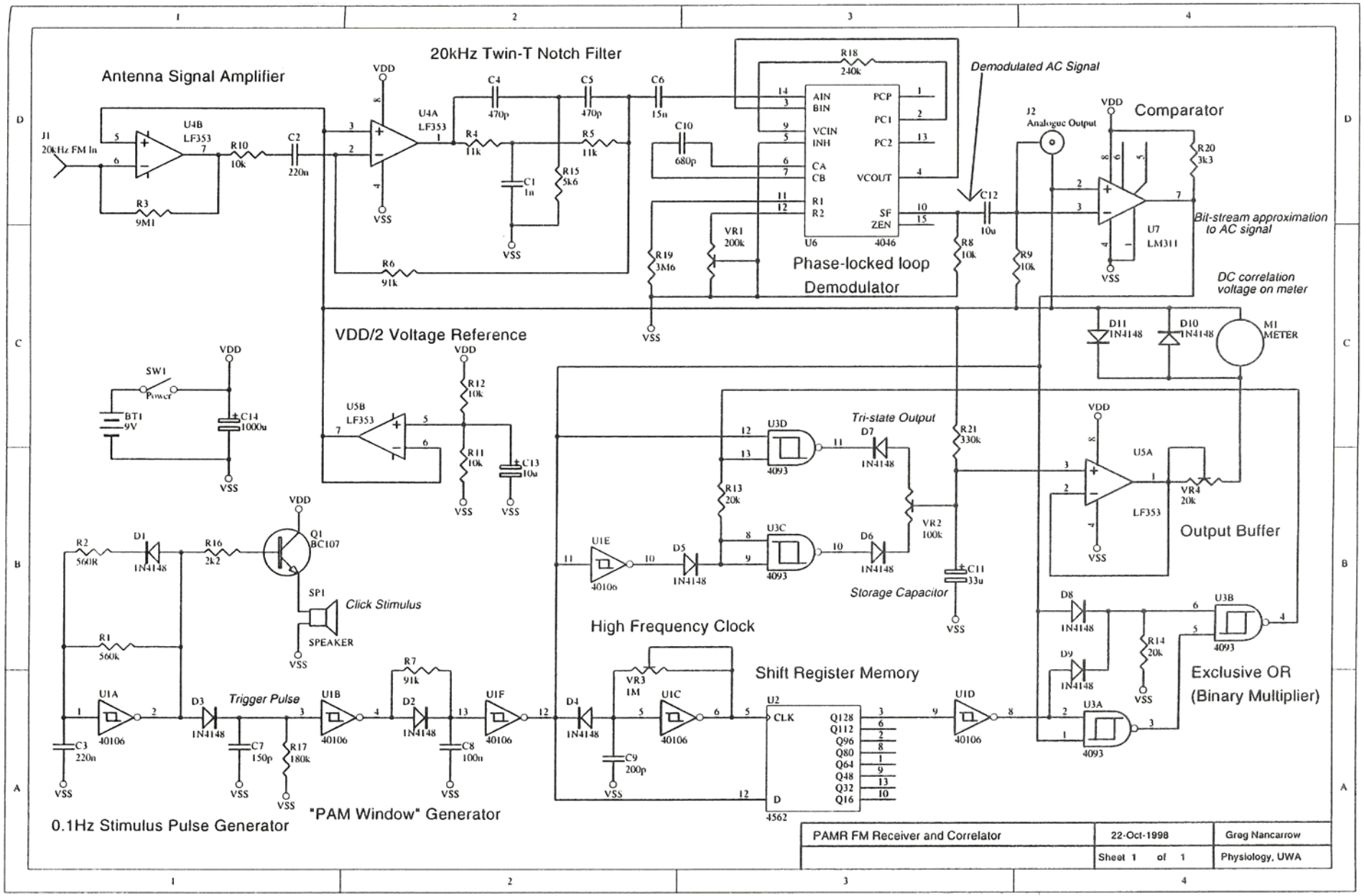

Figure 3.11.6: The circuit diagram for the FM receiver/correlator.

FM receiver/correlator – printed circuit board layout

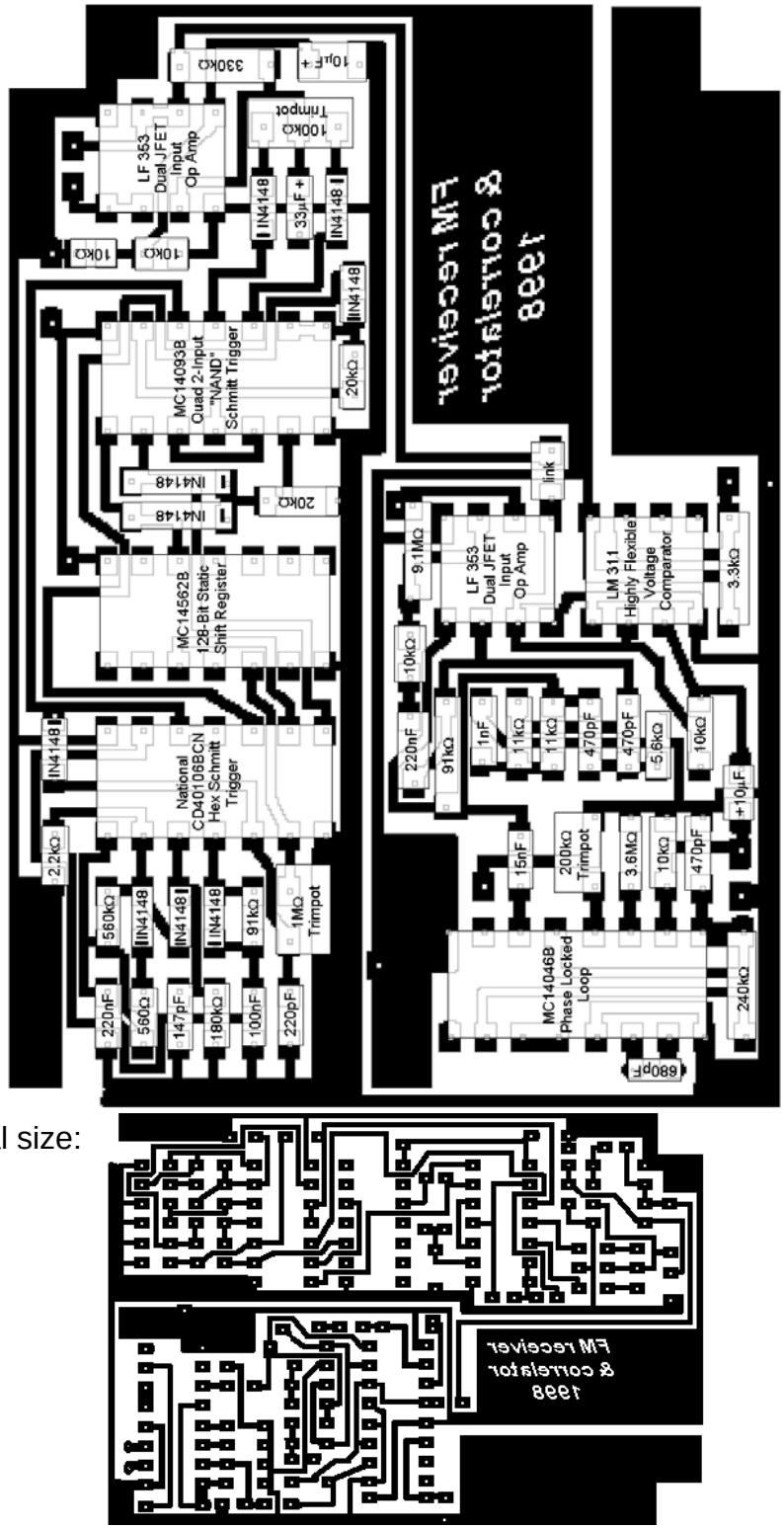

actual size:

Figure 3.11.7: The printed circuit board layout for the FM receiver/correlator circuit.

3.12 PAMR threshold-tracking using a stimulus-level feedback loop

A series of experiments was carried out in which the level of the sound stimulus was automatically adjusted to maintain a constant PAMR correlation level over a period of time. The aim of these experiments was to use the software to automatically and continuously determine the sound level at which the PAMR could be first detected (the PAMR threshold) using the correlation method. As described in Section 3.13, the same technique, using the same software, was later applied to the automatic tracking of the compound action potential (CAP) threshold in the guinea pig.

Due to difficulties involved in producing and attenuating click stimuli using software, a custom-built external click generator and attenuator were used to produce the click stimuli (as described in Sections 2.2 and 2.11). In the custom-built electronics, the stimulus attenuation level could be adjusted manually using a potentiometer, or by using a voltage-controlled attenuator (VCA) circuit that smoothly ramped the attenuation up or down, depending on the presence or absence of a digital TTL (transistor-transistor logic) voltage level delivered to the attenuator circuit from one of the digital outputs of the Lab-PC+ card within the computer. At the same time, the VCA circuit produced a DC voltage output proportional to the decibel attenuation of the stimulus signal, which was fed to the Lab-PC+ card and used by the software to monitor the level of attenuation provided by the circuit.

Using these components, a software feedback loop could be written which automatically raised or lowered the sound level of the click based on the whether the average correlation level between consecutive waveforms was above or below a certain pre-set level. In this way, the system automatically "hunted" or "tracked" the PAMR threshold, as defined by a fixed (pre-set) correlation value. This automatic technique is a variation of the Békésy

audiometric method (von Békésy, 1947), in which a human subject ramps the stimulus level up or down based on whether they can hear the stimulus or not.

3.12.1 The effect of attenuation ramping rate on threshold-tracking

In this study, a comparison was made between the subjective click threshold (the sound level at which the subjects could first hear the clicks), and the automatically-detected PAMR threshold (the sound level at which the PAMR was first detected by the software using the correlation method). The factors that influenced these two thresholds were also studied.

To obtain the subjective click threshold of the subject, the sound level of the click was adjusted manually by the subject (using a potentiometer on the VCA box), so that the click was only just audible. Once this threshold was found, the level of attenuation was read from a meter on the front panel of the VI. Automatic PAMR threshold detection was then carried out using the VI developed for the task, as shown in Appendix One. The criterion for detection of the PAMR was chosen to be a running-point-average correlation level reaching a pre-set value. The correlation value chosen to most effectively indicate the presence of the PAMR is discussed below.

The automatic tracking method is illustrated in Figure 3.12.1. Here, the PAMR threshold of an adult subject was automatically determined by the VI over a three minute period, after which a conductive hearing loss of 30 dB was simulated by attenuating the voltage to the headphones by 30 dB, using a HP 350D resistive attenuator. This attenuation was maintained for a further three minutes, and then removed. Of interest, in this experiment, were the stability of the automatic PAMR threshold measure, and the ability of the tracking software to follow this simulated change in threshold.

Apart from the repetition rate of the stimulus, which was fixed at 8/s, two sources of "sluggishness" were identified in the feedback process. The first was the number of values in the running-point-average of the correlation used by the VI to make its decision, and the second was the ramping rate of the attenuator (shown in Figure 2.10 of the Methods section). The number of values in the running-point-average of the correlation was arbitrarily set at five. There are no physiological sources of sluggishness: any change in the PAMR due to a change in stimulus level was immediate. The correlation set-point value was also of importance, as it was used as the decision boundary for the presence of the PAMR, as described in Section 2.11. The threshold-tracking task described above was carried out using different attenuation ramping rates and different correlation set-point values, as described below.

Shown in Figure 3.12.1 are the threshold-tracking results obtained using attenuation increase and decrease ramping rates of A) –3.5 dB/s and 1.3 dB/s, B) –5.7 dB/s and 2.2 dB/s, and C) –17.6 dB/s and 6.8 dB/s. The ability of the feedback circuit to track the 30 dB threshold increase was assessed subjectively, in terms of the similarity between the time-course of changes in the stimulus sound level and those of the automatically-determined PAMR threshold. According to this subjective measure, the highest similarity in time-courses was achieved by the attenuation increase and decrease ramping rates of –5.7 dB/s and 2.2 dB/s, respectively (Figure 3.12.1 B).

An average correlation level of 0.2 over 5 stimulus presentations was decided upon as the level of correlation required to indicate the presence of the PAMR. Through trial and error, the 0.2 average correlation level was found to provide the best estimate of the visual PAMR threshold: an average level of 0.1 was too commonly achieved during random fluctuations (data not shown), whereas a level of 0.4 was found to overestimate the stimulus intensity

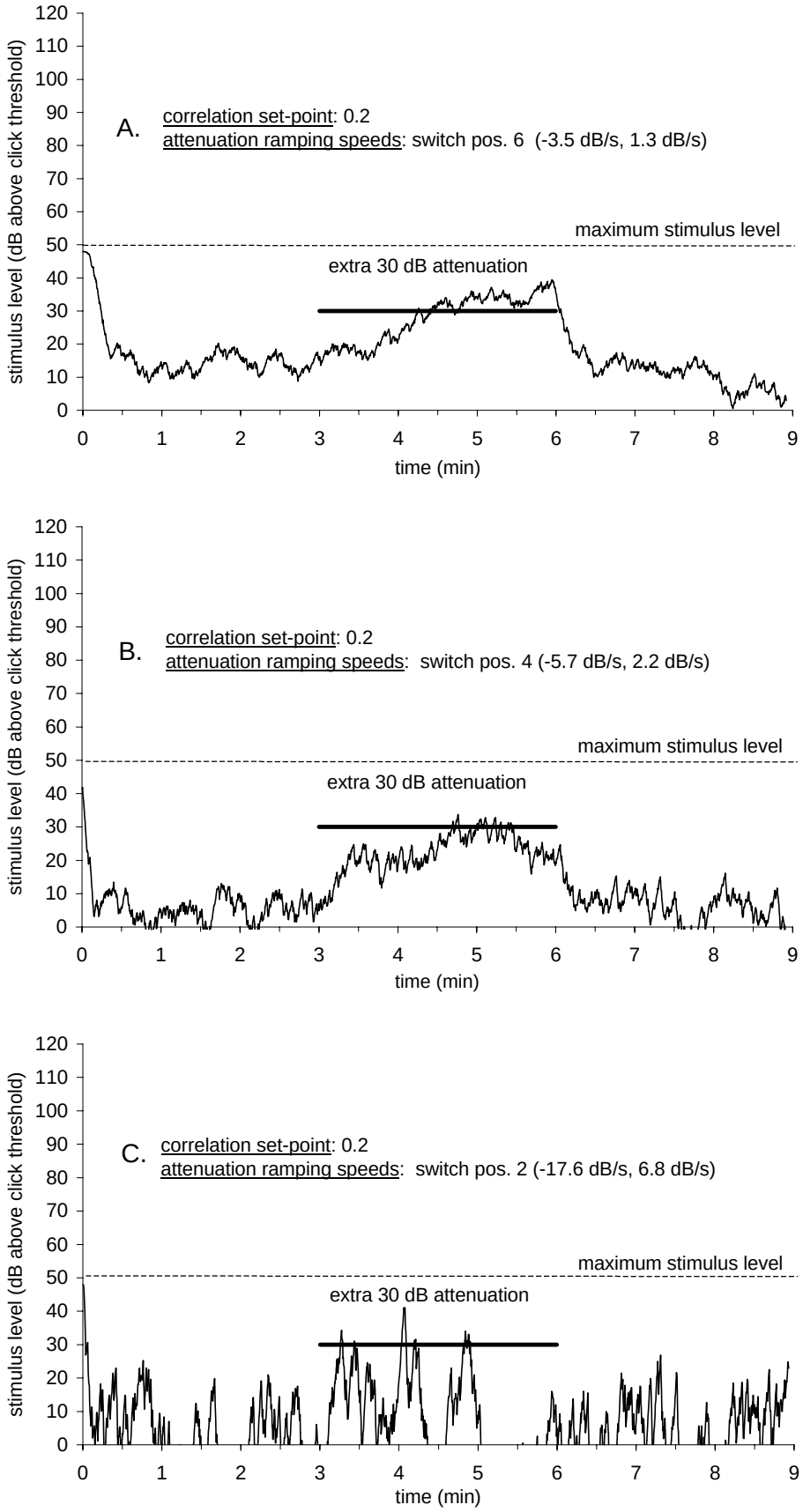

Figure 3.12.1: The effect of attenuation ramping speed on the ability of the software to automatically track the PAMR threshold. The stimulus voltage to the headphones was attenuated by an additional 30 dB in the period between three and six minutes to simulate a rapid change in PAMR threshold.

required for the author to visually identify the PAMR in the raw trace, as shown in Figure 3.12.2. In this example, the stimulus attenuation level required during the 3 to 6 minute period was outside of the range of attenuation that could be provided by the voltage-controlled attenuator, and so the estimate of the PAMR threshold appears clipped during this period.

3.12.2 Effect of muscle tone on the automatically-determined PAMR threshold

The effect of muscle tone on the PAMR threshold was also studied using the automated tracking technique. Figure 3.12.3 shows the PAMR threshold for a subject determined over a period of eight and a half minutes. The subject was quite relaxed at the beginning of this

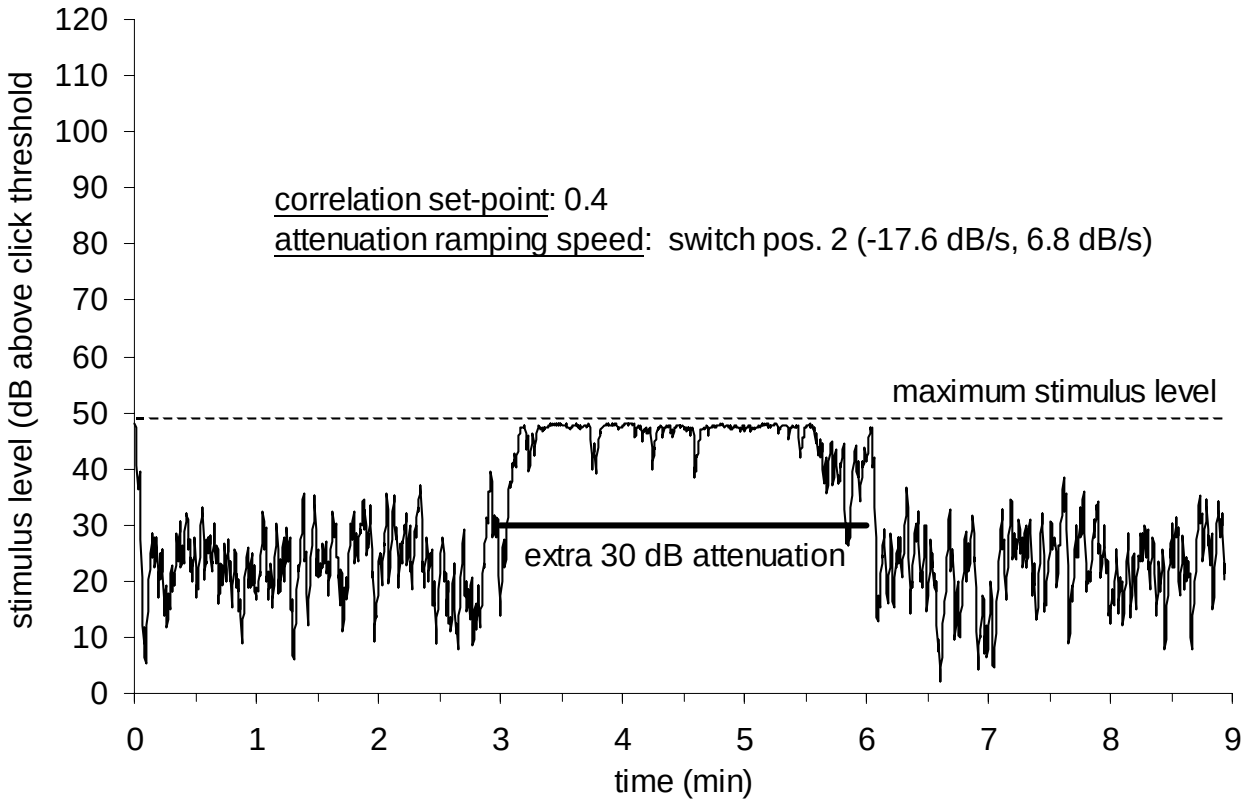

Figure 3.12.2: The overestimation of PAMR threshold when a correlation set-point of 0.4 is chosen. The stimulus voltage to the headphones was attenuated by an additional 30 dB in the period between three and six minutes to simulate a rapid change in PAMR threshold.

period, and consequently the average magnitude of the recorded EMG was only 1.8 μV RMS (± 1.8 μV, due to occasional larger increases in EMG). The eyes of the subject were rotated towards the recording electrodes during the period between 3 minutes and 6 minutes, which increased the average EMG level to 25 μV RMS (± 9.0 μV) in the 4 to 6 minute period. When the gaze angle was returned to a forward position, the EMG decreased to an average level of 11 μV RMS (± 5.5 μV) over the remaining two and a half minutes of the experiment.

The average PAMR threshold measured during the first three minutes of the experiment (with the eyes forward) was 42.3 dB SL (± 4.0 dB), which fell to 11.7 dB SL (± 2.4 dB) during the ipsilateral eye rotation period (measured between 4 and 6 minutes). When the eye rotation ceased and the EMG fell to 11 μV RMS (± 5.5 μV), the estimate of PAMR threshold increased slightly to 13.4 dB SL (± 3.5 dB). Although the experiment was not continued past the 9-minute point, it is safe to assume that as the EMG decreased further, the estimate of the PAMR threshold would have continued to rise until it reached the pre-rotation level. Figure 3.12.4 illustrates the PAMR threshold as a function of EMG. The data is the same as that in Figure 3.12.3.

Recordings of PAMR threshold were also made from a subject in whom the PAMR was always active, and in whom any further increase in muscle tone above resting level caused a *reduction* in correlation level rather than an increase (as seen in other subjects). As shown in Figure 3.12.5, the automatically determined PAMR threshold of this subject actually decreased from an average level of 8.6 dB SL (± 1.4 dB) when the eyes were rotated, to an average threshold level of 4.6 dB SL (± 3.0 dB) when the gaze of the subject was returned to a forward position.

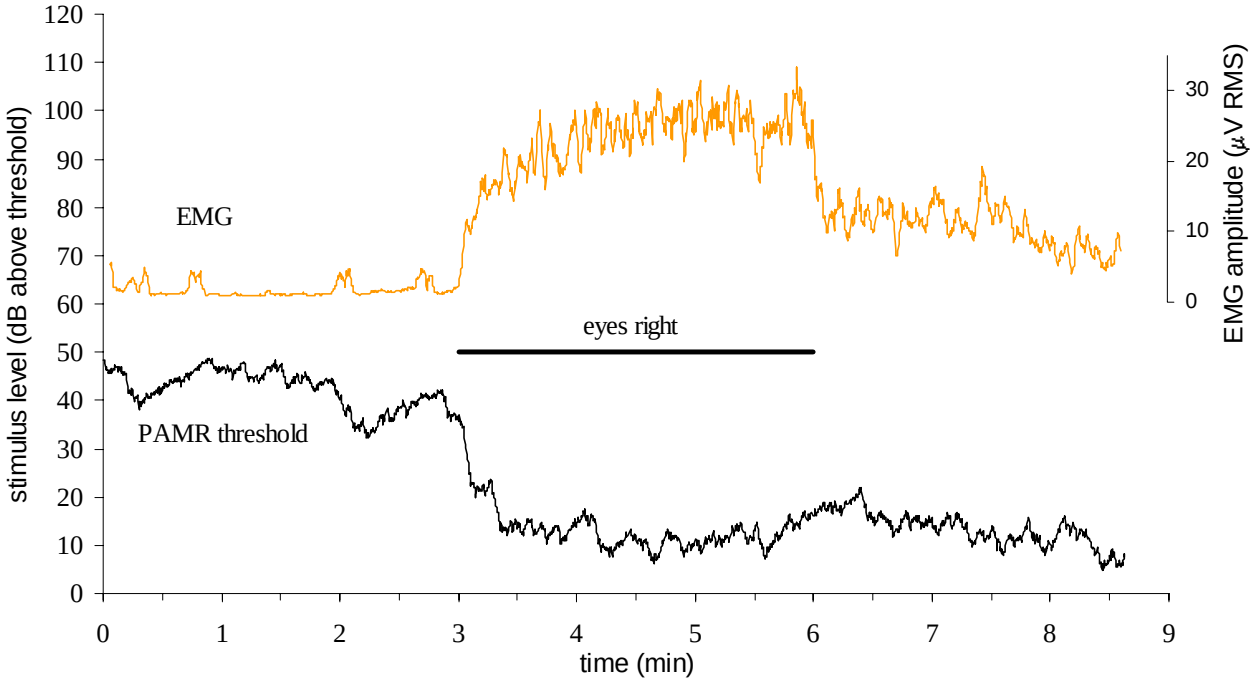

Figure 3.12.3: The effect of muscle tone on the automatically determined PAMR threshold. The eyes of the subject were rotated hard towards the recording electrode between three and six minutes in order to increase the PAM EMG. (Click rate: 8/s. Attenuation ramping rates: -5.7 dB/s, 2.2 dB/s. Correlation set-point: 2).

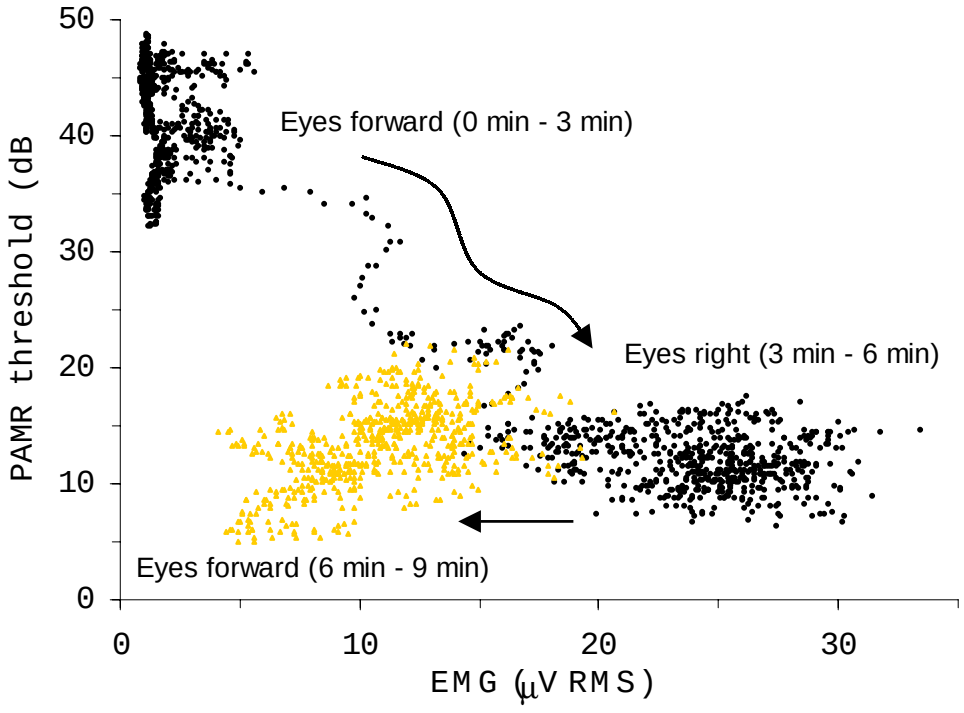

Figure 3.12.4: The effect of muscle tone on the automatically determined PAMR threshold. The data is the same as that plotted in Figure 3.12.3.

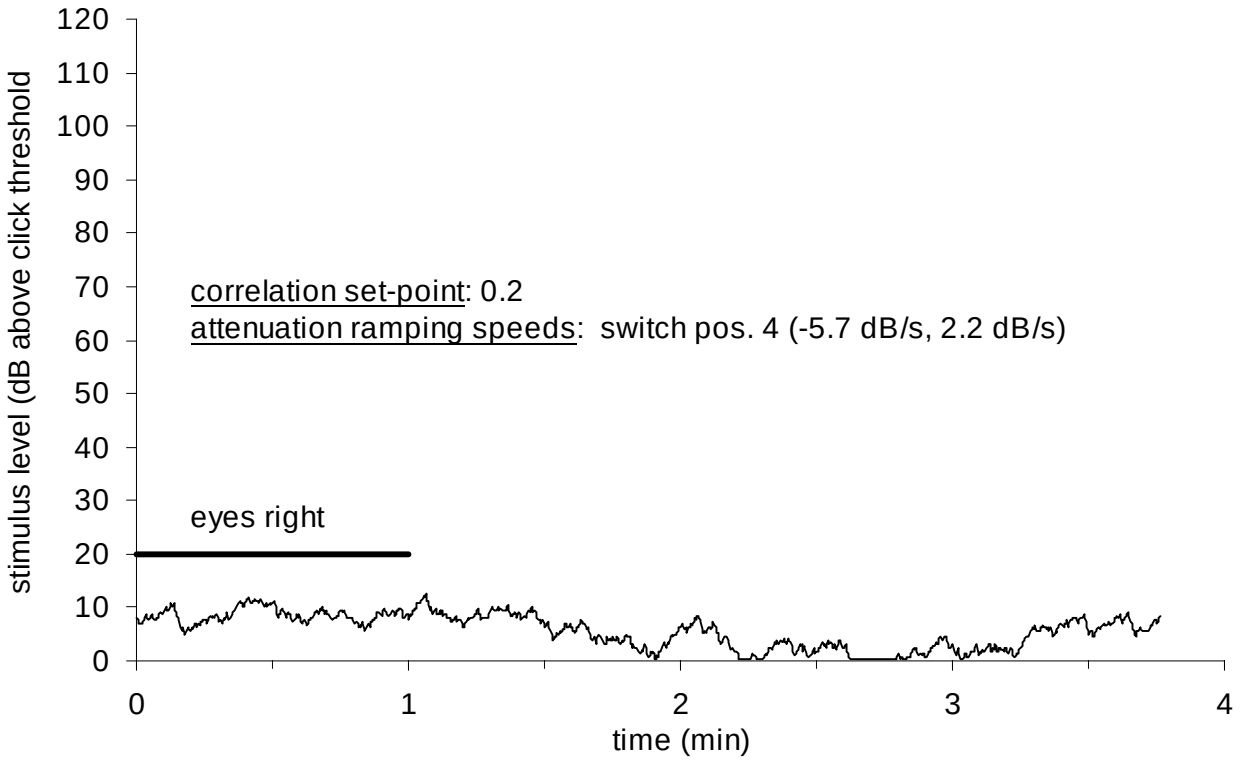

Figure 3.12.5: In subjects in whom the PAMR is always active, an increase in muscle tone can actually increase the automatically determined PAMR threshold, by causing a reduction in correlation level rather than an increase.

Discussion

The feedback loop described above contains the equivalent of three low-pass filters, all of which slow the rate at which the detection of the absence or presence of the PAMR produces an increase or decrease in stimulus level. These three low-pass filters are: i) the repetition rate of the stimulus, ii) the number of running-point averages of the correlation, and iii) the ramping rate of the voltage-controlled attenuator. The repetition rate of the stimulus was fixed at 8/s for both software and physiological reasons, discussed in Sections 1.7.3, 2.2, and 2.5. This meant that the two variables that could be changed to adjust the "tightness" of the feedback loop (the speed with which changes were propagated through the loop) were the number of correlation averages performed and the ramping rate of the attenuator. Adjustment of either of these

variables affects the dynamics and stability of the system, as described below. If the ramping-rate of the attenuator were too rapid, or too few running-point averages were carried out on the correlation, then the system would become unstable, and the fluctuations in the stimulus level would be both large and rapid, making it difficult to determine the actual threshold. If the ramping-rate were too slow, or too many correlation points were included in the running-point average, then the system would be slow to respond to any changes in the *physiological* PAMR threshold. This latter system may be preferable if the evoked-response that used in the threshold determination is a particularly stable one, and if no rapid changes in the threshold are expected. However, if there *are* fluctuations in the actual threshold, and the aim is to track these fluctuations accurately (as it was in these experiments), then the stability of the system must be "traded-off" against the ability to track these changes in threshold.

With reference to the data in Figure 3.12.1, if we assume a constant level of background muscle tone, we would expect the effective PAMR threshold (relative to the click sound level at time 0) to have *increased almost instantaneously* by 30 dB at the 3 minute mark and *decreased almost instantaneously* by 30 dB at the 6 minute mark. The number of points included in the running-point correlation average was fixed at 5 throughout these experiments. However, we *cannot* assume a constant level of background tone[1], and so the 30 dB change in threshold is only approximate[2]. The attenuator ramping rates used in Figure 3.12.1 A, while

---

[1] In retrospect, it would have been better to repeat the 30 dB threshold tracking experiment (shown in Figure 3.12.1) a number of times for each experimental condition, and to average the results of these repeats to reduce the variation in the results due to fluctuations in muscle tone.

[2] A 25 dB change would also have been preferable to avoid approaching the attenuation limit of the VCA circuitry.

providing a stable measurement of threshold, took quite a long time to respond to the change in the threshold at the 3 minute mark. The ramping rates used in Figure 3.12.1 C resulted in an unstable estimate of the PAMR threshold, which would be difficult to determine visually without further low-pass filtering of the threshold data.

The level of low-pass filtering provided by the 5-point running average, combined with attenuation increase and decrease attenuation rates of –5.7 dB/s and 2.2 dB/s, respectively, allowed the system to respond to the threshold changes observed in Figure 3.12.1 B within 30 seconds. These attenuation ramping rates enabled the VI to respond sufficiently quickly to the *trend* of the changes in PAMR threshold, while not being "knocked off course" by the fluctuations ("noise") of the average (n = 5) correlation level.

In the subject whose data is shown in Figures 3.12.3 and 3.12.4, the PAMR threshold was between 30 and 50 dB SL when the average EMG magnitude was below 5 μV RMS, but decreased to between 5 and 20 dB SL when the EMG magnitude was above 5 μV RMS. In Figure 3.12.4, the train of data points that link the eyes-forward (0 – 3 min) group of points to the eyes right (3 – 6 min) group, is probably due to the ramping speed of the attenuator. If this ramping speed had been quicker, it is likely that the transition between the eyes forward and eyes right group of points would have been nearly instantaneous.

Conclusions

From a testing perspective, the results in Figure 3.12.4 reveal an interesting property of the PAMR. Because the data show that the sound level required to evoke an identifiable PAMR is dependent on the EMG in the PAM of the subject (or at least correlates with it), it is likely that the large gap between subjective threshold and PAMR threshold observed by some researchers (e.g. Buffin et al., 1977, shown in Figure 1.6 of Section 1.3), can be attributed to

low EMG levels in the PAMs of their subjects. If it had been widely known that eye rotation was a simple method of increasing this EMG, then this subjective/objective gap would probably have been much lower.

The automatic threshold tracking technique was useful in providing information about the sound level required to evoke the PAMR under different muscle tone conditions, a task that is quite time consuming and difficult to accomplish manually. The technique could conceivably be used as a method of hearing threshold estimation, but only in situations where the EMG of the subject's PAM is sufficiently high that near-hearing-threshold stimuli evoke a PAMR capable of elevating the correlation level above the chosen set-point level.

3.13 CAP threshold-tracking using a stimulus-level feedback loop

A series of experiments was carried out in which the attenuation level of the sound stimulus was automatically adjusted to maintain a constant correlation level. The initial aim of these experiments was to use the software to determine the sound level threshold at which the PAMR could be first detected (the PAMR threshold). It was found that the software and hardware developed for the PAMR threshold-tracking task had the potential to be adapted for use in the tracking of other evoked response thresholds. One response in which threshold determination is routinely carried out for audiometric purposes is the compound action potential (CAP), shown in Figure 1.2 of the Introduction. To illustrate the use of the LabVIEW instrumentation and the threshold tracking technique developed for the PAMR, a set of experiments was carried out in the guinea pig to automatically detect the CAP threshold using the new method at a number of tone-burst frequencies, and to compare the automated and manual techniques.

The CAP arises from the synchronous discharge of many nerve fibres in the auditory nerve at the start of a click or tone-burst, and can be recorded from scala tympani and scala vestibuli (Hall, 1992). The threshold of visual detection of the CAP on an oscilloscope screen can be used as a reliable means of determining auditory sensitivity (Johnstone et al., 1979; Rajan et al., 1991). When using the visual detection method, the sound pressure level (SPL) of the tone-burst stimulus is reduced until the first negative-going deflection of the CAP waveform (N_1) is just visible. This SPL is then taken as the auditory threshold for the particular stimulus frequency.

In these experiments, the CAP of a single 329 g guinea pig was recorded from a hole made at the first turn of the cochlea into scala tympani using a Ag/AgCl electrode placed inside

a perfusion pipette. The anaesthesia and surgical procedures were carried out by Dr. Si-Yi Zhang, and are described elsewhere in detail (Patuzzi et al., 1989a; Marcon, 1995). The 50 ms tone-bursts were generated at a rate of 3 per second using an SRS DS335 Synthesized Function Generator (Stanford Research Systems Inc., CA, USA) gated by a Wilsonics BSIT Cosine Switch. The tone-burst output was attenuated by 50 dB using a Wilsonics PATT Programmable Attenuator before feeding into the input of the VCA circuit. The resulting attenuated tone-bursts were then delivered to the right ear of the guinea pig via a high-voltage, reverse-driven microphone (the Bruel and Kjaer 4134) acting as the sound source.

The CAP thresholds were obtained manually using the visual detection method at tone-burst frequencies of 10, 15, 20, 25, and 30 kHz. To ensure the accuracy of the manual CAP threshold measurements, the visual detection was carried out by Dr. Peter Sellick, a researcher experienced in the task. The stimulus SPL was adjusted manually by Dr. Sellick using a potentiometer on the VCA box. Once the threshold was found, the level of attenuation was read from a meter on the front panel of the VI. This process was repeated for each of the tone-burst frequencies.

Automatic CAP threshold detection was then carried out using the VI developed for the task. The present automated technique calculated the correlation level between successive CAP waveforms over the 1 to 3 ms post-stimulus time-window (the window during which the CAP occurs). Based on the results of the experiments described in Section 3.12, an average correlation level of 0.2 over 5 stimulus presentations was decided upon as the minimum level of correlation required to indicate the presence of the CAP. If the average correlation level for 5 stimulus presentations was under 0.2, the CAP was deemed to be not present, and a TTL output from the Lab-PC+ card was turned on, thus causing the attenuation level to decrease.

As the stimulus became more intense, the CAP increased in amplitude, which was reflected by the increase in correlation level above 0.2. When the average correlation level for 5 stimulus presentations rose above 0.2, the TTL output from the Lab-PC+ card was turned off, and the attenuation progressively became greater, so that the sound stimulus was not sufficiently intense to elicit a CAP. This procedure was carried out for stimulus frequencies of 10, 15, 20, 25, and 30 kHz.

With each stimulus presentation, the output from the VI, which included the attenuation level (in dB), was recorded to an output file for later analysis. The results for the experiment are shown below.

Results

A comparison was made between manual estimation of CAP threshold using the visual detection technique (Johnstone et al., 1979; Rajan et al., 1991), and an automated method which used correlation techniques to detect the presence or absence of the CAP at a given stimulus attenuation level, and increased or decreased the level of attenuation accordingly.

The CAP thresholds were obtained manually by Dr. Peter Sellick using the visual detection method at tone-burst frequencies of 10, 15, 20, 25, and 30 kHz. Thresholds for the same stimulus frequencies were then determined using the automatic CAP threshold detection VI developed for the task. The results of this comparison between manual and automatic threshold levels are shown in Figure 3.13.1.

Because of the ramping method used by the VI and the VCA circuit, the level of attenuation “oscillated” up and down as the VI followed the pattern of detecting the response, increasing the attenuation, losing the response, decreasing the attenuation, and so on. This process is commonly called “hunting”. For this reason, the CAP threshold (that is, the level of

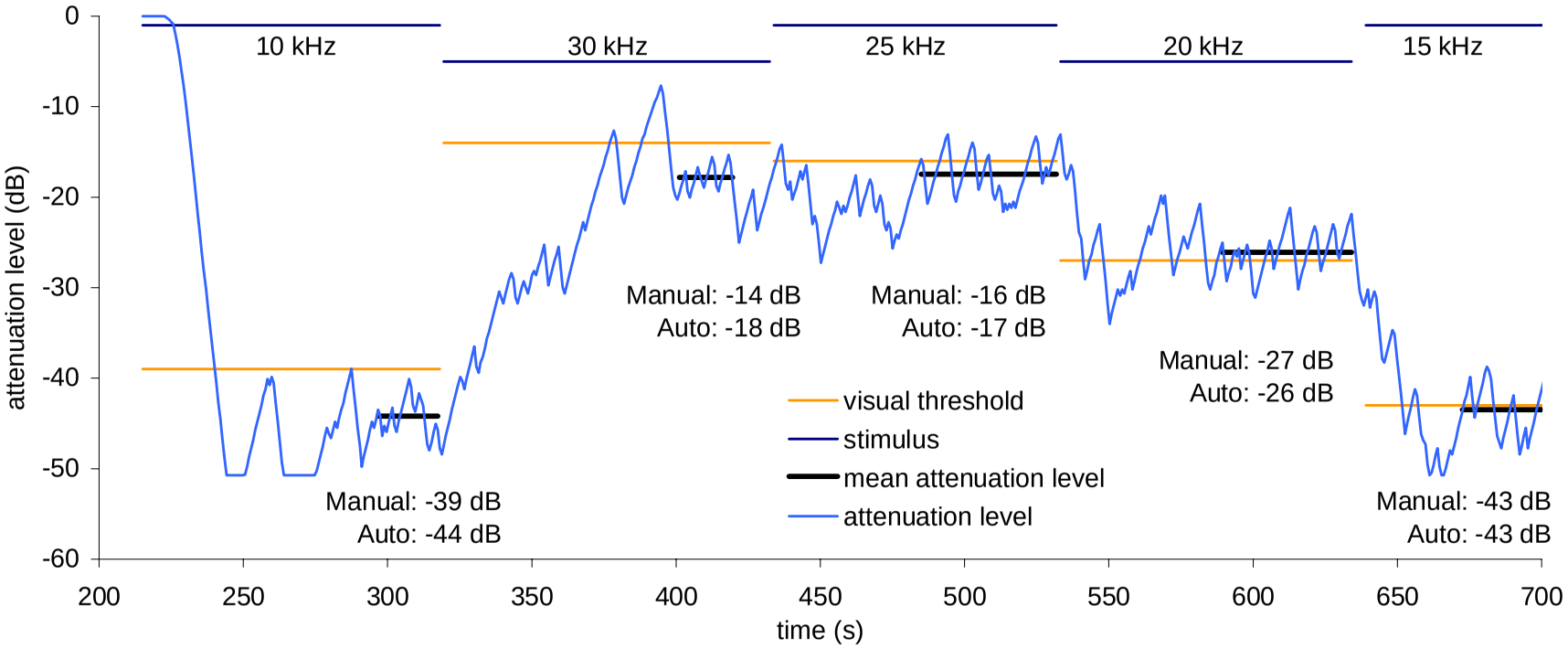

Figure 3.13.1: The results of the experiment comparing manual and automatic threshold determination. The CAP thresholds were obtained manually using the visual detection method at tone-burst frequencies of 10, 30, 25, 20, and 15 kHz. Thresholds for the same stimulus frequencies were then determined using the automatic CAP threshold detection VI developed for the task. Using the VI, the automatically-determined CAP threshold for a stimulus frequency was measured as the average of the oscillating attenuation levels, once the "zigzag" excursions around a particular attenuation level decreased in magnitude and appeared to stabilise.

attenuation at which the VI first detects the response) must lie between the higher and lower attenuation levels reached during the periods of oscillation. Once the "zigzag" excursions around a particular attenuation level decreased in magnitude and appeared to stabilise, the CAP threshold for the stimulus frequency was measured as the simple average of these oscillating attenuation levels. Although the ramping rates are not symmetrical, the average of these oscillations is representative of the detection threshold, as the attenuation level at which the response is detected or lost is independent of the time taken to *reach* the particular attenuation level.

When a stimulus frequency of 10 kHz was used, automatic threshold detection VI was able to detect the presence of the CAP using stimulus sound pressure levels 5 dB quieter than the threshold determined with the visual detection technique by Dr. Sellick. However, with the exception of the 15 kHz threshold measurement, the gap between the automatically detected thresholds and the manual thresholds determined at the beginning of the experiment decreased as the trial progressed, to the point that the automatically detected threshold for 20 kHz was worse than that detected using the manual technique, as shown in Figure 3.13.1.

As the background noise had not appeared to increase greatly during this period, the correlation technique should have been able to detect the CAP at stimulus sound levels lower than those needed for visual detection. The apparent elevation of CAP threshold was likely to be due to either i) a false estimation of threshold due to shortcomings in the correlation technique used, or ii) a real elevation of CAP threshold due to some physiological cause. In order to determine which of these two possibilities was the cause, the CAP thresholds were once again measured manually by Dr. Sellick using the visual detection technique. It was

found that over the 36 minutes of the experiment, the CAP thresholds had changed as shown in Table 3.13.2 below:

Stimulus Frequency:	10 kHz	15 kHz	20 kHz	25 kHz	30 kHz
Manual (0 – 2 min)	-39 dB	-43 dB	-27 dB	-16 dB	-14 dB
Automatic (2-11 min)	-44 dB	-43 dB	-26 dB	-17 dB	-18 dB
Manual (34 – 36 min)	-32 dB	-26 dB	-13 dB	-11 dB	-3 dB

Table 3.13.2: Comparison between CAP thresholds measured using the manual technique in the first two minutes of the experiment, those measured using the automatic technique, and the results obtained when the manual estimation was repeated at the end of the experiment. The total stimulus attenuation level is obtained by subtracting 50 dB from all values.

The cause of the CAP threshold elevation was physiological: on visual inspection of the guinea pig cochlea itself, it was apparent that the basilar membrane had been punctured by the perfusion pipette during surgery. In spite of this surgical problem, the CAP threshold automatic tracking method appeared to work well, on average taking around one minute to find the threshold attenuation level (59 s ± 21 s). The average excursion width about the threshold, once located, was 3.8 dB (± 2.3 dB). No other experiments were attempted, since the goal here was to simply demonstrate that the VI threshold-tracking technique also worked well in guinea-pigs.

Discussion

The speed at which the VI was able to find the threshold attenuation level could be improved in a number of ways. The factors influencing the speed with which the threshold attenuation level was found were: i) the stimulus repetition rate, ii) the ramping speed of the VCA, and iii) the number of points used to calculate the running point average of the

correlation values. Although the VI took around a minute to find the threshold attenuation level with the current settings, once the threshold level is found, the VI would be able to follow it closely for hours.

The conditions under which the CAP tracking experiment was conducted were not ideal. If the stimulus repetition rate of 3 tone-bursts per second used in the experiment were increased to around 10 per second or higher (which is typical in such experimentation), the sensitivity of the tracking would have been greatly increased, resulting in a decreased excursion width about the threshold. In addition, a faster VCA ramping speed would decrease the time taken to first reach the threshold attenuation level. The correlation smoothing level of 5 averages provided an adequate level of sensitivity in detecting the repeated presence of the CAP, whilst reducing the impact of any short-lived random fluctuations in correlation level.

Although the guinea-pig cochlea had been damaged during surgery, the data shown above still provides an indication of the effectiveness of the technique. Initially, the results obtained using the automatic technique were better than those obtained using manual threshold estimation, but the hearing of the animal was progressively deteriorating, and so it is not fair to compare the manual thresholds obtained at the beginning of the experiment with the automatic thresholds measured in the later parts of the experiment.

In summary, the results from this single trial indicate that the automated CAP threshold tracking method presented here is a viable alternative to visual threshold detection, and that the automated method is able to detect the presence of a CAP at stimulus levels at least 2 dB lower than the visual detection method. With the slight modifications of the test procedure described above, the threshold tracking technique could prove useful in situations where it is desirable to observe the changes CAP threshold at a particular frequency over a number of hours.

3.14 Real-time Boltzmann analysis of cochlear microphonic waveforms

Described in previous sections was the development of systems for the detection and analysis of auditory evoked responses, such as the PAMR in the human, and the CAP in the guinea-pig. Using the signal analysis and virtual instrument programming techniques gained during the development of the PAMR acquisition and analysis software, a further set of experiments were carried out using evoked-responses from the guinea-pig. During these experiments, a VI was developed that enabled fast and convenient real-time analysis of mechano-electrical transduction (MET) in outer hair cells (OHCs) *in vivo*.

The technique is an extension of a technique reported recently (Patuzzi and Moleirinho, 1998) in which the low-frequency (200 Hz) cochlear microphonic (CM) potential in the basal turn of the guinea pig cochlea was analysed, assuming that the transfer curve relating instantaneous pressure in the ear canal to the receptor current through OHCs is well described by a first-order Boltzmann activation curve (Holton and Hudspeth, 1986).

In the previous technique (Patuzzi and Moleirinho, 1998), the CM waveforms were analysed using a custom-built electronic circuit which generated its own synthetic "CM waveform", and automatically adjusted its parameters to match the real CM waveform. The circuit's parameters describing the synthetic waveform were then taken to be those describing the real waveform. This analogue device, colloquially known as the "Boltzmatron", was originally developed some years ago, before personal computers were sufficiently fast, and software was sufficiently sophisticated to perform the analysis numerically in real-time. While it was fast and relatively cheap, it had the disadvantage of being restricted in practice to one frequency (200 Hz, because of the circuitry), and required a complex custom-built circuit for each recording set-up. In recent years, however, advances in microprocessor technology and

increasing clock speeds have made it possible to perform this analysis in real-time without the analogue circuitry.

In essence, the CM analysis described can provide information about small, slow movements of the organ of Corti and other subtle changes in cochlear function which may be useful in studying cochlear homeostasis, and a range of other cochlear phenomena.

Because the opening probability of MET channels at the apex of the hair cells follows a Boltzmann activation function (Holton and Hudspeth, 1986), the relationship between instantaneous pressure in the ear canal (P) and the summed current through the OHCs (I_{ohc}) follows a similar function, with $I_{ohc} \approx I_{sat} / [1 + \exp(E_o + Z.P)/kT]$, where:

i) the parameter I_{sat} gives the maximal receptor current change through OHCs for large sinusoidal excursions of their hair bundles,

ii) Z is a sensitivity parameter (in units of eV/Pa) which, when multiplied by pressure, gives the instantaneous potential energy difference between the open and closed states of the MET channels,

iii) E_o is an offset parameter accounting for the fact that I_{ohc} is non-zero for a zero pressure stimulus in the ear canal,

iv) k is the Boltzmann constant and T is the absolute temperature of the population of MET channels.

At mammalian temperatures, the product kT has a value of approximately 27 meV. The significance of these parameters is described more fully in Patuzzi and Moleirinho (1998).

As a result of this nonlinear transduction, an intense but non-traumatic sinusoidal pressure stimulus can produce a decidedly non-sinusoidal CM waveform, as shown in Figure 3.14.1. Because the receptor current through OHCs of the basal turn dominates the low-

frequency CM in that region (Patuzzi et al., 1989), the instantaneous CM potential (V_{cm}) is approximately proportional to both the summed current through the OHCs (I_{ohc}) and the effective resistance of the extracellular fluid (R_{fluid}), so that the CM potential is given by $V_{cm} = R_{fluid}.I_{ohc}$, or:

$$V_{cm} \approx V_{sat} / (1 + \exp[E_0 + Z.P]/kT)$$

Conversely, with sinusoidal stimulation (pure tones), the CM waveform (V_{cm} plotted against time) can provide information about the nonlinear Boltzmann transfer curve governing MET. Assuming a Boltzmann transfer curve, and i) that the pressure stimulus is sinusoidal [$P = P_0.\sin(2\pi f.t + \phi)$], where f is the frequency of the sinusoid and ϕ is its phase relative to some external reference, ii) that there is an additional phase shift ϕ_0 between the CM response and the pressure stimulus due to phase delays in the middle ear and fluid dynamics of the cochlea [notably the high-pass acoustic filtering due to the helicotrema (Ruggero et al., 1986; Dallos, 1970)], and iii) that V_{off} represents some DC offset in the CM recording chain, we have that

$$V_{cm} = V_{off} + V_{sat} / \{1 + \exp[E_o + Z.P_o.\sin(2\pi f + \phi + \phi_0)]\} \qquad \text{(Equation 1)}$$

Previously, this theoretical function has been fitted to the CM waveform data off-line (using the “Solver” function of Microsoft Excel; Patuzzi and Rajan, 1990), or by using the analogue circuitry mentioned previously to accomplish the task in real-time (Patuzzi and Moleirinho, 1998). The present VI eliminates the need for this circuitry, by using a software algorithm to fit the theoretical function to the recorded CM waveform, and extract the Boltzmann parameters in real-time, either online, during an experiment, or offline, using CM waveforms recorded to digital audio tape (DAT).

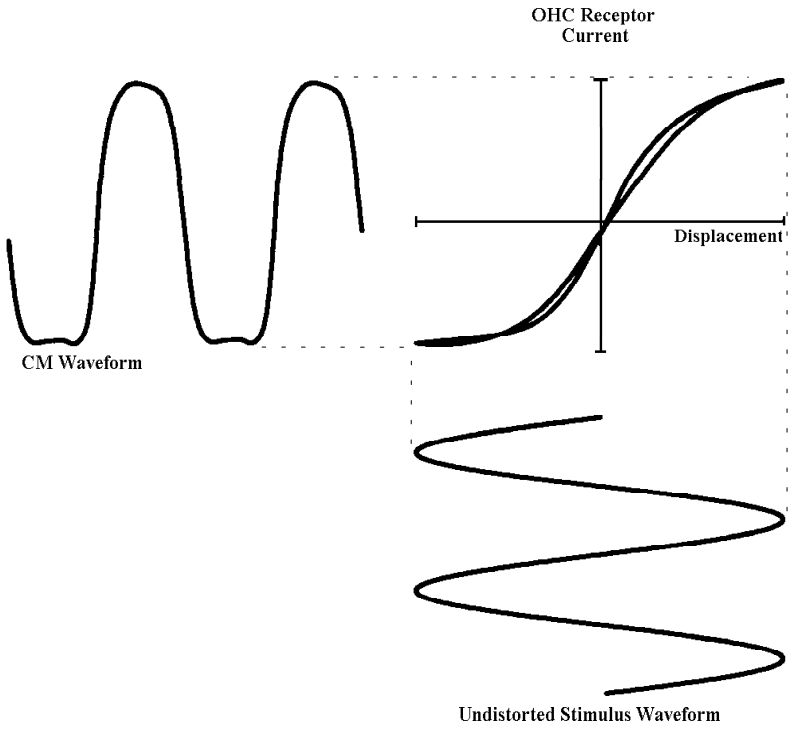

Figure 3.14.1: A Lissajous figure showing the CM waveform that results from the presumed sinusoidal displacement of the cochlear partition in response to an intense but non-traumatic pure-tone stimulus. (Patuzzi and Rajan, 1990).

The software developed in the present study (named the Boltzmatron.vi in honour of its electronic predecessor) samples a number of cycles of the CM waveform recorded from the scala tympani of the guinea pig, and fits the theoretical CM waveform function (Equation 1) using the nonlinear Levenberg-Marquardt (Lev-Mar) numerical method (see LabVIEW Analysis VI Reference Manual p.7-17, 1996).

To demonstrate the functioning of the VI, a CM waveform from a 320g guinea pig was recorded from a hole made at the first turn of the cochlea into scala tympani using a Ag/AgCl electrode placed inside a perfusion pipette. The anaesthesia and preliminary surgical procedures used on the guinea pig were carried out by Dr. Si-Yi Zhang, and are described

elsewhere in detail (Patuzzi et al., 1989a; Marcon, 1995). The animal was first used during another experiment, carried out by Dr. Sellick and Dr. Zhang, in which an electrode was also placed into scala vestibuli, the helicotrema was opened, and scala tympani was perfused with artificial perilymph. The opening at the helicotrema was made to allow a flow of perfused solutions from the base to the apex along the entire cochlea length. Presumably a result of the opening of the helicotrema and the artificial perilymph perfusion, the CAP thresholds of the animal had, on average, been elevated to 40 dB above the thresholds recorded prior to these procedures. In other words, the animal had suffered a hearing loss. Nevertheless, the CM recorded from the animal was still of sufficient amplitude and quality to allow measurement of the Boltzmann parameters.

The 200 Hz stimulus tone was generated by a Hewlett Packard 3325A Synthesizer/Function Generator (Hewlett Packard Corp., CA, USA). The tone was delivered to the guinea pig by a Beyer DT48 headphone coupled to the right hollow ear bar via a 4cm long probe tube. The CM waveform recorded from scala tympani was then amplified by 60 dB before being recorded to DAT using a DTR-2000 DAT recorder (Denon Corp., Japan).

The aim of this experiment was to cause a perturbation to the cochlea and record the changes in the CM waveform using the Boltzmatron VI. One of the simplest perturbations to carry out is to temporarily cut off the supply of oxygen to the animal, and to record the changes in cochlear function that follow.

After recording the CM waveform for approximately 3 minutes, the respirator for the guinea pig was turned off so that any changes in CM with transient hypoxia could be observed. After 9 minutes, the respirator was turned on again and the guinea pig was allowed to recover. After a further 10 minutes, the respirator was again turned off and the CM waveform was

recorded to DAT for further 30 minutes, during which time the guinea pig died. This procedure was carried out in order to allow observation of the changes in the CM waveform when the asphyxia is continued past the point where recovery of the animal is possible. The DAT tape recording of the CM was later played into an analogue input channel of the Lab-PC+ card for analysis by the Boltzmatron VI.

To provide another example of the functioning of the Boltzmatron VI, a DAT recording of a guinea pig CM waveform made by Mr. Simon Marcon in July 1995 was also played into the Lab-PC+ card and analysed by the Boltzmatron VI. The surgery and anaesthesia carried out on the guinea pig are as described elsewhere (Patuzzi et al., 1989a; Marcon, 1995). The CM from this animal was recorded from a hole made at the first turn of the cochlea into scala tympani using a Ag/AgCl electrode placed inside a perfusion pipette. A 207 Hz stimulus tone was generated by a Hewlett Packard 3325A Synthesizer/Function Generator (Hewlett Packard Corp., CA, USA), and was attenuated by 25 dB before being delivered to the guinea pig by a Beyer DT48 headphone coupled to the right hollow ear bar via a 4cm long probe tube.

In that particular experiment, a transient hypoxia was induced by clamping of the tracheal cannula for a period of 3 minutes, after which time oxygen was restored to the guinea pig. The operation of this VI is explained below.

3.14.1 Boltzmatron VI 

The purpose of the following VI was to enable fast and convenient real-time analysis of mechano-electrical transduction (MET) in outer hair cells (OHCs) *in vivo*. A low-frequency cochlear microphonic (CM) waveform recorded from a guinea pig was sampled, and the non-linear Levenberg-Marquardt (Lev-Mar) numerical method was used to continually adjust the parameters of the assumed CM equation (shown below) to obtain the least-squares fit to each sampled waveform. The parameters describing each CM waveform sample were then displayed and stored to disk.

The assumed theoretical function describing the CM waveform is:

$$V_{cm} = V_{off} + V_{sat} / \{1 + \exp[E_o + Z.P_o.\sin(2\pi f + \phi_{tot})]\} \qquad \text{(Equation 2)}$$

where the six parameters are:

i) a DC offset voltage (V_{off})

ii) the frequency of the sinusoidal stimulus (f)

iii) the phase of the sinusoidal stimulus (ϕ_{tot})

iv) the maximal amplitude of the distorted microphonic signal (V_{sat})

v) the sensitivity of the transduction process (Z), and

vi) the operating point on the sigmoidal transfer curve (E_o).

As the sampling and fitting process could be carried out in less than a second (because of the speed of the computer), any changes that occurred in the actual CM waveform characteristics over time were mirrored by changes in the six parameters of the fitted function.

The VI consisted of four major blocks: i) a CM waveform synthesis section (used for tutorial purposes, or teaching about MET in OHCs and the significance of the six parameters); ii) a waveform capture section (used when sampling a real incoming CM waveform); iii) the

nonlinear Lev-Mar fit section (used to obtain the least-squares fit to the six parameters); and iv) the graphical display and data storage section. The operation of the VI is as follows:

If the user had selected the "Save Output" option, on commencement of the running of the VI they were prompted to enter an output data filename, and a header file was written which contained the column headings for the output data, namely:

time offset f phase Vsat Z Eo mserror 10/9/98 @ 14:22

The "date @ time" value changed every time the VI was run, and was used to aid identification of the data at a later date. Once the header file was written, the VI then entered the outer "WHILE" loop, in which the start time of the loop (a large number which indicated the number of seconds that had passed since the 1st of January, 1904) was read from the internal clock of the computer. Once this had been read, the VI entered the next "WHILE" loop. This loop contained the mechanisms for sampling and fitting a single CM waveform, and kept repeating until the stop button was pressed. At this point, a number of values were read from the fields on the front panel, such as the sample rate, the number of points to capture (or generate, depending on which mode the VI was in), the delay time between each iteration of the while loop, the six "First Guess" parameters, and the MODE that the VI was to run in. The MODE button could be set to either "Capture" or "Simulate". These modes are described below:

3.14.1.1 Simulation Mode

In order to use the CM simulation, the MODE button was set to "Simulate". The VI then read the six Simulation parameters entered into the front panel by the user, and generated an artificial CM waveform. The VI constructed the CM waveform according to Equation One, as follows. First, a sine wave was generated, and then this sine wave was distorted by the Boltzmann transfer function.

The "frequency" of the sine wave to be generated was converted from Hertz (cycles/sec) to radians/sec by dividing the "f" parameter from the front panel by the sample rate divided by 2π. If, for example, the sine wave was to consist of 600 points, a one-dimensional array of numbers (0, 1, 2, 3,… …598, 599) was created by a small "FOR" loop, and this 1D array was multiplied by the radians/sec frequency value. The phase of the desired waveform (in radians) was then arithmetically added to each of the values of the scaled 1D array. The sine of each of the 600 points in the array was then calculated, thus creating a 600-point sine wave of specified frequency and phase.

The sine wave was then distorted using the Boltzmann function in the following way. First, the 600-point array containing the sine wave was multiplied by the "Z" sensitivity parameter. The value representing the E_0 operating point was then added to each point of the array, and e was raised to the power of the array. Each value in the array was then increased by 1. A new array was then calculated by dividing the V_{sat} parameter by the current array. Once the V_{off} DC offset value was added, this artificial CM waveform was plotted in the Waveform Display window on the upper right of the front panel. The Noise Amplitude setting on the front panel could be adjusted to vary the amount of uniform white noise added to the artificial CM waveform prior to plotting. In Simulate mode, the Lev-Mar fitting procedure was carried out on this artificial CM. Alternatively, in Capture mode, a real CM waveform was sampled and used, as described below.

3.14.1.2 Capture Mode

In Capture mode, the user-defined data acquisition settings were read from the front panel. These included the data channel (the analogue input channel on the Lab-PC+ card from which to sample the CM), the trigger channel (the analogue input channel on the Lab-PC+ card

used as a trigger for acquisition), the trigger level and slope, and the high and low voltage limits for the acquisition (normally set at ± 5V). When the trigger conditions had been satisfied, a number of points were sampled from the analogue input channel at a rate of 15000 samples/sec. The analogue input could be either the amplified CM voltage coming directly from the Ag/AgCl electrode in scala tympani of the guinea pig, or the CM could first be recorded onto DAT tape to be played back into the analogue input at a later date.

Once the CM waveform was sampled, it was multiplied by a scaling factor to compensate for the gain of the recording chain. So that monitoring of CM waveforms could be done intermittently, as well as continuously, a "threshold" setting was introduced so that the VI did not leave the acquisition WHILE loop *until the sum of the squares of the sampled waveform was above a certain level*. This meant that once the VI was set to run, the low-frequency stimulus tone could be turned off and the VI would not attempt to fit Equation One to a non-existent CM.

In both Capture and Simulate mode, the current time (seconds since 1/1/1904) was again read from the internal clock, and the previously recorded start time was subtracted from this value. The resulting number was the time of the capture or artificial CM generation in seconds since the start of recording.

Now that a CM waveform had been sampled (in Capture mode), or an artificial CM generated (in Simulation mode), the fitting process could begin. Once the VI left the acquisition WHILE loop, the initial guesses for the best-fit parameters (the starting point for the Lev-Mar process) were read from those entered in the "First Guess" fields on the front panel. When using the Simulation mode, the First Guess parameters should be approximately equal to the Simulation parameters. The operation of the non-linear Levenberg-Marquardt

algorithm sub-VI is explained on pages 7 to 17 of the LabVIEW Analysis VI Reference Manual (National Instruments Corp., 1996).

The output from this sub-VI included the values for the six parameters (V_{off}, frequency, phase, V_{sat}, Z, and E_0) that provided the best-fit to the sampled or simulated CM waveform, the fitted waveform generated from the equation using these values, and two measures of the accuracy of the fit to the CM waveform. These were the covariance matrix of the best fit coefficients, and the mean square error. The Lev-Mar fitting process determines the values of the six parameters that minimise this mean square error quantity. Consequently, the "mserror" quantity was also written to the output file, so that the accuracy of the fitted Boltzmann parameters could be assessed.

After each fit, the values of the six best-fit parameters were shown on the front panel of the VI, and stored for output to file. The fitted waveform was also plotted in the same window as the actual CM waveform, so that any obvious differences (if present) between the two waveforms could be seen. When the "STOP" button was pressed, the operation of the VI ceased, and the accumulated data was then appended to the header file, which had been written at the start of the VI. The format of the data file was tab-delimited text, which could be opened and analysed using spreadsheet programs, such as Microsoft Excel. The results of the Boltzmann analysis are discussed in the next section. The diagrams and front panel for this VI are shown in the following pages.

3.14.2 Results of the Boltzmann analysis

The purpose of this part of the study was to develop software that was capable of analysing mechano-electrical transduction (MET) in outer hair cells (OHCs) *in vivo*, and to provide an example of the changes in MET that can be monitored using the technique.

Front Panel: Boltzmatron VI

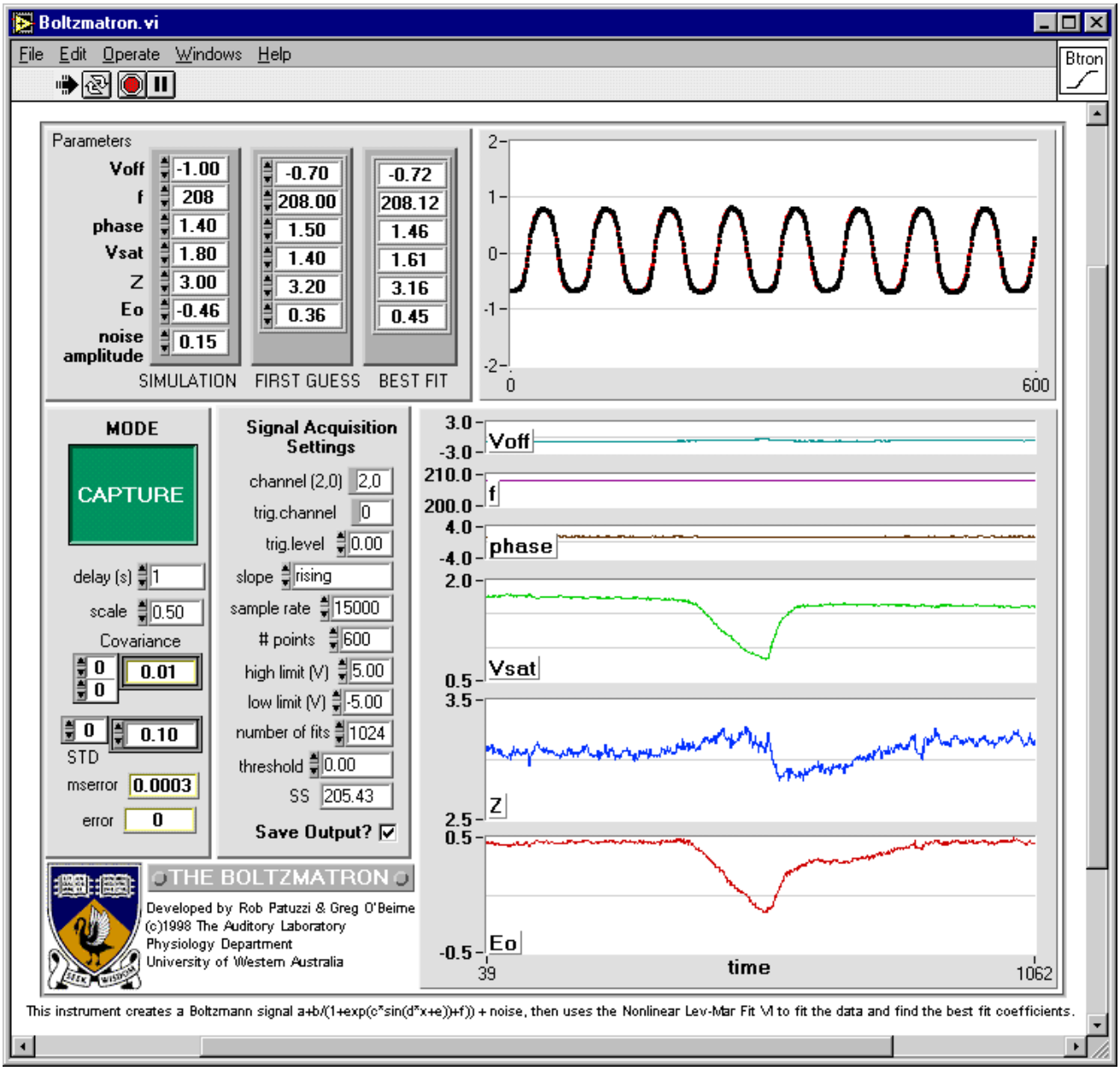

Diagram: Boltzmatron VI ("Simulation" mode)

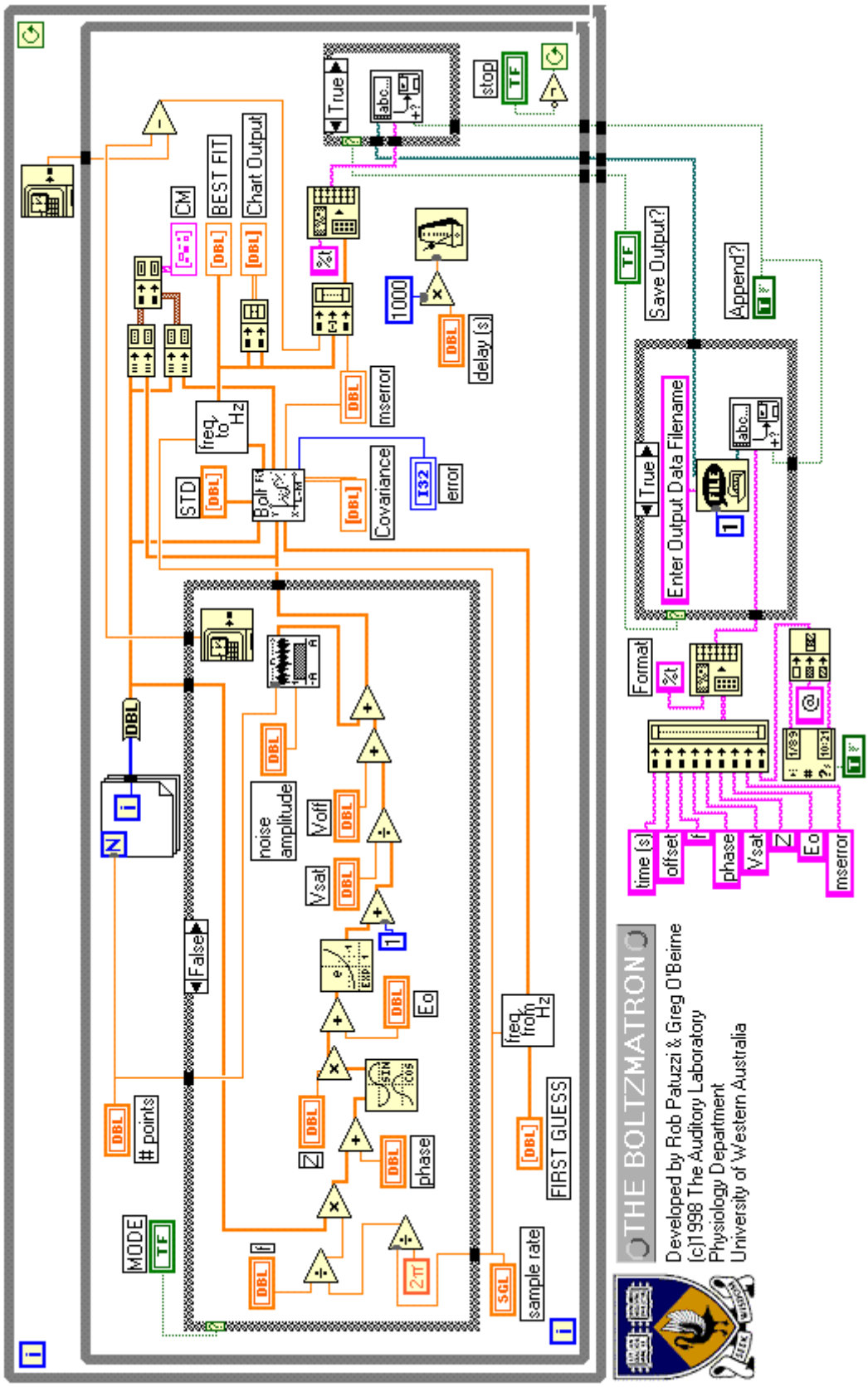

Diagram: Boltzmatron VI ("Capture" mode)

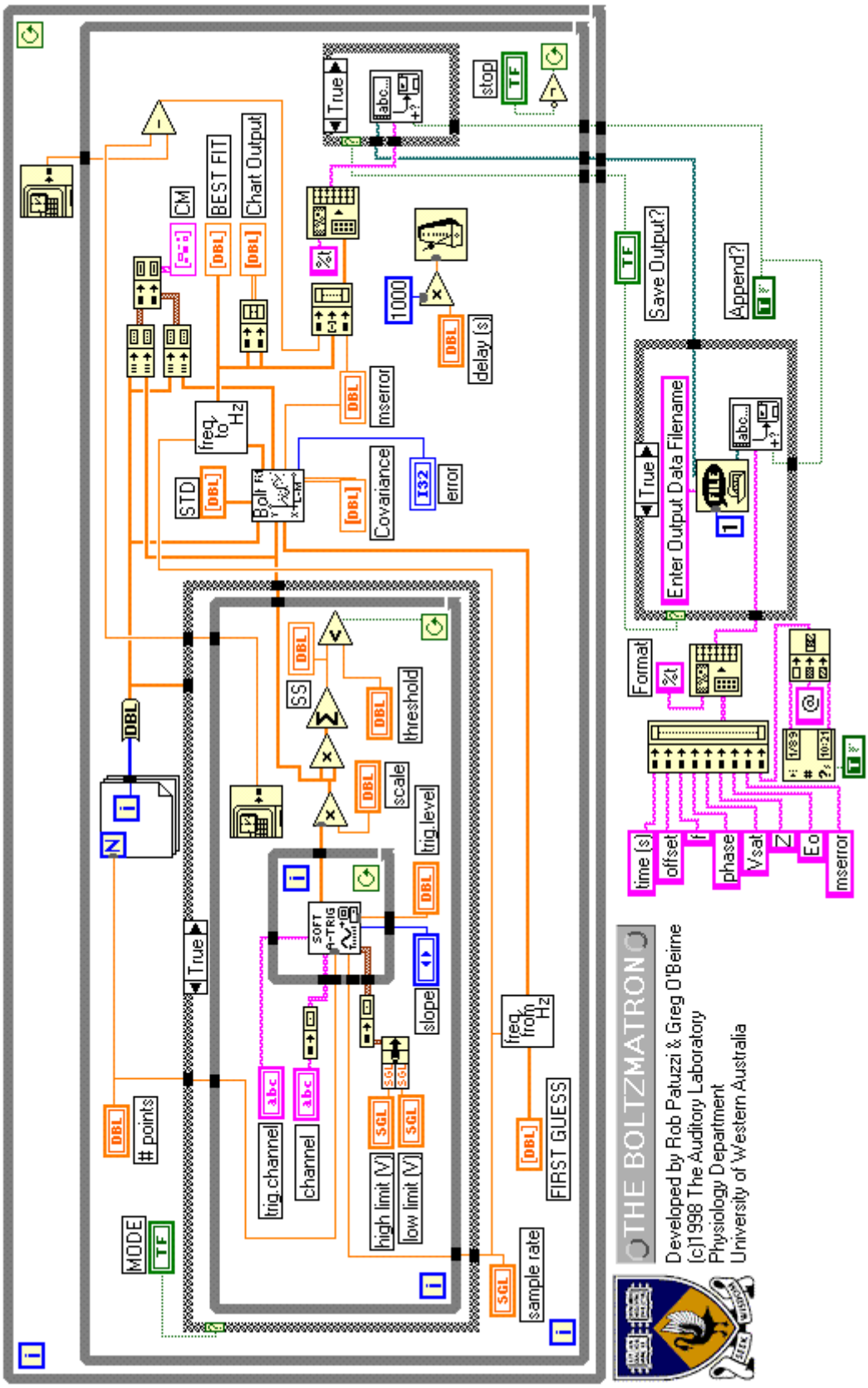

Figure 3.14.2 shows the changes in the 207 Hz CM waveforms recorded from the basal turn of the guinea pig cochlea when the cochlear transduction was disturbed by a transient asphyxia. This particular experiment was performed by Mr. Simon Marcon in 1995. The CM waveforms were recorded to DAT during the experiment, and were analysed using the Boltzmatron VI software during this project.

During asphyxia, there was a characteristic decrease in the endocochlear potential (EP) as the function of stria vascularis was compromised (Konishi et al., 1961). The effects of this fall in EP can be seen as a reduction in CM amplitude approximately two minutes after clamping of the tracheal cannula (Figure 3.14.2). This fall in EP (the driving potential for OHC receptor current) also caused the drop in the V_{sat} parameter. The E_0 parameter changed in a manner consistent with a movement of the OHC hair bundles towards the cell's basal body (i.e. the opening of MET channels and larger clipping on the positive-going CM phase), while the Z parameter showed a slight increase. Even though the V_{sat} parameter was reduced to less than half of its initial value in this case, the Z parameter increased by only 5%.

When the tracheal cannula was unclamped after three minutes, and the supply of oxygen was restored to stria vascularis, the EP and Boltzmann parameters recovered to values close to their starting values. Similar changes have been reported previously using the older analogue method for analysing the CM waveforms, and some of the mechanisms producing these changes have been discussed (Patuzzi and Moleirhino, 1998).

In a separate experiment, shown in Figure 3.14.3, death was the intended end-point for the asphyxia. The V_{sat} parameter had been declining slowly since the previous transient asphyxia (between 4 and 13 minutes, as shown in Figure 3.14.3). The reasons for this slow decline are unknown, and are not reflected in changes in the other Boltzmann parameters.

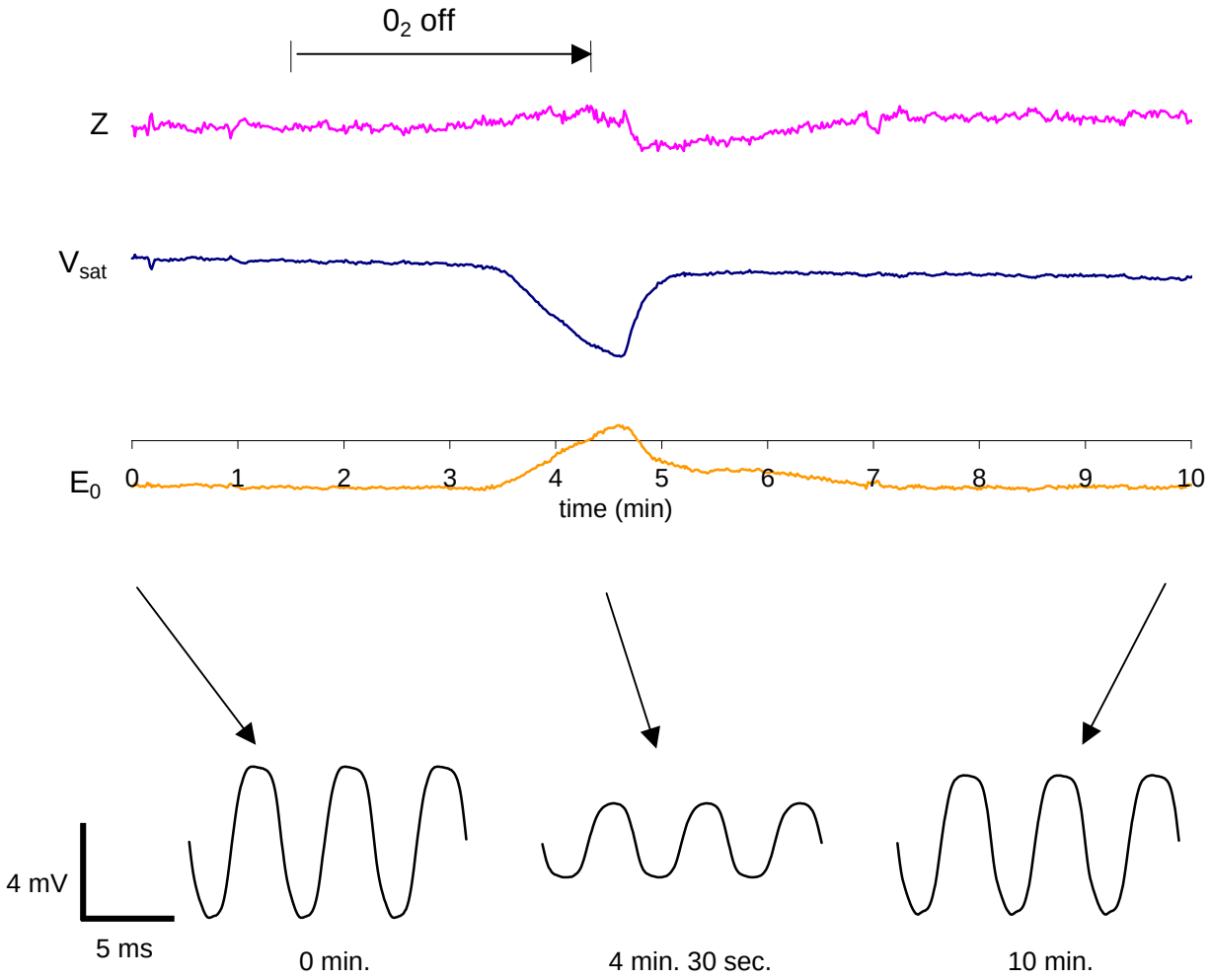

Figure 3.14.2: The changes in CM waveform shape, and the Boltzmann parameters Z, V_{sat} and E_0, during transient asphyxia caused by clamping of the tracheal cannula.

However, eleven minutes after the respirator was turned off (at the 23 minute mark, as shown in Figure 3.14.3), the V_{sat} parameter dropped rapidly for slightly under two minutes, before declining at a slower rate. There was a large, steady increase in the E_0 parameter, consistent with movement of the OHC hair bundle towards the basal body of the cell. The sensitivity of the MET process (reflected in the Z parameter) first declined slightly (by 4%) for approximately one minute, before sharply rising by 23% over 3 minutes. It was then observed to decrease steadily over 9 minutes until it reached values similar to the pre-asphyxia values.

3.14.3 Discussion

It is likely that the long delay between the shutting down of the respirator and the presumed drop in EP that caused the change in V_{sat} is due to the high concentration of O_2 in the tracheal cannula and associated tubes being enough to sustain the guinea pig for several minutes before being depleted. A similar problem was observed during the first transient hypoxia (between 4 and 13 minutes, as shown in Figure 3.14.3). Although the respirator was turned off for over 9 minutes, there was very little change in the characteristics of the CM. From this it can be inferred that clamping of the tracheal cannula is a more reliable method of causing hypoxia than turning off the artificial respirator.

A slight oscillation can be observed in the E_0 trace of Figure 3.14.3 before the presumed drop in EP. The oscillations are possibly due to a rhythmical movement of the basilar membrane, caused by fluctuations in cerebrospinal fluid (CSF) pressure with heartbeat. Ordinarily, these small fluctuations in CSF pressure would not cause such movement, but an earlier experiment on the same animal necessitated opening the helicotrema, which could conceivably cause the cochlear fluids to act in a manner similar to a barometer. The frequency

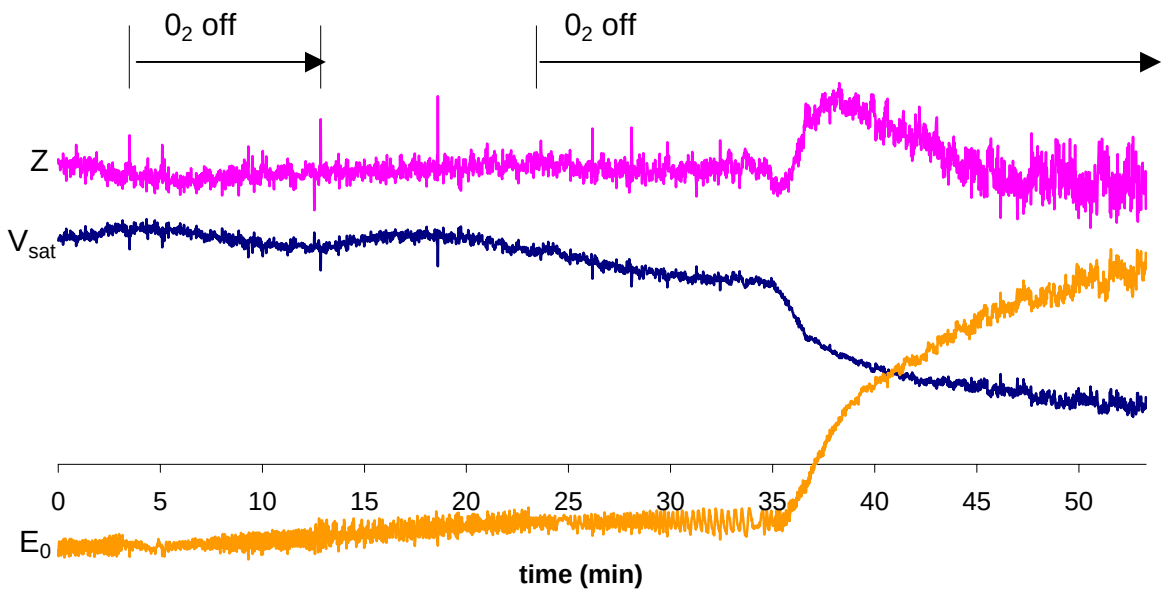

Figure 3.14.3: The changes in the Boltzmann parameters Z, V_{sat} and E_0, during transient asphyxia caused by turning off the artificial respirator (between the 3 to 14 minute marks), and during terminal asphyxia, caused by the same method (at the 23 minute mark). Note the oscillations in the E_0 parameter, possibly caused by fluctuations in cerebrospinal fluid (CSF) pressure with heartbeat.

of the oscillation shown is likely to be a beat frequency, caused by the difference between the frequency of the heartbeat oscillation, and the interval between samples (approximately 1/sec).

3.14.4 Conclusion

The technique described here is a simple *in vivo* method of monitoring MET in OHCs by analysing the extracellular CM in real-time. The V_{off} parameter (the voltage offset) need not have any physiological significance, but may be due to any DC offsets in the recording/playback chain. The V_{sat} parameter is assumed to be affected by (and in some instances approximately proportional to): i) the driving potential for the OHC receptor current (the EP minus intracellular OHC membrane potential), ii) the number of operating MET channels at the apex of the OHCs, iii) the conductance of the basolateral membrane of the OHCs, and iv) various recording conditions, such as the distance of the recording electrode from the relevant OHCs (Patuzzi and Moleirinho, 1998). The Z parameter is, broadly speaking, the horizontal excursion across the Boltzmann transfer curve per unit pressure fluctuation in the ear canal. It is proportional to the sound level of the stimulus in the ear canal, the transfer efficiency through the middle ear (defined as intracochlear pressure fluctuation per unit pressure fluctuation in the ear canal), transverse compliance of the organ of Corti, the efficiency of mechanical coupling from transverse displacement of the organ of Corti to hair bundle displacement, and coupling between hair bundle displacement to energy bias of the MET channels (Patuzzi and Moleirinho, 1998).

Finally, the operating point E_0 is assumed to represent the effective energy bias on the MET channels without sound stimulation. If there were no adaptation in the coupling between hair bundle displacement and MET channel energy bias, then E_0 would also be proportional to the displacement of the OHC hair bundles as well, and presumably the transverse displacement

of the organ of Corti, and the combined hydrostatic and osmotic pressures acting on the organ of Corti (Patuzzi and Moleirinho, 1998). If there is adaptation of the OHC hair bundles, then the E_0 parameter would a measure of the effective energy bias of the OHC hair bundles, but would not be a measure of the hair bundle displacement, or the displacement of the organ of Corti (Patuzzi and Moleirinho, 1998).

As for the derived phase of the CM response (ϕ_{tot} of Eqn.2), the parameter only has a physiological significance if the waveform capture is triggered by an external reference (the electrical drive to the sound system or the sound pressure waveform). In this case, changes in the response phase may indicate changes in the hydrodynamics of the organ of Corti (e.g. phase distortion due to low-pass filtering in the helicotrema) or more complex changes in MET.

This present VI, which is to be made freely available on the Internet, enables automatic monitoring of mechano-electrical transduction (MET) in the guinea pig (and other mammals) to be carried out by any electrophysiologist with a sufficiently fast computer and access to LabVIEW. A stand-alone version of the VI has been also been compiled, which allows only the simulation mode to be run, in the absence of the data-acquisition card or LabVIEW, and may be useful in demonstrating the role of each the Boltzmann parameters in describing the CM.

DISCUSSION
and
SUMMARY

4.0 Discussion and Summary

The discussion of the individual results of this study appeared following the results in each section. This final section consists of a brief summary of the findings of this study and their significance, and suggestions for future improvements and research.

4.1 Summary

A number of characteristics of the human PAMR were studied in both adult and infant subjects. The input/output function of the PAMR in response to click stimuli was measured. Our results indicate that the amplitude of the PAMR increased monotonically with increasing stimulus level over an 80 dB range. Input/output functions for a number of evoked responses do not always show this linearity. For example, a bimodal input/output function is often observed for the compound action potential of the cochlear, because of differential recruitment of hair cells with stimulus intensity (Özdamar and Dallos, 1976). The monotonic increase observed in the PAMR input-output function was consistent with the response being produced by a single, large population of neurones.

The latency of the first and second peaks of the PAMR was also found to decrease with increasing stimulus level (first-peak decreased from 15.5 ms at 10 dB SL to to 13.2 ms at 80 dB SL). These latency shifts were of practical importance to clinical screening using the correlation level between successive waveforms, because of the “windowing” used in the correlation calculations. That is, the correlation level was greatly reduced when the peak of the response fell outside of the time-window over which the correlation was calculated. This was demonstrated empirically by the correlation contour plots shown in Figure 2.9.

Input-output functions were also measured using 38 ms tone-bursts from 500 Hz to 16 kHz, and at stimulus levels from 0 dB SL to 80 dB SL (Figures 3.2.1). These data showed that in two subjects the PAMR could be evoked using frequency-specific stimuli (rather than clicks) at stimulus levels of 40 dB SL or less. This result indicated that the PAMR has the potential to be used as an objective hearing test that can provide information as to whether a subject has a high-frequency or a low-frequency hearing loss.

The distribution of the PAMR over the skin surface was studied for a number of reasons. Firstly, it was important to gain information about how the electrode location affects the size of the measured response, and because the correlation level of successive waveforms gives a measure of the signal-to-noise ratio of the response. It was important to record the response from locations that i) maximised the size of the PAMR, and ii) minimised electrical artefacts, both from external and biological sources, so that the correlation measure of signal-to-noise ratio accurately reflected the presence of an evoked response. It was found that the peak-to-peak amplitude of the response was largest when recorded with an active electrode situated directly over the body of the PAM, but decreased with electrode locations further away from the body of the muscle. It was also found that an inverted version of the PAMR could be recorded with reduced amplitude from the dorsal surface of the pinna. Whatever the explanation for the inversion may be, we found that by recording the PAMR with reference to a pinna electrode (rather than a forehead electrode), the signal-to-noise ratio was improved in two ways. Firstly, the amplitude of the signal was increased due to subtraction of the inverted pinna waveform. Secondly, there was decreased electrical noise from biological sources such as blink artefacts, and from external sources, because the active and reference locations were physically closer together. For these reasons, all subsequent measurements of the PAMR were

made with reference to the pinna. This electrode placement was also convenient from a practical point of view, as it allowed the development of a hinged "wedge" electrode which fitted snugly into the fold behind the ear.

Because testing of the PAMR in infants was likely to be carried out using free-field stimuli, rather than headphones, it was important to understand how the PAMR was changed by the direction of the stimuli (i.e. loudest in the ear on the same side of the head as the recording electrodes, on the opposite side of the head as the recording electrodes, or equally loud in both ears). It was found that the PAMR waveform evoked by binaural clicks was very similar, in both magnitude and latency, to the sum of the two monaural waveforms. Significant differences in first-peak latency were observed between the binaurally-evoked PAM, the PAMR evoked with contralateral-monaural stimuli, and the PAMR evoked with ipsilateral-monaural stimuli. The difference in peak latency of the ispsilaterally- and contralaterally-evoked PAMR waveforms is probably due to a slight difference in the length of neurones in the crossed and uncrossed pathways through the brainstem. Although these latency differences were significant, the maximum latency difference we observed was still less than 1 ms. Because the correlation window was set quite wide, these small shifts did not have a significant impact on the correlation levels we recorded.

It has been reported that the latency of the PAMR is significantly extended in infancy (Buffin et al., 1977). In the present study, recordings of the PAMR were made from two infant subjects. One of these subject was 4½ months old, and the other was one year old. When the first-peak latencies of the averaged waveforms recorded from these subjects were compared with those from an adult subject, it was found that while the first-peak latency of the PAMR recorded from the 1 year old subject was similar to that of the adult, the first-peak latency of

the PAMR recorded from the 4½ month old subject was, on average, 2 ms longer than that of the adult subject. Our results are consistent with those of Buffin et al. (1977).

As described previously, the latency of the peaks of the PAMR from a subject is highly relevant to the correlation measure of the response, if these peaks occur outside the chosen correlation window. To allow for the shifts of latency that occur with maturation, a correlation window of 10 ms to 24 ms was chosen, as it provided an adequate level of correlation for both adult and infant subjects. This window could still have been chosen even if the correlation device was to be used only on infants and children, as the peak latencies recorded from the one year old subject were similar to those from the adult subject.

In the present study, the effect of eye movement on a number of characteristics of the PAMR was examined using custom-designed virtual instruments capable of simultaneously measuring and averaging the peak-to-peak amplitude and latency of the PAMR, the EMG of the PAM, and the correlation level between successive PAMR waveforms. Our initial hypothesis was that if eye rotation potentiated the PAMR at some point along the reflex pathway through the brainstem, we would expect that eye rotation would increase the size of the sound-evoked response <u>without altering the level of background EMG</u> in the muscle. However, if the enhancement of the reflex with eye rotation occurred at the motor nucleus of the facial nerve, then we would expect that eye rotation would increase the amplitude of the sound-evoked PAMR <u>and</u> the background EMG simultaneously. This hypothesis was later revised, as described below.

In brief, we found that the arguments in favour of a causal relationship between the EMG and the peak-to-peak height of the PAMR were that: i) in most cases, any method that increased the EMG of the PAM (from a low level to a high level) also increased the amplitude

of the PAMR *if it was present*, and ii) any action that increased the peak-to-peak amplitude of the PAMR (other than altering the acoustic stimulus) also increased the EMG of the PAM, even when the action was performed in the absence of sound stimuli. Viewed in terms of our initial hypothesis (but not our *final* one), our results suggested that the increases in both the amplitude of the PAMR and the background EMG was likely to be caused by a change in membrane potential of the neurones in the motor nucleus of the facial nerve.

This initial hypothesis had to be modified. In summary, the above experiments have found that the enhancement of the PAMR during eye movement coincides with increased electrical activity (EMG) in the post-auricular muscle observed during this manoeuvre, and that any procedure which increases electrical activity in the PAM enhances the PAMR if it is present. The similar time-courses of these changes indicate that the mechanisms that increase the EMG *and* the PAMR probably occur at a common point. However, due to a lack of neuro-anatomical evidence, we cannot distinguish whether this common point is the motor nucleus of the facial nerve, as we had originally thought, or is within the auditory brainstem. Despite the lack of evidence as to the precise mechanisms by which it occurs, ipsilateral rotation of the eyes was found to be a convenient and efficient method of enhancing the PAMR in most of our subjects, including infants.

The correlation measure of the PAMR was also found to be an effective measure of the response in both adult and infant subjects. For this reason, the correlation measure was used as the basis of a cheap and portable device for measurement of the PAMR developed during this study. The software developed during this study to analyse the PAMR was also easily adapted for automated measurement of CAP thresholds in the guinea-pig, where it performed well.

While not directly relevant to our results from the PAMR, the expertise gained during the development of the systems described above allowed software to be written for the real-time Boltzmann analysis of the cochlear microphonic waveform of the guinea-pig. This software has already proved very useful in studying outer hair-cell function, and is now regularly used within our laboratory.

4.2 Shortcomings of the study

In this study, most of the data was obtained from one subject only, except where indicated. It would have been advantageous to carry out these experiments on a greater range of adult and infant subjects. However, the primary aim of the study was to develop the techniques for measurement of the response, and to see if this measurement could be done cheaply and reliably using the correlation measure. While this aim has been achieved, a population study using these techniques must be carried out before clinical implementation of the device can take place.

4.3 Suggestions for future improvements and research

There are a number of ways in which the correlator device developed in this study can be improved, as described in Section 3.11. The FM link between the subject and the correlator is a source of some of these problems, because the FM receiver lost lock on the signal if there were fluctuations in the power supply. The “wedge” electrode is, in principle, a good design, but as our prototypes were made from self-adhesive foam off-cuts from normal ECG electrodes. If these electrodes were to be properly manufactured, the electrode design could be improved to make it easier to place, and to make it less likely to fall off during recordings.

It may be possible to develop a hybrid PAMR measurement system, consisting of components of the correlator device and the LabVIEW software, for use in maternity hospitals. It is conceivable that the correlator device, including the speaker, could be built into the crib containing the baby. The crib electronics could produce the click stimuli, amplify the signal from the electrodes, carry out the bitstream approximation and calculate the correlation level between the successive responses. The correlation voltage from the crib could be displayed by a peak-meter, which would record the highest level of correlation achieved over the time of the test. Using a simple lap-top computer and the crib electronics, a large number of babies could be tested in parallel, with the results of the test from each baby displayed on the screen. Babies who failed to show an average correlation level above a chosen level, such as 0.2, with moderate level click stimuli (45 – 50 dB HL) would be referred for further testing.

The correlation measure of the presence of the PAMR was assessed throughout this study, and was found to give a good approximation of the signal-to-noise ratio of the response. It was noticed during this study that another method of detecting the presence of the PAMR would be to calculate the RMS magnitudes of both the pre-trigger and post-trigger epochs (shown in Figure 2.8 of the Methods section), and to subtract the pre-trigger value from the post-trigger value. The logic behind this calculation is that the post-trigger epoch contains both the signal (the PAMR) and noise (the EMG), whereas the pre-trigger epoch contains only the noise (the EMG), and so:

RMS magnitude of window containing (PAMR + EMG)

subtract *RMS magnitude of window containing EMG only*

= RMS magnitude of PAMR.

When the PAMR is absent, there should be no difference in the average RMS amplitude of the two windows over time. However, when the PAMR is present, the RMS amplitude of the post-trigger window would, on average, be larger than that of the pre-trigger window. Preliminary trials of this technique have indicated that this measure could be just as effective as the correlation measure in detecting the PAMR. An advantage to using this technique is that it is simpler to implement electronically than the correlation measure, but further research needs to be done in order to assess its strengths and weaknesses.

4.4 Concluding remarks

Currently, the PAMR is treated with a degree of contempt in many circles. For example, Hall (1992) lists the PAMR under the "muscular artefact" section of his book. He states: "*It is noteworthy to point out that not long ago, PAM activity was, in fact, a desired response (vs. an artefact), recorded intentionally as a measure of auditory function. Ironically, the PAM response was proposed for essentially the same clinical purpose as the AMLR, namely as an "objective" technique for auditory assessment in patient populations that were difficult to test by behavioural audiometry*." From paragraphs such as these the reader gets the impression that the PAM is not really an objective technique. However, this is not the case.

The PAMR seems to have been dismissed because it is a muscle response, rather than a solely neural one, but to some extent this is an advantage. It is unique in that it is the only convenient objective measure of hearing that can be used in active, restless, or "difficult-to-test" children. Based on his own research, Gibson (1975) concluded that tests based on the PAMR appeared to provide an excellent method of assessing the hearing acuity of children during a clinic: "*The advantages of the test are that all manner of children, normally untestable without sedation, can be rapidly screened during the course of the actual clinic*." He felt that the unique advantage of the PAMR was that "*since it is a muscle response, the tense child difficult to test by other means gives clear responses*."

In fact, as this research and that of other groups have pointed out, the PAMR is a useful, reliable indicator of hearing. The development of a cheap test for this response changes the weighting in considering the PAMR as a viable alternative to the objective tests currently available. We have done just that.

REFERENCES

References

Abe, M. (1954). Electrical responses of the human brain to acoustic stimulus. Tohuku J.Expt.Med. 60 (1), 47-58.

von Békésy, G. (1947). A new audiometer. Arch.Otolaryngol. 35, 411-422.

Bench, R.J. and Boscak, N. (1969). Some applications of signal detection theory to paedo-audiology. Sound. 58-61.

Bess, F.H. and Paradise, J.L. (1994). Universal Screening for Infant Hearing Impairment: Not Simple, Not Risk-Free, Not Necessarily Beneficial, and Not Presently Justified. Pediatrics 93(2), 330-334.

Bickford, R.G., Jacobson, J.L. and Cody, D.T.R. (1964). Nature of averaged evoked potentials to sound and other stimuli in man. Ann.New York Acad.Sci. 112, 204-223.

Bickford, R.G., Jacobson, J.L. and Galbraith, R.F. (1963). A new audio motor system in man. Electroenceph.Clin.Neurophysiol. 15, 921-925.

Bochenek, W. and Bochenek, Z. (1976). Postauricular (12 msec latency) responses to acoustic stimuli in patients with peripheral, facial nerve palsy. Acta Otolaryngol. 81, 264-269.

Boeder, P. (1961). The co-operation of the extraocular muscles, Am.J.Opthalmol. 51, 469.

Boston, J.R. and Møller, A.R. (1985). Brainstem auditory-evoked potentials. Crit.Rev. Biomed.Eng. 13(2), 97-123.

Buffin, J.T., Connell, J.A. and Stamp, J.M. (1977). The post-auricular muscle response in children. J.Laryng.Otol. 91(12), 1047-1062.

Burde, R.A. and Feldon, S.E., (1987). Actions of the extraocular muscles, in Moses, R.A., and Hart, W.M. (eds.) "Adler's Physiology of the Eye" 8th Ed., C.V. Mosby Co., St. Louis, MO, USA. 95-110.

Celesia, G.G. (1976). Organization of auditory cortical areas in man. Brain 99, 403-414.

Celesia, G.G. and Puletti, F. (1971). Auditory input to the human cortex during states of drowsiness and surgical anaesthesia. Electroenceph.Clin.Neurophysiol. 31, 603-609.

Clifford-Jones, R.E., Clarke, G.P. and Mayles, P. (1979). Crossed acoustic response combined with visual and somatosensory evoked responses in the diagnosis of multiple sclerosis. J.Neurol.Neurosurg.Psychiat. 42, 749-752.

Cody, D.T.R. and Bickford, R.G. (1969). Averaged evoked myogenic responses in normal man. Laryngoscope 79, 400-416.

Cody, D.T.R., Jacobson, J.L., Walker, J.C. and Bickford, R.G. (1964). Averaged evoked myogenic and cortical potentials to sound in man. Ann.Otol.Rhinol.Laryngol. 73, 763-777.

Creel, D., Boxer, L.A. and Fauci, A.S. (1983). Visual and auditory anomalies in Chediak-Higashi syndrome. Electroenceph.Clin.Neurophysiol. 55, 252-257.

Dallos, P. (1970). Low-frequency auditory characteristics: species dependence. J.Acoust.Soc.Am. 48, 489-499.

Davis, H. (1976). Principles of electric response audiometry. Ann.Otol.Rhinol.Laryngol 85 Suppl. 28, 1-96.

Davis, H. (1976). Brain stem and other responses in electric response audiometry. Ann.Otol.Rhinol.Laryngol 85, 3-14.

Davis, H., Lowell, E. and Goldstein, R. (1965). Sonomotor Reflexes: Myogenic Evoked Potentials. Acta Otolaryngol. 206, 122-128.

Davis, H., Mast, T., Yoshie, N. and Zerlin, S. (1966). The slow response of the human cortex to auditory stimuli: Recovery process. Electroenceph.Clin.Neurophysiol. 21, 105-113.

De Grandis, D. and Santoni, P. (1980). The post-auricular response: a single motor unit study. Electroenceph.Clin.Neurophysiol. 50, 437-440.

Desmedt, J.E. and Robertson D. (1977). Differential enhancement of early and late components of the cerebral somatosensory evoked potentials during forced-paced cognitive tasks in man. J Physiol (Lond). 271(3):761-82.

Don, M., Elberling, C. and Waring, M. (1984). Objective detection of averaged auditory brainstem responses. Scand.Audiol. 13, 219-228.

Douek, E.E., Gibson, W.P.R. and Humphries, K.N. (1975). The crossed acoustic response. Revue de Laryngologie 96 (No.3-4), 121-126.

Douek, E., Gibson, W. and Humphries, K. (1973). The crossed acoustic response. J.Laryngol.Otol., 711-726.

Douek, E.E., Gibson, W.P.R. and Humphries, K.N. (1974). The Crossed Acoustic Response and Objective Tests of Hearing. Develop.Med.Child.Neurol. 16, 32-39.

Dus, V. and Wilson, S.J. (1975). The click-evoked post-auricular myogenic response in normal subjects. Electroenceph.Clin.Neurophysiol. 39, 523-525.

Eggermont, J.J. (1985). Evoked potentials as indicators of auditory maturation. Acta Otolaryngol. (Suppl)., 421, 41-47.

Erwin, R.J. and Buchwald, J.S. (1986). Midlatency auditory evoked responses: Differential recovery cycles characteristics. Electroenceph.Clin.Neurophysiol. 64, 417-423.

Erwin, R. and Buchwald, J.S. (1986). Midlatency auditory evoked responses: Differential effects of sleep in the human. Electroenceph.Clin.Neurophysiol. 65, 383-392.

Feldon, S.E., and Burde, R.A. (1987). The oculomotor system, in Moses, R.A., and Hart, W.M. (eds.) "Adler's Physiology of the Eye" 8th Ed., C.V. Mosby Co., St. Louis, MO, USA. 122-168.

Feliciano, M., Saldaña, E., and Mugnaini, E. (1995). Direct projections from the rat primary auditory neocortex to nucleus sagulum, paralemniscal regions, superior olivary complex and cochlear nuclei. Aud.Neurosci. 1, 287-308.

Feneis, H. (1994). Pocket atlas of human anatomy: based on the international nomenclature. (English translation). Theieme Medical Publishers, Stuttgart.

Feuer, A., and Goodwin, G.C. (1996). "Sampling in Digital Signal Processing and Control", Birkhäuser Boston, Cambridge, MA, USA, 73.

Flood, L.M., Fraser, J.G., Conway, M.J. and Stewart, A. (1982). The Assessment of Hearing in Infancy using the Post-Auricular Myogenic Response. Brit.J.Audiology 16, 211-214.

Geisler, C.D., Frishkopf, L.S. and Rosenblith, W.A. (1958). Extracranial responses to acoustic clicks in man. Science 128, 1210-1211.

Gerber, S.E. (1977), Audiometry in Infancy, Grune & Stratton Inc.: New York, NY, USA., 183-203.

Gibson, W.P.R. (1975). The Crossed Acoustic Response - A Post-Aural Myogenic Response. Thesis - Doctor of Medicine. University of London, UK.

Glattke, T.J. (1978). Ch.31: Electronystagmography. in Katz, J (ed.) "Handbook of Clinical Audiology (2nd Ed.)", Williams & Wilkins Co, Baltimore, MD, USA. 375-387.

Goetzinger, C.P. (1962). Effects of small perceptive losses on language and on speech discrimination. Volta Rev. 64, 408-414.

Goldstein, P.J., Krumholz, A., Felix, J.L., Shannon, D., and Carr, R.F. (1979). Brainstem evoked responses in neonates. Am.J.Obst.Gyn. 135, 622-631.

Goff, G.D., Matsumiya, Y., Allison, T. and Goff, W.R. (1977). The scalp topography of human somatosensory and auditory evoked potentials. Electroenceph.Clin.Neurophysiol. 42, 57-76.

Hall, J.W. (1992). Post-auricular muscle (PAM) activity. in "Handbook of Auditory Evoked Responses", 101-103. Allyn & Bacon, MA, USA.

Halliday, A. (1994). Development of a unit for the screening of neonates with hearing impairment using auditory evoked potentials. Unpublished report, Physiology Dept., University of Western Australia, 1-12.

Holton, T. and Hudspeth, A.J. (1986). The transduction channel of hair-cells from the bull-frog characterised by noise analysis. J.Physiol. 375, 195-227.

Humphries, K.N., Gibson, W.P.R. and Douek, E.E. (1976). Objective methods of hearing assessment: a system for recording the crossed acoustic response. Med.Biol.Eng 14(1), 1-7.

Ifeachor, E.C., and Jervis, B.W. (1993). "Digital signal processing: a practical approach." Addison-Wesley Publishers Ltd., U.K., p.280-284.

Jacobson, J.L., Cody, D.T., Lambert, E.H. and Bickford, R.G. (1964). Physiological Properties of the Post-Auricular Responses (Sonomotor) in Man. The Physiologist 7, 167-167.

Jacobson, J.T., Jacobson, C.A., and Spahr, R.C. (1990). Automated and conventional ABR screening techniques in high-risk infants. J.Am.Acad.Audiol. 1, 187-195.

Johnstone, J.R., Adler, V.A., Johnstone, B.M., Robertson, D., and Yates, G.K. (1979). Cochlear action potential threshold and single unit thresholds. J.Acoust.Soc.Am. 65(1), 254-257.

Joseph, J.P. and Boussaoud, D. (1985). Role of the cat substantia nigra pars reticular in eye and head movements. I. Neural activity. Exp. Brain Res. 57, 286-296.

Katz, B., and Miledi, R. (1965). Propagation of electric activity in motor nerve terminals. Proc. Roy. Soc. (Biol.), 161, 453-482.

KEMH (1997). Early detection aim for hearing tests. Inside Edition, King Edward Memorial Hospital Public Relations Dept., Western Australia 4(3), 3-3.

Kemp, D.T. (1978). Stimulated acoustic emissions from within the human auditory system. J.Acoust.Soc.Am. 64(5), 1386-1391.

Khadori, R., Soler, N.G., Good, D.C., DevlescHoward, A.B., Broughton, D. and Walbert, J. (1986). Brainstem auditory and visual evoked potentials in Type 1 (insulin-dependent) diabetic patients. Diabetologia 29, 362-365.

Kiang, N.Y., Crist, A.H., French, M.A. and Edwards, A.G. (1963). Postauricular electrical response to acoustic stimuli in humans. Massachusetts Institute of Technology Quarterly Progress Report 68, 218-225.

Kim, D.O. (1986). Active and nonlinear cochlear biomechanics and the role of outer-hair-cell subsystem in the mammalian auditory system. Hearing Res. 22, 105-114.

Lille, F., Audin, G. and Hazemann, P. (1975). Effects of time and tasks upon auditory and somatosensory evoked potentials in man. Electroenceph.Clin.Neurophysiol. 39, 239-246.

Marcon, S. (1995). The influence of the perilymphatic potassium concentration on the mammalian cochlea. BSc. Honours Thesis, Physiology Department, University of Western Australia.

Mast, T (1963). Muscular vs. cerebral sources for the short-latency human evoked responses to clicks. The Physiologist 6, 228-229.

McGee, T., Kraus, N., and Nicol, T. (1997). Is it really a mismatch negativity? An assessment of methods for determining a response validity in individual subjects. Electroenceph.Clin.Neurophysiol. 104, 359-368.

Mendel, M.I. (1977). Evoked Cochlear Potentials. In Gerber, S.E. (ed.), "Audiometry in Infancy", Grune & Strattion Inc.: New York, NY, USA., 183-203.

Nober, E.H. and Nober, L.W. (1977). Effects of hearing loss on speech and language in the postbabbling stage. In B.F.Jaffe (ed.), "Hearing Loss In Children", University Park Press: Baltimore, MD, USA., 621-629.

Norton, M.P. (1989) "Fundamentals of noise and vibration analysis for engineers", Cambridge University Press, Cambridge, UK, 361-364.

Özdamar, Ö. and Dallos, P. (1976). Input-output functions of cochlear whole nerve action potentials: Interpretation in terms of one population of neurons. J.Acoust.Soc.Am. 59, 143-147

Özdamar, Ö. and Delgado, R.E. (1996). Measurement of signal and noise characteristics in ongoing auditory brainstem response averaging. Ann.Biomed.Eng. 24, 702-715.

Özdamar, Ö., Kraus, N. and Curry, F. (1982). Auditory brain stem and middle latency responses in a patient with cortical deafness. Electroenceph.Clin.Neurophysiol. 53, 224-230.

Oudesluys-Murphy, A.M., Van Straaten, H.L., Bholasingh, R. and Van Zanten, G.A. (1996). Neonatal hearing screening. Eur.J.Ped. 155 (6), 429-435.

Patuzzi, R.B. and Moleirinho, A. (1998). Automatic monitoring of mechano-electrical transduction in the guinea pig cochlea. Hearing Res. 125, 1-16.

Patuzzi, R.B. and Rajan, R. (1990). Does electrical stimulation of the crossed olivo-cochlear bundle produce movement of the organ of Corti? Hearing Res. 45, 15-32.

Patuzzi, R.B. and Thomson, S.M. (1995). Development of a simple evoked-response averaging system for neonatal screening. Report, Physiology Dept., University of Western Australia, 1-16.

Patuzzi, R.B. and Thomson, S.M. (1999). The Post-Auricular Muscle Response (PAMR) Revisited. (*in preparation*)

Patuzzi, R.B., Yates, G.K. and Johnstone, B.M. (1989a). The origin of the low-frequency microphonic in the first cochlear turn of the guinea-pig. Hearing Res. 30, 83-98.

Picton, T.W. and Hillyard, S.A. (1974). Human auditory evoked potentials. II: Effects of Attention. Electroenceph.Clin.Neurophysiol. 36, 191-199.

Picton, T.W., Hillyard, S.A. and Galambos, R. (1973). Ch.8.: Habituation and Attention in the Auditory System. Handbook of Sensory Physiology: The Auditory System 3, 343-389.

Picton, T.W., Hillyard, S.A., Galambos, R. and Schiff, M. (1971). Human Auditory Attention: A Central or Peripheral Process?. Science 173, 351-353.

Picton, T.W., Hillyard, S.A., Krausz, H.I. and Galambos, R. (1974). Human auditory evoked potentials. 1: Evaluation of components. Electroenceph.Clin.Neurophysiol. 36, 179-190.

Populin, L.C. and Yin, T.C.T. (1998). Pinna movements of the cat during sound localization. J. Neuroscience, 18(11), 4233 – 4243.

Probst, R., Lonsbury-Martin, B.L. and Martin, G.K. (1991). A review of otoacoustic emissions. J.Acoust.Soc.Am. 89(5), 2027-2067.

Qiu, W., Chan, F.H.Y., Lam, F.K., Poon, P.W.F. (1994). An enhanced approach to adaptive processing of the brainstem auditory evoked potential. Australasian Physical & Engineering Sciences In Medicine 17(3), 131-135.

Rajan, R., Irvine, D.R. and Cassell, J.F. (1991). Normative N_1 audiogram data for the barbiturate-anaesthetised domestic cat. Hearing Res. 53, 153-158.

Robinson, K. and Rudge, P. 1977). Abnormalities of the auditory evoked potentials in patients with multiple sclerosis. Brain 100, 19-40.

Rodieck, R.W. (1979). Visual Pathways. Ann.Rev.Neurosci. 2, 193-225.

Ruggero, M.A., Robles, L. and Rich, N.C. (1986). Basilar membrane mechanics at the base of the chinchilla cochlea: II. Responses to low-frequency tones and the relationship to microphonics and spike initiation in the VIII nerve. J.Acoust.Soc.Am. 80, 1375-1383.

Schwarz, D.M., Morris, M.D. and Jacobson, J.T. (1994). The Normal Auditory Brainstem Response and its Variants. in Jacobson, J.T. (Ed.) "Principles and Applications in Auditory Evoked Potentials". Allyn & Bacon, Boston, MA. USA.

Seales, D.M., Torkelson, R.D., Shuman, R.M., Rossiter, V.S.and Spencer, J.D. (1981). Abnormal brainstem auditory evoked potentials and neuropathology in "locked-in" syndrome. Neurology 31, 893-896.

Spehlmann, R. (1985) Evoked potential primer. Butterworth Publishers, Boston, MA, USA.

Stein, L., Tremblay, K., Pasternak, J., Banerjee, S., Lindemann, K., and Kraus, N. (1996). Brainstem abnormalities in neonates with normal otoacoustic emissions. Seminars in Hearing. 17(2), 197-212.

Streletz, L.J., Katz, L., Hohenberger, M. and Cracco, R.Q. (1977). Scalp recorded auditory evoked potentials and sonomotor responses: An evalutation of components and recording techniques. Electroenceph.Clin.Neurophysiol. 43, 192-206.

Teas, D.C., Klein, A.J., and Kramer, S.J. (1982). An analysis of auditory brainstem responses in infants. Hearing Research 7(1), 19-54.

Thornton, A.R.D. (1975a). Distortion of averaged post-auricular muscle responses due to system bandwidth limits. Electroenceph.Clin.Neurophysiol. 39, 195-197.

Thornton, A.R.D. (1975b). The use of post-auricular muscle responses. J.Laryngol.Otol. 89, 997-1010.

Thornton, A.R.D. and Coleman, M.J. (1975). The adaptation of cochlear and brainstem auditory evoked potentials in humans. Electroenceph.Clin.Neurophysiol. 39, 399-406.

Totsuka, G., Nakamura, K. and Kirikae, I. (1954). Studies of the acoustic reflex. Part I. Electromyographic studies of the acoustic-auricular reflex. Ann.Otol.Rhinol.Laryngol. 63, 939-949.

Weber, B.A. and Jacobson, C. (1994). Newborn Hearing Screening. in Jacobson, J.T. (Ed.) "Principles and Applications in Auditory Evoked Potentials". Allyn & Bacon, Boston, MA. USA. 357-383.

White. K.R. and Maxon, A.B. (1994). Universal screening for infant hearing impairment: simple beneficial, and presently justified. Int.J.Ped.Otorhinolaryngol. 32, 201-211.

Wilson, W.R. and Richardson, M.A. (1991). Behavioural audiometry. Otolaryngol.Clin.North Am. 24(2), 285-297.

Wolpaw, J.R. and Wood, C.C. (1982). Scalp distribution of human auditory evoked potentials. I. Evaluation of reference electrode sites. Electroenceph.Clin.Neurophysiol. 54, 15-24.

Yoshie, N. and Okudaira, T. (1969). Myogenic evoked potential responses to clicks in man. Acta Otolaryngol.Supp. 252, 89-103.

Zerlin, S. and Davis, H. (1967). The variability of single evoked vertex potentials in man. Electroenceph.Clin.Neurophysiol. 23, 468-472.

APPENDIX ONE:
Virtual Instruments

PAMoMATIC VI 

The purpose of this VI was to sample, display, and average waveforms, to calculate the correlation value between successive waveforms, to calculate and display the background EMG level of the post-auricular muscle, and to allow the user to save this information to external spreadsheet files for later analysis.

The operating sequence of the PAMoMATIC VI was as follows. If the "Save Summary Data" box on the front panel had been ticked, on starting the VI a file requester asked the user to enter the name of the file that the Summary Data was to be saved under. A "header" file was then created by the VI, which contained the names of the columns that the Summary Data was to be saved under at the end of the operation of the VI. Also stored in this header was other information such as the date, time, sample rate, number of averages per "run", BIO Amp filter settings, correlation window times, and comments. The file format was tab-delimited text. When read by a spreadsheet program such as Excel, this header file appeared as one row, with each item of the header appearing in separate columns. The "Comments" box on the front panel was used for entering miscellaneous information, such as the name of the subject, or any information relevant to that experiment. The BIO Amp filter settings were not used in calculations, but were saved with the data file for future reference. An example of the Header file is shown below:

run p-p-height ave.corr. corr.stdev ave.EMG EMGstdev PAMR.rms Prms.StDev atten.dB. max.time min.time corrSig? *7/05/98 @ 13:47 20 Aves/Run Sample Rate: 5000Hz HP: 10 Hz LP: 200 Hz Notch CorrWindow: 10 - 24ms Subject: G.O'B.*

The BIO Amp "Range" setting was used to scale the input voltages from the BIO Amp to correct for the gain associated with that Range setting. All of the above occurred outside the

main WHILE loop, which ensured that the above was completed before the data acquisition commenced. The VI contained a number of loops in which iterative calculations were carried out. These loops are described below. The "Number of Runs" input, read from the front panel, set the number of iterations of the following FOR loop. A "run" was defined as a number of sets of *x* averages, as specified by the "Averages per Run" input on the front panel.

FOR Loop

Within this FOR loop, the Data Acquisition settings were read from the front panel. These settings defined the analog input channel from which to trigger, the analog input from which to sample the waveform, the number of pre-trigger and post-trigger samples to take, the upper and lower voltage limits of the acquisition, the trigger voltage, and the edge of the trigger pulse from which to trigger (the rising or falling edge). Also generated at this stage was the correlation window array. The Window VI is described in more detail on page A 9. Once this was done, the program entered another WHILE loop, as described below.

WHILE Loop

This loop contained the main computational tasks of the VI, such as the Averager and Correlation VIs. The acquisition settings were first read by the Software Analog Trigger VI, which was located in it's own WHILE loop to ensure that acquisition of the waveform was complete before attempting to display or carry out calculations on it. The Software Analog Trigger VI waited for the trigger conditions on the appropriate channel to be satisfied before it began acquisition. When triggered, the VI sampled the specified number of pre-trigger samples and post-trigger samples from the specified channel at the specified rate. The Software Analog Trigger VI was modified from a pre-existing one, so that it supplied the

"waveform" array and the "trigger" arrays separately, as well as a "1/rate" output, which could be used to convert the sample numbers into milliseconds. Once acquisition of the waveform was complete, the waveform array was divided by the BIO Amp gain factor, and converted from volts to microvolts. The trigger array was displayed on a side area of the front panel of the VI for equipment diagnostic purposes. The waveform array then passed to the Subtract DC Offset VI. This sub-VI is shown in more detail on page A 10. The VI subtracted the mean value of the waveform from the array in order to eliminate any DC offset and thus further AC couple the waveform. The array was then split into the pre-trigger and post-trigger arrays. The root mean square amplitude of the pre-trigger array was calculated by the RMS VI, shown in more detail on page A 9. This RMS value was displayed on the EMG meter of the front panel. It was also placed on a shift register and averaged over the number of "Averages Per Run" for output of the mean and standard deviation of the EMG to the Summary Data file. This process was also carried out for the post-trigger array, so that it could be directly compared to the EMG in some experiments. The post-trigger array was also displayed on the front panel as the "raw" waveform, and was passed to the Averager VI, shown in more detail on page A 6. Each raw waveform was placed in a shift register, summed with the previous waveforms, and divided by the number of waveforms making up the sum (taken from the iteration number of the WHILE loop). The averaged waveform was displayed on the front panel, while the raw waveform was passed to the Correlator VI. Both the Averager and Correlator VIs were reset if the iteration number of the WHILE loop was 1. The Correlator VI is shown in more detail on page A 7. The output of the correlator (the correlation value of the current raw waveform and the waveform from the previous iteration) was sent to a Stack Averager, which calculated a running point average of the past *n* correlation values for graphing (where *n* was specified by

the “Correlation Graph Smoothing Level” on the front panel). The output of the correlator was also passed to an averager, which calculated the mean and standard deviation of the correlation over the number of “Averages Per Run” (from the front panel) for output in the summary data file. The standard deviation of the correlation was also represented graphically on the front panel. If the operator of the VI was interested in examining the correlation values of each pair of raw waveforms, he or she was able to tick the “Save All Corr. Data?” box on the front panel, and this correlation data was then written to a file at the end of every run. The attenuation voltage from the voltage-controlled attenuator was read from the relevant channel at this stage. As the attenuation level was not expected to change very rapidly, it was not converted to dB or displayed until the end of every run, which saved processor time. This WHILE loop continued until the current iteration number was larger than the “Averages Per Run” value specified on the front panel.

On exiting this WHILE loop, some primary summary data for the run were generated. The following data were bundled for output to the Summary Data file at the end of the “Number Of Runs” (the end of the operation of the VI):

i) The run number (from the iteration number of the “for” loop).

ii) The peak-to-peak height of the averaged waveform. This was calculated by subtracting the array minimum from the array maximum, which were both displayed on the front panel.

iii) The mean and standard deviation of the correlation, calculated over the number of averages in that run.

iv) The mean and standard deviation of the RMS of the EMG window, calculated over the number of averages in that run.

v) The mean and standard deviation of the RMS of the PAMR window, calculated over the number of averages in that run.

vi) The attenuation level (in dB), calculated from the attenuation voltage by the Attenuation-to-dB VI (shown in more detail on page A 16) which was displayed on the front panel.

vii) The time at which the maximum peak of the averaged waveform occurred, and

viii) The time at which the minimum peak of the averaged waveform occurred.

At this point in the operation of the VI, an unpaired T-Test was carried out on the correlation value to ascertain whether the mean correlation value for the run was significantly different from zero. The operation of the T-Test VI is described further on page A 12.

This "for" loop then repeated. A beep was given by a Beep VI every *x* runs (where *x* is specified by the "Beep every… runs" input on the front panel). This was done in order to alert the self-experimenter to the current run number if he or she had his or her eyes closed, or the monitor off,. The "for" loop continued for the number of iterations specified by "Number of Runs".

On exiting this "for" loop, the Summary Data bundle was written to a file, whose name was specified in the opening file-request dialog. If the user wanted to save the averaged waveforms, he or she was able to tick the "Save Waveforms" box on the front panel, and a file requestor asked them to enter a filename. The waveforms were then saved as a tab-delimited text file, and the VI stopped operation.

Front Panel: PAMoMATIC VI

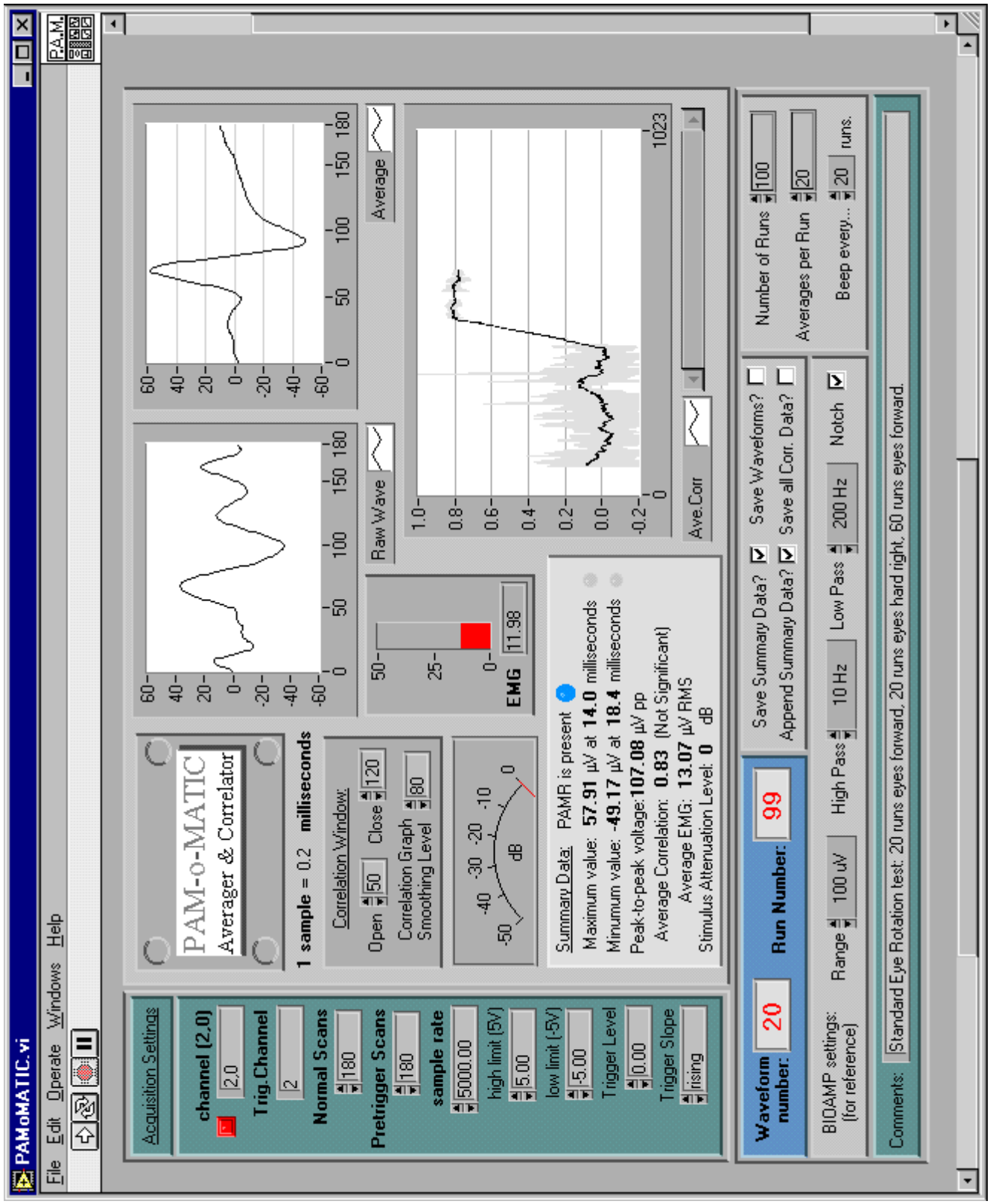

Diagram: PAMoMATIC VI

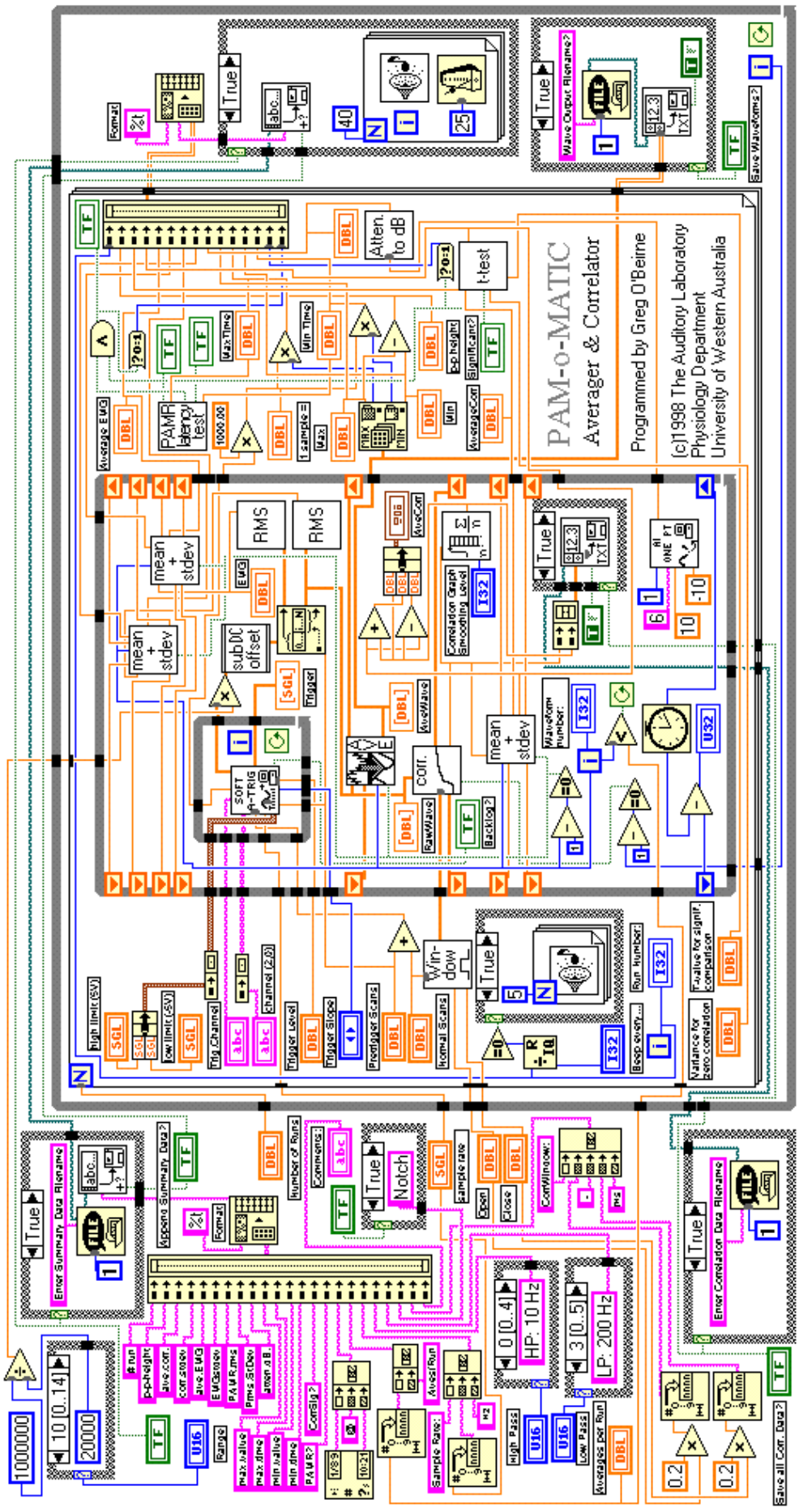

Averager VI

The purpose of this VI was to calculate the average of a number of "raw" (or unaveraged) waveform arrays.

On the first iteration, if the “Reset?” Boolean value was True, the input waveform was passed, without modification, via a shift register to the next iteration, where it became the "Sum Data In" array. A copy of the waveform array was displayed on the front panel as the Averaged Waveform (i.e. an average of 1 waveform).

On the second and subsequent iterations, the input waveform array was added to an array (called "Sum Data In") that was the sum of the previous waveforms. This new array (called "Sum Data Out") was then passed via a shift register to the next iteration, where it was used as the Sum Data In array, and so on. A copy of the Sum Data Out array was divided by the iteration number (i.e. the number of waveforms making up the Sum Data array) and displayed graphically on the front panel as the Averaged Waveform.

Diagram (first iteration):

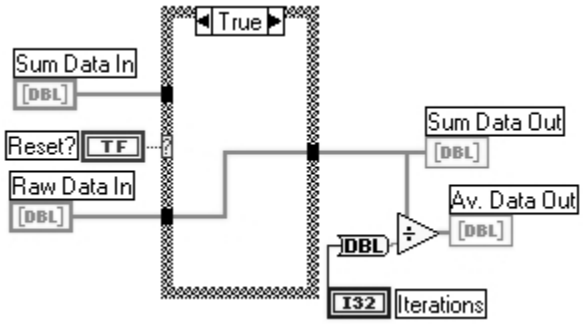

Diagram (second & subsequent iterations):

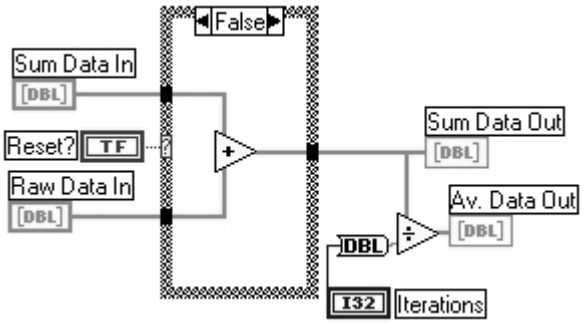

Correlator VI 

The purpose of this VI is to calculate the correlation value between successive waveforms.

On the first iteration, if the "Reset?" boolean value is True, the output of the correlator is set as zero, and the current waveform (the "*n*" data in, where *n* = this iteration) is passed via a shift register to the next iteration, where it becomes the "*n-1*" data in.

On the second and subsequent iterations, the "*n*" waveform array and the "*n-1*" waveform array are both multiplied by the window array, which is set by the Window VI (described on page A 9). This limits the period over which the correlation value is calculated, as described in Section 2.6. The windowed "*n*" and "*n-1*" arrays are multiplied together, and then summed over their length, also as described in Section 2.6. This sum is then divided by the square root of [the (sum of the square of waveform "*n*") multiplied by the (sum of the square of waveform "*n-1*")]. This output is the correlation value of the two waveforms, which can be read and plotted from outside the VI.

The current waveform array, "*n*", is then passed to the shift register where it becomes the "*n-1*" waveform array for the next iteration.

Diagram (first iteration):

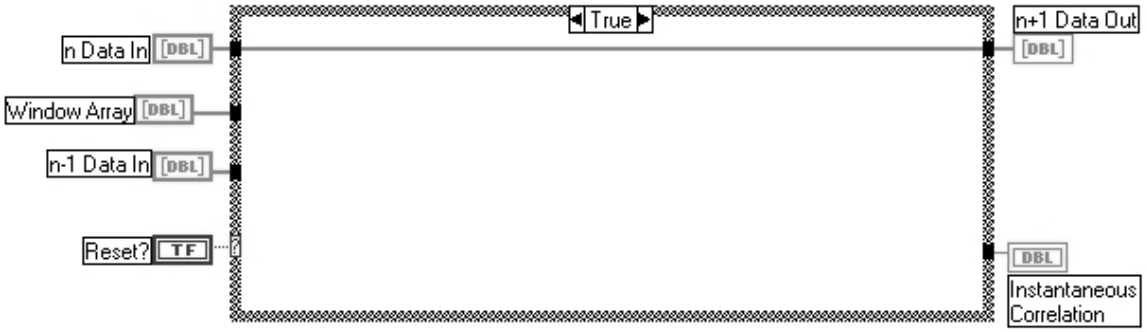

Diagram (second & subsequent iterations):

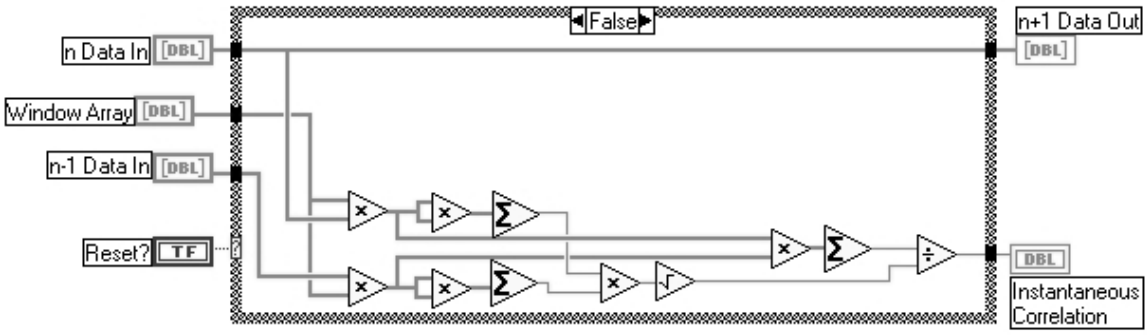

Window VI 

The purpose of this VI was to generate a window array that could be used in the calculation of the correlation value of successive waveforms.

The length of window array was determined by the number of iterations of a “for” loop. The “open” and “close” times for the window were set by the user via controls on the front panel. At each iteration of the “for” loop, if the iteration number was between the window “open” and “close” times, the output of the VI was a “1”, otherwise it was a “0”. The result at the completion of the VI was an array of zeros and ones that was used in the Correlator VI described on page A7.

Diagram:

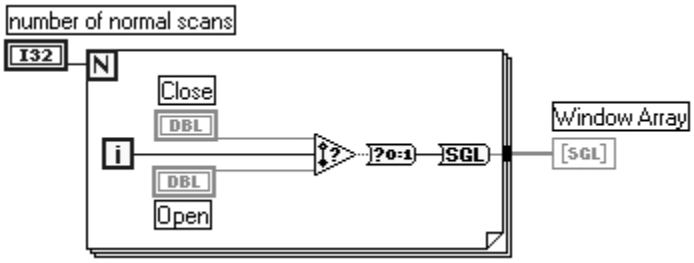

RMS VI 

The purpose of this VI was to calculate the root mean square amplitude of an array. The input array was first multiplied by itself, and the sum of this squared array was calculated over its length. This sum was then divided by the length of the array, and the square-root was calculated. This output was the RMS value of the input array.

Diagram:

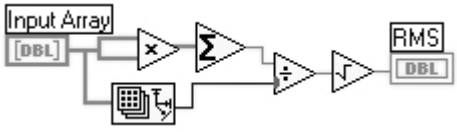

Subtract DC Offset VI 

The purpose of this VI was to remove any possible DC offset in a waveform array. This was done by subtracting the mean value from the array. The mean of the input array was first calculated by summing the array over its length, and dividing this sum by the length if the array. This mean value was then subtracted from the input array, so that the mean of the output array was zero.

Diagram: 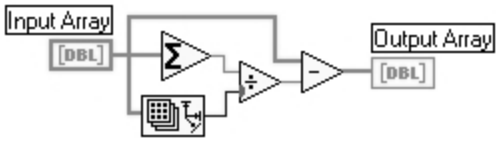

Mean & StDev VI 

The purpose of this VI was to calculate the mean and standard deviation of a set of numbers. The sample standard deviation was calculated as the square root of the sample variance, where the variance was calculated using the formula:

$$s^2 = \frac{\Sigma X^2 - [(\Sigma X)^2 / n]}{n - 1} \qquad \text{where } s^2 = \text{variance of sample}$$

On the first iteration, if the “Reset?” Boolean value was True, the input number was passed via a shift register to the next iteration, where it became the "Sum Data In" number. It was simultaneously multiplied by itself, and passed via another shift register to the next

iteration, where it became the “Sum Squares Data In” number. On the first iteration, the “Av.Data Out” is simply the “Raw Data In” number divided by one.

On the second and subsequent iterations, the “Raw Data In” input is added to the “Sum Data In” input, and divided by the current iteration number to give the mean of the “Raw Data In” inputs over those iterations. The “Raw Data In” value is simultaneously multiplied by itself and added to the “Sum Squares Data In” value

Diagram (first iteration):

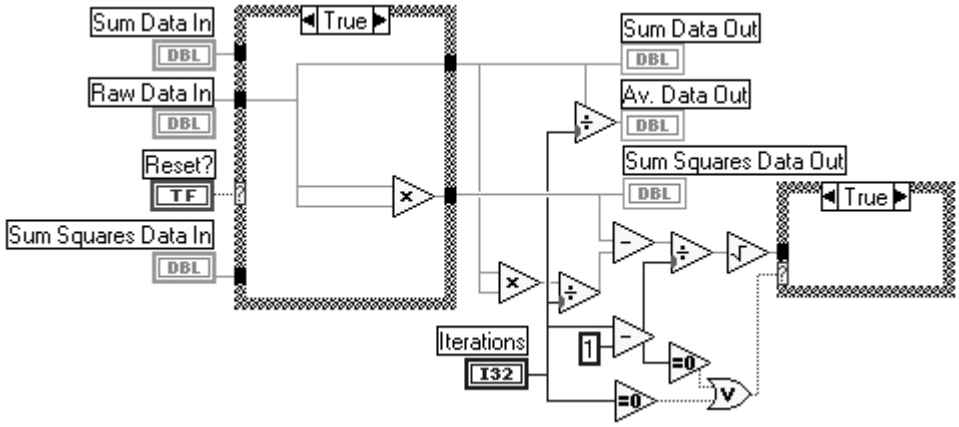

Diagram (second & subsequent iterations):

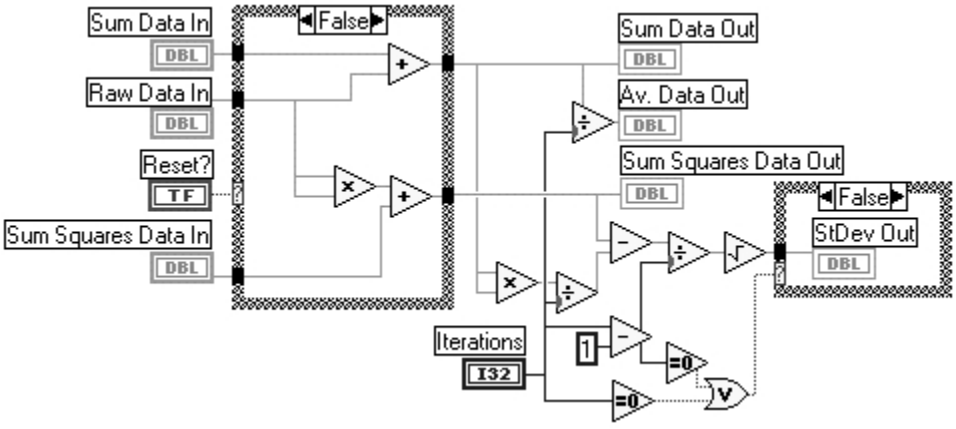

T-Test VI 

The purpose of this VI was to conduct an unpaired Student's T-Test on the mean correlation value in order to determine whether it was significantly different from zero at the 5% level. The test statistic, t, was calculated using the following formula:

$$t = \frac{|(\overline{x}_1 - \overline{x}_2)|}{s^2x_1 + s^2x_2}$$

where $\overline{x}_1$ = average correlation value
$\overline{x}_2$ = zero correlation
s^2x_1 = variance of correlation
s^2x_2 = variance for zero correlation

The mean and standard deviation of the 20 individual correlation values in each run was calculated by the Mean & StDev VI, shown on page A 10. The variance for the zero correlation value was taken to be 0.17, which was the mean of the variance of correlation values around zero for a number of subjects (n = 3). The mean correlation value over each run (of 20 averages) was determined to be significantly different from zero at the 5% level if the calculated test statistic was greater than 2.021, which was the 0.05 value of the t-distribution for 38 degrees of freedom (38 = 20+20–2). Although negative correlation values can also be significantly different from zero, they do not indicate the presence of a PAMR. For this reason, the VI allowed "Significant" result to be shown only if the correlation value was greater than zero. In practice, however, a far more reliable and useful measure of the presence of the PAMR was simply to state whether the average correlation level was above 0.2. For this reason, this T-Test VI was rarely used.

Diagram:

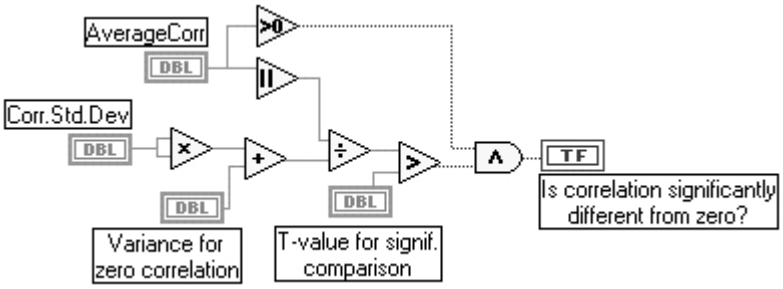

Latency Test VI 

The purpose of this VI was to determine whether the peaks of the averaged waveform fell into approximately the same time periods that would contain the peaks of the PAMR if it were present.

To satisfy the latency criteria for the PAMR, the maximum value of the waveform array had to occur between 10 and 20 ms, the minimum value had to occur between 15 and 30 ms, and the maximum value had to have occurred earlier than the minimum value. The ranges for the peaks were made sufficiently broad so as to allow for the latency shifts found in different age groups (as described in Section 3.5).

Diagram:

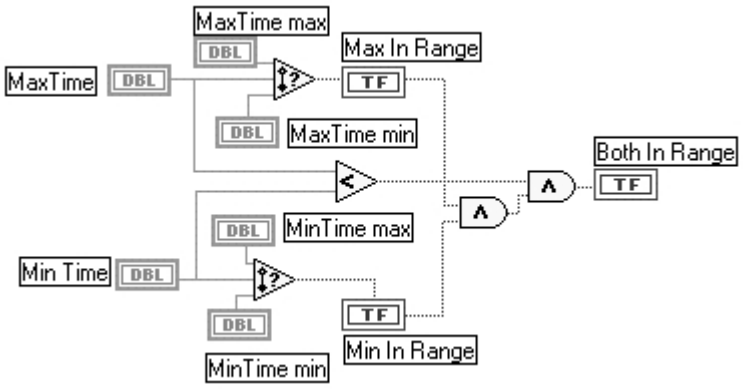

3D Correlation Graph VI 

The purpose of the following VI was to calculate the average correlation value of a set of "*n*" waveforms, measured using every possible correlation window start and stop time. Although this VI was capable of using window increments of 0.2 ms (the length of one sample period), using window increments of 1 ms brought the time taken to complete this task down from several hours to around 30 minutes. This VI used the Correlation VI (shown on page A 7) and the Window VI (shown on page A 9) within a for loop, whose number of iterations was set by the number of waveforms over which the correlation values were to be calculated. The Window start and stop times were taken from the iteration numbers of two "while" loops. The operation of the VI was as follows.

Firstly, the user was prompted to enter the names of the input and output files for the VI. The input was a file containing the waveforms that correlation values were to be calculated from, an the output was the file that will contain the start and stop time defining the correlation window, and the average correlation value measured over that window. If the user had chosen to use window increments of 5 samples (equivalent to 1 ms), each iteration number was multiplied by 5 before being used as a window time. At each iteration of the inside "while" loop, the input file was loaded, and the waveform arrays were fed to the Correlator VI inside the "for" loop. Using the window array generated by the Window VI, the Correlator VI calculated the correlation values of every successive waveform pair. The output of the "for" loop was an array containing these correlation values. This was then summed, and divided by the number of waveforms that the correlation was calculated over, to give the average correlation value of those waveforms using that correlation window. This average correlation value, and the start and stop window times were then saved as one row of a text file.

On the next iteration of the inner “while”, the stop window increment increased by 1ms, and the inner “for” loop repeated. When the maximum stop window time was reached, the outer “while” loop advanced one iteration, which increased the window “start” time by 1ms, and inner “while” loop repeated. At each iteration of the outer “while” loop, the percentage progress was displayed on the front panel.

As only those correlation windows in which the “stop” time occurred after the “start” time produced an output that was a real number (i.e. the sum was not divided by zero), the average correlation value was checked to see if it was a real number before writing to the file, which saved having to edit these values out of the output file before plotting the data.

Diagram:

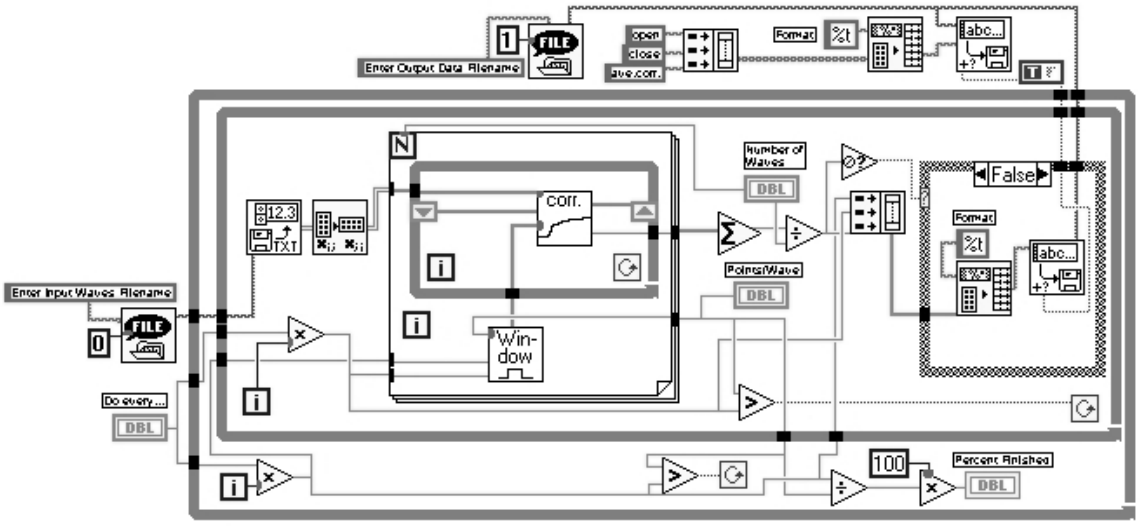

Attenuation to dB VI 

The purpose of this VI was to convert a DC voltage output from a voltage-controlled attenuator to an attenuation level in decibels (calculated from the percentage reduction off peak-to-peak height of the square-wave pulse used to generate the click stimuli).

The three functions defining the conversion curve were as follows:

Let x = Attenuation voltage (V)

Let y = Peak-to-peak voltage of square-wave pulse used to generate the click stimulus.

If $0.42 \leq x < 1.04$ then $y = 10^{(4.610567x - 3.84991)}$

If $1.04 \leq x \leq 1.08$ then $y = 10^{(1.168585x - 0.26909)}$

If $1.08 < x$ then $y = 9.8$ volts.

The peak-to-peak height was then converted to a value in decibels relative to the peak-to-peak height of the unattenuated square-wave pulse (9.8 volts) by the formula:

$$\text{Attenuation Level (dB)} = 20 \cdot \log_{10}(y / 9.8)$$

The VI shown overleaf is the LabVIEW equivalent to the formulae above, and was used to convert the attenuation voltage to an attenuation level in decibels.

Diagram (showing “True” case structures):

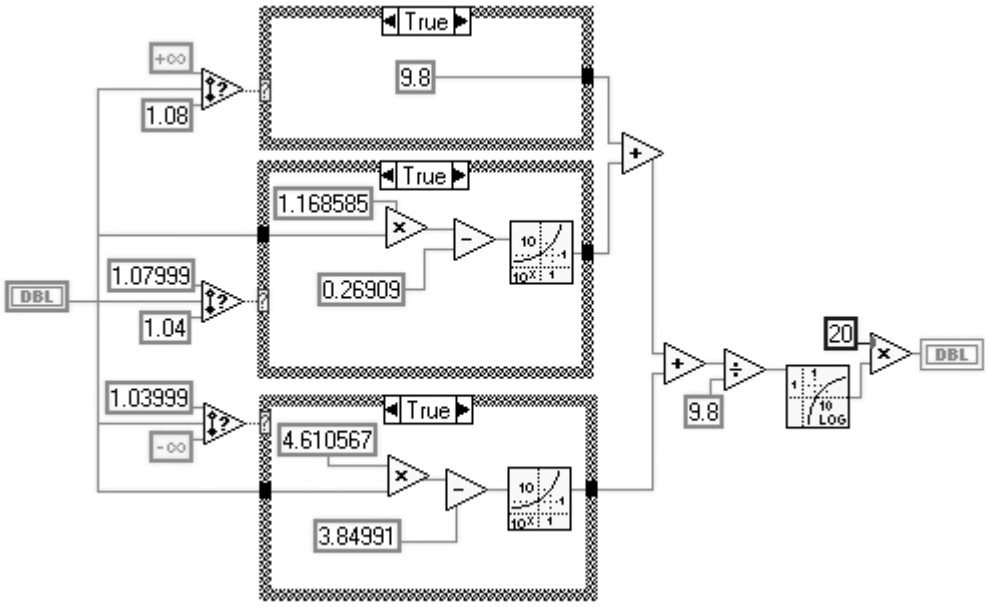

Diagram (showing “False” case structures):

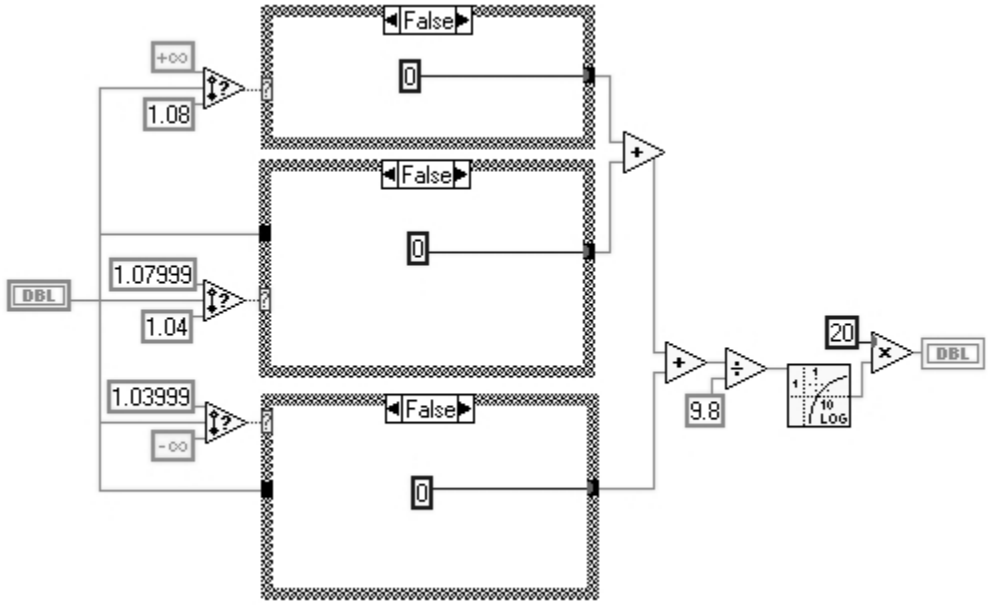

Stimulus-level feedback loop VI components

The purpose of these VI components were to ramp the sound level of the stimulus up or down manually (in manual mode), or automatically, in which case the sound level was ramped up or down to maintain either a constant correlation level, or a constant stimulus attenuation level. They were placed in the main data acquisition loop of the PAMoMATIC VI and used in the experimental series described in Sections 3.12 and 3.13.

In the automatic "iso-correlation" mode, the "smoothed" correlation level from the correlator was compared to a set-point value, and the TTL output was set to high ("1") if the level was below the set-point, and to low ("0") if it was above. The high TTL output caused the stimulus attenuator to decrease the level of attenuation, and so increase the sound level of the stimulus, while a low TTL output increased the attenuation level and made the sound stimuli quieter. In the automatic iso-attenuation mode, the same process was used to maintain the stimulus attenuation level within a certain, tight, range. The attenuation or correlation set-point was written to the file output to allow assessment of the success of the VI in maintaining the attenuation or correlation level near the set-point.

The diagrams for these components showing both the "true" and "false" cases structures are shown overleaf.

Diagram (showing “True” case structures):

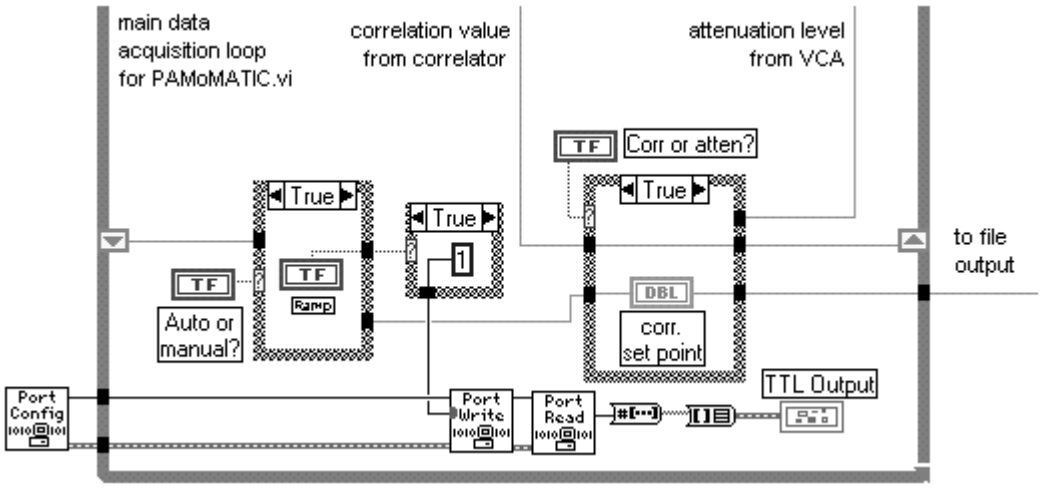

Diagram (showing “False” case structures):

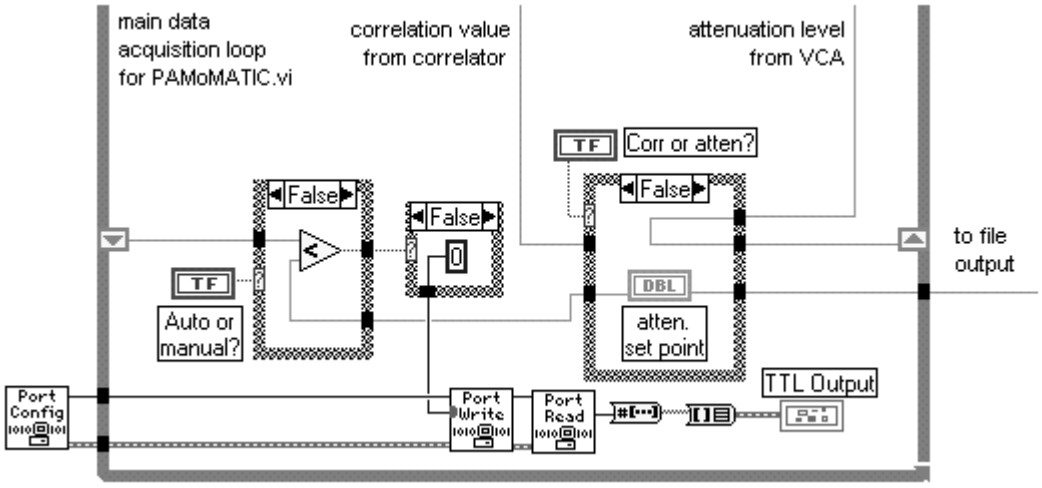

APPENDIX TWO:
Information Sheets and Consent Forms

The University of Western Australia

Dr Robert Patuzzi
The Auditory Laboratory
Department of Physiology
The University of Western Australia
Nedlands, Western Australia 6009
Telephone (09)-380-1422
Facsimile (09)-380-1025
Email rpatuzzi@cyllene.uwa.edu.au

Development of a simple evoked-response averaging system for neonatal audiometric screening.

Information and Consent Form

The purpose of this study is to develop a new technique for detecting hearing loss in adults and babies by measuring a small electrical signal from a muscle behind the ear. The measurement is perfectly safe and involves no discomfort. In this initial stage of development, we need to measure responses from a large number of people, and your participation in this study is greatly appreciated.

Small self-adhesive button contacts will be placed on the skin of the head and neck, after a light wiping with alcohol to clean the surface. Normal signals from the muscle will be recorded with and without a soft clicking sound presented from a small speaker. You do not need to do anything for the signal to be measured, although you may be asked to move your eyes from side to side to increase the signal slightly.

If you wish to end the test at any time, you are welcome to do so.

Declaration

I (the participant) have read the information above and any questions I have asked have been answered to my satisfaction. I agree to participate in this activity, realising that I may withdraw at any time without prejudice.

I understand that all information provided is treated as strictly confidential and will not be released by the investigator unless required to do so by law.

I agree that research data gathered for the study may be published provided my name or other identifying information is not used.

_____ _____

Participant Date

The Committee for Human Rights at the University of Western Australia requires that all participants are informed that, if they have any complaint regarding the manner in which a research project is conducted, it may be given to the researcher or, alternatively, to the Secretary, Committee for Human Rights, Registrar's Office, University of Western Australia, Nedlands, WA 6907 (telephone number 9380 3703). All study participants will be provided with a copy of the Information Sheet and Consent Form for their personal records.

The University of Western Australia

Dr Robert Patuzzi
The Auditory Laboratory
Department of Physiology
The University of Western Australia
Nedlands, Western Australia 6009
Telephone (09)-380-1422
Facsimile (09)-380-1025
Email rpatuzzi@cyllene.uwa.edu.au

Development of a simple evoked-response averaging system for neonatal audiometric screening.

Information and Consent Form

The purpose of this study is to develop a new technique for detecting hearing loss in adults and babies by measuring a small electrical signal from a muscle behind the ear. The measurement is perfectly safe and involves no discomfort. In this initial stage of development, we need to measure responses from a large number of infants, and your participation in this study is greatly appreciated.

Small self-adhesive button contacts will be placed on the skin of the head and neck, after a light wiping with alcohol to clean the surface. Normal signals from the muscle will be recorded with and without a soft clicking sound presented from a small speaker. You do not need to do anything for the signal to be measured, although you may be asked to gently rock your child from side to side to increase the signal slightly.

If you wish to end the test at any time, you are welcome to do so.

Declaration

I (the parent or legal guardian of the participant) have read the information above and any questions I have asked have been answered to my satisfaction. I agree to allow my child to participate in this activity, realising that I may withdraw them at any time without prejudice.

I understand that all information provided is treated as strictly confidential and will not be released by the investigator unless required to do so by law.

I agree that research data gathered for the study may be published provided my child's name or other identifying information is not used.

_____ _____

Parent/Legal Guardian of Participant Date

The Committee for Human Rights at the University of Western Australia requires that all participants are informed that, if they have any complaint regarding the manner in which a research project is conducted, it may be given to the researcher or, alternatively, to the Secretary, Committee for Human Rights, Registrar's Office, University of Western Australia, Nedlands, WA 6907 (telephone number 9380 3703). All study participants will be provided with a copy of the Information Sheet and Consent Form for their personal records.